THE UNIVERSITY of ADELAIDE

Holocene hydroclimate variability in south-eastern Australia; validation and application of cellulose oxygen isotopes at Lake Surprise, Victoria, Australia.

Batugoda Pussepitiye Gedara Asika Manohari Kumari Dharmarathna

Department of Earth Sciences

School of Physical Sciences

University of Adelaide

This thesis is submitted in fulfilment of the requirements for the degree of Doctor of Philosophy

December 2022

Table of Contents

Abstract

Understanding decadal-millennial scale patterns of climate variability are essential to provide context for future climate projections and to support climate mitigation actions. In south-eastern Australia, which has been vulnerable to climate extremes in recent decades, the relatively short (<125 years) instrumental climate record does not capture the full range of natural climate variability, undermining efforts to model and predict future droughts. In this context, there remains a need for decadal-scale palaeoclimate records which are well-dated and provide robust reconstructions of hydroclimate change based on a firm understanding of the contemporary proxy system.

This thesis presents a new Holocene palaeoclimate record for south-eastern Australia using oxygen isotopes in aquatic cellulose, preserved in the sediments of Lake Surprise, Victoria.

The palaeoclimate record is supported by,

i. A combined monitoring and modelling program to quantify the link between climate, lake hydrology and the oxygen isotope composition of lake waters, with a particular focus on lake-groundwater interaction. Precipitation and lake waters were monitored for major ions and oxygen and hydrogen isotopes. These data were interpreted using the lake isotope mass balance modelling approach.

ii. A robust chronology based on combined ^{210}Pb, Pu and ^{14}C analyses, as well as independent chronomarkers, with ^{14}C measured on bulk sediment, plant macrofossils and pollen extracts. An age model was developed using Bayesian *Plum* modelling, and chronological biases with pollen radiocarbon dates were examined in detail.

iii. Palaeoclimate validation-in-time by comparing the recent sedimentary record with climate data for the instrumental period. Correlations between instrumental precipitation-evaporation data with sedimentary oxygen isotope data provide greater confidence in the fidelity of the Holocene climate reconstruction. Changes in sediment carbonate concentration and carbon isotopes in organic matter appear to relate to changes in groundwater influence and aquatic primary productivity.

The Holocene palaeoclimate record of lake water oxygen isotopes derived using cellulose oxygen isotope analysis agrees with previous studies from western Victoria, which indicate a relatively wet early-mid Holocene and a prolonged period of drier climate after ~4500 cal yr

BP. It is suggested that the late Holocene drying was influenced by an increase in the frequency of El-Niño events. In contrast to previous studies, the Lake Surprise record indicates that the early Holocene wet period was not a singular event, but instead, three periods of wetter climate occurred from ~10850 – 10000 cal yr BP, 7400 – 7000 cal yr BP and 5600 – 4500 cal yr BP. These wet intervals are consistent with inferred periods of weaker and northward migration of the Southern Westerly Winds. By constraining the timing of major hydroclimate shifts in south-eastern Australia, the new record from Lake Surprise contributes to a deeper knowledge of the Holocene climate in the region, which can assist in modelling hydroclimate responses to global change. Furthermore, the modern monitoring, modelling and validation lay the foundation for replicating the Lake Surprise record to develop regional scale, quantitative records of hydrological change.

Declaration

I certify that this work contains no material which has been accepted for the award of any other degree or diploma in my name, in any university or other tertiary institution and, to the best of my knowledge and belief, contains no material previously published or written by another person, except where due reference has been made in the text. In addition, I certify that no part of this work will, in the future, be used in a submission in my name, for any other degree or diploma in any university or other tertiary institution without the prior approval of the University of Adelaide and where applicable, any partner institution responsible for the joint award of this degree.

I give permission for the digital version of my thesis to be made available on the web, via the University's digital research repository, the Library Search and also through web search engines, unless permission has been granted by the University to restrict access for a period of time.

I acknowledge the support I have received for my research through the provision of an Australian Government Research Training Program Scholarship.

Batugoda Pussepitiye Gedara Asika Manohari Kumari Dharmarathna 16th December 2022

Acknowledgements

First and foremost, I would like to give my sincere thanks to my principal supervisor, Jonathan Tyler and my co-supervisors John Tibby and Cameron Barr for giving me the opportunity to be a part of this project. None of this work would have succeeded without your unwavering support and belief in me. Jon, thank you very much for always being there when I needed the support, and guiding me in the right direction. I've always been fascinated with the enthusiasm and interest that you have shown for this project and the work I've produced. You have encouraged me to take many opportunities that I have been lucky to have had during the time of my PhD. John, you were always willing to make time whenever I needed advice and I've always been inspired by your knowledge and insights. Thank you very much for the encouragement and invaluable support. Cameron, even though it was just two years, working with you was a wonderful experience and thank you very much for the enormous support provided not only during the fieldwork but also in the lab. Thank you very much for sharing your knowledge, skills and experience as a scientist and for the constant support provided until this day. I'm also extremely thankful to all the other co-authors for their contribution, insightful comments and suggestions and also for being patient with me and my work.

I'd also like to acknowledge the ARC Discovery grant, which is the main funding body for this project and also the AINSE limited for their financial assistance provided through the Post Graduate Research Award and the other research grants awarded, giving me the opportunity to spend time at ANSTO, collaborating with many knowledgeable people. A special thanks go to my ANSTO co-supervisor Carol Tadros not only for the support and guidance provided in sample analysis and data interpretation but also for being a good friend and mentor. I'd also deeply appreciate the contribution and guidance provided by Matthew Jones in lake modelling aspects. Working with you has broadened my knowledge and helped me to develop my skills.

I'm also grateful to Victoria Parks Team for providing access to Lake Surprise and also for their immense support with monthly sample collections even during the covid pandemic. I'm also thankful to Damian Bell and the Guditjmara Corporation for enlightening our knowledge about the invaluable history of the Guditjmara people. I gratefully acknowledge the expertise and assistance given by Tony Hall and Robert Klaeb, during my time in the laboratory. The quality of this work was greatly improved by the consistent support provided to advance the technical and instrumental approaches and also you have given me the maximum help at times of laboratory difficulties. I also thank to staff at Flinders Analytical, AWQC, Adelaide and

ALS laboratory Melbourne for their assistance in water sample analysis. I'm thankful for the support given by Martin Hand in providing me with the XRF analyser and I'd also like to express my sincere thanks to John Sherwood and Julie Mondon for offering help with sample collection during the covid pandemic. I'm also thankful to the coring team and my colleagues, who made my fieldwork enjoyable and a memorable experience. A special thanks go to Haidee for her immense support and contribution provided for the benefit of this project. I also thankful for the assistance given by Simon Harbele for completion of this thesis during the last 6 months of my PhD.

Many thanks go to my PhD colleagues, for their support in good times as well as in bad times and especially to my past and present office mates for sharing the journey with me. I owe a great deal and gratitude to my beloved family, thank you very much for believing in me and my desires. Although you were not physically being with me, you have always been there for me to help through my darkest moments and to share the joy during my brightest. The unending love, support and encouragement you have shown me over the years helped me to come this far in my life. Last but not least, I'd like to express sincere thanks to my partner, Udara. Thank you very much for being my best friend for all these years. This work has been so much easier with the boundless support, encouragement and love that you have shown me throughout this PhD.

This thesis is lovingly dedicated to my Mom & Dad, for their unwavering love, support and encouragement throughout my life.

Publications arising from this Ph.D. research

Conference abstracts -

Dharmarathna A., Tyler J., Tibby J., Barr, C., Cadd H., Ankor M., Jones M., Tadros, C., Hua Q., Child D., Zawadski A., Hotchkis M., Gadd, P., Klaeb, R., Hall, T., A detailed study of Holocene climate variability in south-east Australia based on cellulose inferred lake water isotopes and monitoring ad modelling approach at Lake Surprise, Victoria. *Australian Quaternary Association (AQUA). (2022) Adelaide, Australia*

Dharmarathna, A., Tyler, J., Barr, C., Tibby, J., Jones, M., Ankor, M., & Zolitschka, B. et al. (2022). Holocene climate variability in south-east Australia; inferred from oxygen isotopes in sedimentary cellulose at Lake Surprise, Victoria. *EGU 2022, Vienna, Austria.*

Dharmarathna A., Tyler J., Barr C., Tibby J., Jones M., Ankor M., Gadd P., Hua Q., Child D., Zawadski A., Hotchkis M., Zolitschka B., Cadd H., Holocene climate variability in south-east Australia; inferred from oxygen isotopes in sedimentary cellulose at Lake Surprise, Victoria. *Australian Quaternary Association (AQUA). (2021) Australia.*

Dharmarathna A., Barr C., Tyler J., Tibby J., Gadd P., Ankor M., Jones M., Lake geochemical response to decadal scale climate variability; evidence from a 150 year sediment record from Lake Surprise, Victoria. *GSA Earth Sciences Student Symposium. (2020) South Australia.*

Dharmarathna A., Tyler J., Barr C., Tibby J., Cadd H., Zolitschka B., Ankor M., Holocene climate variability in south-eastern Australia; inferred from oxygen isotopes in sedimentary cellulose at Lake Surprise, Victoria. *Adelaide Physical Sciences Postgraduate Student Symposium. (2021) University of Adelaide, Australia.*

Dharmarathna A., Tyler J., Barr C., Tibby J., Gadd P., Ankor M., Jones M., Holocene climate variability in south-east Australia; an integrated isotope data – modelling approach at Lake Surprise, Victoria. *GSA Earth Sciences Student Symposium. (2019) South Australia.*

CHAPTER 1

Introduction and thesis outline

1 Introduction and thesis outline

1.1 Modern climate in south-east Australia

Climate change represents one of the major threats to societies and the environment, with projected global warming of 1.5℃ by 2040 predicted to result in major changes in water resources, food production and the risks of climate extremes (Rogelj et al., 2012; IPCC, 2022). Projecting the future of Earth's climate relies on a combination of cutting-edge climate modelling and the development of palaeoclimate records that can both provide long-term context for future climate change but also assist in the calibration and validation of climate models. Importantly, long-term records of past hydroclimate provide insights into the nature and causes of natural variability in the climate system, which can assist in the estimation and projection of future climate risks.

This thesis aims to develop Australia's record of past hydroclimate variability over the last 11,000 years by developing a mechanistically grounded record of hydroclimate variability from western Victoria. Using oxygen isotope analysis of lake sedimentary cellulose, the thesis provides the first two studies of lake geochemical responses to recent/contemporary climate variability, before applying this knowledge to reconstruct past hydroclimate change for the last 11,000 years. The results of the research are relevant for understanding the underlying drivers of hydroclimate variability in south-eastern Australia, as well as the prediction of future drought risk.

Australia, which is one of the driest, inhabited continents on Earth, experiences a highly variable climate due to the influence of large-scale atmospheric and oceanic circulations arising from the surrounding Indian, Pacific and Southern Oceans (Cleverly et al., 2016; Dey et al., 2019, 2021). The rapid transition of climate extremes from multi-decadal scale droughts to exceptionally heavy rains or flooding is no longer a hypothesis for the continent (King et al., 2020). These extreme climate conditions resulted in severe agricultural losses with far-reaching socio-economic impacts, especially in the south-east Australian region, which produces a significant share of Australia's agricultural output and houses the majority of its population (Murphy and Timbal, 2008; Ummenhofer et al., 2009; Kiem et al., 2016). Murray-Darling Basin in South-eastern Australia is the Australia's largest river basin and the major source of water for human and animal consumption and agriculture (Chiew et al., 2011; Holland et al., 2015). Instrumental observations provide evidence of a long-term decline in rainfall causing

intense droughts, particularly "The Millennium Drought", a decade of low rainfall (1997 – 2010) (Van Dijk et al., 2013; Kiem et al., 2016; Jiao et al., 2020). However, record-breaking rainfall initiated from 2010 – 2011 caused devastating floods in the south and east coasts of the region (Flack et al., 2020; King et al., 2020). Furthermore, many parts of south-eastern Australia have recently experienced heat extremes and catastrophic bushfires that were almost unprecedented, especially in early 2013 and in 2019 – 2020 ("Black summer fires") (Head et al., 2014; Filkov et al., 2020; Abram et al., 2021; Reddy et al., 2022b). As climate model projections suggest, these extreme events are expected to continue with high amplitude changes in intensity and duration (Kiem et al., 2016; Dixon et al., 2019).

Variability in the magnitude and timing of climate extremes is strongly influenced by the behaviour of the large-scale climate drivers such as the El-Niño Southern Oscillation (ENSO), Southern Annular Mode (SAM) and the Indian Ocean Dipole (IOD) (Risbey et al., 2009; Gouramanis et al., 2013; Ashcroft et al., 2016; Cleverly et al., 2016). ENSO, the major mode of variability within the Pacific Ocean, is considered to be the largest and leading driver of global and Australian climate, particularly in eastern Australia (Cleverly et al., 2016). El- Niño events are typically manifest as warm, dry conditions and La- Niña events with wetter conditions particularly over the spring to mid-summer period of the year (Ashcroft et al., 2016; Barr et al., 2019; Liguori et al., 2022). The IOD describes differential sea surface temperatures in the western and eastern Indian Ocean, with a significant effect on Australian rainfall, particularly across the north-west cloud band, a band of weather that stretches from the northwest to southeast of the continent (Evans et al., 2009; Ummenhofer et al., 2009; Gouramanis et al., 2013). The SAM is strongly associated with the position (north-south) and strength of the Southern Westerly Winds (SWW) and acts as the major source of rainfall for much of southern Australia (Meneghini et al., 2007; Fletcher & Moreno, 2012; Saunders et al., 2018). Additionally, other modes of internal variability, such as Interdecadal Pacific Oscillation (IPO) and Madden-Julian oscillation (MJO), also influence the Australian climate at different timescales (Risbey et al., 2009; Vance et al., 2015; Dey et al., 2019).

However, the short-term instrumental climate data (~100-year record) currently available for Australia does not fully reflect the natural climate variability and cannot be used to resolve low-frequency climate fluctuations and to elucidate their interactions with climate drivers (Kiem et al., 2016; Armstrong et al., 2020). As a consequence, significant uncertainties remain in both the modern and future climate projections (Kirono et al., 2020). This highlights the

importance of better understanding long-term patterns of climate variability, including constraints upon the frequency, magnitude and causation of climate variance in the region (Murphy and Timbal, 2008; Grant et al., 2013). In this context, palaeoclimatology, which is the study of past climates, is crucial for comprehending the nature of long-term (century- to millennium-scale) climatic variability.

1.2 Holocene climate variability in the region

An ample amount of research has been produced from the south-east Australian region, covering the Holocene epoch (~11,500 – 0 cal yr BP) that is strongly connected with the present-day climate. Lakes that are spatially distributed across the region, particularly in the western Victorian plains, serve as excellent archives of past climates. Lacustrine sediment records from the region further provide evidence of global climate events such as the Last Glacial Maximum (LGM) and Little Ice Age (LIA) (Black et al., 2006; Builth et al., 2008; Barr et al., 2014; Falster et al., 2018; Filkov et al., 2020). The region is believed to have undergone an abrupt shift from a climatically humid, more variable early-mid Holocene to a relatively arid and late Holocene (Bowler & Hamada, 1971; Dodson, 1974; Chivas et al., 1986; Kemp et al., 2012; Gouramanis et al., 2013; Wilkins et al., 2013). The transition of climate from a SWW dominant phase to an ENSO-driven climate from around 5000 cal yr BP (Beck et al., 2017; Mariani & Fletcher, 2017), is believed to influence the prolonged aridity in the region. Amplification of El-Niño events is thought to be responsible for declining rainfall, marked lake level decline, consecutive fire events and significant transition of flora and fauna from mid-late Holocene (Gouramanis et al., 2013; Petherick et al., 2013; Barr et al., 2019). Correspondingly, these estimates of a multi-centennial period of rainfall decline during the mid to late Holocene in southern Australia, are a causal lesson for recent rainfall decline and rapid warming over the region (Wilkins et al., 2013). Previous records from the region also provide the context and demonstrate the possibility of more severe droughts and unpredictable weather than that have occurred since the European colonisation began (Millennium Drought etc.) (Barr et al., 2014). Since European settlement after the mid-19th century, the climate of south-eastern Australia transitioned to a relatively dry phase which coincided with the introduction of agriculture and land clearance (Jones, 2014; Tibby et al., 2018; Morgan et al., 2020).

Palaeoclimate studies further demonstrated that teleconnections between major climate drivers are likely to cause intensified high-amplitude changes in climate, resulting extensive droughts,

bushfires, heat waves and floods, compared to the impact of any individual climate mode (Risbey et al., 2009; Gouramanis et al., 2013; Cleverly et al., 2016). A commonly observed effect is that of coupled ENSO-IOD variability, which largely affects the winter and spring precipitation in south-east Australia (Meyers et al., 2007; Abram et al., 2009; Risbey et al., 2009; Cai et al., 2011c; Holgate et al., 2022). Recent studies demarcate that the co-occurrence of El-Niño and positive IOD phases had a significant impact on the recent major droughts and catastrophic bushfires/heatwaves (Abram et al., 2021; Liguori et al., 2022; Reddy et al., 2022a; b). Studies have proposed similar interactions between climate drivers such as IOD-SAM, ENSO-SAM and ENSO-IPO that may be associated with climate extremes (Hughes, 2003; Cai et al., 2011a; b; Gouramanis et al., 2013; Dey et al., 2021). Yet, unlike the ENSO-IOD behaviour, most of these correlations remain either weaker or uncertain (Risbey et al., 2009; Gouramanis et al., 2013). The interaction of these climate modes has not only influenced extreme climate change, but also indirect effects such as enhanced productivity across Australia contributing mainly to the 2011 global land carbon sink anomaly (Cleverly et al., 2016). Despite the palaeoclimate interpretations of major climate drivers and their impact on the Australian climate, many challenges still exist in defining their individual or compound effects and inclusive mechanisms (Gouramanis et al., 2013; Dey et al., 2019; Abram et al., 2020a). Controversies remain about the effect of ENSO and IOD on decadal-scale drought occurrence and temperature variations in the region (Hughes, 2003; Gouramanis et al., 2013; McIntosh & Hendon, 2018; Dey et al., 2021) and also rainfall predictions in the region remain in dispute, due to the lack of precise global circulation models (Shi et al., 2008; CSIRO, 2018; Dey et al., 2019).

Major advances have been made in understanding the Holocene climate variability in south-eastern Australia, including a recent study from off-shore southern Australia that identifies a relatively warmer and wetter period referred to as the Holocene Hypsithermal that existed approximately from 8200 – 5500 cal yr BP (De Deckker, 2022) across south-east Australia, which also corresponds with existing terrestrial records from the Lynds Cave in Tasmania (eg. Xia et al., 2001). Off-shore sediment cores further suggest a switch from a mid-Holocene La-Niña-like state (7400 – 3500 cal yr BP) to a late-Holocene El-Niño-like state (3500 cal yr BP) (Perner et al., 2018). However, much of what we understand about Holocene climate variability on land hinges on largely indirect tracers of past climate, such as those indicated by changes in vegetation (pollen), fire (charcoal), dust deposition or sediment grain size as a proxy for lake depth (Dodson, 1974; Mooney, 1997; Stanley & De Deckker, 2002; Wilkins et al., 2013; Marx

et al., 2018; De Deckker, 2019; Martin et al., 2019; Mooney et al., 2020; Adeleye et al., 2021). Therefore, there remains a need for additional palaeoclimate reconstructions that are (a) based on physically-grounded proxies that respond predictably to past climate; (b) that have robust proxy-climate validation; (c) that can be supported by a strong mechanistic understanding of the climate influence upon the proxy; and (d) are sampled at a suitable resolution to detect decadal-scale climate variability. Oxygen isotopes in lake sediment provide one such physically based proxy for past hydroclimate (Talbot & Kelts, 1990; Leng et al., 2005; Von Grafenstein et al., 2013; Jones et al., 2016b; Jones & Dee, 2018; Konecky et al., 2020;). In addition, through monitoring and modelling contemporary lake systems, it is possible to develop a strong quantitative understanding of the processes that drive isotope variability in the sediment record (Shapley et al., 2008; Gibson et al., 2016; Jones et al., 2016). Chronological resolution and accuracy are also important factors for high-quality palaeoclimate records, and this has been identified as being lacking for many Australian Holocene records (Gouramanis et al., 2013; Petherick et al., 2013; Dixon et al., 2017).

Most of the previous chronological records that are derived using ^{14}C analysis of bulk sediment (single grains) are shown to be largely affected by older carbon derived from geologic sources or materials synthesised from geologic carbon dissolved in groundwater (Wilkins et al., 2012; Martin et al., 2019). Multiple lake studies from the region have reported radiocarbon age offsets varying from approximately 200 – 670 years (Wilkins et al., 2012; Barr et al., 2014; Gouramanis et al., 2010). The Holocene sediments of Lake Surprise had previously been dated using a combination of bulk sediment and pollen radiocarbon dates, as well as 210Pb analyses. However, these chronologies have run into a number of problems, including pollen contamination, potential groundwater effects, and age reversals (Barr et al., 2014; Falster et al., 2018). A common challenge with Australian lake sediments is the sparsity of plant microfossils upon which to base radiocarbon chronologies (Cadd et al., 2022). However, the recent refinement of radiocarbon dating of pollen grains (Cadd et al., 2022), provides a potential solution to this problem.

1.3 Lakes as palaeoarchives

Lake sediments have been used for several decades as important terrestrial palaeoarchives to infer past climate and environmental changes, given their rapid response to climate change and continuous sediment accumulation over timescales of centuries to millions of years (Cohen,

2003; Smol, 2008). Climate changes are directly or indirectly linked to the lake water column and subsequently transferred to lake sediments, which preserves a wide range of physical, chemical and biological proxies (Cohen, 2004; Adrian et al., 2009; Bradley, 2015). Pollen, diatoms, chironomids, macrofossils and charcoal remnants are among the most often exploited biological proxies (Battarbee, 2000; Bradley, 2015). However, these biological proxies respond to the climate indirectly and nonlinearly, and for many of them, the reaction is mediated by other physical and chemical variables, leading to uncertain and debatable climate interpretations (Bigler, 2009).

Stable isotopes in lake waters are independent of these biological activities and are a direct consequence of climate change (Leng & Marshall, 2004). Oxygen isotope ratios of lake waters reflect a combination of the source and history of precipitation and water vapour reaching the lake, including the condensation temperature, as well as the subsequent evaporation of lake and catchment waters following precipitation (Leng & Marshall, 2004; Jonsson et al., 2010; Rozanski et al., 2010; Gibson et al., 2016; Jones et al., 2016a, b; Cluett & Thomas, 2020; Tyler et al., 2022). Therefore, oxygen isotope variation preserved in a wide array of inorganic and organic compounds in lake sediments is used as a more reliable indicator of past climate variability. Among these proxies, the most extensively used is the oxygen isotope analysis of carbonate minerals, either authigenic or biogenic (Talbot & Kelts, 1990; Leng & Marshall, 2004; van Hardenbroek et al., 2018; Li et al., 2020). Oxygen isotope analysis of diatom silica is also increasingly applied but to a much lesser extent (Leng et al., 2001; Leng & Marshall, 2004; Leng & Barker, 2006; Rozanski et al., 2010; van Hardenbroek et al., 2018). However, both carbonates and silicates are subject to temperature-dependant isotope fractionation, and resolving the dual effects of temperature and the lake water oxygen isotope composition presents a challenge to quantitative palaeoclimate reconstructions (Kim & O'Neil, 1997; Leng & Marshall, 2004; Heikkilä et al., 2010; Rozanski et al., 2010). Carbonates are also only intermittently preserved in a relatively narrow range of lake sediments, and in many lake systems carbonate minerals formed in the upper waters are then dissolved in organic and acidic deep waters and sediments (Dean, 1999). In these instances, oxygen isotope analysis of aquatic cellulose provides a useful alternative.

The oxygen isotope composition of aquatic cellulose is independent of temperature and is therefore a useful yet infrequently applied palaeoclimate proxy (Edwards & McAndrews, 1989; Heikkilä et al., 2010; Rozanski et al., 2010). Since Edwards & McAndrews, (1989), lake

sediment cellulose has been increasingly used as a direct tracer of lake water isotope composition in a diverse range of lakes worldwide, particularly in organic-rich, freshwater lakes (Sternberg et al., 1984; Abbott et al., 2000; Wolfe et al., 2000; 2001a,b, 2007; Beuning et al., 2002; Brahney et al., 2010; Heikkilä et al., 2010; Rozanski et al., 2010; Heyng et al., 2014; Street-Perrott et al., 2018; Stojakowits et al., 2020). Interpretation of cellulose oxygen isotopes as a lake water proxy, however, requires cellulose to be of aquatic origin (algae, aquatic macrophytes and aquatic vegetation) – i.e. changes in the mixture of terrestrial and aquatic cellulose can confuse the interpretation (Edwards & McAndrews, 1989; Street-Perrott et al., 2018). As a consequence, most studies target fine-grained (<150 µm) organic matter for cellulose extraction, to eliminate woody material and leaves. A constant cellulose-water oxygen isotope fractionation is also required for cellulose oxygen isotopes to be used as a reliable climate proxy (Edwards & McAndrews, 1989; Street-Perrott et al., 2018). This isotope fractionation factor has been demonstrated to be constant, whereby $\alpha = 1.028 \pm 0.003$ (DeNiro & Epstein, 1981; Sternberg, 1989; Street-Perrott et al., 2018; Savage et al., 2021), and independent of factors such as plant species, photosynthetic pathway, growth stage, and oxygen isotopes in dissolved CO_2 (Street-Perrott et al., 2018). Extraction of pure cellulose is crucial since the accuracy of oxygen isotope measurements depends mostly on the extraction quality (Wissel et al., 2008). Some studies have found the extraction of cellulose to be challenging and time-consuming, especially in highly organic lakes where organic contaminants were often found in extracted cellulose (Beuning et al., 2002; Wolfe et al., 2007). However, these effects were minimised and pure cellulose was yielded with methodological advancements such as wet-oxidation-based cellulose dissolution in cuprammonium by Wissel et al., (2008). As a consequence, oxygen isotope analysis of cellulose provides a significant potential to provide new insights into past climate variability in Australia.

1.4 Study area – Lake Surprise

The research in this thesis is focused on Lake Surprise, a volcanic crater lake (Timms, 1975) located in western Victoria in the newer volcanic province. Lake Surprise is selected as an ideal study site because of its rapid sediment accumulation rate (Falster et al., 2018), finely laminated sediment that indicates a lack of bioturbation and undisturbed nature (Ankor & Tyler, 2022), lack of evidence of any human disturbance (Tibby et al., 2006; Barr et al., 2014) and organic-rich sediment that indicates a cellulose enriched environment. Lake Surprise is located within the Budj Bim Cultural Landscape, which is a part of the Gunditjmara country and home to the

Dhauwurd Wurrung people of the Gunditjmara nation (Parks Victoria, 1996; Builth, 2004; Bell & Johnston, 2008). Between 1960 and 2004, the region was known as the Mt Eccles National Park. Budj Bim was open for public access in 1926, proclaimed a national park on 7th June 1960 (Parks Victoria, 1996), and included in the United Nations Educational, Scientific and Cultural Organization (UNESCO) World Heritage list in July 2004 recognizing its outstanding cultural value (Bell & Johnston, 2008). The surface area of the Budj Bim National Park is ~6000 ha and is located at an elevation of 114 mAHD (Australian Height Datum) within the Newer Volcanic Province of western Victoria (Barr et al., 2014). As per the most recent field measurements, the lake is approximately 600 m long and 200 m wide at its longest and widest points (Appendix 1).

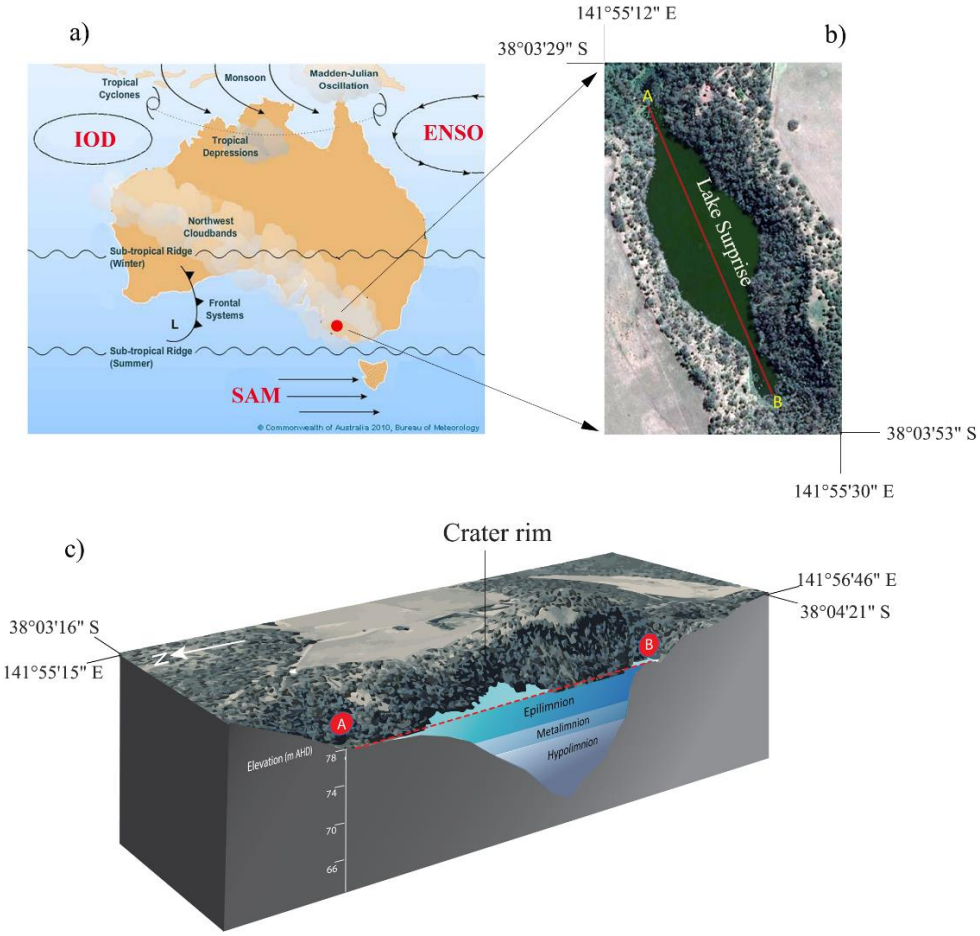

Figure 1. a) Approximate location of Lake Surprise and representation of the behavioural pattern major climate systems, El-Niño Southern Oscillation (ENSO), Indian Ocean Dipole (IOD) and Southern Annular Mode (SAM), Source: Commonwealth of Australia 2010, Bureau of Meteorology (www.bom.gov.au/climate/about/). b) Aerial view of Lake Surprise, c) cross-section of the lake along the AB line as shown in the aerial view. (The actual measurements were inferred from the lake bathymetry developed in 2019 (Appendix 1).

The funnel-shaped lake basin is located on tertiary limestone, marl and thick basalt layers (Barr et al., 2014; Ankor, 2020) and the lake is approximately 11.5 m deep. The freshwater (pH = ~7 – 9), deep lake environment is characterised by thermal stratification, with oxygenated epilimnion and de-oxygenated hypolimnion possibly occurring during late spring and summer (Figure 1c) (Timms, 1975; Barr et al., 2014; Chapter 2, Figure 2b). The lake has an approximately 1.5 m deep Secchi depth ("photic zone"), however, previous evidence suggests that there were times when this depth was much higher (~8 m) in the past (Timms, 1975). A crater wall that slopes from steep to vertical is approximately 49 m high and acts as a wind barrier (Timms, 1975; Barr et al., 2014). Due to the absence of any surface drainage, the "closed" lake basin is primarily fed by precipitation and groundwater (Barr et al., 2014). The densely vegetated lake catchment is abundant with *Eucalyptus viminalis* ("manna gum") and *Acacia melanoxylon* ("blackwood"). Ground cover is mainly composed of Poaceae, Asteraceae, *Pteridium esculuntum* ("bracken") and *Banksia marginanta* (Tibby et al. 2006; Builth et al., 2008). Shallow water margins support a rich, although frequently constrained zone of aquatic vegetation mostly composed of floating plants (*Lemna sp.* and *Azolla filiculoides*) and emergent macrophytes (*Carex appressa, Triglochin procera, Rumex brownii, R. bidens* and *Urtica incisa*) in sheltered open water (Tibby et al. 2006).

According to traditional knowledge, this spiritually and culturally rich landscape is intimately linked to an ancestral creation being (Bell & Johnston, 2008).

"The ancestral creation-being is revealed in the landscape of south-western Victoria at Budj Bim (Mt Eccles). At Mount Eccles the top of his head is revealed, his teeth 'tung att' is the scoria cones. His spirit is embedded deep in this place and in the people – Gunditjmara." (Bell & Johnston, 2008).

According to western knowledge Lake Surprise was formed in the crater of Mt Eccles by adjoining three consecutive volcanic eruptions approximately around 37000 years ago (Timms, 1975; Matchan et al., 2020). This consequently led to an elongated lake with a larger main lagoon and two smaller lagoons at either end (Timms, 1975). The Mt Eccles lava flow is considered to be one of Victoria's longest and most scenic lava flows covering approximately 165 km^2 of the surrounding landscape (Builth, 2004; Builth et al., 2008). According to oral records from the Gunditjmara people, it is likely that people lived in the Budj Bim landscape

before the volcanic eruptions (Bell & Johnston, 2008; Builth et al., 2008). However, there is not much proof available to validate this assumption (Builth et al., 2008).

The Newer volcanic province does not appear to have experienced any further volcanic activity, since approximately the mid-Holocene (Sherwood et al., 2004). The geology of the western plains is dominated by tertiary-cretaceous sediments and volcanic rocks of the Otway Basin (Boyce, 2013; Iverach et al., 2020). The western plains also consist of more than half of the eruption points in the newer volcanic province that interacts with the underlying aquifers of the Otway Basin (Boyce, 2013; Webb, 2016). The base of the stratigraphic sequence consists of Late Jurassic – late cretaceous rocks, whereas overlying the base are the Cenozoic sedimentary and volcanic rocks which form the major aquifers of the region (Iverach et al., 2020). Of the many volcanic formations, the western Victorian plains are mainly composed of scoria cones, lava volcanoes and maars (Barr et al., 2014; Boyce et al., 2014). Oldest lava flows form relatively thick kaolinite weathering profiles, whereas younger lava flows form “stony rises”; rocky outcrops with stony basalt rises and sharp boundaries (Boyce, 2013; Ankor, 2020). Volcanic craters have changed over time to create a variety of crater lakes and groundwater flows are essential for maintaining lake hydrology due to the relatively weak surface drainage system in the region (Webb, 2016; Yihdego et al., 2016).

The Otway Basin is underlain by sedimentary formations of the Gellibrand Marl or Port Campbell Limestone onshore (Ankor, 2020; Radke et al., 2022). As per the Western Victorian Groundwater Framework Lake Surprise sits ~15m below the upper surface of the Port Campbell Limestone and approximately 60 m above the Gellibrand Marl formation (Victorian Department of Sustainability and Environment, 2014; Ankor, 2020) (Supplementary Figure I). Aquifer and aquitard units (along the sediment stratigraphy) of the western plains are summarized in the supplementary table I (Iverach et al., 2020). Port Campbell Limestone is a permeable, unconsolidated to semi-consolidated, karstic aquifer of bioclastic carbonate formation and marls (Radke et al., 2022). The Port Campbell Limestone holds the majority of the Otway Basin's water table and the total amount of dissolved solids in the groundwater is often less than 1000 ppm, although it tends to be "hard" due to the dissolving of limestone (Hortle et al., 2011). The aquifer is dominated by Na-Ca-HCO_3-type water and is mainly sourced from surface infiltration (Iverach et al., 2020). The Gellibrand Marl is a several hundred meters thick aquitards composed of mainly clay minerals and minor amounts of marl

(Ankor, 2020; Radke et al., 2022). More compact sedimentation led to limited permeability and relatively lower diagenetic alteration in the marl formation (Radke et al., 2022).

The palaeoclimate significance of Lake Surprise is well emphasised by its continuous sedimentation that allows comparison analysis for approximately 30000 years and its characteristic features such as its closed nature and lack of human impact (Tibby et al. 2006; Builth et al., 2008; Falster et al., 2018). It is believed that the lake has been free of major catchment disturbances and thus preserves a predominantly natural climate signal in the sediments (Builth et al., 2008; Barr et al. 2014). Following the monitoring work led by Timms, (1975), Lake Surprise has been studied for both the recent and long-term climate and environmental changes using proxy-based reconstructions such as pollen and diatom assemblages, carbon isotope ratios and element geochemistry (Tibby et al. 2006; Builth et al., 2008; Barr et al., 2014; Falster et al., 2018). Diatom-inferred conductivity measurements from Lake Surprise sediments provide evidence of the timing of the LIA for the very first time from mainland Australia (Barr et al., 2014). The same record suggests that, at least within the last two millennia, there have been more severe droughts than those experienced since European settlement in the region (Barr et al., 2014). The beginning of drier, 'LGM-like' conditions at Lake Surprise have been observed at approximately 28000 cal yr BP, indicating that the LGM in the Southern Hemisphere mid-latitudes may have occurred much earlier than the timing of the global LGM (~ 23000 cal yr BP) (Falster et al., 2018).

An overall reduction in lake level corresponding to a significantly drier climate around 3750 cal yr BP is further indicated by increased dryland taxa obtained from pollen and diatom records at Lake Surprise ((Tibby et al. 2006; Builth et al., 2008). However, lower resolution and poor chronological control in this record appeared to hinge the possible interpretations, particularly during the late Holocene (Builth et al., 2008). Relatively high-resolution records developed later were limited to the late Holocene and Pleistocene periods respectively and also encountered several chronological issues such as older carbon contamination, age-reversals and loss of basal age in ^{210}Pb age modelling (Barr et al., 2014; Falster et al., 2018). Therefore, a high resolution, continuous Holocene record with a well-dated chronology from Lake Surprise is crucial to understand climate-derived changes in the region.

Figure 2. View of Lake Surprise and the immediate catchment as looking south from the crater rim of Mt Eccles (Photo courtesy of John Tibby).

1.5 Thesis aims and objectives

This thesis aims to reconstruct the Holocene climate variability in south-eastern Australia by developing a new, physically-based and validated palaeoclimate record based on oxygen isotope analysis of Lake Surprise sediments. This aim will be achieved by:

- Developing a lake model using monitoring and instrumental data to understand the contemporary lake hydrology and major controls of lake water isotopes.
- Developing a well-constrained chronology for the Holocene period using multiple dating techniques.
- Understanding the proxy-climate relationship for oxygen isotopes in cellulose and associated lake sediment geochemical properties by validating these palaeoclimate proxies against instrumental climate data.
- Developing a well-dated, high-resolution lake water oxygen isotope record using oxygen isotope analysis of lacustrine cellulose for the Holocene period.

1.6 Thesis outline

Chapter 2: Lake hydrological response to climate variability; a coupled monitoring and isotope mass balance modelling approach applied to Lake Surprise, Victoria, Australia.

In this chapter, I present a detailed assessment of modern lake hydrology using both observational data and modelling. The stable isotope measurements of lake water and rainwater samples, lake water chemistry data and field measurements collected over two years were used to determine the modern hydrochemistry of the lake, dominant sources of major ions into the lake and major controls of lake water isotopes. The data were combined with previous monitoring work done by Timms, (1975) and Barr et al., (2014), to obtain the longest possible monitoring dataset. Multiple qualitative analyses (Piper trilinear plots, Gibbs model plots and deuterium-excess analysis) were performed to explore the observational data. A stable isotope mass balance modelling approach was utilised for the lake, to evaluate the observational data and thereby quantify the groundwater influence on the lake, as well as to determine major controls of stable oxygen isotope variability in lake water. The results from both the monitoring and modelling, show that the lake is heavily influenced by groundwater inflow and outflow, and lake surface evaporation is likely the main factor affecting the oxygen isotope composition of lake water. This understanding of the hydrological behaviour of Lake Surprise is crucial for making reliable climate and environmental interpretations for both the past and future. Therefore, the outcomes of this study have significant implications for long-term climate reconstructions derived using lake water isotopes.

This chapter is written in manuscript format for future publication in the *Journal of Hydrology* with the following authors and title of the manuscript: Dharmarathna, A., Tyler, J., Jones, M., Tadros, C., Ankor, M., Tibby, J., Barr, C., Zolitschka, B., Hughes, C., Lake hydrological response to climate variability; a coupled monitoring and isotope mass balance modelling approach applied to Lake Surprise, Victoria, Australia.

Chapter 3: Pollen radiocarbon dating of lake sediments; a cautionary tale from Lake Surprise, Victoria, Australia.

In this chapter, I developed a well-dated chronology for the Holocene sediments of Lake Surprise. Recent sediment was analysed for ^{210}Pb activity and Pu isotope concentrations. Radiocarbon dating was performed on a combination of terrestrial macrofossil and pollen samples selected across the sediment depth. A recently developed pollen isolation procedure

discussed in Cadd et al., (2022) was followed to minimise contamination. Pollen extracts were screened for contamination using Fourier Transform Infra-Red (FTIR) analysis. Additionally, bulk sediment samples were dated for comparison. A combined ^{210}Pb and ^{14}C chronology was established for the Holocene period using the Bayesian *Plum* software (Aquino-López et al., 2018) and comparisons were made to the more conventional Constant Flux Constant Sedimentation (CFCS) and Constant Rate of Supply (CRS) models (Appleby & Oldfield, 1978; Appleby, 2001). The accuracy and precision of different age models were assessed using recent chronomarkers obtained from this study and previous work by Barr et al., (2014). Developing robust interpretations of climate and environmental changes beyond the instrumental period has strongly relied on the accuracy and reliability of the chronological control. Since the development of many palaeoclimate records in south-eastern Australia has been undermined by chronological control, the outcomes of this study will have a significant impact on the development of more reliable climate records from the region.

This chapter is written in manuscript format for future publication in the Journal of *Radiocarbon* with the following authors and title of the manuscript: Dharmarathna, A., Tyler, J., Tibby, J., Cadd, H., Barr, C., Hua, Q., Child, D., Hotchkis, M., Zawadski, A., Francke, A., Pollen radiocarbon dating of lake sediments; a cautionary tale from Lake Surprise, western Victoria, Australia.

Chapter 4: Validating lake sediment palaeoclimate proxies against instrumental climate records; isotope and major element data from Lake Surprise, Victoria, Australia.

In Chapter 4, I compare sediment proxy data with instrumental climate data (1890 – 2020 CE) to identify their contemporary relationship and to evaluate the most commonly used past climate interpretations. The sediments of Lake Surprise provide a rare opportunity in this respect, since the catchment, which consists of steep volcanic crater walls, has experienced limited disturbance throughout the post-colonial era. Furthermore, the sediments accumulated rapidly at over 1 cm/year, thus allowing a high-resolution proxy record for comparison to instrumental climate. Sediments were analysed for their major element concentrations, stable carbon and nitrogen isotopes and oxygen isotopes in cellulose. Ca content (indicating calcium carbonate), oxygen and carbon isotope data were compared against average annual climate variables approximately for the last 200 years using both qualitative and statistical approaches. The results of this correlation validate the assumption that lake water oxygen isotopes derived using cellulose reflect changes in lake water hydrological balance (precipitation–evaporation),

and are thus a reliable proxy for long-term climate reconstruction. Changes in carbonate concentration also positively correlated with rainfall amount, possibly indicating a role of groundwater influx or primary productivity, which is also reflected in the carbon isotope composition of organic matter. This validation exercise provides confidence in the interpretation of past climate from sediment geochemical data from Lake Surprise, as well as similar sites worldwide.

This chapter is written in manuscript format for future publication in the *Journal of Paleolimnology* with the following authors and title of the manuscript: Dharmarathna, A., Tyler, J., Barr, C., Cadd, H., Tibby, J., Klaebe, R., Hall, T., Hua, Q., Child, D., Hotchkis, M., Zawadski, A., Validating lake sediment proxies against instrumental climate records; isotope and major element data from Lake Surprise, Victoria, Australia.

Chapter 5: Holocene climate variability in south-eastern Australia; inferred from oxygen isotopes in sedimentary cellulose at Lake Surprise, Victoria, Australia.

In Chapter 5, I report a high-resolution, continuous record of lake water balance throughout the Holocene, using oxygen isotopes in cellulose to infer past lake water oxygen isotope composition. Although the lake sediment is composed of finely laminated carbonate throughout the sediment core, the carbonate concentration remains generally low limiting the oxygen isotope analysis of sedimentary carbonate. Instead, organic-rich fine-grained sediments present the opportunity to extract and analyse cellulose oxygen isotopes as a palaeoclimate proxy from this lake. Carbon isotopes and carbon and nitrogen elemental composition data were used to infer the primary source of organic matter, which was aquatic throughout this period. Findings from Chapters 2, 3, and 4 were employed as a foundation for improving the accuracy of this Holocene record. Then I assess my findings in the view of previous Holocene reconstructions from western Victoria and the long-term behaviour of major climate drivers. This study provides evidence of major wet phases that were not previously recognised in other palaeoclimate records and that lake water isotopes have a strong coherence to SWW throughout the Holocene. The outcomes of this work highlight the importance of developing long-term past climate records with a well-constrained chronology, knowledge of contemporary hydrology, and the potential of sediment proxies to be used as climate indicators.

This chapter is written in manuscript format for future publication in the Journal of *Quaternary Science Reviews* with the following authors and title of the manuscript: Dharmarathna, A.,

Tyler, J., Tibby, J., Barr, C., Cadd, H., Ankor, M., Klaebe, R., Hall, T., Hua, Q., Child, D., Hotchkis, M., Zawadski, A., Holocene climate variability in south-eastern Australia; inferred from oxygen isotopes in sedimentary cellulose at Lake Surprise, Victoria, Australia.

Chapter 6: Key outcomes and suggestions for future research

In this chapter, I summarise the key outcomes of this thesis and provide concluding statements and recommendations for future research.

1.7 List of references cited

Abbott, M. B., Wolfe, B. B., Aravena, R., Wolfe, A. P., & Seltzer, G. O. (2000). Holocene hydrological reconstructions from stable isotopes and paleolimnology, Cordillera Real, Bolivia. *Quaternary Science Reviews*, *19*(17–18), 1801–1820. https://doi.org/10.1016/S0277-3791(00)00078-0

Abram, N. J., Hargreaves, J. A., Wright, N. M., Thirumalai, K., Ummenhofer, C. C., & England, M. H. (2020). Palaeoclimate perspectives on the Indian Ocean Dipole. *Quaternary Science Reviews*, *237*, 106302. https://doi.org/10.1016/j.quascirev.2020.106302

Abram, N. J., Henley, B. J., Gupta, A. Sen, Lippmann, T. J. R., Clarke, H., Dowdy, A. J., Sharples, J. J., Nolan, R. H., Zhang, T., Wooster, M. J., Wurtzel, J. B., Meissner, K. J., Pitman, A. J., Ukkola, A. M., Murphy, B. P., Tapper, N. J., & Boer, M. M. (2021). Connections of climate change and variability to large and extreme forest fires in southeast Australia. *Communications Earth and Environment*, *2*. https://doi.org/10.1038/s43247-020-00065-8

Abram, N. J., McGregor, H. V., Gagan, M. K., Hantoro, W. S., & Suwargadi, B. W. (2009). Oscillations in the southern extent of the Indo-Pacific Warm Pool during the mid-Holocene. *Quaternary Science Reviews*, *28*(25–26), 2794–2803. https://doi.org/10.1016/j.quascirev.2009.07.006

Adeleye, M. A., Haberle, S. G., Harris, S., Connor, S. E., & Stevenson, J. (2021). Assessing Long-Term Ecological Changes in Wetlands of the Bass Strait Islands, Southeast Australia: Palaeoecological Insights and Management Implications. *Wetlands*, *41*(7). https://doi.org/10.1007/s13157-021-01480-z

Adrian, R., O'Reilly, C. M., Zagarese, H., Baines, S. B., Hessen, D. O., Keller, W., Livingstone, D. M., Sommaruga, R., Straile, D., Van Donk, E., Weyhenmeyer, G. A., & Winder, M. (2009). Lakes as sentinels of climate change. *Limnology and Oceanography*, *54*(6 PART 2), 2283–2297. https://doi.org/10.4319/lo.2009.54.6_part_2.2283

Ankor, M. J. (2020). *Hydrologic and Isotopic Lake Modelling for Palaeoclimate Research*.

January.

Ankor, M. J., & Tyler, J. J. (2022). A computational method for rapid orthographic photography of lake sediment cores. *Journal of Paleolimnology*, *0123456789*. https://doi.org/10.1007/s10933-022-00241-0

Appleby, P. G. (2001). *in Recent Sediments*. *1*, 171–172.

Appleby, P. G., & Oldfield, F. (1978). The calculation of lead-210 dates assuming a constant rate of supply of unsupported 210Pb to the sediment. *Catena*, *5*(1), 1–8. https://doi.org/10.1016/S0341-8162(78)80002-2

Aquino-López, M. A., Blaauw, M., Christen, J. A., & Sanderson, N. K. (2018). Bayesian Analysis of 210 Pb Dating. *Journal of Agricultural, Biological, and Environmental Statistics*, *23*(3), 317–333. https://doi.org/10.1007/s13253-018-0328-7

Armstrong, M. S., Kiem, A. S., & Vance, T. R. (2020). Comparing instrumental, palaeoclimate, and projected rainfall data: Implications for water resources management and hydrological modelling. *Journal of Hydrology: Regional Studies*, *31*(July), 100728. https://doi.org/10.1016/j.ejrh.2020.100728

Ashcroft, L., Gergis, J., & Karoly, D. J. (2016). Long-term stationarity of El Niño–Southern Oscillation teleconnections in southeastern Australia. *Climate Dynamics*, *46*(9–10), 2991–3006. https://doi.org/10.1007/s00382-015-2746-3

Barr, C., Tibby, J., Gell, P., Tyler, J., Zawadzki, A., & Jacobsen, G. E. (2014). Climate variability in south-eastern Australia over the last 1500 years inferred from the high-resolution diatom records of two crater lakes. *Quaternary Science Reviews*, *95*, 115–131. https://doi.org/10.1016/j.quascirev.2014.05.001

Barr, C., Tibby, J., Leng, M. J., Tyler, J. J., Henderson, A. C. G., Overpeck, J. T., Simpson, G. L., Cole, J. E., Phipps, S. J., Marshall, J. C., McGregor, G. B., Hua, Q., & McRobie, F. H. (2019a). Holocene El Niño–Southern Oscillation variability reflected in subtropical Australian precipitation. *Scientific Reports*, *9*(1), 1–9. https://doi.org/10.1038/s41598-019-38626-3

Barr, C., Tibby, J., Leng, M. J., Tyler, J. J., Henderson, A. C. G., Overpeck, J. T., Simpson, G. L., Cole, J. E., Phipps, S. J., Marshall, J. C., McGregor, G. B., Hua, Q., & McRobie, F. H. (2019b). Holocene El Niño–Southern Oscillation variability reflected in subtropical Australian precipitation. *Scientific Reports*, *9*(1), 1–9. https://doi.org/10.1038/s41598-019-38626-3

Battarbee, R. W. (2000). Palaeolimnological approaches to climate change, with special regard to the biological record. *Quaternary Science Reviews*, *19*(1–5), 107–124. https://doi.org/10.1016/S0277-3791(99)00057-8

Beck, K. K., Fletcher, M. S., Gadd, P. S., Heijnis, H., & Jacobsen, G. E. (2017). TITLE: An early onset of ENSO influence in the extra-tropics of the southwest Pacific inferred from a 14, 600 year high resolution multi-proxy record from Paddy's Lake, northwest

Tasmania. *Quaternary Science Reviews*, *157*, 164–175. https://doi.org/10.1016/j.quascirev.2016.12.001

Bell, D., & Johnston, C. (2008). Budj Bim; Caring for the spirit and the people. *Finding the Spirit of Place : Between Tangible and Intangible Heritage. (16th ICOMOS General Assembly and International Scientific Symposium, Quebec, 2008)*, 213-224. http://openarchive.icomos.org/12/%5Cnhttp://openarchive.icomos.org/12/1/77-7xnf-104.pdf

Beuning, K. R. M., Kelts, K., Russell, J., & Wolfe, B. B. (2002). Reassessment of Lake Victoria-Upper Nile River paleohydrology from oxygen isotope records of lake-sediment cellulose. *Geology*, *30*(6), 559–562. https://doi.org/10.1130/0091-7613(2002)030<0559:ROLVUN>2.0.CO;2

Black, M. P., Mooney, S. D., & Martin, H. A. (2006). A >43,000-year vegetation and fire history from Lake Baraba, New South Wales, Australia. *Quaternary Science Reviews*, *25*(21–22), 3003–3016. https://doi.org/10.1016/j.quascirev.2006.04.006

Boyce, J. (2013). The Newer Volcanics Province of southeastern Australia: A new classification scheme and distribution map for eruption centres. *Australian Journal of Earth Sciences*, *60*(4), 449–462. https://doi.org/10.1080/08120099.2013.806954

Boyce, J., Nicholls, I., Keays, R., & Hayman, P. (2014). Victoria erupts: The Newer Volcanics Province of south-eastern Australia. *Geology Today*, *30*(3), 105–109. https://doi.org/10.1111/gto.12054

Bradley, R. S. (2015). Lake Sediments. In *Paleoclimatology* (3rd ed.). Elsevier Inc. https://doi.org/10.1016/b978-0-12-386913-5.00009-0

Brahney, J., Clague, J. J., Edwards, T. W. D., & Menounos, B. (2010). Late Holocene paleohydrology of Kluane Lake, Yukon Territory, Canada. *Journal of Paleolimnology*, *44*(3), 873–885. https://doi.org/10.1007/s10933-010-9459-8

Builth, H. (2004). Mt Eccles lava flow and the Gunditjmara connection: A landform for all seasons. *Proceedings of the Royal Society of Victoria*, *116*(1), 163–182.

Builth, H., Kershaw, A. P., White, C., Roach, A., Hartney, L., McKenzie, M., Lewis, T., & Jacobsen, G. (2008). Environmental and cultural change on the Mt Eccles lava-flow landscapes of southwest Victoria, Australia. *Holocene*, *18*(3), 413–424. https://doi.org/10.1177/0959683607087931

Cadd, H., Sherborne-Higgins, B., Becerra-Valdivia, L., Tibby, J., Barr, C., Forbes, M., Cohen, T. J., Tyler, J., Vandergoes, M., Francke, A., Lewis, R., Arnold, L. J., Jacobsen, G., Marjo, C., & Turney, C. (2022). the Application of Pollen Radiocarbon Dating and Bayesian Age-Depth Modeling for Developing Robust Geochronological Frameworks of Wetland Archives. *Radiocarbon*, *64*(2), 213–235. https://doi.org/10.1017/RDC.2022.29

Cai, W., Sullivan, A., & Cowan, T. (2011a). Interactions of ENSO, the IOD, and the SAM in

CMIP3 models. *Journal of Climate*, *24*(6), 1688–1704. https://doi.org/10.1175/2010JCLI3744.1

Cai, W., van Rensch, P., & Cowan, T. (2011b). Influence of global-scale variability on the subtropical ridge over Southeast Australia. *Journal of Climate*, *24*(23), 6035–6053. https://doi.org/10.1175/2011JCLI4149.1

Cai, W., van Rensch, P., Cowan, T., & Hendon, H. H. (2011c). Teleconnection pathways of ENSO and the IOD and the mechanisms for impacts on Australian rainfall. *Journal of Climate*, *24*(15), 3910–3923. https://doi.org/10.1175/2011JCLI4129.1

Chiew, F. H. S., Young, W. J., Cai, W., & Teng, J. (2011). Current drought and future hydroclimate projections in southeast Australia and implications for water resources management. *Stochastic Environmental Research and Risk Assessment*, *25*(4), 601–612. https://doi.org/10.1007/s00477-010-0424-x

Clarke, J. D. A., Fontaine, K., Lewis, S. J., Stewart, G., & Kilgour, P. L. (2015). *Regional Hydrogeological Characterisation of the Otway Basin, Victoria and South Australia: Technical report for the National Collaboration Framework Regional Hydrogeology Project*. Geoscience Australia.

Cleverly, J., Eamus, D., Luo, Q., Coupe, N. R., Kljun, N., Ma, X., Ewenz, C., Li, L., Yu, Q., & Huete, A. (2016). The importance of interacting climate modes on Australia's contribution to global carbon cycle extremes. *Scientific Reports*, *6*(November 2015), 1–10. https://doi.org/10.1038/srep23113

Cluett, A. A., & Thomas, E. K. (2020). Resolving combined influences of inflow and evaporation on western Greenland lake water isotopes to inform paleoclimate inferences. *Journal of Paleolimnology*, *63*(4), 251–268. https://doi.org/10.1007/s10933-020-00114-4

Cohen, A. S. (2004). Paleolimnology: the history and evolution of lake systems. In *Choice Reviews Online* (Vol. 41, Issue 06). https://doi.org/10.5860/choice.41-3461

da Silveira Lobo Sternberg, L. (1989). *Oxygen and Hydrogen Isotope Ratios in Plant Cellulose: Mechanisms and Applications*. 124–141. https://doi.org/10.1007/978-1-4612-3498-2_9

De Deckker, P. (2019). An evaluation of Australia as a major source of dust. *Earth-Science Reviews*, *194*(June 2018), 536–567. https://doi.org/10.1016/j.earscirev.2019.01.008

De Deckker, P. (2022). The Holocene hypsithermal in the Australian region. *Quaternary Science Advances*, *7*(July), 100061. https://doi.org/10.1016/j.qsa.2022.100061

Dean Jr., W. E. (1999). The carbon cycle and biogeochemical dynamics in lake sediments. *Journal of Paleolimnology*, *21*(1997), 375–393.

DeNiro, M. J., & Epstein, S. (1981). Isotopic composition of cellulose from aquatic organisms. *Geochimica et Cosmochimica Acta*, *45*(10), 1885–1894. https://doi.org/10.1016/0016-7037(81)90018-1

Dey, R., Bador, M., Alexander, L. V., & Lewis, S. C. (2021). The drivers of extreme rainfall event timing in Australia. *International Journal of Climatology*, *41*(15), 6654–6673. https://doi.org/10.1002/joc.7218

Dey, R., Lewis, S. C., Arblaster, J. M., & Abram, N. J. (2019). A review of past and projected changes in Australia's rainfall. *Wiley Interdisciplinary Reviews: Climate Change*, *10*(3), 1–23. https://doi.org/10.1002/wcc.577

Dixon, B. C., Tyler, J. J., Lorrey, A. M., Goodwin, I. D., Gergis, J., & Drysdale, R. N. (2017). Low-resolution Australasian palaeoclimate records of the last 2000 years. *Climate of the Past*, *13*(10), 1403–1433. https://doi.org/10.5194/cp-13-1403-2017

Dixon, B., Tyler, J., Henley, B. J., & Drysdale, R. (2019). Regional patterns of hydroclimate variability in southeastern Australia over the past 1200 years. *Earth and Space Science Open Archive*. https://doi.org/10.1002/essoar.10501482.1

Edwards, T. W. D., & McAndrews, J. H. (1989). Paleohydrology of a Canadian Shield land inferred from 18O in sediment cellulose. *Canadian Journal of Earth Sciences*, *26*(9), 1850–1859. https://doi.org/10.1139/e89-158

Evans, A. D., Bennett, J. M., & Ewenz, C. M. (2009). South Australian rainfall variability and climate extremes. *Climate Dynamics*, *33*(4), 477–493. https://doi.org/10.1007/s00382-008-0461-z

Falster, G., Tyler, J., Grant, K., Tibby, J., Turney, C., Löhr, S., Jacobsen, G., & Kershaw, A. P. (2018). Millennial-scale variability in south-east Australian hydroclimate between 30,000 and 10,000 years ago. *Quaternary Science Reviews*, *192*, 106–122. https://doi.org/10.1016/j.quascirev.2018.05.031

Filkov, A. I., Ngo, T., Matthews, S., Telfer, S., & Penman, T. D. (2020). Impact of Australia's catastrophic 2019/20 bushfire season on communities and environment. Retrospective analysis and current trends. *Journal of Safety Science and Resilience*, *1*(1), 44–56. https://doi.org/10.1016/j.jnlssr.2020.06.009

Flack, A., Kiem, A., Vance, T., Tozer, C., & Roberts, J. (2020). Comparison of published palaeoclimate records suitable for reconstructing annual to sub-decadal hydroclimatic variability in eastern Australia: implications for water resource management and planning. *Hydrology and Earth System Sciences Discussions*, *June*, 1–25. https://doi.org/10.5194/hess-2020-314

Fletcher, M. S., & Moreno, P. I. (2012). Have the Southern Westerlies changed in a zonally symmetric manner over the last 14,000 years? A hemisphere-wide take on a controversial problem. *Quaternary International*, *253*, 32–46. https://doi.org/10.1016/j.quaint.2011.04.042

Gibson, J. J., Birks, S. J., & Yi, Y. (2016). Stable isotope mass balance of lakes: A contemporary perspective. *Quaternary Science Reviews*, *131*, 316–328. https://doi.org/10.1016/j.quascirev.2015.04.013

Gouramanis, C., Deckker, P. De, Switzer, A. D., & Wilkins, D. (2013a). Earth-Science Reviews Cross-continent comparison of high-resolution Holocene climate records from southern Australia — Deciphering the impacts of far- fi eld teleconnections Austra l Winte r ITCZ today mer I ral Sum TCZ to Approx . position of today. *Earth Science Reviews*, *121*, 55–72. http://dx.doi.org/10.1016/j.earscirev.2013.02.006

Gouramanis, C., Deckker, P. De, Switzer, A. D., & Wilkins, D. (2013b). Earth-Science Reviews Cross-continent comparison of high-resolution Holocene climate records from southern Australia — Deciphering the impacts of far- fi eld teleconnections Austra l Winte r ITCZ today mer I ral Sum TCZ to Approx . position of today. *Earth Science Reviews*, *121*, 55–72. https://doi.org/10.1016/j.earscirev.2013.02.006

Grant, S. B., Fletcher, T. D., Feldman, D., Saphores, J. D., Cook, P. L. M., Stewardson, M., Low, K., Burry, K., & Hamilton, A. J. (2013). Adapting urban water systems to a changing climate: Lessons from the millennium drought in southeast Australia. *Environmental Science and Technology*, *47*(19), 10727–10734. https://doi.org/10.1021/es400618z

Head, L., Adams, M., Mcgregor, H. V., & Toole, S. (2014). Climate change and Australia. *Wiley Interdisciplinary Reviews: Climate Change*, *5*(2), 175–197. https://doi.org/10.1002/wcc.255

Heikkilä, M., Edwards, T. W. D., Seppä, H., & Sonninen, E. (2010). Sediment isotope tracers from Lake Saarikko, Finland, and implications for Holocene hydroclimatology. *Quaternary Science Reviews*, *29*(17–18), 2146–2160. https://doi.org/10.1016/j.quascirev.2010.05.010

Heyng, A. M., Mayr, C., Lücke, A., Wissel, H., & Striewski, B. (2014). Late Holocene hydrologic changes in northern New Zealand inferred from stable isotope values of aquatic cellulose in sediments from Lake Pupuke. *Journal of Paleolimnology*, *51*(4), 485–497. https://doi.org/10.1007/s10933-014-9769-3

Holgate, C., Evans, J. P., Taschetto, A. S., Gupta, A. Sen, & Santoso, A. (2022). The Impact of Interacting Climate Modes on East Australian Precipitation Moisture Sources. *Journal of Climate*, *35*(10), 3147–3159. https://doi.org/10.1175/JCLI-D-21-0750.1

Holland, J. E., Luck, G. W., & Max Finlayson, C. (2015). Threats to food production and water quality in the Murray-Darling Basin of Australia. *Ecosystem Services*, *12*, 55–70. https://doi.org/10.1016/j.ecoser.2015.02.008

Hortle, A., De Carita, P., Stalvies, C., & Jenkins, C. (2011). Groundwater monitoring at the Otway Project site, Australia. *Energy Procedia*, *4*, 5495–5503. https://doi.org/10.1016/j.egypro.2011.02.535

Hughes, L. (2003). *Climate change and Australia : Trends , projections and impacts*. 423–443.

IPCC. (2022). Summary for Policymakers: Climate Change 2022_ Impacts, Adaptation and Vulnerability_Working Group II contribution to the Sixth Assessment Report of the

Intergovernamental Panel on Climate Change. In *Working Group II contribution to the Sixth Assessment Report of the Intergovernamental Panel on Climate Change* (Issue August). https://doi.org/10.1017/9781009325844.

Iverach, C.P., O'Neill, C., Bold, T.A. & Hocking, M., 2020. A regional baseline of quality and hydrocarbon occurrence in groundwater, Onshore Otway Basin, Victoria. *Victorian Gas Program Technical Report 21. Geological Survey of Victoria.* Department of **J**obs, Precincts and Regions. Melbourne, Victoria. 42pp.

Jiao, T., Williams, C. A., Rogan, J., De Kauwe, M. G., & Medlyn, B. E. (2020). Drought Impacts on Australian Vegetation During the Millennium Drought Measured With Multisource Spaceborne Remote Sensing. *Journal of Geophysical Research: Biogeosciences*, *125*(2), 1–19. https://doi.org/10.1029/2019JG005145

Jones, M. D., Cuthbert, M. O., Leng, M. J., McGowan, S., Mariethoz, G., Arrowsmith, C., Sloane, H. J., Humphrey, K. K., & Cross, I. (2016a). Comparisons of observed and modelled lake δ18O variability. *Quaternary Science Reviews*, *131*, 329–340. https://doi.org/10.1016/j.quascirev.2015.09.012

Jones, M. D., Dee, S., Anderson, L., Baker, A., Bowen, G., & Noone, D. C. (2016b). Water isotope systematics: Improving our palaeoclimate interpretations. *Quaternary Science Reviews*, *131*, 243–249. https://doi.org/10.1016/j.quascirev.2015.11.014

Jones, M. D., & Dee, S. G. (2018). Global-scale proxy system modelling of oxygen isotopes in lacustrine carbonates : New insights from isotope-enabled-model proxy-data comparison. *Quaternary Science Reviews*, *202*, 19–29. https://doi.org/10.1016/j.quascirev.2018.09.009

Jones, R. (2014). *Natural and Human Influences on the Distribution and Extent of Victorian Lowland Grasslands*. *January 1999*.

Jonsson, C. E., Andersson, S., Rosqvist, G. C., & Leng, M. J. (2010). Reconstructing past atmospheric circulation changes using oxygen isotopes in lake sediments from Sweden. *Climate of the Past*, *6*(1), 49–62. https://doi.org/10.5194/cp-6-49-2010

Kemp, J., Radke, L. C., Olley, J., Juggins, S., & De Deckker, P. (2012). Holocene lake salinity changes in the Wimmera, southeastern Australia, provide evidence for millennial-scale climate variability. *Quaternary Research*, *77*(1), 65–76. https://doi.org/10.1016/j.yqres.2011.09.013

Kiem, A. S., Johnson, F., Westra, S., van Dijk, A., Evans, J. P., O'Donnell, A., Rouillard, A., Barr, C., Tyler, J., Thyer, M., Jakob, D., Woldemeskel, F., Sivakumar, B., & Mehrotra, R. (2016). Natural hazards in Australia: droughts. *Climatic Change*, *139*(1), 37–54. https://doi.org/10.1007/s10584-016-1798-7

Kirono, D. G. C., Round, V., Heady, C., Chiew, F. H. S., & Osbrough, S. (2020). Drought projections for Australia: Updated results and analysis of model simulations. *Weather and Climate Extremes*, *30*, 100280. https://doi.org/10.1016/j.wace.2020.100280

Konecky, B. L., McKay, N. P., Churakova, O. V., Comas-Bru, L., Dassié, E. P., DeLong, K. L., Falster, G. M., Fischer, M. J., Jones, M. D., Jonkers, L., Kaufman, D. S., Leduc, G., Managave, S. R., Martrat, B., Opel, T., Orsi, A. J., Partin, J. W., Sayani, H. R., Thomas, E. K., … Yoshimura, K. (2020). The Iso2k database: A global compilation of paleo-δ18O and δ2H records to aid understanding of Common Era climate. *Earth System Science Data*, *12*(3), 2261–2288. https://doi.org/10.5194/essd-12-2261-2020

Leng, M., Barnker, P., Greenwood, P., Roberts, N., & Reed, J. (2001). Oxygen isotope analysis of diatom silica and authigenic calcite from Lake Pinarbasi, Turkey. *Journal of Paleolimnology*, *25*(3), 343–349. https://doi.org/10.1023/A:1011169832093

Leng, M. J., & Barker, P. A. (2006). A review of the oxygen isotope composition of lacustrine diatom silica for palaeoclimate reconstruction. *Earth-Science Reviews*, *75*(1–4), 5–27. https://doi.org/10.1016/j.earscirev.2005.10.001

Leng, M. J., Lamb, A. L., Marshall, J. D., Wolfe, B. B., Jones, M. D., Holmes, J. A., & Arrowsmith, C. (2005). NERC Isotope Geosciences Laboratory British Geological Survey Nottingham NG12 5GG, UK. *Encyclopedia of Atmospheric Sciences*, *4*(December 2007), 147–184. http://cdiac.esd.ornl.gov/oceans/GLODAP/glodap_pdfs/Thermohaline.web.pdf

Leng, M. J., & Marshall, J. D. (2004). Palaeoclimate interpretation of stable isotope data from lake sediment archives. *Quaternary Science Reviews*, *23*(7–8), 811–831. https://doi.org/10.1016/j.quascirev.2003.06.012

Li, H., Liu, X., Tripati, A., Feng, S., Elliott, B., Whicker, C., Arnold, A., & Kelley, A. M. (2020). Factors controlling the oxygen isotopic composition of lacustrine authigenic carbonates in Western China: implications for paleoclimate reconstructions. *Scientific Reports*, *10*(1), 1–17. https://doi.org/10.1038/s41598-020-73422-4

Liguori, G., McGregor, S., Singh, M., Arblaster, J., & Di Lorenzo, E. (2022). Revisiting ENSO and IOD Contributions to Australian Precipitation. *Geophysical Research Letters*, *49*(1), 1–12. https://doi.org/10.1029/2021GL094295

Mariani, M., & Fletcher, M. S. (2017). Long-term climate dynamics in the extra-tropics of the South Pacific revealed from sedimentary charcoal analysis. *Quaternary Science Reviews*, *173*, 181–192. https://doi.org/10.1016/j.quascirev.2017.08.007

Martin, L., Goff, J., Jacobsen, G., & Mooney, S. (2019). The radiocarbon ages of different organic components in the mires of Eastern Australia. *Radiocarbon*, *61*(1), 173–184. https://doi.org/10.1017/RDC.2018.118

Marx, S. K., Kamber, B. S., McGowan, H. A., Petherick, L. M., McTainsh, G. H., Stromsoe, N., Hooper, J. N., & May, J. H. (2018). Palaeo-dust records: A window to understanding past environments. *Global and Planetary Change*, *165*(March), 13–43. https://doi.org/10.1016/j.gloplacha.2018.03.001

Matchan, E. L., Phillips, D., Jourdan, F., & Oostingh, K. (2020). Early human occupation of southeastern Australia: Newinsights from 40Ar/39Ar dating of young volcanoes.

Geology, *48*(4), 390–394. https://doi.org/10.1130/G47166.1

Meneghini, B., Simmonds, I., & Smith, I. N. (2007). Association between Australian rainfall and the Southern Annular Mode. *International Journal of Climatology*, *27*(1), 109–121. https://doi.org/10.1002/joc.1370

Meyers, G., McIntosh, P., Pigot, L., & Pook, M. (2007). The years of El Niño, La Niña and interactions with the tropical Indian Ocean. *Journal of Climate*, *20*(13), 2872–2880. https://doi.org/10.1175/JCLI4152.1

Mooney, S. D., Hope, G., Horne, D., Kamminga, J., & Williams, A. N. (2020). Fire, humans and climate as drivers of environmental change on Broughton Island, New South Wales, Australia. *Holocene*, *30*(11), 1528–1539. https://doi.org/10.1177/0959683620941067

Morgan, G. W., Tolhurst, K. G., Poynter, M. W., Cooper, N., Mcguffog, T., Ryan, R., Wouters, M. A., Stephens, N., Black, P., Sheehan, D., Leeson, P., & Whight, S. (2020). Prescribed burning in south-eastern Australia : history and future directions. *Australian Forestry*, *83*(1), 4–28. https://doi.org/10.1080/00049158.2020.1739883

Parks Victoria. (1996). *Mount Eccles National park and Mount Napier state park; management plan*.

Perner, K., Moros, M., De Deckker, P., Blanz, T., Wacker, L., Telford, R., Siegel, H., Schneider, R., & Jansen, E. (2018). Heat export from the tropics drives mid to late Holocene palaeoceanographic changes offshore southern Australia. *Quaternary Science Reviews*, *180*, 96–110. https://doi.org/10.1016/j.quascirev.2017.11.033

Petherick, L., Bostock, H., Cohen, T. J., Fitzsimmons, K., Tibby, J., Fletcher, M. S., Moss, P., Reeves, J., Mooney, S., Barrows, T., Kemp, J., Jansen, J., Nanson, G., & Dosseto, A. (2013). Climatic records over the past 30ka from temperate Australia - a synthesis from the Oz-INTIMATE workgroup. *Quaternary Science Reviews*, *74*, 58–77. https://doi.org/10.1016/j.quascirev.2012.12.012

Radke, B., Champion, D. C., Gallagher, S. J., Wang, L., De Vleeschouwer, D., Kalinowski, A., Tenthorey, E., Urosevic, M., & Feitz, A. (2022). Geology, geochemistry and depositional history of the Port Campbell Limestone on the eastern flank of the Otway Basin, southeastern Australia. *Australian Journal of Earth Sciences*, *69*(4), 509–538. https://doi.org/10.1080/08120099.2022.1998220

Reddy, P. J., Perkins-Kirkpatrick, S. E., Ridder, N. N., & Sharples, J. J. (2022a). Combined role of ENSO and IOD on compound drought and heatwaves in Australia using two CMIP6 large ensembles. *Weather and Climate Extremes*, *37*(December 2021), 100469. https://doi.org/10.1016/j.wace.2022.100469

Reddy, P. J., Perkins-Kirkpatrick, S. E., & Sharples, J. J. (2022b). Interactive influence of ENSO and IOD on contiguous heatwaves in Australia. *Environmental Research Letters*, *17*(1). https://doi.org/10.1088/1748-9326/ac3e9a

Risbey, J. S., Pook, M. J., McIntosh, P. C., Wheeler, M. C., & Hendon, H. H. (2009). On the

remote drivers of rainfall variability in Australia. *Monthly Weather Review*, *137*(10), 3233–3253. https://doi.org/10.1175/2009MWR2861.1

Rogelj, J., Meinshausen, M., & Knutti, R. (2012). Global warming under old and new scenarios using IPCC climate sensitivity range estimates. *Nature Climate Change*, *2*(4), 248–253. https://doi.org/10.1038/nclimate1385

Rozanski, K., Klisch, M. A., Wachniew, P., Gorczyca, Z., Goslar, T., Edwards, T. W. D., & Shemesh, A. (2010). Oxygen-isotope geothermometers in lacustrine sediments: New insights through combined δ18O analyses of aquatic cellulose, authigenic calcite and biogenic silica in Lake Gościaz, central Poland. *Geochimica et Cosmochimica Acta*, *74*(10), 2957–2969. https://doi.org/10.1016/j.gca.2010.02.026

Saunders, K. M., Roberts, S. J., Perren, B., Butz, C., Sime, L., Davies, S., Van Nieuwenhuyze, W., Grosjean, M., & Hodgson, D. A. (2018). Holocene dynamics of the Southern Hemisphere westerly winds and possible links to CO2 outgassing. *Nature Geoscience*, *11*(9), 650–655. https://doi.org/10.1038/s41561-018-0186-5

Shapley, M. D., Ito, E., & Donovan, J. J. (2008). Isotopic evolution and climate paleorecords: Modeling boundary effects in groundwater-dominated lakes. *Journal of Paleolimnology*, *39*(1), 17–33. https://doi.org/10.1007/s10933-007-9092-3

Stanley, S., & De Deckker, P. (2002). A holocene record of allochthonous, aeolian mineral grains in an australian alpine lake; implications for the history of climate change in southeastern australia. *Journal of Paleolimnology*, *27*(2), 207–219. https://doi.org/10.1023/A:1014249404845

Sternberg, L., Deniro, M. J., & Keeley, J. E. (1984). Hydrogen, oxygen, and carbon isotope ratios of cellulose from submerged aquatic crassulacean acid metabolism and non-crassulacean acid metabolism plants. *Plant Physiology*, *76*(1), 68–70. https://doi.org/10.1104/pp.76.1.68

Stojakowits, P., Mayr, C., Lücke, A., Wissel, H., Hedenäs, L., Lempe, B., Friedmann, A., & Diersche, V. (2020). Impact of climatic extremes on Alpine ecosystems during MIS 3. *Quaternary Science Reviews*, *239*. https://doi.org/10.1016/j.quascirev.2020.106333

Street-Perrott, F. A., Holmes, J. A., Robertson, I., Ficken, K. J., Koff, T., Loader, N. J., Marshall, J. D., & Martma, T. (2018). The Holocene isotopic record of aquatic cellulose from Lake Äntu Sinijärv, Estonia: Influence of changing climate and organic-matter sources. *Quaternary Science Reviews*, *193*, 68–83. https://doi.org/10.1016/j.quascirev.2018.05.010

Talbot, M. R., & Kelts, K. (1990). Paleolimnological signatures from carbon and oxygen isotopic ratios in carbonates from organic carbon-rich lacustrine sediments. *Lacustrine Basin Exploration - Case Studies and Modern Analogs*, 99–112.

Tibby, J., Tyler, J. J., & Barr, C. (2018). *Post little ice age drying of eastern Australia con fl ates understanding of early settlement impacts*. *202*, 45–52. https://doi.org/10.1016/j.quascirev.2018.10.033

Timms, B. V. (1976). A Comparative Study of the Limnology of Three Maar Lakes in Western Victoria. I. physiography and physicochemical features. *Marine and Freshwater Research*, *27*(1), 35–60. https://doi.org/10.1071/MF9760035

Tyler, J. J., Marshall, J. C., Schulz, C., Barr, C., Hofmann, H., Blessing, J. J., Mccoy, K., Mcgregor, G. B., & Tibby, J. (2022). *Hydrological and Isotopic Variability of Perched Wetlands on North Stradbroke Island (Minjerribah), Australia : Implications for Understanding the Effects of Past and Future Climate Change*. *10*(July), 1–21. https://doi.org/10.3389/fenvs.2022.868114

Ummenhofer, C. C., England, M. H., Mcintosh, P. C., Meyers, G. A., Pook, M. J., Risbey, J. S., & Gupta, A. Sen. (2009). *What causes southeast Australia ' s worst droughts ? 36*, 1–5. https://doi.org/10.1029/2008GL036801

Van Dijk, A. I. J. M., Beck, H. E., Crosbie, R. S., De Jeu, R. A. M., Liu, Y. Y., Podger, G. M., Timbal, B., & Viney, N. R. (2013). The Millennium Drought in southeast Australia (2001-2009): Natural and human causes and implications for water resources, ecosystems, economy, and society. *Water Resources Research*, *49*(2), 1040–1057. https://doi.org/10.1002/wrcr.20123

Vance, T. R., Roberts, J. L., Plummer, C. T., Kiem, A. S., & Ommen, T. D. Van. (2015). *Interdecadal Pacific variability and eastern Australian megadroughts over the last millennium*. 129–137. https://doi.org/10.1002/2014GL062447.Abstract

Von Grafenstein, U., Belmecheri, S., Eicher, U., van Raden, U. J., Erlenkeuser, H., Andersen, N., & Ammann, B. (2013). The oxygen and carbon isotopic signatures of biogenic carbonates in Gerzensee, Switzerland, during the rapid warming around 14,685 years BP and the following interstadial. *Palaeogeography, Palaeoclimatology, Palaeoecology*, *391*, 25–32. https://doi.org/10.1016/j.palaeo.2013.08.018

Webb, J. A. (2016). *Chapter 18 the evolution of Victorian landscapes*. *January 1991*.

Wilkins, D., De Deckker, P., Fifield, L. K., Gouramanis, C., & Olley, J. (2012). Comparative optical and radiocarbon dating of laminated Holocene sediments in two maar lakes: Lake Keilambete and Lake Gnotuk, south-western Victoria, Australia. *Quaternary Geochronology*, *9*, 3–15. https://doi.org/10.1016/j.quageo.2012.01.008

Wilkins, D., Gouramanis, C., de Deckker, P., Fifield, L. K., & Olley, J. (2013). Holocene lake-level fluctuations in Lakes Keilambete and Gnotuk, southwestern Victoria, Australia. *Holocene*, *23*(6), 784–795. https://doi.org/10.1177/0959683612471983

Wissel, H., Mayr, C., & Lücke, A. (2008). A new approach for the isolation of cellulose from aquatic plant tissue and freshwater sediments for stable isotope analysis. *Organic Geochemistry*, *39*(11), 1545–1561. https://doi.org/10.1016/j.orggeochem.2008.07.014

Wolfe, B. B., Aravena, R., Abbott, M. B., Seltzer, G. O., & Gibson, J. J. (2001a). Reconstruction of paleohydrology and paleohumidity from oxygen isotope records in the Bolivian Andes. *Palaeogeography, Palaeoclimatology, Palaeoecology*, *176*(1–4), 177–192. https://doi.org/10.1016/S0031-0182(01)00337-6

Wolfe, B. B., Edwards, T. W. D., Aravena, R., Forman, S. L., Warner, B. G., Velichko, A. A., & MacDonald, G. M. (2000). Holocene paleohydrology and paleoclimate at treeline, north-central Russia, inferred from oxygen isotope records in lake sediment cellulose. *Quaternary Research*, *53*(3), 319–329. https://doi.org/10.1006/qres.2000.2124

Wolfe, B. B., Edwards, T. W. D., Elgood, R. J., & Beuning, K. R. M. (2001b). 14 . Carbon and oxygen isotope analysis of lake sediment cellulose : methods and applications, Department of Earth Sciences Canada N2L 3G1 Department of Earth and Environmental Sciences. *Tracking Environmental Change Using Lake Sediments*, *2*, 1–28.

Wolfe, B. B., Falcone, M. D., Clogg-Wright, K. P., Mongeon, C. L., Yi, Y., Brock, B. E., Amour, N. A. S., Mark, W. A., & Edwards, T. W. D. (2007). Progress in isotope paleohydrology using lake sediment cellulose. *Journal of Paleolimnology*, *37*(2), 221–231. https://doi.org/10.1007/s10933-006-9015-8

Xia, Q., Zhao, J. xin, & Collerson, K. D. (2001). Early-mid Holocene climatic variations in Tasmania, Australia: Multi-proxy records in a stalagmite from Lynds Cave. *Earth and Planetary Science Letters*, *194*(1–2), 177–187. https://doi.org/10.1016/S0012-821X(01)00541-6

Yihdego, Y., Webb, J., & Leahy, P. (2016). Modelling water and salt balances in a deep, groundwater-throughflow lake—Lake Purrumbete, southeastern Australia. *Hydrological Sciences Journal*, *61*(1), 186–199. https://doi.org/10.1080/02626667.2014.975132

Supplementary data

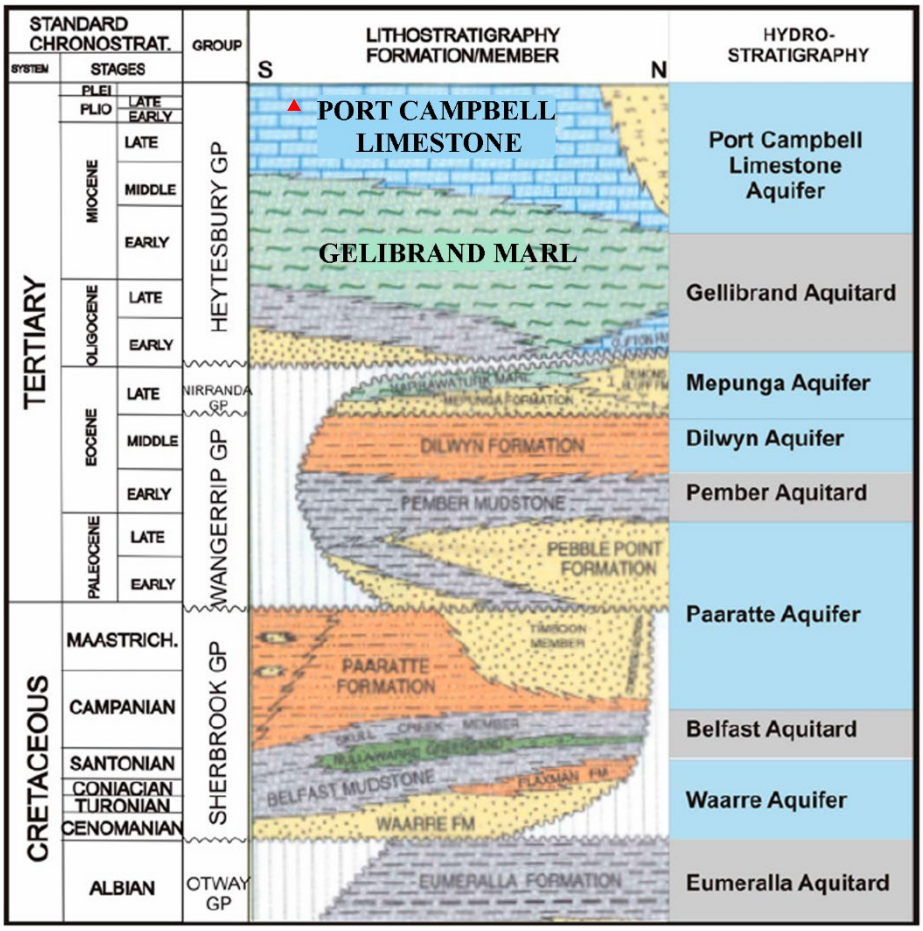

Figure I. Hydrostratigraphic sequence of the Port Campbell limestone (PCL) in the Otway basin (source: Hortle et al., 2011). Red triangle represents an approximate position of the Lake Surprise, where it underlies 15 m below the upper surface of the PCL and 60m above the Gellibrand Marl (Ankor, 2020).

Era	Period	Hydrostratigraphic unit	Formation
Cenozoic	Quaternary	Quaternary Aquifer	Unconsolidated alluvial sediments
		Upper Tertiary/ Quaternary Basalts	Newer Volcanic group
	Neogene	Upper Tertiary Aquifer (Marine)	Whalers Bluff Formation Parilla Sand Black Rock Sandstone
		Upper Mid-Tertiary Aquifer	**Port Campbell Limestone** Gambier Limestone (west)
		Upper Mid-Tertiary Aquitard	**Gellibrand Marl (east)**
	Palaeogene	Lower Mid-Tertiary Aquifer	Clifton Formation
		Lower Mid-Tertiary Aquitard	Narrawaturk Marl Mepunga Formation
		Lower Tertiary Aquifer	Dilwyn Formation Pember Mudstone Member Pebble Point Formation Moomowroong Sand Member Wirdjil Gravel Timboon Sand
Mesozoic	Cretaceous	Upper Cretaceous Sediments	Paaratte Formation Nullawarre Greensand Belfast Mudstone Flaxman Formation Waarre Formation
		Upper Jurassic to Lower Cretaceous Sediments and Lower Palaeozoic Bedrock	Eumeralla Formation Katnook Sandstone Laira Formation Pretty Hill Formation Casterton Formation

Table I. Hydrostratigraphic units (aquifer/aquitard) of the Otway Basin according to the Victorian Aquifer Framework (Source: Clarke et al., 2015; Iverach et al., 2020).

CHAPTER 2

Dharmarathna, A., Tyler, J., Jones, M., Tadros, C., Ankor, M., Tibby, J., Barr, C., Zolitschka, B., Hughes, C., Lake hydrological response to climate variability; a coupled monitoring and isotope mass balance modelling approach applied to Lake Surprise, Victoria, Australia.

Supplementary information concerning this chapter follows the text. Data tables concerning this chapter are provided in Appendix 2.

Statement of Authorship

Title of Paper	Lake hydrological response to climate variability; a coupled monitoring and isotope mass balance modelling approach applied to Lake Surprise, Victoria, Australia.
Publication Status	☐ Published ☐ Accepted for Publication ☐ Submitted for Publication ☑ Unpublished and Unsubmitted work written manuscript style
Publication Details	Dharmarathna, A., Tyler, J., Jones, M., Tadros, C., Ankor, M., Tibby, J., Barr,C., Zolitschka, B., Hughes, C., Lake hydrological response to climate variability; a coupled monitoring and isotope mass balance modelling approach applied to Lake Surprise. *Journal of Hydrology* **in prep.**

Principal Author

Name of Principal Author (Candidate)	Asika Dharmarathna		
Contribution to the Paper	Field sample collection, sample preparation for analysis, Assisted in instrumental analysis, Data interpretation and modelling, Writing the manuscript and acting as the corresponding author		
Overall percentage (%)	70%		
Certification:	This paper reports on original research I conducted during the period of my Higher Degree by Research candidature and is not subject to any obligations or contractual agreements with a third party that would constrain its inclusion in this thesis. I am the primary author of this paper.		
Signature		Date	10/12/2022

Co-Author Contributions

By signing the Statement of Authorship, each author certifies that:

i. the candidate's stated contribution to the publication is accurate (as detailed above);

ii. permission is granted for the candidate in include the publication in the thesis; and

iii. The sum of all co-author contributions is equal to 100% less the candidate's stated contribution.

Name of Co-Author	Jonathan Tyler		
Contribution to the Paper	Field work assistance, Funding support, guidance in data analysis and interpretation, Manuscript evaluation and review		
Signature		Date	5/12/22

Name of Co-Author	Matthew Jones		
Contribution to the Paper	Provided guidance in lake modelling and interpretation of data		
Signature		Date	22/11/2022

Name of Co-Author	Carol Tadros		
Contribution to the Paper	Provided guidance in data interpretation, Assistance in instrumental analysis of lake water isotope data		
Signature		Date	23/11/2022

Name of Co-Author	Martin Ankor		
Contribution to the Paper	Preparation of 3D printed sediment trap and rainfall sampler for modern sample collection, provided monitoring data from the period of 2015 – 2018, provided guidance in data analysis		
Signature		Date	23/11/2022

Name of Co-Author	John Tibby		
Contribution to the Paper	Field work assistance, provided guidance in data interpretation, Manuscript evaluation and review		
Signature		Date	1/12/2022

Name of Co-Author	Cameron Barr		
Contribution to the Paper	Field work assistance, provided guidance in data interpretation,		
Signature		Date	23/11/2022

Name of Co-Author	Bernd Zolitschka		
Contribution to the Paper	Field work assistance, provided lake measurement data		
Signature		Date	November 11, 2022

Name of Co-Author	Catherine Hughes		
Contribution to the Paper	Provided updated GNIP data (2014 -2019) for comparison with our data		
Signature		Date	23/11/2022

2 Lake hydrological response to climate variability; a coupled monitoring and isotope mass balance modelling approach applied to Lake Surprise, Victoria, Australia.

Abstract

The application of oxygen isotopes to infer past climate from lake sediments is helped by a thorough understanding of the hydrological and isotopic states of the modern lake environment. Such data are also useful for understanding the response of lake systems to future climate change. This study presents a coupled observational and modelling study at Lake Surprise, a crater lake in western Victoria, Australia, using data collected over a five-year monitoring period. Isotope mass balance models based on observational measurements are used to estimate the hydrologic budget and evaluate the key variables impacting the fluctuation of lake water isotopes.

Gibbs plots and Piper diagram analysis indicate weathering of basalts and carbonate dissolution via groundwater are the main sources of Na^+ and HCO_3^- ions in lake water. Similar results collected over the last 50 years suggest that this lake's hydrological state is relatively constant. Stable oxygen and hydrogen isotopes in lake water ($\delta^{18}O$ and $\delta^{2}H$) defined a local evaporation line (LEL) that deviates significantly from the precipitation-defined local meteoric water line (LMWL) indicating that evaporative enrichment has a significant impact on the isotope composition of lake water, and comparison to an index lake model indicates groundwater dominance at Lake Surprise. The water balance model estimates groundwater inflow (79%) and outflow (67%) to be higher than the contribution from precipitation and evaporation, explaining the stability of Lake Surprise through recent droughts. Sensitivity tests using the lake water isotope mass balance model indicate that evaporation relative to rainfall plays a major role in determining the oxygen and hydrogen isotope composition of water at Lake Surprise, whereas the lake water isotopes are relatively insensitive to changes in groundwater throughflow. Overall, this study demonstrates how a combination of long-term monitoring and modelling is needed to better understand a lake system in response to climate and environmental changes and support to make reliable palaeoclimate reconstructions.

2.1 Introduction

Lake sediments are important archives of past climate and environment, spanning a diverse range of localities and time scales (Cohen 2003; Fritz 2008; Adrian et al. 2009). Most of these palaeoclimate interpretations rely on indirect measurements of biological, geochemical and isotopic tracers preserved in lake sediments or on long-used palaeo-assumptions (Battarbee et al., 2012). Individual sediment proxies, however, may respond to climate change in a non-linear manner given that lakes are complex systems and made up of fundamentally different properties, making palaeo-interpretations more challenging (Battarbee, 2000; Fritz, 2008; Jones & Dee, 2018). This is generally true for the interpretation of oxygen isotopes in lakes, as well as processes such as carbonate deposition, both of which are affected by often unknown and variable groundwater influence on the lake system (Dean et al., 2015; Jones et al., 2016; Li et al., 2020; Şehnaz et al., 2020). Therefore, in order to make reliable reconstructions of past climates, it is crucial to have a thorough understanding of the behaviour of lakes over a variety of hydroclimate circumstances via both lake monitoring and modelling (Jones & Dee, 2018; Tyler et al., 2022).

Lake water hydrological and geochemical monitoring provides a fundamental understanding of the physical and chemical characteristics of the modern lake system, including the key controls of lake water isotope variability, and responses to climate change (Dean et al., 2015). Major ions in surface waters have been extensively studied to determine the sources of water and material loading, water-rock interaction and natural processes that affect water chemistry including precipitation, evaporation, rock weathering and soil erosion (Zhu & Yang, 2007; Xu et al., 2010; Xiao et al., 2015; Li et al., 2016; Liu et al., 2019). Major ions also act as tracers of various climate and human-induced activities that may impact lake-specific mechanisms such as photosynthesis, respiration, mineral deposition and dissolution (carbonate, pyrite etc.), nutrient loading and biogeochemical cycling (Li et al., 2011; Xiao et al., 2012; Liu et al., 2019). Major ionic data can be evaluated using the Gibbs envelope plots and Piper trilinear plots. The Gibbs plot is used to distinguish the major controlling hydrochemical mechanisms of water bodies such as atmospheric precipitation, regional rock weathering, and evaporation and crystallization processes (Gibbs, 1970; Xu et al. 2010; Liu et al. 2020; Şehnaz et al. 2020).

Piper trilinear diagram analysis provides a graphical representation of the major ion distribution in a water body, which enables the classification of different water types depending on the similarities and differences in chemical composition (Piper, 1944), and has been applied to

investigate the hydrogeological evolution of lakes (Darwesh et al., 2019; Liu et al., 2019; Wei et al., 2020). A wide range of major ion ratios are also used to explain hydrochemical processes and their controlling mechanisms, for instance, the ionic ratio of HCO_3^-/Cl^- has been used to differentiate between groundwater and surface water–fed lakes in western Victoria, Australia (Barton et al., 2013). In this region, groundwater is thought to have high salinity and lower HCO_3^- owing to carbonate precipitation and evapotranspiration in the soil zone, meaning that surface water and interflow are responsible for mineral weathering that results in high HCO_3^- and low Cl^- (Barton et al., 2013).

Stable oxygen and hydrogen isotopes ($\delta^{18}O$ and $\delta^{2}H$) in lake water have been extensively used in understanding the hydrological processes including sources of water flux, the origin of groundwater resources and to determine the impact of climate and hydrological change on lake water balance (Craig & Gordon, 1965; Leng & Marshall, 2004; Dean et al., 2015; Gibson et al., 2016; Cluett & Thomas, 2020; Wu et al., 2021; Li et al., 2022). Several different sedimentary materials record changes in past lake water oxygen isotope composition (Leng & Marshall, 2004; Jones et al., 2007; Gat, 2010; Gibson et al., 2016; Dean et al., 2018; Li et al., 2021), including sedimentary cellulose which is considered a direct proxy of lake water $\delta^{18}O$ (Wolfe et al., 2001, 2007; Heikkilä et al., 2010; Street-Perrott et al., 2018). However, the majority of lake water isotope interpretations are based on qualitative assessment, which limits the understanding of lake hydrology and its response to climate change (Jones & Imbers, 2010; Jones & Dee, 2018). Numerical analysis of lake water isotopes can be achieved using a coupled hydrologic-isotopic mass balance approach, which balances the amount of incoming and outgoing water and the oxygen/hydrogen isotope composition of such water (Dincer, 1968; Gat, 1995; Gibson et al., 2002, 2016; Jones et al., 2005; Li et al., 2022).

Isotope mass balance models are practical and adaptable, enabling research that advances the interpretation of past climate from lake sediment isotopes (Steinman et al., 2010; Jones & Dee, 2018). In addition, stable hydrogen and oxygen isotope mass-balance models are employed to compare and evaluate multi-year observational records (Tyler et al., 2007; Jones et al., 2016) and to provide estimates of the water balance of lakes, particularly when observational data are absent (Haig et al., 2020). In general, this isotope mass balance approach has been predominantly applied to northern hemisphere lakes, where more reliable palaeoclimate interpretations and projections of the future climate have been generated thus far (Gibson &

Edwards, 2002; Jones et al., 2005, 2016; Jones & Imbers, 2010; Gibson & Reid, 2014; Jones & Dee, 2018; Lacey & Jones, 2018).

Several lakes in southeast Australia have been used to reconstruct past climate change based on their sediment composition. Even though numerous amount of qualitative research is available for the region, a very limited number of studies have taken a quantitative approach either by lake monitoring or modelling (Jones et al., 1998; Jones et al., 2001; Tibby and Tiller, 2007; Yihdego et al., 2015, 2016; Yihdego and Webb, 2016). Many of the climate interpretations available rely mostly on multiple evidence from sediment proxy data and qualitative conceptual models (Tyler et al., 2015). However, some studies have used a quantitative approach to determine the hydraulic budget in western Victorian lakes, to estimate the groundwater flux and to determine the role of climate in lake level changes (Jones et al., 1998; Jones et al., 2001; Tweed et al., 2009). By comparing historical and simulated water levels Jones et al., (2001) constructed a lake water balance model, which has since been replicated and expanded upon for several other lakes in western Victoria (Kirono et al., 2009; Tweed et al., 2009; Ankor, 2020). However, the accuracy of this method relies on estimates of groundwater inflow/outflow from a water body (Lee, 1996; Yang et al., 2014; Yihdego et al., 2016). In addition, the difference method, and modified-difference water budget methods were applied in calculating the hydraulic budget and most of these models applied Darcy's law to estimate the groundwater flux (Yihdego et al., 2015, 2016). However, these methods may produce poor outcomes if the hydraulic gradient or conductivity cannot be precisely determined or if the groundwater fluxes are small (Yihdego & Webb, 2012, 2015, 2016; Yihdego et al., 2015, 2016). Furthermore, the majority of these models have focused only on the water balance relationship. As yet, no published studies in south-east Australia have undertaken isotope mass balance modelling to constrain contemporary lake water hydrology.

Lake Surprise, a crater lake located in western Victoria, Australia, is an important archive of past climate and environment, due to its geological location, confined basin, and lack of major post-colonial human impact. Several studies have analysed the sediments of Lake Surprise to reconstruct hydroclimate variability using fossil diatom assemblages, carbon isotopes and inorganic geochemistry (Tibby et al., 2006; Builth et al., 2008; Barr et al., 2014; Falster et al., 2018). Most of these palaeo-interpretations rely on the assumption that the lake's hydrological balance is driven by precipitation and evaporation. That the lake has continued to deposit sediment near-continuously throughout the last ~30,000 years suggests some degree of

groundwater recharge into or out of the lake, particularly during dry climates (Barr et al., 2014; Falster et al., 2018). However, none of these assumptions has been experimentally tested to date. The lake was initially surveyed from July 1971 – February 1972(Timms, 1975). This work investigates the modern climate and hydrological controls over Lake Surprise and its geochemical budget, using oxygen and hydrogen isotope data, the major ionic composition of lake water and local climate records spanning a total of five years (2015 – 2018 and 2019 – 2022). Further, the data is used to calibrate a coupled hydrologic and stable isotope mass balance model to quantify the lake water balance and to determine the sensitivity of both lake level and oxygen isotope composition to climate change.

2.2 Study area

2.2.1 Regional climate and geological setting

Lake Surprise is situated in the western plains of the Newer Volcanic province in Victoria, south-east Australia. The majority of volcanoes in the Newer Volcanic province are concentrated in the western plains (Boyce, 2013; Barr et al., 2014; Boyce et al., 2014). The plain overlies Cretaceous sandstone, Tertiary-Quaternary marl and limestone of the Otway Basin (Price et al., 1997; Barr et al., 2014). The volcanic plain has produced approximately 400 eruption centres with both simple and complicated magmatic characteristics, yet the system appears to have been dormant since the mid-Holocene (Joyce et al., 1988; Boyce, 2013; Webb, 2016; Smith et al., 2017). Extensive volcanic eruptions have left basaltic lava flows across the region with a significant amount of scoria cones and maars, particularly towards the north of the western plains (Price et al., 1997; Boyce, 2013; Webb, 2016). Major unconfined to semi-confined regional aquifer systems are formed by these thick basaltic lava flows and the majority of the maar volcanoes are connected to Mesozoic structures and aquifers beneath the Cenozoic Otway Basin sediments (Joyce, 1975; Boyce, 2013; Yihdego et al., 2016). The regolith profile of the plains consists of thick kaolinite layers and clay and nodular ironstone, which are formed by weathering of older lava flows. Younger lava flows remain as “stony rises”, which are rocky outcrops formed especially around individual volcanoes like Mt. Eccles (Budj Bim) (Yihdego et al., 2015; Webb, 2016). Volcanic craters in the region have changed through time to form a diverse range of crater lakes, ranging from freshwater (<0.5 mS/cm to hypersaline (>400 mS/cm) and shallower (<5 m) to deeper (>60 m) (Webb, 2016; Yihdego et al., 2016; Ankor, 2020). A generally poor surface drainage system across the region means that groundwater flows are crucial for sustaining lake hydrology (Webb, 2016; Yihdego et al., 2016).

The modern climate of the region is characterised as a temperate or Mediterranean-like climate with relatively dry summers and mild, wet winters (Barr et al., 2014; Falster et al., 2018). The majority of the precipitation is winter dominant (June to August) and brought to the region by mid-latitudinal shifts of southern westerly winds originating in the Southern Ocean (Murphy and Timbal, 2008; Tweed et al., 2009; Barr et al., 2014). Average annual precipitation across the region varies from ~500 – 1500 mm (BOM, 2022). However, according to climate measurements obtained from the closest rain gauge station, which is located approximately 10 km north of the study site at Macarthur (090055), the annual precipitation near Lake Surprise varies from 500 – 1000 mm over the last 30 years (BOM, 2022). Annual evaporation at this location exceeds precipitation with values varying from 1100 – 1400 mm (BOM, 2022). The mean annual minimum and maximum temperature over the last 30 years varies from 13 – 15℃ and 18 – 20℃ respectively (BOM, 2022).

2.2.2 Lake Surprise

Lake Surprise was formed following the eruption of Mt. Eccles (Budj Bim) volcano approximately 37,000 years ago (Matchan et al., 2020). The lake is located within Budj Bim National park (formerly known as Mt. Eccles National Park), a UNESCO World Heritage Site (Bell & Johnston, 2008; Smith et al., 2019). The initial lake bathymetry by Timms, (1975) suggests that the irregularly shaped lake was formed by the integration of a larger eruption site in the middle and a smaller eruption site at each end, creating an extended lake with little "lagoons" at both ends. According to the reports of the Western Victorian Groundwater Framework, the bottom of Lake Surprise sits ~15m below the upper-surface of the Port Campbell Limestone, a permeable and generally unconsolidated carbonate formation of Upper Miocene age; and ~60 m above the Gellibrand Marl formation, a several hundred meters thick aquiclude of clay and marl (Jones et al., 2001; Ankor, 2020). A more recent lake bathymetry surveyed in 2019 (see Methods) indicated that the main lagoon was ~11.5 m deep (~78 mAHD), ~600 m long and ~200 m wide at its longest and widest points (Appendix 1). The funnel-shaped lake basin alters the lake volume and surface area along the depth profile. Depth profile measurements obtained in 2019, provide evidence of thermal stratification with the presence of sharp horizontal boundaries between the oxygenated epilimnion and an underlying anoxic hypolimnion (Figure 1b). A relatively small catchment area and densely vegetated, steep and high crater walls (~49 m) limit the inflow of detrital material and wind-blown particles into the lake (Builth et al., 2008; Barr et al., 2014; Falster et al., 2018).

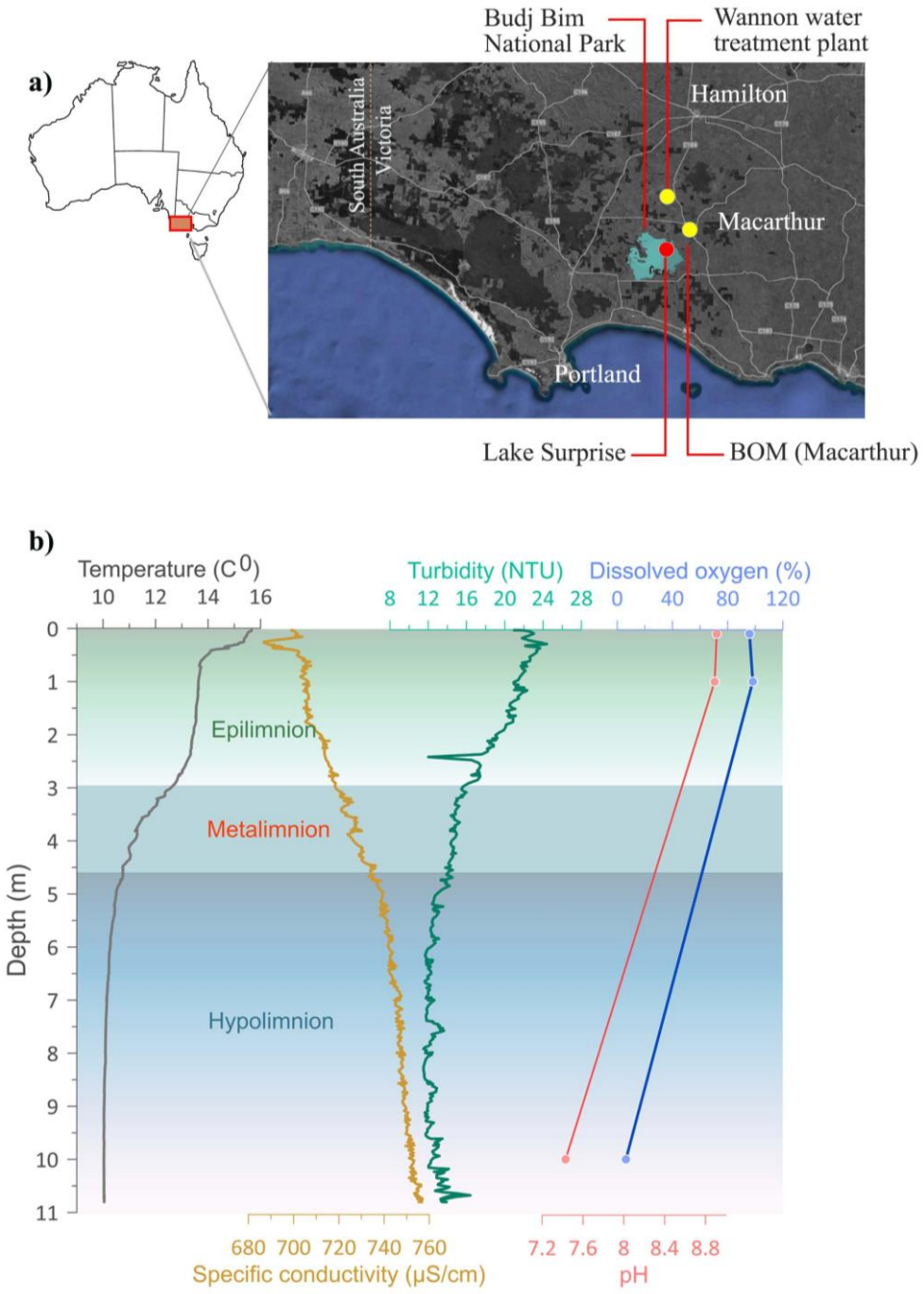

Figure 1. a) Figure representing the detailed view of Lake Surprise, along with locations of the Macarthur weather station (instrumental climate data) and Wannon water treatment plant, (location of rainwater sample collection) and b) lake water depth profile measurements obtained in 2019.

2.3 Materials and methods

2.3.1 Fieldwork

Lake water sampling and physical properties were measured from Lake Surprise during five field visits conducted from October 2019 to April 2022. In addition, monthly lake water samples were collected for isotopes with the help of the local community (Rangers). All the water samples were taken at around 0.5 m depth to eliminate water-air isotope exchange and the majority of the water samples were taken from the middle of the lake to represent overall lake features. In October 2019, a complete lake depth profile was measured for pH, temperature, turbidity, specific conductivity and dissolved oxygen concentration measured using a "CTD sonde XR-620 sensor''. The lake bathymetry using a Lowrance HDS – 5 echo sounder coupled to a Leica 1200GG RTK GPS antenna with corrections from the Smartnet CORS network, mounted on a pedal-powered Native Watercraft Mariner 12.5 kayak. The GPS antenna was installed 1.1 m above the depth sounder transducer, which was situated 0.2 m below the water's surface. A 30 m tape with a 150 g lead weight was used for manual sounding to validate the electronic depth soundings. The combined vertical + height inaccuracy for GPS QA was set at 1 m. During the survey, only a small number of auto-logged points were lost, although it was observed that the maximum QA tolerance was occasionally used, mainly due to the very poor sky visibility in the crater. The lake was surveyed with loops spaced approximately 20 metres apart. 940 sounding sites and 17 manually taken depth measurements were obtained. Surveying closer to the shoreline was restricted by the presence of fallen trees, rocks, and other navigational hazards. The sounding line closest to the shoreline is about 1 m deep and ~10m away from the shoreline. Bathymetry was not defined using specific GPS heights. Instead, the average height of all 940 auto-logged points was utilised. The horizontal quality is greater than 0.1 m for about 75% of auto-logged locations, and within 0.5 m for the remaining 25% of points (Appendix 1, Figure I).

Leak-proof HDPE bottles (30 ml) rinsed three times with the lake water were used in sampling and missing data indicate periods when sampling was not possible due to heavy rains, fires and the travel restriction during the covid–19 situation. A separate set of lake water samples were collected into acid-washed bottles (500 ml) to measure major ions and nutrients, where samples for the major ions were filtered in-site using a 0.45μm filter. These samples were sent to the laboratory immediately after collection. Physical measurements (water temperature, pH, conductivity (EC) / Total Dissolved Solids (TDS), Dissolved oxygen (DO)) were recorded

using a Hanna 98194 water meter. Single-point calibrations were conducted before each field visit using 5000 µS/cm conductivity standard, 3-point pH calibration standards 4.01, 7.01, 10.01 and DO calibration using DI water. A quick calibration was performed in the field right before taking measurements. A hand-held depth sounder and a Secchi disk were occasionally used for in-depth measurements and identification of the photic zone. A 3D-printed autonomous rainfall sampler was designed to meet the needs of stable isotope analysis that is capable of collecting daily and monthly rainwater samples approximately for three consecutive months (Ankor et al., 2019). The sampler was installed at the Wannon water treatment plant, Macarthur, 10 km North of Lake Surprise on 30th October 2019. All the water samples were stored in a cool foam box immediately after collection and refrigerated at 4°C upon return to the laboratory.

2.3.2 Laboratory analysis

Stable oxygen and hydrogen isotopes of water samples collected from 2019 – 2021 were analysed using the L2130-i Picarro Cavity Ring-Down Spectrometer at the Flinders analytical laboratory and the last batch of samples collected in April 2022 was measured at the Australian Nuclear Science and Technology Organization (ANSTO), Lucas Heights, New South Wales. The Picarro at Flinders analytical laboratory was calibrated using three in-house standards (DESAL, EVIAL and a QC sample check against RAIN) and sample processing was conducted using seven injections per sample with the first three injections being discarded to reduce the memory effect. Results were reported with a precision of ±0.07‰ for $\delta^{18}O$ and ±0.58‰ for $\delta^{2}H$. Similarly, six standard reference materials were used in the calibration of Piccaro at ANSTO, with three in-house standards (AILS – 006, AILS – 012 and AILS – 013) with a QC sample check against three other standards (AILS – 008, AILS – 009 and AILS – 014). Samples and standards were injected 20 times with the first eight being rejected to reduce the memory effect. Results were reported with an accuracy of ±0.15‰ for $\delta^{18}O$ and ±1‰ for $\delta^{2}H$. All the isotope results were given as delta notation per mille (‰) with reference to the international primary standard VSMOW2 (Vienna Mean Standard Ocean Water). Water samples for nutrients and major cations ($Ca^{2+}, Mg^{2+}, Na^{+}, K^{+}$) and anion ($HCO_3^-, CO_3^{2-}, SO_4^{2-}, Cl^-$) analysis was sent to the Australian Laboratory Services (ALS) water chemistry lab in Melbourne and Australian Water Quality Centre (AWQC) in Adelaide immediately after collection. Major cations were determined using Inductively Coupled Plasma Mass Spectrometry (ICP-MS).

Anions such as SO_4^{2-}, Cl^- were measured in the Discrete Analyser whereas carbonate/bicarbonate analysis was performed using a PC Titrator.

2.3.3 Data acquisition

Data from the initial monitoring work done by Timms, (1975) and Ankor, (2020) were used in this work to expand the monitoring record at Lake Surprise. (Ankor, 2020) consists of stable isotopes, major ions and field measurements collected on a monthly basis from 2015 – 2018. In addition, climate data were obtained from the nearest rain gauge station at Macarthur (station number 090055) located about 9 km northeast of the study site. The data in this station is recorded by the Australian Bureau of Meteorology (BOM) since 1889. However, the Scientific Information for Land Owners (SILO) database (https://www.longpaddock.qld.gov.au/silo/) created by the Queensland Government in collaboration with the BOM provides post-processed observational data that are ready to use in scientific studies. Therefore, in this study, post-processed data from the SILO database were utilised for a higher degree of accuracy. Due to the absence of stable isotope values in precipitation at Macarthur (BOM data), $\delta^{18}O$ and $\delta^{2}H$ values at Melbourne were obtained from the Global Network of Isotopes in precipitation (GNIP) database. Groundwater chemistry data and the nearby borehole logs were acquired from the "Visualizing Victoria's groundwater" database and the "Groundwater Explorer" database developed by the Australian Bureau of Meteorology.

2.3.4 Lake modelling

Model development for Lake Surprise was performed based on the lake isotope mass balance (IMB) theory (Craig & Gordan., 1965; Dincer, 1968; Gat, 1995; Gibson et al., 2002; 2016). Index lake approach and steady-state lake modelling were applied to Lake Surprise following Lacey & Jones, (2018) isotope mass balance calculations. Thenceforward, the lake modelling approach used in Attenborough lakes (Jones et al., 2016) was applied in this study to test the sensitivity of the lake model.

Considering a lake in a steady state, the water balance equation is given as follows,

$$\frac{dV}{dt} = P + Qi - E - Qo \qquad \text{Equation 1}$$

Where, $\frac{dV}{dt}$ is the change in lake volume per given time, P is the precipitation on the lake, E is the evaporation from the lake and Qi and Qo are the inflow and outflow respectively, which separate into surface inflow (Si) and outflow (So) and groundwater inflow (Gi) and outflow (Go) respectively.

Given that Lake Surprise is not connected to any of the tributaries or streams from the surrounding catchment, Si and So can be eliminated from the equation. In addition, due to the smaller and steep catchment water does not flow across the surface, but permeates through fractured basaltic terrain and therefore accounts for groundwater. The primary water inflow and outflow to/from the lake can be assumed as precipitation and evaporation. Groundwater inflow/outflow to/from the lake has not been estimated up to date. However, given that the lake remains permanent with minimal water level fluctuation, particularly during arid periods and the limestone and basaltic terrain that underlies the lake catchment, suggests that groundwater is a potential component of the lake water balance. This has also been mentioned in previous work on Lake Surprise (Barr et al., 2014; Falster et al., 2018). Therefore, the isotope mass balance of Lake Surprise is expressed by the following equation (Gibson et al., 2002, 2016; Steinman et al., 2010; Jones et al., 2016; Lacey & Jones, 2018).

$$\frac{d}{dt}(V\delta_{L)} = P\delta_P + Gi\delta_{Gi} - E\delta_E - Go\delta_{Go} \qquad \text{Equation 2}$$

Where, δ_P, δ_E , δ_{Gi}, δ_{Go} & δ_L explain isotope values of precipitation, evaporation, groundwater inflow and outflow and lake water correspondingly. Delta notation represents the isotope ratios of stable isotopes of oxygen ($^{16}O/^{18}O$) and hydrogen ($^{1}H/^{2}H$) relative to VSMOW2. δ_P and δ_L values obtained by averaging the direct measurements of rainwater and lake water samples collected during the monitoring period (from 2019 – 2022). Average $\delta^{18}O$ and $\delta^{2}H$ values of precipitation are -2.80‰ and -14.40‰ respectively. The average isotope composition of lake water for the same period (2019 – 2022) was 3.16‰ for $\delta^{18}O$ and 11.99‰ for $\delta^{2}H$. The isotope composition of evaporation (δ_E) was calculated using the Craig and Gordon (1965) evaporation model (Steinman et al., 2010).

$$\delta_E = \frac{\alpha^*\delta_L - h\delta_A - \varepsilon}{1 - h + 0.001\varepsilon_K} \qquad \text{Equation 3}$$

Where h is the relative humidity normalised to surface water temperature, ε_K is the kinetic fractionation factor and δ_A is the isotope composition of atmospheric moisture over the lake. ε is the total isotope fractionation which is equal to $\varepsilon = \varepsilon^* + \varepsilon_K$, whereas $\varepsilon_K = 1000(1 - \alpha^*)$. $\delta^{18}O$ and δ^2H values of ε_K are shown to approximate $14.2 \times (1 - h)$ and $12.5 \times (1 - h)$ respectively. The normalised relative humidity is obtained from the following equation (Steinman et al., 2010).

$$h = RH \times \frac{e_{s-a}}{e_{s-w}} \quad \text{Equation 4}$$

Where, e_{s-a} and e_{s-w} are saturation vapour pressures of the overlying air and the surface water temperature in millibars respectively. e_{s-a} & $e_{s-w} = 6.108 \times \exp(\frac{17.27 \times T}{T+237.7})$, in which T is the average annual temperature of air or lake water in℃. RH is the average relative humidity (%) at Macarthur, acquired from BOM monthly statistical data from 1971 – 2000.

α^*, the reciprocal of the isotope fractionation factor (α) of $\delta^{18}O$ and δ^2H were calculated using the following equations, in which Tw indicates the lake surface water temperature in degrees Kelvin (K), where ℃ is approximated to be 287.2 K (Horita & Wesolowski, 1994; Lacey & Jones, 2018).

For $\delta^{18}O$,

$$ln\,\alpha = 0.35041(\frac{10^6}{T_w^3}) - 1.6664\left(\frac{10^3}{T_w^2}\right) + 6.7123\left(\frac{1}{T_w}\right) - 7.685 \times 10^{-3} \quad \text{Equation 5}$$

For δ^2H,

$$ln\,\alpha = 1.1588\left(\frac{T_w^3}{10^9}\right) - 1.6201\left(\frac{T_w^2}{10^6}\right) + 0.79484\left(\frac{T_w}{10^3}\right) + 2.9992\left(\frac{10^6}{T_w^3}\right) - 161.04 \times 10^{-3}$$

Equation 6

In addition, given that the lake has no surface water flux, δ_{Gi} and δ_{Go} are assumed to have the same isotope composition as precipitation and lake water respectively.

2.3.4.1 Calculating the lake water budget

Considering the lake is at a steady state where volumetric change is minimal and hydrologic flow remains constant for a given period,

$$\frac{dV}{dt} = 0 \quad \text{Equation 7}$$

Therefore, the sum of water inputs is equivalent to the sum of water outputs as revised from Equation 1

$$P + Gi = E + Go \quad \text{Equation 8}$$

Total precipitation at Lake Surprise was calculated using annual average values recorded for the last 30 years at the Macarthur rain gauge station. The precipitation over the last 30 years varies between 505.8 mm/year to 893.8 mm/year, whereas the average precipitation is 694.6 mm/year. Given that the surface area of the lake is corresponding to the water depth at the time of monitoring (~11m), which was 57430 m^2, the total amount of precipitation that fell across the entire surface area of the Lake is estimated to be $1.26*10^{-3}$ m^3/s.

Provided that the evaporation from a surface water body is a non-measurable parameter, here the formula discussed in Linacre, (1992) (Equation 5) is used to estimate the evaporation rate. Accordingly, evaporation at Lake Surprise is equivalent to $2.00*10^{-3}$ m^3/s.

$$E = [0.015 + 4 * 10^{-4}T_a + 10^{-6}z] * \left[\frac{480(T_a+0.006z)}{(84-A)-40+2.3u(T_a-T_d)}\right] mm/day. \quad \text{Equation 9}$$

Where Ta is the average air temperature (°C), Td is the dew point air temperature (°C), z, A, and u are altitude, latitude and wind speed respectively.

The following equation was used in calculating the dew point temperature (Lacey & Jones, 2018).

$$T_d = 0.52T_{min} + 0.60T_{max} - T_{max}^2 - 2.0℃ \quad \text{Equation 10}$$

Temperature variation over the last 30 years was calculated using the Macarthur data. According to the calculations, average, maximum and minimum air temperatures were 13.9°C, 18.9°C and 8.9°C respectively. In addition, the mean wind speed was calculated using the direct measurements taken at 9 am and 3 pm for 30 years (1971 – 2000) at Macarthur (BOM data) and the mean wind speed was 4.5 m/s.

Groundwater component can be further simplified by substitution of precipitation and evaporation values in Equation 8,

$$Gi - G0 = 0.0011 \text{ m}^3/\text{s} \quad \text{Equation 11}$$

Given that the lake volume is in the steady state, equation 2 can be re-expressed as follows,

$$P\delta_P + Gi\delta_{Gi} = E\delta_E + Go\delta_{Go} \quad \text{Equation 12}$$

According to the calculation of isotope composition in evaporation based on equation 3, δ_E for $\delta^{18}O$ and $\delta^{2}H$ are -14.78‰ and -55.11‰ respectively (Spreadsheet 1).

Due to the absence of any tributaries or springs, except for areas where there is considerable groundwater-surface water interaction, isotopic values of groundwater inflow likely reflect the composition of long-term average precipitation and the groundwater outflow is equivalent to the lake water isotopic composition for the given period.
Therefore the revised equation can be written as,

$$P\delta_P + Gi\delta_P = E\delta_E + Go\delta_L \quad \text{Equation 13}$$

The groundwater budget (Gi and Go) at Lake Surprise were calculated by substitution of measured values of P, δ_P and δ_L and calculated values of E and δ_E using both equations 11 and 13 (Supplementary data, Section 1).

2.3.4.2 Index lake approach

Considering that the lake is a terminal (zero throughflow) lake where long-term evaporation balances inflow and prevents liquid outflow (Qo = 0), (Gibson et al., 2002, 2016) Such that,

$$P\delta_P + Gi\delta_P = E\delta_E \quad \text{Equation 14}$$

Where, δ_P should equal to δ_E, hence the values of δ_P were substituted to δ_E in equation 3, calculate the isotope composition for the index lake as follows (Supplementary data, Section 2),

For $\delta^{18}O$,

$$-2.8 = \frac{\alpha^* \delta_L - h\delta_A - \varepsilon}{1 - h + 0.001\varepsilon_K}$$

For $\delta^{2}H$,

$$-14.4 = \frac{\alpha^* \delta_L - h\delta_A - \varepsilon}{1 - h + 0.001\varepsilon_K}$$

2.3.4.3 Stable isotope mass balance modelling of lake water oxygen isotopes

The isotope mass balance modelling approach discussed in Jones et al., (2016) (lakes in the Attenborough Nature Reserve), is used for Lake Surprise to evaluate how sensitive the lake

water isotopes are to different climate variables and to estimate the lake water level fluctuations. Equations 1 and 2 were combined to calculate the change in the isotopic value of lake water for a given time. Given that monthly data acquired from the GNIP and BOM database are used in these equations, the time difference can be assumed to be 30 days (Δt = 30 days). Equation (2) has been used in place of the expanded left side of equation (1), to make dependencies of δ_L more apparent (Jones & Imbers, 2010; Jones et al., 2016).

$$\frac{d}{dt}(V\delta_{L)} = V\ \frac{d\delta_L}{dt} + \delta_L \frac{dV}{dt} = \delta_L(P + Gi - E - Go) + V\ \frac{d\delta_L}{dt} \qquad \text{Equation 15}$$

Then δ_E was re-written as a linear function of δ_L using equation 3 as shown below,

$$\delta_E = A\delta_L + C \qquad \text{Equation 16}$$

As per equation 3,

A and C can be defined as $((\alpha^*)/(1 - h + 0.001\varepsilon_K))$ and $-((h\delta_A + \varepsilon)/(1 - h + 0.001\varepsilon_K))$ respectively.

The following equation was derived by replacing δ_E in equations 2 and 15 using equation 16

$$V\ \frac{d\delta_L}{dt} + \delta_L(P + Gi - E - Go) = \delta_P(P + Gi) - E(A\delta_L + C) - Go\delta_L \qquad \text{Equation 17}$$

Equation 17 was simplified and re-expressed as,

$$V\ \frac{d\delta_L}{dt} = (P + Gi)\delta_P - EC - (P + Gi - E(1 - A))\delta_L \qquad \text{Equation 18}$$

To simplify the notations in the following equations, β and λ were expressed as;

$\beta = (P + Gi)\delta_P - EC$ and $\lambda = P + Gi - E(1 - A)$, therefore Equation 18 can be modified as follows,

$$V\ \frac{d\delta_L}{dt} = \lambda - \beta\delta_L \qquad \text{Equation 19}$$

Provided that β and λ were generated using experimental data, they tend to take distinct values for each time step (for this study it is monthly).

Since dt is small, equations (1) and (2) characterise a lake's dynamics in a continuous form; nevertheless, field observations are often made in discrete time increments, as is the case with

the datasets presented in this analysis (dt =1 month). Because all other variables are likewise entered into the model as rates per month, dV/dt may be accurately estimated as the change in volume over 1 month.

To obtain a value for changes in δ_L for each month, the first approximation was introduced by assuming a constant value for the volume (V) for each month. This estimate is consistent with P and Gi having constant values throughout each month. V is specified as follows,

$$\bar{V} = \frac{V_{30} - V_0}{2} \qquad \text{Equation 20}$$

Where V_0 represents the starting volume on the first day of the month and V_{30} represents the total volume on the final day of each month.

Integration of equation (20) into Equation 19 yields,

$$\ln\left(\frac{\lambda - \beta\delta_{L0}}{\lambda - \beta\delta_L}\right) = \frac{\beta}{\bar{V}}\Delta t \qquad \text{Equation 21}$$

Where Δt stands for 1 for each monthly step and δ_{L0} represents the initial isotopic composition at the beginning of each month. The final expression for δ_L is given by exponentials on both sides of equation 21 as below,

$$\delta_L = \frac{1}{\beta}(\lambda - (\lambda - \beta\delta_{L0}))\exp\left(-\frac{\beta}{V}\right) \qquad \text{Equation 22}$$

Equation 22 was used in the lake model to estimate the lake level fluctuation with lake water isotope composition. Values of monthly evaporation and precipitation amount were extracted from the BOM (Macarthur) data from 2015 – 2020. Average monthly air temperature and mean relative humidity as a percentage were calculated by averaging the maximum and minimum values for the same period. Given that $\delta^{18}O$ values in precipitation are not available for the Macarthur station (BOM), isotope values were extracted from the Melbourne station (GNIP). The correlation between Macarthur and Melbourne precipitation data was tested using the linear regression analysis. Accordingly, seasonal cycling patterns in both stations are approximately similar and Macarthur precipitation shows a moderate correlation to $\delta^{18}O$ values ($R^2 = 0.27$) (Supplementary data, Section 3). Missing data (monthly $\delta^{18}O$ value) in the GNIP record, was estimated by calculating the mean value of data available for the particular month throughout the dataset (2015 – 2020). $\delta^{18}O$ values of monthly precipitation were obtained from the GNIP database at Melbourne. According to the lake bathymetry, the lake has an elongated surface area and a funnel-shaped basin (Spreadsheet 2). Due to the non-linear hypsometric relationship between lake volume and area, lake surface area also changes with volume at the

end of the given period (Δt = 30 days). The spreadsheet-based model has been modified accordingly by calculating the responsive area and depth based on the linear regression analysis of the volume vs area and volume vs depth relationship of actual measurements of the lake. The retaining lake volume at the end of each month was used in calculating the lake water oxygen and isotope ratios (Spreadsheet 2).

Based on our calculations it can be assumed that a substantial quantity of groundwater inflow and outflow occurs to and from the lake monthly, given the limited understanding of the groundwater system at Lake Surprise. Further, given that evaporation is higher than precipitation, a simple mass balance calculation demonstrates that lake water inflow should be greater than the lake water outflow for the lake to exist (Jones et al., 2016). Considering that the lake may acquire and lose the groundwater to the same basaltic and limestone deposit, Gi and Go are assumed to be constant through time (Jones et al 2016). The values of Gi and Go were changed until the normalised root mean square error of a comparison between the modelled and observed (measured) lake water isotope composition was minimised. These parameters were obtained by optimising the model output to the measured data using the Microsoft Excel Solver add-in (Spreadsheet 2).

2.4 Results

2.4.1 Physical and chemical properties of the lake

During the monitoring period, lake water depth varies from 11.02 – 12.04 m, with the greatest water level being observed between the end of 2016 and 2017. Despite the subsequent fall in water depth observed afterwards, two measurements obtained in October 2019 and December 2020 represent a similar value (11.20 m), suggesting a relatively minimal change in water depth. Measurements of Total Dissolved Solids (TDS) represent lake water salinity that ranges from 277 – 470 mg/L with an average value of 331 mg/L. TDS values remained relatively stable over time, except for the minor rise recorded after 2020. pH values range from 7.70 – 9.28, with an average value of 8.75. Relatively low salinity and high pH values indicate an alkaline, freshwater environment. During the period of more frequent/regular sampling (2015 – 2018), surface water temperature shows large fluctuations (Figure 2).

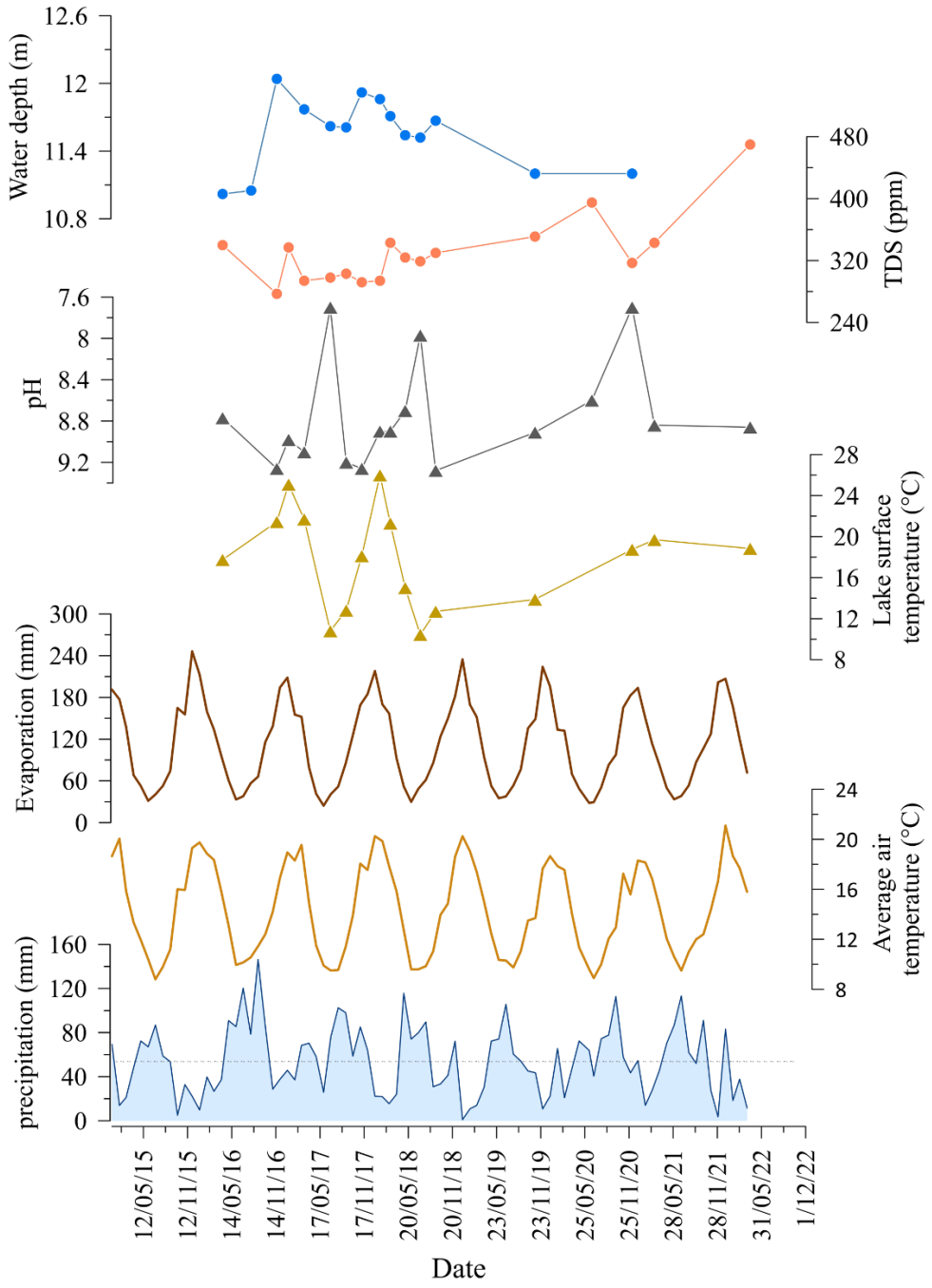

Figure 2. Time series of Lake Surprise water measurements of lake water depth, TDS, pH and surface temperature, together with monthly rainfall, mean air temperature and evaporation data at Macarthur (BOM) for the monitoring period (2015 – 2022). Lake water measurements from 2015 – 2018 were acquired from Ankor, (2020). The average precipitation value (54.7 mm) for the monitoring period is illustrated by the dotted line.

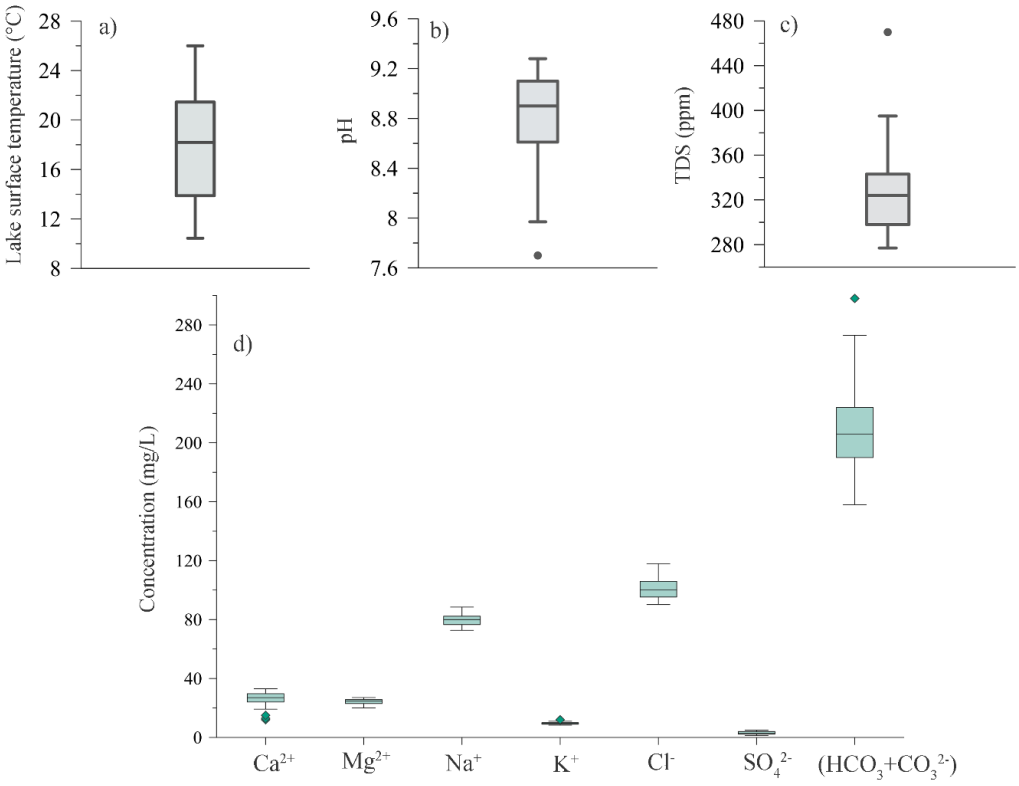

Figure 3. Descriptive statistics of hydroclimate parameters a) Lake temperature, b) pH c) TDS and d) major ions in Lake Water as Box-plot representation. Possible outliers are represented in circles and diamonds.

The surface water temperature at Lake Surprise exhibits a significant variation from 10.44 – 26℃ during the monitoring period with a mean temperature value of 17.73℃ (Appendix 2, Table II). According to the climate data recorded during the monitoring period (from January 2015 – April 2022), monthly precipitation, evaporation and mean air temperature at Macarthur vary from 1 – 146.3 mm, 24.3 – 246.3 mm and 8.8 – 21.1℃ respectively, whereas the average value for precipitation for the monitoring period is recorded as 54.7 mm. Intra-annual variation of monthly evaporation and mean air temperature variability is nearly consistent over the monitoring period, whereas monthly precipitation exhibits inconsistent variability with frequent occurrence of below-average rainfall events over the last three years. Further, climate data illustrates a considerable decrease in precipitation and a corresponding increase in evaporation and mean temperature during summer/spring months and vice versa. According to total annual precipitation data, 2016 and 2017 had the highest recorded rainfall (787.3 mm and 790.4 mm, respectively) whereas 2019 recorded the lowest rain amount (522.2 mm) for the

monitoring period. Even though there isn't a noticeable relationship between lake water parameters and climate data, the relative increase in water depth and decrease in salinity corresponds with the high rainfall events recorded between 2016 and 2017. Similarly, continuous decline in water depth and gradual increase in salinity is in agreement with rainfall decline through time.

2.4.2 General lake water chemistry

The Piper trilinear diagram represents the water chemistry of five water samples collected during the monitoring period from 2019 – 2022, the major ion chemistry of lake water samples collected from 2015 – 2018 and the average composition of lake water samples collected from 1971 – 1972.

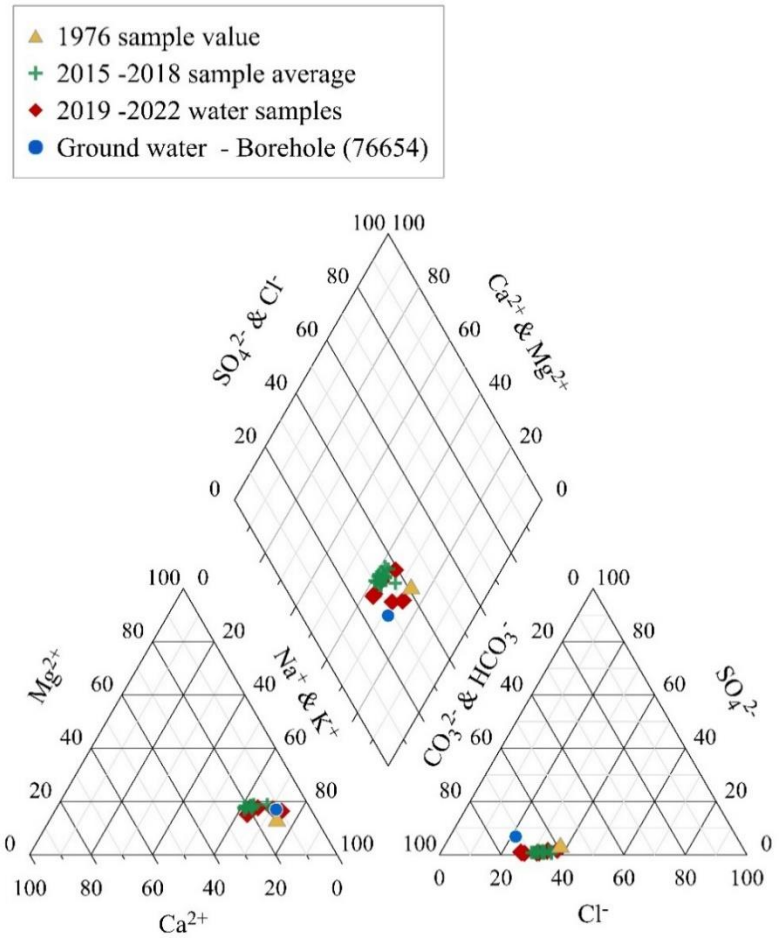

Figure 4. Piper diagram showing the chemical composition of Lake Surprise water from Timms, (1975) and the chemical composition of water samples collected from 2015 – 2018 (Ankor, 2020) and monitoring data from 2019 – 2022. Groundwater chemistry data were obtained from the nearest borehole (<2km) location to Lake Surprise.

Accordingly, lake water samples concentrate within the Na-HCO_3 type region, indicating increased dominance of (Na^+) and (HCO_3^-+CO_3^{2-}) ions. Further, the major ion concentration of groundwater obtained from the nearest borehole, which is ~1.8 km towards the south-east of Lake Surprise also indicates a similar composition to Lake Surprise water chemistry. Lake water samples collected over an approximately 50-year period (from 1971 – 2022) plot within the same region representing a similar lake water chemistry.

The cation and anion abundance in Lake Surprise was in the order of Na^+> Ca^{2+}>Mg^{2+}>K^+ and (HCO_3^-+ CO_3^{2-})>Cl^->SO_4^{2-}respectively (Figure 3d). $Na^+$is the dominant cation which varies from 72.76 – 88.50 mg/L, with an average of 79.74 mg/L (Appendix 2, Table 1). Ca^{2+} and Mg^{2+} are roughly equal in their concentrations with values ranging from 12 – 33 mg/L and 20 – 27.09 mg/L and their average concentrations are 25.56 and 24.30 mg/L, respectively. Considerably lower K^+content varies from 8.31 – 12 mg/L with an average concentration of 9.46 mg/L. The dominant anion concentration of (HCO_3^-+ CO_3^{2-}) vary from 158 – 298 mg/L with an average of 212.89 mg/L. Cl^-content also remained high with values varying from 90.20 – 118 mg/L and its average concentration is 101.09 mg/L. SO_4^{2-}concentration, which is the least abundant in Lake Surprise range from 1.24 – 5 mg/L with an average value of 3.01 mg/L. The total anion concentration is higher compared to the total cation concentration in the lake water. The considerably lower number of outliers illustrated in the statistical analysis (Figure 3d) of major ions suggests that the values are consistent. The correlation matrix of the major cation/anions (Table 1) illustrates a strong association between Ca – Mg (r>0.7) and a moderate (r = 0.5 – 0.6) to good (r = 0.6 – 0.7) association between Na – K, K – Cl and Na – Cl. Additionally, Ca – K and Ca – Cl ion pairs represent a moderate to good negative correlation.

Table 1. Correlation matrix of major ions in Lake Surprise. (*P<0.05 level of significance correlation)

	Ca^{2+}	Mg^{2+}	Na^+	K^+	Cl^-	SO_4^{2-}	HCO_3^-+CO_3^{2-}
Ca^{2+}	1						
Mg^{2+}	0.74*	1					
Na^+	-0.19	0.3	1				
K^+	-0.63*	-0.37	0.62*	1			
Cl^-	-0.57*	-0.08	0.61*	0.53*	1		
SO_4^{2-}	-0.25	-0.41	-0.23	-0.06	-0.04	1	
HCO_3^-+CO_3^{2-}	-0.01	0.05	0.11	0.28	0.35	-0.37	1

The Gibbs plot, derived from the weight ratio of $Na^+/ (Na^+ + Ca^{2+})$ and $Cl^-/(Cl^- + HCO_3^-)$ against the salinity variation (TDS) explains the relative significance of the main natural mechanisms affecting the chemistry of surface water such as evaporation–crystallization, rock weathering, and meteoric precipitation. The region within the dashed lines symbolises the end member series of three major sources of dissolved ions in the majority of the world's surface water (Gibbs, 1970; Khadka & Ramanathan, 2013; Marandi & Shand, 2018; Liu et al., 2019). Na – Cl rich, high salinity region represents the evaporation-fractional crystallization process, low salinity, Na – Cl rich region illustrates the atmospheric dominant sources whereas the opposite end member of both series represents the carbonate-rich rock dominant region (Gibbs, 1970).

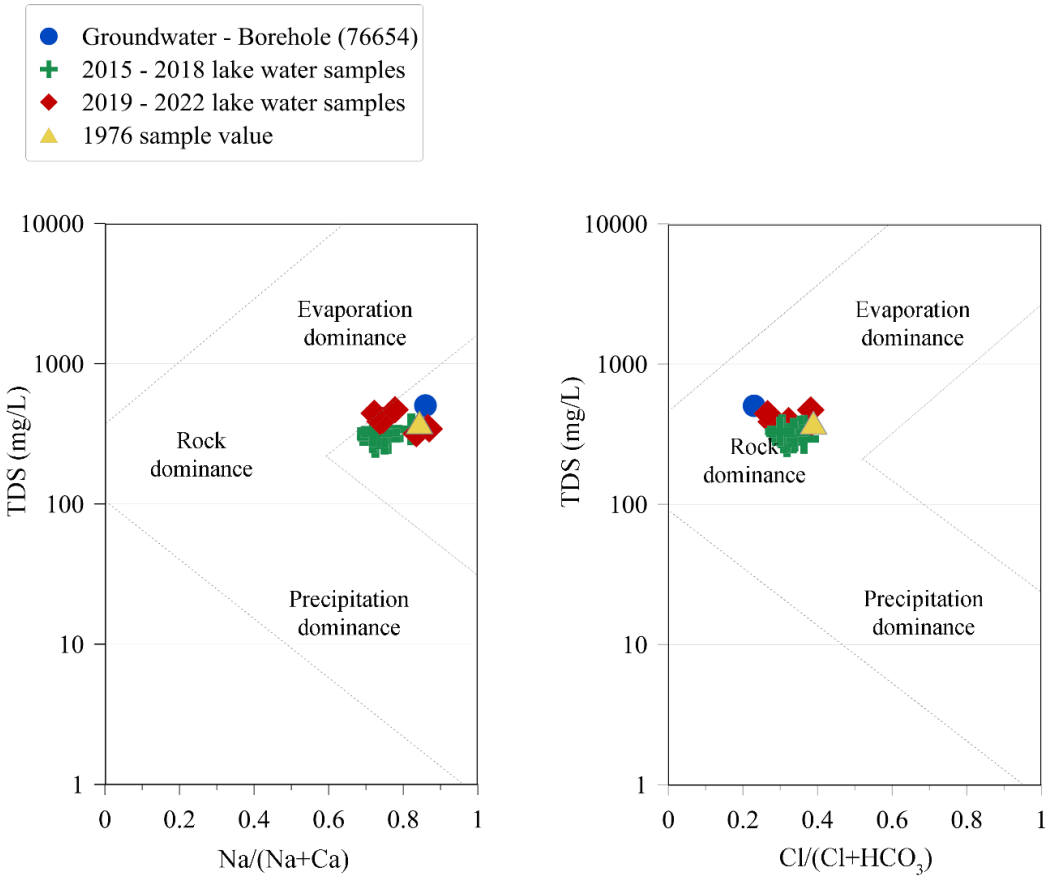

Figure 5. Gibbs representation of the chemical composition of Lake Surprise monitoring data from 2019-2022, from 2018-2015 by Ankor, (2020), Timms, 1975 and groundwater chemistry of the nearest borehole.

Accordingly, Lake Surprise ion concentration falls near the rock-dominant region representing relatively low TDS values and high carbonate content (low $Cl^-/(Cl^- + HCO_3^-)$. However, the majority of the data points in the $(Na^+/ (Na^+ + Ca^{2+})$ plot accumulate towards the edge, exhibiting low salinity but a considerably high amount of Na in lake water. However, water

chemistry still accounts for the rock-dominant zone. Likewise, groundwater chemistry (Borehole 76654) also plots near the rock-dominant zone as expected. Additionally, it is acceptable that depending on the regional differences in hydrologic flow patterns and biogeochemical processes, lake water chemistry can exceed the original Gibbs envelope (Xu et al., 2010).

2.4.3 Stable oxygen and hydrogen isotopes in lake water

Using deuterium excess (d-excess) and HCO_3^-/Cl^- ratio of western Victorian lakes, Barton et al., (2013) proposed a method that can be used to define the groundwater influence and residence time of lakes. Accordingly, HCO_3^-/Cl^-ratio may indicate whether a lake is groundwater-fed or surface water-fed, where lakes have greater HCO_3^-/Cl^- ratio are considered to be surface water-fed lakes and vice versa (Barton et al., 2013). Similarly, the d-excess value derived using the lake water oxygen ($\delta^{18}O_{LW}$) and hydrogen ($\delta^{2}H_{LW}$) isotopes were used to calculate the lake's residence time, in which the lake's lower d-excess values are taken to indicate that lakes have a longer residence time and preferably a terminal lake. Whereas, lakes with higher d-excess value are primarily through-flow lakes with a shorter residence time (Barton et al., 2013). Based on the range of lakes in western Victorian plains, (Barton et al., 2013) proposed boundaries between lower and Higher categories of HCO_3^-/Cl^-ratio and d-excess value as 0.08 and (-2‰) respectively.

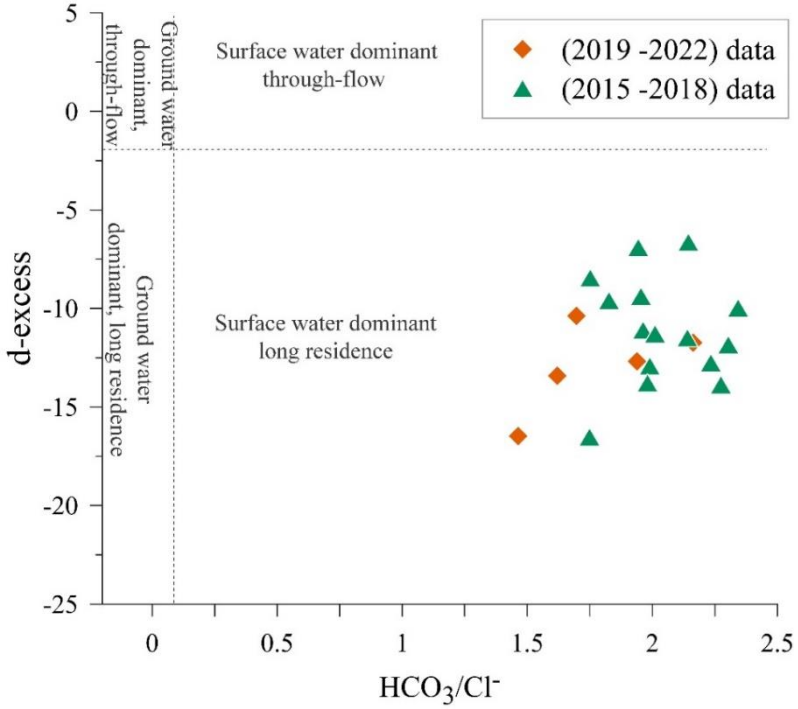

Figure 6. Deuterium excess vs HCO_3^-/Cl^- ratio of lake water samples

Deuterium excess of Lake Surprise water samples collected from 2015 – 2022 range from (- 19.94 to -6.64‰), whereas the HCO_3^-/Cl^- ratio varies from 1.46 to 2.34. Following the boundaries explained above all the lake water samples were placed in the surface water dominant, long-residence time category with relatively high HCO_3^-/Cl^- ratios (>0.08) and lower d-excess values (<-2‰) (Figure 6). Lake water oxygen ($\delta^{18}O_{LW}$) and hydrogen ($\delta^{2}H_{LW}$) isotopes vary from 1.68 – 4.41‰ and 6.7 – 17.32‰ with mean values of 2.95‰ and 11.23‰ respectively, between 2015 and April 2022 (Appendix 2, Table II). Isotope values of precipitation collected at Macarthur (from 2019 – 2021) illustrate considerably depleted values compared to lake water isotopes with $\delta^{18}O$ varying from -8.92 – 1.89‰ and $\delta^{2}H$ from -67.65 – 15.52‰ (Appendix 2, Table III). The linear correlation between $\delta^{18}O$ and $\delta^{2}H$ of precipitation and lake water is defined by the LMWL and the LEL as illustrated in figure 7.

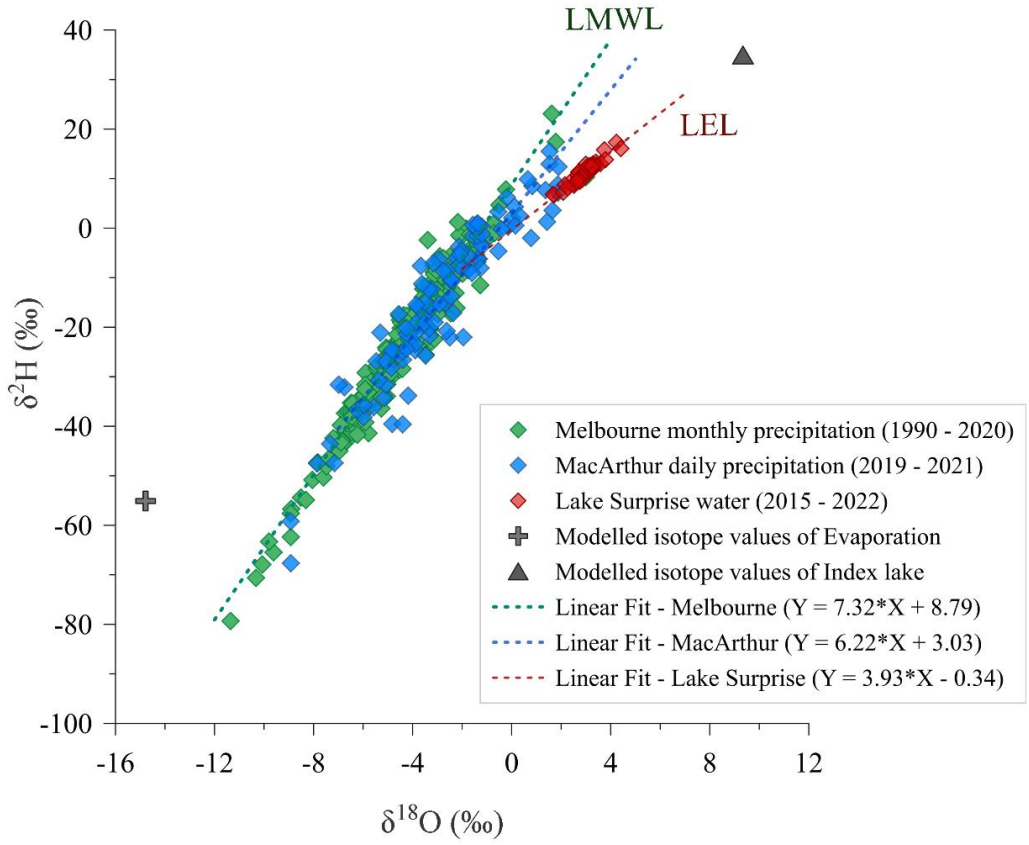

Figure 7. Bi-plot of $\delta^{2}H$ – $\delta^{18}O$ for lake water and precipitation and representation of the isotope composition of the evaporation in the lake during steady-state (cross) and isotope composition of lake water for the Index Lake (triangle). Local Meteoric Water line (LMWL) for Melbourne precipitation data and Local Evaporation Line (LEL) for lake water isotope data along with Ordinary Linear Square Regression line (OLSR) for Macarthur precipitation are shown in the plot.

Linear regression analysis of Macarthur precipitation data represents a slightly smaller slope (m = 6.22) in comparison to the slope of the LMWL (m = 7.32) derived from the Melbourne precipitation values (Figure 7). LEL deviates from the LMWL with a slope of 3.93, where the majority of the lake water isotopes remained enriched throughout the monitoring period. LMWL and LEL intersect at an isotopic value of -2.69‰ for $\delta^{18}O$ and -10.91‰ for $\delta^{2}H$.

2.4.4 Lake isotope mass balance modelling

2.4.4.1 Hydrologic budget calculation for Lake Surprise

Table 2. Water budget for Lake Surprise based on coupled hydrologic and isotopic mass balance calculations for the period of 2019 – 2022 (Spreadsheet 1).

	Source	Flow rate ($*10^{-3}m^3/s$)	Percentage (%)	$\delta^{18}O$	$\delta^{2}H$
Input	Precipitation - P	1.26	21	-2.80	-14.40
	Surface inflow	0.00	0	-	-
	Groundwater inflow - Gi	4.80	79	-2.80	-14.40
Output	Evaporation - E	2.00	33	-14.78	-55.11
	Surface outflow	0.00	0	-	-
	Groundwater outflow - Go	4.06	67	3.16	11.99

According to the lake water balance calculations, the flow rates of Gi and Go account for $4.80*10^{-3}$ m^3/s and $4.06*10^{-3}$ m^3/s respectively, establishing a novel water balance estimate for Lake Surprise. The total water input and output into/from the lake at a steady state are calculated to be $6.06*10^{-3}$ m^3/s (Table 2). Overall, the groundwater contributes 79% of the lake's water input remaining 21% is from precipitation, whilst water outflow from the lake is estimated to be a combination of 67% of groundwater and 33% of evaporation. When the total water inflow is combined with the lake volume at its maximum water depth (~12m), which is $3.114*10^{4}$ m^3, the water residence time of the lake is accounted to be approximately 1.36 years. $\delta^{18}O$ and $\delta^{2}H$ values of calculated evaporation at Lake Surprise following Equation 3, plots towards the negative end of the LEL (Figure 7). The isotope composition of the theoretical Index lake calculated based on Equation 13, sits at the positive end of the LEL with enriched $\delta^{18}O$ and $\delta^{2}H$ values of 9.29‰ and 34.47‰ (Figure 7) (Supplementary data, Section 2). Isotope composition of the evaporation (δ_E) is comparably depleted with values of -14.78‰ for $\delta^{18}O$

and -55.11‰ for δ^2H at the steady state of the lake. δ_E lies towards the left extension of the LEL (Figure 7). Index lake method based δ_A results noticeably lower values for $\delta^{18}O$ and δ^2H as -12.66‰ and -94.2‰ respectively, which plot close to along the LMWL (Figure 7).

2.4.4.2 Lake model performance

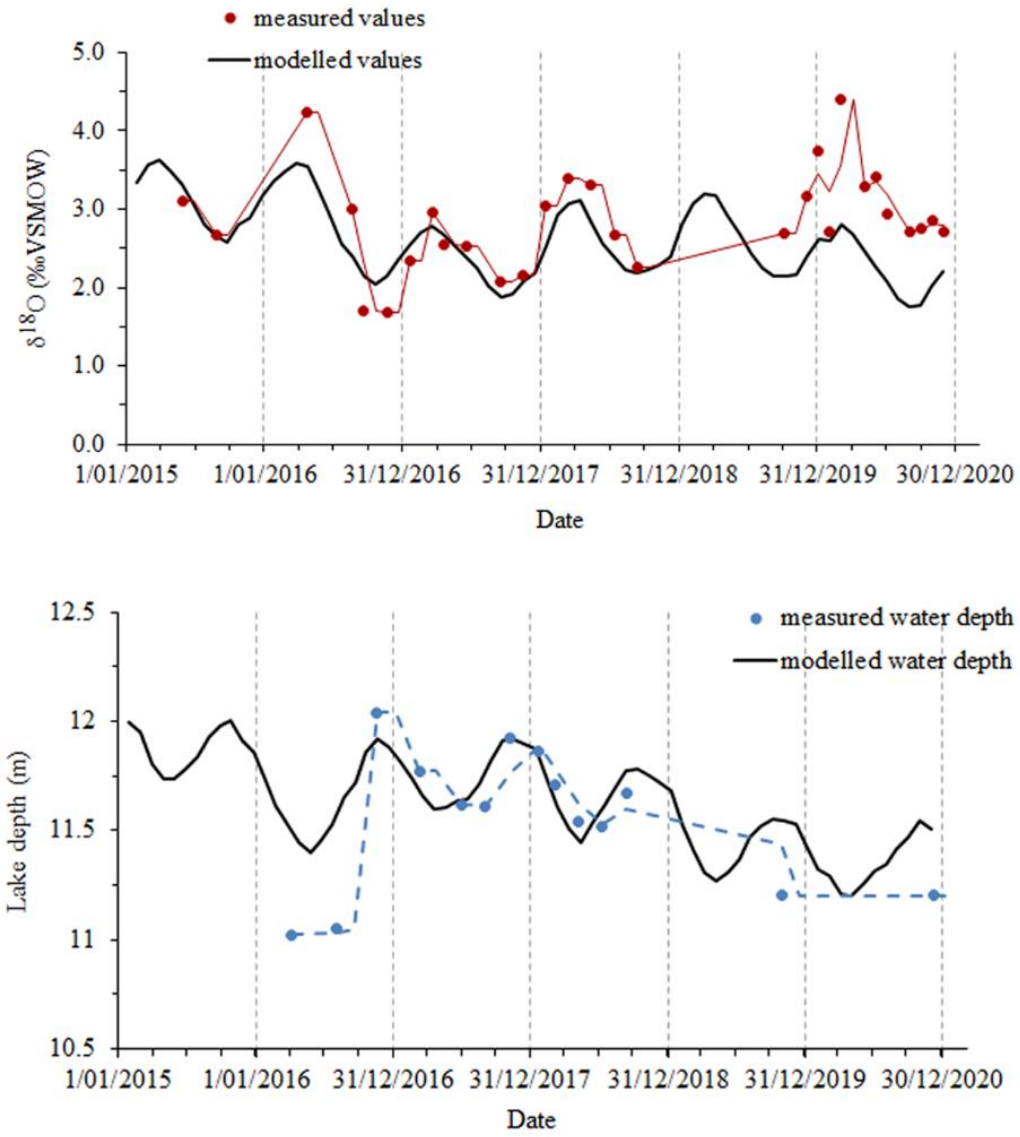

Figure 8. Measured and modelled (black) comparison of $\delta^{18}O$ model for Lake Surprise. Best-fit of the modelled and measured water depth is shown in the bottom diagram. Vertical dashed lines mark calendar years.

The amount of total Gi and Go needed to obtain the best-fit model for Lake Surprise, are 7500 m^3/month and 5490 m^3/month respectively (Spreadsheet 2). However, these values slightly deviate from the estimated total groundwater inflow ($4.80*10^{-3}$ m^3/s) and total groundwater outflow ($4.06*10^{-3}$ m^3/s) rates of the steady-state model (Table 2). The accuracy of the model was assessed by comparing the water depth measurements against the modelled water level. Despite the fact there are multiple occurrences of missing data, The average value of the simulated water depth (11.62 ±0.21 m) is nearly equivalent to the average of the measured water depth (11.55±0.32 m). Similarly, the average modelled lake water $\delta^{18}O$ value (2.61±0.49) is comparable with the measured value of 2.86±0.63 (Spreadsheet 2). The model simulates an intra-annual variability pattern that is approximately consistent with the measured values throughout the monitoring period. When lake water isotope measurements are significantly higher than average, there is a greater divergence between the model and data comparison, especially after 2019 (Spreadsheet 2).

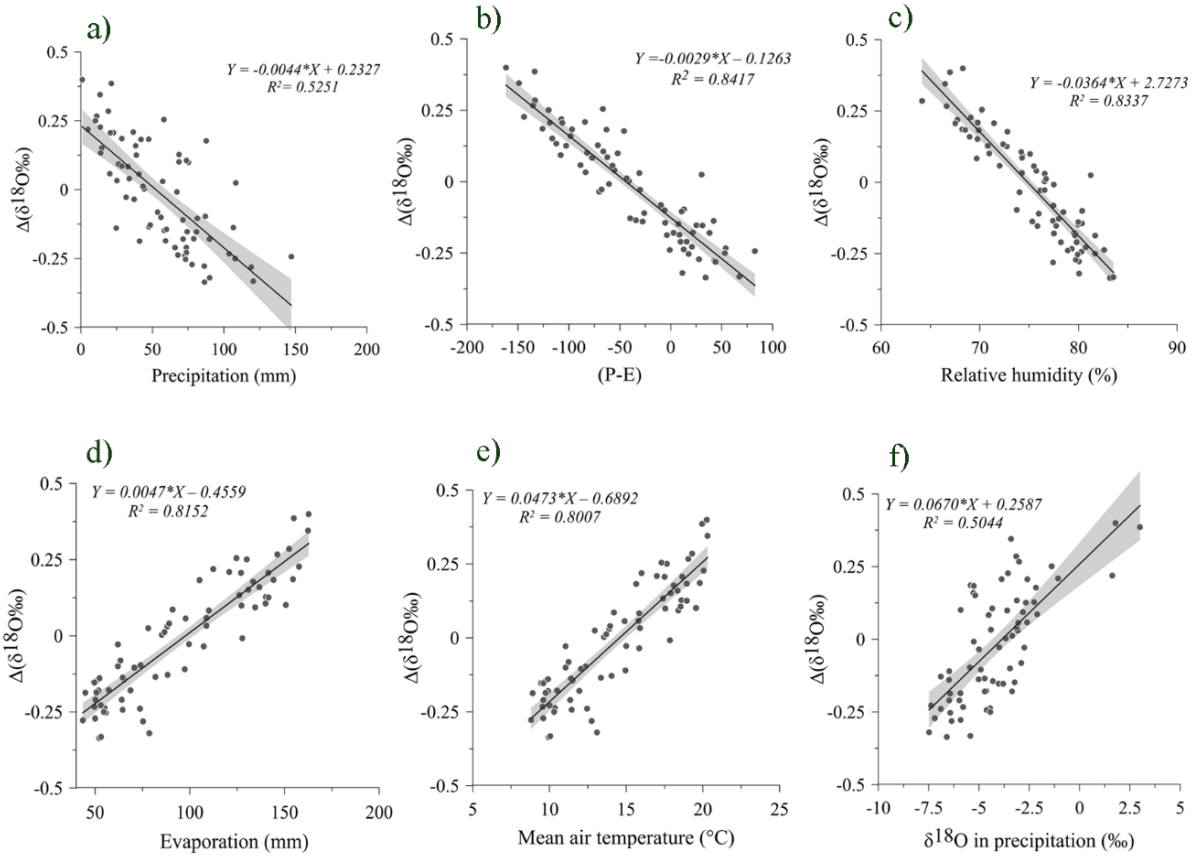

Figure 9. Linear correlation between modelled lake water isotope change ($\Delta\delta^{18}O‰$) for a given period (dt = 30 days) and climate variables of precipitation, evaporation, effective precipitation (P-E), Mean air temperature, relative humidity and $\delta^{18}O$ in precipitation. (P value <0.0001). The Grey shaded area represents the 95% confidence interval of the data.

Climate variables seem to correspond well with the change in the modelled lake water isotopes ($\Delta\delta^{18}O$) for a given period, for which 30 days in this study compared to the modelled water isotopes alone (Figure 9). Effective precipitation (P-E), mean air temperature, relative humidity and precipitation represent a negative linear correlation, whereas evaporation and isotope values in precipitation ($\delta^{18}O_P$) positively correlate with the model ($\Delta\delta^{18}O$). Evaporation, mean air temperature, relative humidity and effective precipitation strongly correlate with the $\Delta\delta^{18}O$‰ ($R^2 \geq 0.80$), whilst precipitation and $\delta^{18}O_P$ demonstrate moderate correlations (R^2 = 0.50 – 0.53).

2.5 Discussion

Groundwater is thought to play a significant role in maintaining water levels in western Victorian crater lakes, due to the limited runoff from the surrounding catchment and considerably lower rainfall recorded in the region (Jankowski & Jacobson, 1989; Tweed et al., 2009; Barton et al., 2013; Yihdego et al., 2016; Yihdego & Webb, 2012, 2015). Several hydrogeological features in the region, including groundwater discharge (springs) at the break of slope and regional groundwater discharge when shallow bedrock ridges act as hydraulic barriers to lateral groundwater flow, have been recognised as significant controls of groundwater inflow to lakes (Yihdego & Webb, 2015). According to previous records, many of these lakes were identified as throughflow lakes, in which both inflow and outflow occur via groundwater system (Lake Mumblin, Lake Purrumbete, Lake Colongulac, and Lake Weering) and some as discharge lakes where surface water outlets remove water from the lake (Lake Beeac) (Barton et al., 2013; Ankor, 2020). The majority of the lakes that are considered to be influenced by groundwater are either shallow lakes (Lake Colac, Lake Weering) that are hydraulically related to the nearby unconfined aquifer systems or saline to hyper-saline lakes (Lake Keilambete, East and West Basin,), in which prolonged drying may cause permanent disappearance or noticeable lowering of the water level (Winter, 1981; Yihdego & Webb, 2015). Using this study it can be demonstrated that groundwater flux has a greater contribution to the hydraulic budget of Lake Surprise which belongs to very few freshwater lakes available in the western plains.

2.5.1 Sources of dissolved ions and major mechanisms that control lake hydrochemistry

As illustrated in the Gibbs model, the lake water is mainly governed by water-rock interaction and the abundance of major cations Na^+, Ca^{2+} and anions of HCO_3^- in surface water further, support our observation. Strong consistency between lake water and nearby groundwater composition demonstrates groundwater is likely to be the dominant source of lake water hydrochemistry. However, according to lake classification by (Barton et al., 2013), Lake Surprise falls into the surface water dominant, long-residence time category (Ankor, 2020). Gibbs model analysis and the long-term freshwater environment observed in this study suggest that groundwater flow exceeds the impact of precipitation or evaporation on lake water chemistry. A High HCO_3^-/Cl^- ratio may explain the groundwater flow across "stony rises", less weathered, yet more fractured younger basalt layers where greater HCO_3^- production occurs due to higher recharge rates (Nolan, 1990; Dessert et al., 2003; Ankor, 2020). Provided that these stony rise basalts are highly permeable and frequently have springs at their margins, thin soils that overlie these basalts allow rapid recharging, producing the least saline groundwater in the region (Raiber et al., 2009; Yihdego et al., 2015; Webb, 2016). Unlike many other lakes in the western plains, Lake Surprise shows minimal water level fluctuations, especially during periods of historical droughts and the lack of surface drainage further demonstrates that the lake is likely to be fed by groundwater, besides precipitation (Barr et al., 2014).

According to geological records, carbonate dissolution and silicate weathering may be the most prominent sources of groundwater chemistry in the region. It is estimated that the Port Campbell Limestone, that underlain Lake Surprise has more than 25% of permeability and porosity throughout and is dominated by carbonates, calcites and to a lesser amount dolomites (Radke et al., 2022). Weathering of plagioclase and silica-dominant basaltic lava flows produces thick layers of kaolinite as the initial by-product and other clay minerals (Boyce, 2013; Boyce et al., 2014; Webb, 2016). Hydrolysis plagioclase and carbonate dissolution may have contributed to dominant ions in lake water such as Na^+, Ca^{2+}, Mg^{2+} and HCO_3^-. Correlation between Ca^{2+} and Mg^{2+} ions and Na and K^+ ions may reflect that both ions share a common source and potential cation exchange between these ions. Yet, a lesser amount of K^+ demonstrates a deficiency of alkali feldspar in basaltic environments. Possible chemical reactions for both carbonate dissolution and silicate weathering can be explained as follows (Chae et al., 2006; Zhang et al., 2020).

Carbonate dissolution for alkaline water,

$$CaCO_3 + H_2O = Ca^{2+} + HCO_3^- + OH^- \quad \text{Equation 23}$$

Plagioclase hydrolysis

$$(NaCa)AlSiO + H_2O + CO_2 = Na^+ + Ca^{2+} + Al_2Si_2O_5(OH)_4 + H_4SiO_4 + HCO_3^- \quad \text{Equation 24}$$

Relatively high Na-normalised molar ratios were observed in lake water (Na^+/Cl^-, Na^+/Mg^{2+}, Na^+/Ca^{2+}, Na^+/K^+>1) and the groundwater sample suggests that silicate weathering is likely to be the predominant source of water chemistry (Appendix 2, Table I) (Dessert et al., 2003; Zhang et al., 2020). This is supported by the high $Na^+/(Na^+ + Ca^{2+})$ ratio in the Gibbs envelop model, which suggests silicate weathering overrides carbonate dissolution (Gascoyne, 2004; Banks & Frengstad, 2006). However, the ratios of (Na^+/K^+)/total cation and $(Ca^{2+}+Mg^{2+})$/total cations vary from ~0.50 to 0.65 and 0.36 to 0.50 respectively, suggesting that the predominance of silicate weathering relative to carbonate dissolution is lesser (Zhang et al., 2020; Gaur et al., 2022). This is further highlighted by the (Na^+/HCO_3^-) ratio which is approximately near or above 1. Additionally, cation exchange, particularly in Na-HCO_3-type waters may also lead to carbonate depletion by the removal of carbonates from the solution (Chae et al., 2006). $Ca^{2+}+Mg^{2+}$ vs Na^+ is used as an indicator of the ion exchange process in water bodies (Appendix 2, Table I). Na-dominated bicarbonate waters (Na-HCO_3) can originate from Ca-Mg-HCO_3 by cation exchange on clay minerals. This indicates input from groundwater in contact with calcite since Ca-Mg-HCO_3 waters are typically produced by the dissolution of carbonate minerals (i.e., calcite and dolomite) (Xiao et al., 2015; Zhang et al., 2020). The presence of samples on both sides of the 1:1 equiline, suggests both ion exchange and reverse exchange influence water chemistry (Gaur et al., 2022). Hypothetical ion exchange and reverse ion exchange equations are represented by equations 25 and 26 respectively,

$$2Na^+ + CaX_2 = Ca^{2+} + 2NaX \quad \text{Equation 25}$$

$$Ca^{2+} + 2NaX = 2Na^+ + CaX_2 \quad \text{Equation 26}$$

Besides rock weathering, atmospheric rainfall that drains into the groundwater system or directly falls on the lake also contributes to Na^+ and Cl^- ions in the lake water. SO_4^{2-} ions in

lake water are considerably lower compared to other major ions and may have derived either from weathering of evaporative minerals such as gypsum and anhydrite or the oxidation of pyrite. Previous studies from Lake Surprise provide evidence of gypsum formation under evaporative conditions (Falster et al., 2018). In addition, major ion concentration in lake water may vary depending on the lake-specific processes such as primary productivity, organic matter decomposition and evaporation.

2.5.2 Stable isotope variation in lake water

The linear correlation between $\delta^{18}O$ and $\delta^{2}H$ in water bodies is used for the qualitative analysis of isotopic separation between different sources of water. The Global Meteoric Water Line (GMWL) was first defined by (Craig, 1961), using the least square regression analysis of more than 400 water samples collected globally and is considered to be comparable to the LMWL, which is usually constrained to a specific region. The LEL reflects the degree to which individual lakes deviate from the LMWL to denote the proportion of water lost to evaporation (Gibson et al., 2002; Yi et al., 2008; Shi et al., 2017; Vystavna et al., 2021). Due to the increasing removal of lighter molecules during evaporation, lake water bodies become enriched in $\delta^{18}O$, which generates considerably higher values of isotope readings (Craig, 1961; Gat, 1995; Gibson et al., 2002; Leng & Marshall, 2004; Horita et al., 2008; Jones et al., 2016). Diffusion-controlled kinetic fractionation of water molecules initiates the deviation of the evaporation trend from the meteoric water line (Craig and Gordon, 1965; Shapley et al., 2008). Accordingly, more positive $\delta^{18}O$ and $\delta^{2}H$ values in Lake Surprise that produces the LEL indicate evaporation as one of the major controls of Lake Isotope variability. This agrees with the idea of evaporative enrichment of lake isotopes in temperate climates with an intermediate slope between LEL and LMWL (Gibson et al., 2016).

The slope of the LMWL at Melbourne is generally calculated to be ~7 (Liu et al., 2010; Hughes & Crawford, 2012), however, precipitation isotope data collected at Macarthur slightly deviates (~1 degree) from LMWL denoting the presence of erroneous measurements. Therefore, all data points were equally weighted using the ordinary least squares regression (OLSR) analysis and residual regression analysis was applied to eliminate outliers in the data set (Payne, 1991; Fischer and Treble, 2008). According to the residual regression of the deuterium excess value (difference between the response variable and the predicted variable), few data points (four data points) plot further than the two–standard deviation limit (±10.85), indicating isotope

reading may not be the cause of the deviation (Supplementary data, Section 4). Therefore, comparatively high isotopic values in precipitation may indicate the effects of evaporation from sample containers with a smaller amount of precipitation or isotopic fractionation that occurred between air and water during transferring of samples for analysis. Given that the OLSR method doesn't rely on precipitation data, it is believed that the results may indicate unintended consequences of the amount of precipitation (Hughes & Crawford, 2012). However, these biases may be addressed by applying effective methods like Precipitation Weighted Linear Square Regression (PWLSR), which takes into account the amount of precipitation in the calculation (Hughes & Crawford, 2012). Yet, the application of PWLSR was limited in this study due to the absence of precipitation amount data from the same location.

However, the slope of the evaporation line can also change with, the modification of lake water isotope composition due to other factors such as lake size, residence time, latitude, humidity and atmospheric moisture conditions (Gibson & Edwards, 2002; Leng & Marshall, 2004; Gibson et al., 2016). The approximate source composition of the lake water isotopes (in this study, $\delta_I = \delta_P$) are illustrated by the intersection point between LMWL and LEL (Gat, 1995; Yi et al., 2008; Bowen et al., 2018; Li et al., 2022). Even though, both precipitation and groundwater inflow account for the total water input at Lake Surprise, assuming groundwater also originated from precipitation, the intersection value should correspond with the average isotope composition of precipitation. The source water isotope composition observed in these samples is approximately close to the average precipitation value recorded at Macarthur (from 2019 – 2022), with 0.1‰ offset for $\delta^{18}O$ and ~3.4‰ offset for $\delta^{2}H$. However, previous studies have also identified that frequently employed linear extrapolation methods may represent a mixture of the water sources that are (linearly) weighted, which may undermine the individual sources (Bowen et al., 2018).

2.5.3 Lake Isotope mass balance modelling

With the need for an additional equation to resolve multiple unknown components (groundwater inflow and outflow) in the water balance equation, Dincer, (1968) noted that incorporation of the isotope component (deuterium and oxygen) in the water balance equations can be more reliable, as water isotope tracers cannot be removed from a system via adsorption, precipitation, or any other biological or chemical processes, which can result in less spatial and temporal variability. Natural isotopic enrichment in lake water isotopes; in which lighter

isotopes preferentially remove from a system during evaporation has been used as the basis for these isotopic parameters (Dincer, 1968; Gat, 1995; Krabbenhoft et al., 1990; Gibson, 2001). With the theoretical framework for simulating and quantitatively interpreting isotopic signals, the isotope mass balance approach has been increasingly used in estimating the hydrologic budget and correctly interpreting climate signals in both open and closed lakes.

2.5.3.1 Lake Surprise water balance and groundwater flux estimations

For a system that may be considered to be at an isotopic and hydrologic steady state, the isotope mass balance equation (Equation 8) can be used most simply and accurately, to determine the components of the hydrologic budget (Krabbenhoft et al., 1990; Gat, 1995; Jones & Imbers, 2010; Gibson & Reid, 2014; Lacey & Jones, 2018). However, given that δ_E depends on the molecular exchange between the lake and atmospheric moisture (δ_A) (Equation 3), determining δ_A is difficult since it demands the collection of a direct sample, which might result in unexpected isotopic fractionation (Gat, 1995; Yi et al., 2008). Since then multiple attempts have been taken to measure δ_A such as the evaporation-pan model and application of assumptions like evaporation flux-weighted local precipitation and atmospheric moisture are in isotopic equilibrium (Welhan & Fritz, 1977; Zuber, 1983; Gibson et al., 1993, 1999, 2002; Edwards, 2004). Yet, these methods were not successful because of the faster integration times in these evaporation pans and equilibrium fractionation between precipitation and atmospheric moisture may not valid when there is considerable terrestrial recycling of evapotranspirative vapour (Gat, 1995; Yi et al., 2008).

Dincer, (1968) suggested a more promising approach, namely the usage of an "index lake", which is a terminal lake with zero through flow where total inflow is balanced by evaporation (E/I =1), (Gat, 1995; Gibson et al., 2002, 2016; Yi et al., 2008). However, this approach has been used for multiple other lakes with known water and isotope balances to calculate the limiting isotope enrichment, the maximal isotopic composition achievable in the given atmospheric circumstances a lake draws nearer to desiccation (Gat, 1995; Yi et al., 2008; Gibson & Reid, 2014; Gibson et al., 2016). As explained by Gibson et al., (2016), δ_A can be defined using the measurements of LEL. The Index lake approach was used as a starting point in this study, considering $\delta_E = \delta_P$, to determine the δ_L of the index lake (Equation 14). As expected, more enriched $\delta^{18}O$ and $\delta^{2}H$ values of the index lake plots at the maximum end of the projected LEL and away from the actual measurements of δ_L demonstrating that the lake

does not exist in a terminal state (Gibson et al., 2016), but the groundwater influx may affect the lake hydrology (Shapley et al., 2008).

Our interpretation of observational data, which indicates a groundwater-dominant, through-flow lake condition, is further supported by the index lake approach (Gibson & Reid, 2014). In agreement with the Craig – Gordan model, evaporative flux in the lake during the steady state is more depleted in heavy isotopes suggesting increased dominance of lighter isotopes in the evaporation vapour (Gat, 1995; Gibson et al., 2002; Horita et al., 2008; Liu et al., 2019). Similarly, δ_E lies along the left end of the extended LEL, referring to light and heavy isotopic fractionation that originates from the lake water (Yi et al., 2008). Similarly, more depleted values of δ_A indicate the abundance of lighter isotopes in the atmospheric moisture that may resultant from the local precipitation (Gibson et al., 2002, 2016). According to the coupled hydrologic-isotopic water balance derived for Lake Surprise, the majority of the water balance is controlled by the groundwater flux. However, the lake's isotopic composition is likely to be balanced by atmospheric precipitation and evaporation as no known surface drainage connects with the lake (Timms, 1975; Barr et al., 2014; Falster et al., 2018).

The presence of stony rise basalts, thick layers of weathered basalts and limestone well explain the dominance of groundwater inflow into the lake (Boyce, 2013; Webb, 2016; Ankor, 2020). Similarly, significant depth (>10 m) and the steep, inclined catchment and funnel-shaped lake basin induce the hydraulic gradient between lake water and groundwater level, increasing groundwater inflow/outflow. Since the water depth was first monitored in 1971 and even during the Millennium Drought (1997–2010), water depth at Lake Surprise illustrated a minimal change, fluctuating within a range of 1 – 2.6 m (Timms, 1975; Barr et al., 2014; Ankor, 2020). Relatively high groundwater outflow in comparison to evaporation, and associated removal of salt from the lake may also account for the fresh water conditions in the lake. Considerably low surface area to water depth ratio and dense vegetation that reduces the approximate open surface area further supports the idea of the extensive impact of groundwater recharge compared to the impact of evaporation on the lake water balance. A similar argument has been made previously for lakes Purrumbete and Burrumbeet, which are freshwater, and deep crater lakes and also account for considerable groundwater flux. (Yihdego & Webb, 2015; Yihdego et al., 2016).

2.5.3.2 Model Performance and sensitivity at Lake Surprise

A spreadsheet-based model using a stable isotope mass balance equation for a well-mixed lake was initially developed by Jones et al., (2016) to evaluate the model performance and to investigate dominant controls of lake isotope variability in the Attenborough Ponds, Nottingham, United Kingdom. The same model was adopted for Lake Surprise but with certain modifications. Given that Lake Surprise has no evidence of surface inflow or flooding, threshold values in absolute and effective rainfall were eliminated, in which if the thresholds are surpassed, surface inflow occurs and the lake fills to its maximum depth. Evaluation of the model performance was limited to some extent due to the inadequate coverage and inconsistency of the observation data. The inadequacy of monitoring data (missing data and erroneous observations due to instrumental failures) also caused limitations in the comparison of the model output to the actual lake status. The greater deviation between the model output and the lake water isotopes when $\delta^{18}O$ values were higher may indicate a weakening of the model sensitivity to increased thermal stratification caused by either a long-term decline of rainfall or due to low wind stress and warm conditions (Figure 8). During summer stratification, lack of mixing causes the lake epilimnion to act as a separate floating system with more enriched heavy isotopes compared to the hypolimnion and thermocline (Gat, 1995; Rivera et al., 2007). This effect has previously been noted for deeper lakes (>30 m), and solved by adding lake water isotope composition of epilimnion and hypolimnion separately into the mass balance equation (Lerman, 1971; Gat, 1995). The offset observed in this study is probably not too significant given that Lake Surprise is only 10–12 m deep and undergoes seasonal stratification and mixing cycles. Further, these limitations may have caused an offset in the resultant value of groundwater flux in this model approach and steady-state lake. Despite these limitations, nearly equal average values of modelled and measured data and the minimal offset between the best-fit model and the actual lake variability demonstrate that the model output is acceptable.

2.5.4 Major controls of Lake Surprise isotope variability

A strong linear correlation of $\Delta\delta^{18}O$ with effective precipitation and evaporation (Figure 9b & d) indicates that lake water isotope variability is likely to be controlled by the balance of precipitation vs. evaporation. These variables are indirectly governed by air temperature and relative humidity, which are key controls of lake water evaporation, where the rise in temperature increases evaporation and decreases the relative humidity (Supplementary data,

Figure IV) (Gibson et al., 2016; Shi et al., 2017; Vystavna et al., 2021). This observation may be further evaluated by assessing the model performance while the climatic variables are changing (Table 1).

Table 3: Response model output (average lake water depth ± standard deviation) for variations in the groundwater inflow and outflow

Variable	Best-fit model	(+10‰) Gi & Go	(-10‰) Gi & Go	(+20‰) Gi & Go	(-20‰) Gi & Go
$\delta^{18}O_{LW}$ (‰)	2.57±0.50	2.39±0.52	2.75±0.48	2.23±0.54	2.95±0.46
Water depth (m)	11.59±0.23	11.73±0.18	11.46±0.28	11.86±0.16	11.33±0.35

Changing both Gi and Go at the same time impacts the model output by fluctuating simulated water isotopes and the responsive water depth depending on whether the groundwater values are lowered or raised. When groundwater values were increased by 10‰ and 20‰, average water depth decreased by approximately 0.2‰ and 0.4‰ respectively while increasing the responsive water level. Similarly, decreasing both the Gi and Go by the same percentage, raises the mean value of lake isotopes to the same proportion. Thus, the linear relationship between modelled lake isotopes and climate variables remained consistent with the original model output.

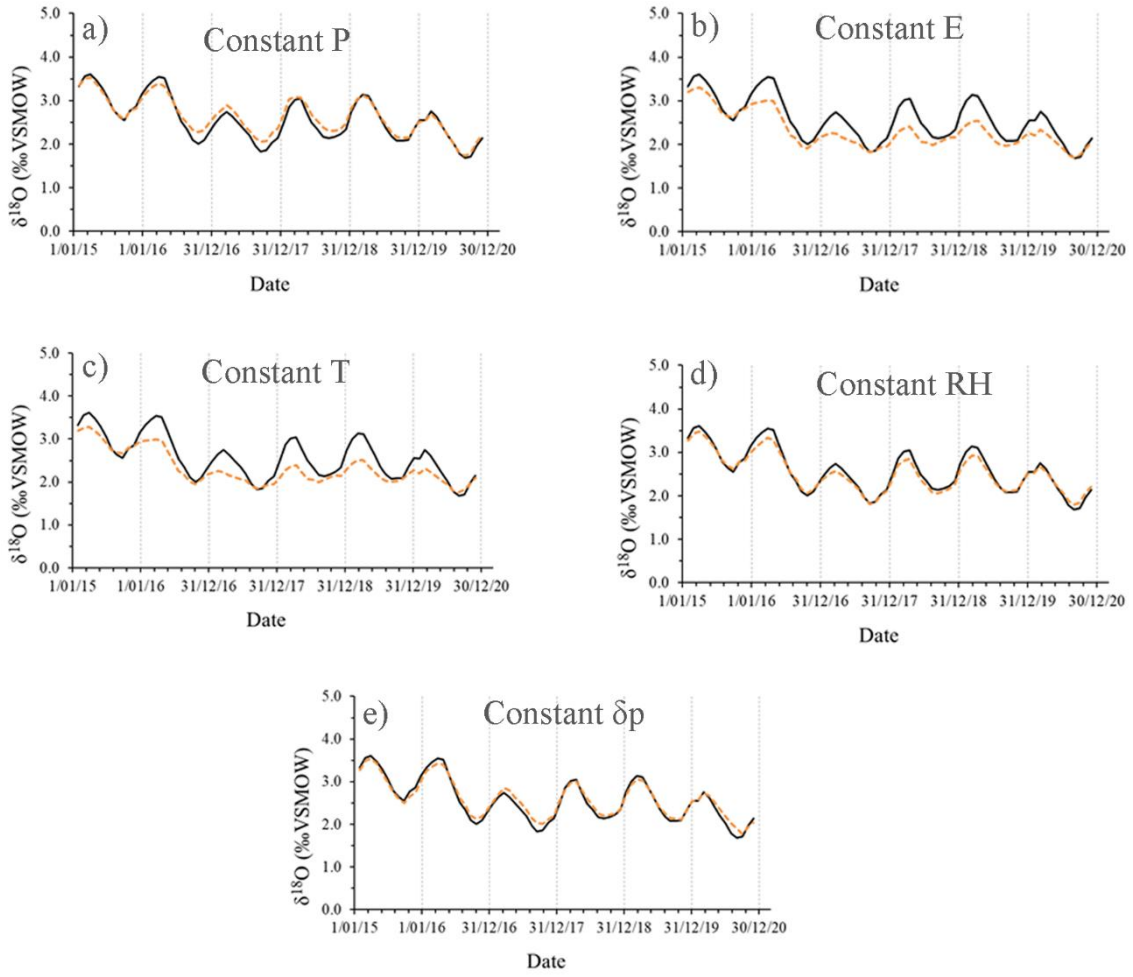

Figure 10: Sensitivity tests of the mass balance model response if different climate variables are held constant at their mean values through the monitoring period compared to the best-fit model (black line). The dashed orange line represents the response of the modelled $\delta^{18}O$ (‰) in lake water.

The sensitivity of the model output was tested by holding the climate variables (precipitation, evaporation, mean air temperature, relative humidity and $\delta^{18}O_P$) constant at their mean values through the monitoring period. When either evaporation or temperature was maintained as constant, a noticeable change in model water isotopes occurred (Figure 10b and c), noting that temperature is a key component of modelled evaporation (Equation 9). By contrast, under constant precipitation, relative humidity and $\delta^{18}O_P$ modelled water isotopes remained nearly consistent with the full model runs, including intra-annual variability (Figure 10a, d and e). This is consistent with the linear relationship between the model output and climatic variables and suggests that the influence of evaporation on lake water isotope composition dominates,

compared to the effect of changing precipitation amount. This analysis further indicates that a relatively short-term change in the average $\delta^{18}O_P$ would have little or no impact on lake water isotope composition. However, if the average value of $\delta^{18}O_P$ were to change, the model's isotope variability may shift while maintaining a similar trend. Our interpretation is consistent with numerous other studies that indicate evaporation predominantly influences the isotope composition of evaporative, closed lakes, whilst hydrologically open systems are mainly driven by precipitation (Leng & Marshall, 2004; Jones et al., 2016; Vystavna et al., 2021). However, the calculation of $\delta^{18}O_{LW}$ variation in response to evaporation or more specifically by the change in P-E was possible with lake modelling. This will eventually enable us to make rough quantitative estimates of how much lake isotopes varied at a longer time scale. It should be emphasised that this basic model still has certain limitations, which may be improved in the future by increasing the accuracy and reliability of measurements and increasing the monitoring period. To comprehend the regional variability of lake water isotopes in response to lake stratification, more complicated modelling is required.

2.6 Conclusion

In this study, contemporary hydrological behaviour and isotopic controls of Lake Surprise were investigated, to highlight the significance of lake monitoring and modelling approaches for testing the hypotheses and contributing to more accurate past climate interpretations, as well as to prepare for likely future changes in water resources. According to observational data, the lake is a through-flow lake that is dominated by groundwater, with waters of the Na-HCO_3 type coming predominantly from weathering and dissolutions basalts and carbonate in the immediate surroundings. Unlikely many other crater lakes in the western plains, approximately similar physiochemical parameters obtained from historical samples indicate that the lake remained nearly consistent and permanent at least for the last 50 years. Despite the spatial distribution of $\delta^{18}O$ and $\delta^{2}H$ in lake water suggesting a heavy isotope enrichment in comparison to precipitation, the application of the index lake approach indicated that evaporation is not as significant as in a terminal lake or zero through-flow lake. The novel water balance estimate developed for Lake Surprise by incorporating contemporary hydrological and isotope data into steady-state isotope mass balance models showed that the majority of water input and output occurred through groundwater. Application of the spreadsheet-based isotope mass balance model developed by Jones et al., (2016) for Lake Surprise, demonstrated that from the two independent climate variables (P and E), changing evaporation has a significant influence on

lake isotopic variability. Further, the model implied that it may be possible to model past lake variability using the isotopic average of precipitation, which maintains the constant lake variability, similar to field measurements. Coupled monitoring and modelling work was beneficial to assess the hypothesis utilised by previous authors when interpreting proxy records, which is the groundwater influence on Lake Surprise and to enhance the knowledge of water-rock interactions. However, results from this study could be further tested by a longer dataset based on numerous annual readings.

2.7 List of references cited

Adrian, R., O'Reilly, C. M., Zagarese, H., Baines, S. B., Hessen, D. O., Keller, W., Livingstone, D. M., Sommaruga, R., Straile, D., Van Donk, E., Weyhenmeyer, G. A., & Winder, M. (2009). Lakes as sentinels of climate change. *Limnology and Oceanography*, *54*(6 PART 2), 2283–2297. https://doi.org/10.4319/lo.2009.54.6_part_2.2283

Ankor, M. J. (2020). *Hydrologic and Isotopic Lake Modelling for Palaeoclimate Research*. *January*.

Ankor, M. J., Tyler, J. J., & Hughes, C. E. (2019). Development of an autonomous , monthly and daily , rainfall sampler for isotope research. *Journal of Hydrology*, *575*(April), 31–41. https://doi.org/10.1016/j.jhydrol.2019.04.074

Banks, D., & Frengstad, B. (2006). Evolution of groundwater chemical composition by plagioclase hydrolysis in Norwegian anorthosites. *Geochimica et Cosmochimica Acta*, *70*(6), 1337–1355. https://doi.org/10.1016/j.gca.2005.11.025

Barr, C., Tibby, J., Gell, P., Tyler, J., Zawadzki, A., & Jacobsen, G. E. (2014). Climate variability in south-eastern Australia over the last 1500 years inferred from the high-resolution diatom records of two crater lakes. *Quaternary Science Reviews*, *95*, 115–131. https://doi.org/10.1016/j.quascirev.2014.05.001

Barton, A. B., Herczeg, A. L., Dahlhaus, P. G., & Cox, J. W. (2013). A geochemical approach to determining the hydrological regime of wetlands in a volcanic plain, South-Eastern Australia. *Groundwater and Ecosystems*, 69–79. https://doi.org/10.1201/b15003-12

Battarbee, R. W. (2000). Palaeolimnological approaches to climate change, with special regard to the biological record. *Quaternary Science Reviews*, *19*(1–5), 107–124. https://doi.org/10.1016/S0277-3791(99)00057-8

Battarbee, R. W., Anderson, N. J., Bennion, H., & Simpson, G. L. (2012). Combining limnological and palaeolimnological data to disentangle the effects of nutrient pollution and climate change on lake ecosystems: Problems and potential. *Freshwater Biology*, *57*(10), 2091–2106. https://doi.org/10.1111/j.1365-2427.2012.02860.x

Bell, D., & Johnston, C. (2008). Budj Bim; Caring for the spirit and the people. *Finding the Spirit of Place : Between Tangible and Intangible Heritage. (16th ICOMOS General Assembly and International Scientific Symposium, Quebec, 2008)*, 213-224. http://openarchive.icomos.org/12/%5Cnhttp://openarchive.icomos.org/12/1/77-7xnf-104.pdf

Boyce, J. (2013). The Newer Volcanics Province of southeastern Australia: A new classification scheme and distribution map for eruption centres. *Australian Journal of Earth Sciences*, *60*(4), 449–462. https://doi.org/10.1080/08120099.2013.806954

Boyce, J., Nicholls, I., Keays, R., & Hayman, P. (2014). Victoria erupts: The Newer Volcanics Province of south-eastern Australia. *Geology Today*, *30*(3), 105–109. https://doi.org/10.1111/gto.12054

Builth, H., Kershaw, A. P., White, C., Roach, A., Hartney, L., McKenzie, M., Lewis, T., & Jacobsen, G. (2008). Environmental and cultural change on the Mt Eccles lava-flow landscapes of southwest Victoria, Australia. *Holocene*, *18*(3), 413–424. https://doi.org/10.1177/0959683607087931

Chae, G. T., Yun, S. T., Kim, K., & Mayer, B. (2006). Hydrogeochemistry of sodium-bicarbonate type bedrock groundwater in the Pocheon spa area, South Korea: water-rock interaction and hydrologic mixing. *Journal of Hydrology*, *321*(1–4), 326–343. https://doi.org/10.1016/j.jhydrol.2005.08.006

Cluett, A. A., & Thomas, E. K. (2020). Resolving combined influences of inflow and evaporation on western Greenland lake water isotopes to inform paleoclimate inferences. *Journal of Paleolimnology*, *63*(4), 251–268. https://doi.org/10.1007/s10933-020-00114-4

Craig, H. (1961). Isotopic variations in meteoric waters. *Science*, *133*(3465), 1702–1703. https://doi.org/10.1126/science.133.3465.1702

Darwesh, N., Allam, M., Meng, Q., Helfdhallah, A. A., Naser Ramzy, S. M., Kharrim, K. El, Al Maliki, A. A., & Belghyti, D. (2019). Using piper trilinear diagrams and principal component analysis to determine variation in hydrochemical faces and understand the evolution of groundwater in sidi slimane region, Morocco. *Egyptian Journal of Aquatic Biology and Fisheries*, *23*(5 Special Issue), 17–30. https://doi.org/10.21608/ejabf.2019.63248

Dean, J. R., Eastwood, W. J., Roberts, N., Jones, M. D., Yiğitbaşioğlu, H., Allcock, S. L., Woodbridge, J., Metcalfe, S. E., & Leng, M. J. (2015). Tracking the hydro-climatic signal from lake to sediment: A field study from central Turkey. *Journal of Hydrology*, *529*(P2), 608–621. https://doi.org/10.1016/j.jhydrol.2014.11.004

Dean, J. R., Jones, M. D., Leng, M. J., Metcalfe, S. E., Sloane, H. J., Eastwood, W. J., & Roberts, C. N. (2018). Seasonality of Holocene hydroclimate in the Eastern Mediterranean reconstructed using the oxygen isotope composition of carbonates and diatoms from Lake Nar, central Turkey. *Holocene*, *28*(2), 267–276.

https://doi.org/10.1177/0959683617721326

Dessert, C., Dupré, B., Gaillardet, J., François, L. M., & Allègre, C. J. (2003). Basalt weathering laws and the impact of basalt weathering on the global carbon cycle. *Chemical Geology*, *202*(3–4), 257–273. https://doi.org/10.1016/j.chemgeo.2002.10.001

Edwards, T. W. D. (2004). *Department of Earth Sciences University of Waterloo Waterloo, Ontario N2L 3G1, Canada*. 187–207.

Falster, G., Tyler, J., Grant, K., Tibby, J., Turney, C., Löhr, S., Jacobsen, G., & Kershaw, A. P. (2018). Millennial-scale variability in south-east Australian hydroclimate between 30,000 and 10,000 years ago. *Quaternary Science Reviews*, *192*, 106–122. https://doi.org/10.1016/j.quascirev.2018.05.031

Fritz, S. C. (2008). Deciphering climatic history from lake sediments. *Journal of Paleolimnology*, *39*(1), 5–16. https://doi.org/10.1007/s10933-007-9134-x

Gascoyne, M. (2004). Hydrogeochemistry, groundwater ages and sources of salts in a granitic batholith on the Canadian Shield, southeastern Manitoba. In *Applied Geochemistry* (Vol. 19, Issue 4). https://doi.org/10.1016/S0883-2927(03)00155-0

Gaur, N., Sarkar, A., Dutta, D., Gogoi, B. J., Dubey, R., & Dwivedi, S. K. (2022). Evaluation of water quality index and geochemical characteristics of surfacewater from Tawang India. *Scientific Reports*, *12*(1), 1–26. https://doi.org/10.1038/s41598-022-14760-3

Gibson, J. J. (2001). Forest-tundra water balance signals traced by isotopic enrichment in lakes. *Journal of Hydrology*, *251*(1–2), 1–13. https://doi.org/10.1016/S0022-1694(01)00428-0

Gibson, J. J., Birks, S. J., & Yi, Y. (2016). Stable isotope mass balance of lakes: A contemporary perspective. *Quaternary Science Reviews*, *131*, 316–328. https://doi.org/10.1016/j.quascirev.2015.04.013

Gibson, J. J., & Edwards, T. W. D. (2002). Regional water balance trends and evaporation-transpiration partitioning from a stable isotope survey of lakes in northern Canada. *Global Biogeochemical Cycles*, *16*(2), 10-1-10–14. https://doi.org/10.1029/2001gb001839

Gibson, J. J., Edwards, T. W. D., Bursey, G. G., & Prowse, T. D. (1993). Estimating Evaporation Using Stable Isotopes: Quantitative Results and Sensitivity Analysis for. *Nordic Hydrology*, *24*, 79–94.

Gibson, J. J., Edwards, T. W. D., & Prowse, T. D. (1999). Pan-derived isotopic composition of atmospheric water vapour and its variability in northern Canada. *Journal of Hydrology*, *217*(1–2), 55–74. https://doi.org/10.1016/S0022-1694(99)00015-3

Gibson, J. J., Prepas, E. E., & McEachern, P. (2002). Quantitative comparison of lake throughflow, residency, and catchment runoff using stable isotopes: Modelling and results from a regional survey of Boreal lakes. *Journal of Hydrology*, *262*(1–4), 128–144. https://doi.org/10.1016/S0022-1694(02)00022-7

Gibson, J. J., & Reid, R. (2014). Water balance along a chain of tundra lakes: A 20-year isotopic perspective. *Journal of Hydrology*, *519*(PB), 2148–2164. https://doi.org/10.1016/j.jhydrol.2014.10.011

Haig, H. A., Hayes, N. M., Simpson, G. L., Yi, Y., Wissel, B., Hodder, K. R., & Leavitt, P. R. (2020). Comparison of isotopic mass balance and instrumental techniques as estimates of basin hydrology in seven connected lakes over 12 years. *Journal of Hydrology X*, *6*(November 2019). https://doi.org/10.1016/j.hydroa.2019.100046

Heikkilä, M., Edwards, T. W. D., Seppä, H., & Sonninen, E. (2010). Sediment isotope tracers from Lake Saarikko, Finland, and implications for Holocene hydroclimatology. *Quaternary Science Reviews*, *29*(17–18), 2146–2160. https://doi.org/10.1016/j.quascirev.2010.05.010

Horita, J., Rozanski, K., & Cohen, S. (2008). Isotope effects in the evaporation of water: A status report of the Craig-Gordon model. *Isotopes in Environmental and Health Studies*, *44*(1), 23–49. https://doi.org/10.1080/10256010801887174

Horita, J., & Wesolowski, D. J. (1994). Horita and Wesolowski 1994. *Geochimica et Cosmochimica Acta*, *58*(16), 1–13. papers2://publication/uuid/F9BCD32F-8569-4ACF-81AF-08518BF40A32

Hughes, C. E., & Crawford, J. (2012). A new precipitation weighted method for determining the meteoric water line for hydrological applications demonstrated using Australian and global GNIP data. *Journal of Hydrology*, *464–465*, 344–351. https://doi.org/10.1016/j.jhydrol.2012.07.029

Jankowski, J., & Jacobson, G. (1989). *Hydrochemical Evolution of Regional Groundwaters ~*. *108*.

Jones, M. D., Cuthbert, M. O., Leng, M. J., Mcgowan, S., Mariethoz, G., Arrowsmith, C., Sloane, H. J., Humphrey, K. K., & Cross, I. (2016a). Comparisons of observed and modelled lake d 18 O variability. *JQSR*, *131*, 329–340. https://doi.org/10.1016/j.quascirev.2015.09.012

Jones, M. D., & Dee, S. G. (2018a). Global-scale proxy system modelling of oxygen isotopes in lacustrine carbonates : New insights from isotope-enabled-model proxy-data comparison. *Quaternary Science Reviews*, *202*, 19–29. https://doi.org/10.1016/j.quascirev.2018.09.009

Jones, M. D., & Imbers, J. (2010). Modeling Mediterranean lake isotope variability. *Global and Planetary Change*, *71*(3–4), 193–200. https://doi.org/10.1016/j.gloplacha.2009.10.001

Jones, M. D., Leng, M. J., Roberts, C. N., & Tu, M. (2005). *A coupled calibration and modelling approach to the understanding of dry-land lake oxygen isotope records*. 391–411. https://doi.org/10.1007/s10933-005-6743-0

Jones, M. D., Roberts, C. N., & Leng, M. J. (2007). Quantifying climatic change through the

last glacial-interglacial transition based on lake isotope palaeohydrology from central Turkey. *Quaternary Research*, *67*(3), 463–473. https://doi.org/10.1016/j.yqres.2007.01.004

Jones, R. N., McMahon, T. A., & Bowler, J. M. (2001). Modelling historical lake levels and recent climate change at three closed lakes, Western Victoria, Australia (c.1840-1990). *Journal of Hydrology*, *246*(1–4), 159–180. https://doi.org/10.1016/S0022-1694(01)00369-9

Khadka, U. R., & Ramanathan, A. L. (2013). Major ion composition and seasonal variation in the Lesser Himalayan lake: Case of Begnas Lake of the Pokhara Valley, Nepal. *Arabian Journal of Geosciences*, *6*(11), 4191–4206. https://doi.org/10.1007/s12517-012-0677-4

Kirono, D. G. C., Jones, R. N., Kent, D., & Leahy, P. (2009). Modelling lake levels under climate change conditions: Three closed lakes in Western Victoria. *18th World IMACS Congress and MODSIM 2009 - International Congress on Modelling and Simulation: Interfacing Modelling and Simulation with Mathematical and Computational Sciences, Proceedings, July*, 4312–4318.

Krabbenhoft, D. P., Bowser, C. J., Anderson, M. P., & Valley, J. W. (1990). Estimating groundwater exchange with lakes: 1. The stable isotope mass balance method. *Water Resources Research*, *26*(10), 2445–2453. https://doi.org/10.1029/WR026i010p02445

Lacey, J. H., & Jones, M. D. (2018). Quantitative reconstruction of early Holocene and last glacial climate on the Balkan Peninsula using coupled hydrological and isotope mass balance modelling. *Quaternary Science Reviews*, *202*, 109–121. https://doi.org/10.1016/j.quascirev.2018.09.007

Lee, T. M. (1996). Hydrogeologic controls on the groundwater interactions with an acidic lake in karst terrain, Lake Barco, Florida. *Water Resources Research*, *32*(4), 831–844. https://doi.org/10.1029/96WR00162

Leng, M. J., & Marshall, J. D. (2004). Palaeoclimate interpretation of stable isotope data from lake sediment archives. *Quaternary Science Reviews*, *23*(7–8), 811–831. https://doi.org/10.1016/j.quascirev.2003.06.012

Li, H., Liu, X., Tripati, A., Feng, S., Elliott, B., Whicker, C., Arnold, A., & Kelley, A. M. (2020). Factors controlling the oxygen isotopic composition of lacustrine authigenic carbonates in Western China: implications for paleoclimate reconstructions. *Scientific Reports*, *10*(1), 1–17. https://doi.org/10.1038/s41598-020-73422-4

Li, J., Song, F., Bao, Z., Fan, H., & Wu, H. (2022). Insights into Shallow Freshwater Lakes Hydrology in the Yangtze Floodplain from Stable Water Isotope Tracers. *Water (Switzerland)*, *14*(3), 1–14. https://doi.org/10.3390/w14030506

Li, S., Lu, X. X., He, M., Zhou, Y., Bei, R., Li, L., & Ziegler, A. D. (2011). Major element chemistry in the upper Yangtze River: A case study of the Longchuanjiang River. *Geomorphology*, *129*(1–2), 29–42. https://doi.org/10.1016/j.geomorph.2011.01.010

Li, X., Zhou, X., Liu, W., Wang, Z., He, Y., & Xu, L. (2016). Carbon and oxygen isotopic records from Lake Tuosu over the last 120 years in the Qaidam Basin, Northwestern China: The implications for paleoenvironmental reconstruction. *Global and Planetary Change*, *141*, 54–62. https://doi.org/10.1016/j.gloplacha.2016.04.006

Li, Y., Tian, L., Bowen, G. J., Wu, Q., Luo, W., Chen, Y., Wang, D., Shao, L., Cai, Z., & Tao, J. (2021). Deep lake water balance by dual water isotopes in Yungui Plateau, southwest China. *Journal of Hydrology*, *593*(December 2020), 125886. https://doi.org/10.1016/j.jhydrol.2020.125886

Liu, J., Fu, G., Song, X., Charles, S. P., Zhang, Y., Han, D., & Wang, S. (2010). Stable isotopic compositions in Australian precipitation. *Journal of Geophysical Research Atmospheres*, *115*(23), 1–16. https://doi.org/10.1029/2010JD014403

Liu, J., Gao, Z., Wang, M., Li, Y., Yu, C., Shi, M., Zhang, H., & Ma, Y. (2019). Hydrochemical and isotopic characteristics of surface water in the Lhasa River basin. *Arabian Journal of Geosciences*, *12*(16). https://doi.org/10.1007/s12517-019-4690-8

Liu, M., Zhao, L., Lin, L., Li, Q., Hu, Y., Tao, J., Zou, J. Y., & Tang, X. (2020). Water chemistry and source analysis of major ions of Bangong Lake in Tibetan Plateau. *IOP Conference Series: Earth and Environmental Science*, *427*(1). https://doi.org/10.1088/1755-1315/427/1/012016

Marandi, A., & Shand, P. (2018). Groundwater chemistry and the Gibbs Diagram. *Applied Geochemistry*, *97*(July), 209–212. https://doi.org/10.1016/j.apgeochem.2018.07.009

Matchan, E. L., Phillips, D., Jourdan, F., & Oostingh, K. (2020). Early human occupation of southeastern Australia: Newinsights from 40Ar/39Ar dating of young volcanoes. *Geology*, *48*(4), 390–394. https://doi.org/10.1130/G47166.1

Piper, A. M. (1944). A graphic procedure in the geochemical interpretation of water-analyses. *Eos, Transactions American Geophysical Union*, *25*(6), 914-928.

Price, R. C., Gray, C. M., & Frey, F. A. (1997). Strontium isotopic and trace element heterogeneity in the plains basalts of the Newer Volcanic Province, Victoria, Australia. *Geochimica et Cosmochimica Acta*, *61*(1), 171–192. https://doi.org/10.1016/S0016-7037(96)00318-3

Radke, B., Champion, D. C., Gallagher, S. J., Wang, L., De Vleeschouwer, D., Kalinowski, A., Tenthorey, E., Urosevic, M., & Feitz, A. (2022). Geology, geochemistry and depositional history of the Port Campbell Limestone on the eastern flank of the Otway Basin, southeastern Australia. *Australian Journal of Earth Sciences*, *69*(4), 509–538. https://doi.org/10.1080/08120099.2022.1998220

Raiber, M., Webb, J. A., & Bennetts, D. A. (2009). Strontium isotopes as tracers to delineate aquifer interactions and the influence of rainfall in the basalt plains of southeastern Australia. *Journal of Hydrology*, *367*(3–4), 188–199. https://doi.org/10.1016/j.jhydrol.2008.12.020

Şehnaz, Ş., Şener, E., Davraz, A., & Varol, S. (2020). Hydrogeological and hydrochemical investigation in the Burdur Saline Lake Basin, southwest Turkey. *Chemie Der Erde*, *80*(4). https://doi.org/10.1016/j.chemer.2019.125592

Shapley, M. D., Ito, E., & Donovan, J. J. (2008). Isotopic evolution and climate paleorecords: Modeling boundary effects in groundwater-dominated lakes. *Journal of Paleolimnology*, *39*(1), 17–33. https://doi.org/10.1007/s10933-007-9092-3

Shi, X., Pu, T., He, Y., Qi, C., Zhang, G., & Xia, D. (2017). Variability of stable isotope in lakewater and its hydrological processes identification in Mt. Yulong region. *Water (Switzerland)*, *9*(9). https://doi.org/10.3390/w9090711

Smith, A., McNiven, I. J., Rose, D., Brown, S., Johnston, C., & Crocker, S. (2019). Indigenous Knowledge and Resource Management as World Heritage Values: Budj Bim Cultural Landscape, Australia. *Archaeologies*, *15*(2), 285–313. https://doi.org/10.1007/s11759-019-09368-5

Steinman, B. A., Rosenmeier, M. F., Abbott, M. B., & Bain, D. J. (2010). The isotopic and hydrologic response of small, closed-basin lakes to climate forcing from predictive models: Application to paleoclimate studies in the upper Columbia River basin. *Limnology and Oceanography*, *55*(6), 2231–2245. https://doi.org/10.4319/lo.2010.55.6.2231

Street-Perrott, F. A., Holmes, J. A., Robertson, I., Ficken, K. J., Koff, T., Loader, N. J., Marshall, J. D., & Martma, T. (2018). The Holocene isotopic record of aquatic cellulose from Lake Äntu Sinijärv, Estonia: Influence of changing climate and organic-matter sources. *Quaternary Science Reviews*, *193*, 68–83. https://doi.org/10.1016/j.quascirev.2018.05.010

The Bureau of Meteorology, & CSIRO. (2020). *Report at a glance Key points*.

Tibby, J., & Tiller, D. (2007). Climate-water quality relationships in three Western Victorian (Australia) lakes 1984-2000. *Hydrobiologia*, *591*(1), 219–234. https://doi.org/10.1007/s10750-007-0804-5

Timms, B. V. (1975). Basic limnology of two crater lakes in western Victoria.

Tweed, S., Leblanc, M., & Cartwright, I. (2009). Groundwater-surface water interaction and the impact of a multi-year drought on lakes conditions in South-East Australia. *Journal of Hydrology*, *379*(1–2), 41–53. https://doi.org/10.1016/j.jhydrol.2009.09.043

Tyler, J. J., Leng, M. J., & Arrowsmith, C. (2007). Seasonality and the isotope hydrology of Lochnagar, a Scottish mountain lake: Implications for palaeoclimate research. *Holocene*, *17*(6), 717–727. https://doi.org/10.1177/0959683607080513

Tyler, J. J., Mills, K., Barr, C., Sniderman, J. M. K., Gell, P. A., & Karoly, D. J. (2015). Identifying coherent patterns of environmental change between multiple, multivariate records: an application to four 1000-year diatom records from Victoria, Australia. *Quaternary Science Reviews*, *119*, 94–105.

https://doi.org/10.1016/j.quascirev.2015.04.010

Vystavna, Y., Harjung, A., Monteiro, L. R., Matiatos, I., & Wassenaar, L. I. (2021). Stable isotopes in global lakes integrate catchment and climatic controls on evaporation. *Nature Communications*, *12*(1), 1–7. https://doi.org/10.1038/s41467-021-27569-x

Webb, J. A. (2016). *Chapter 18 the evolution of Victorian landscapes*. *January 1991*.

Welhan, J. A., & Fritz, P. (1977). Evaporation pan isotopic behavior as an index of isotopic evaporation conditions. *Geochimica et Cosmochimica Acta*, *41*(5), 682–686. https://doi.org/10.1016/0016-7037(77)90306-4

Winter, T. C. (1981). Effects of water-table configuration on seepage through lakebeds. *Limnology and Oceanography*, *26*(5), 925–934. https://doi.org/10.4319/lo.1981.26.5.0925

Wolfe, B. B., Edwards, T. W. D., Elgood, R. J., & Beuning, K. R. M. (2001). 14 . Carbon and oxygen isotope analysis of lake sediment cellulose : methods and applications. Department of Earth Sciences Canada N2L 3G1 Department of Earth and Environmental Sciences. *Tracking Environmental Change Using Lake Sediments*, *2*, 1–28.

Wolfe, B. B., Falcone, M. D., Clogg-Wright, K. P., Mongeon, C. L., Yi, Y., Brock, B. E., Amour, N. A. S., Mark, W. A., & Edwards, T. W. D. (2007). Progress in isotope paleohydrology using lake sediment cellulose. *Journal of Paleolimnology*, *37*(2), 221–231. https://doi.org/10.1007/s10933-006-9015-8

Wu, H., Huang, Q., Fu, C., Song, F., Liu, J., & Li, J. (2021). Stable isotope signatures of river and lake water from Poyang Lake, China: Implications for river–lake interactions. *Journal of Hydrology*, *592*(October 2020), 125619. https://doi.org/10.1016/j.jhydrol.2020.125619

Xiao, J., Jin, Z. D., Zhang, F., & Wang, J. (2012). Solute geochemistry and its sources of the groundwaters in the Qinghai Lake catchment, NW China. *Journal of Asian Earth Sciences*, *52*, 21–30. https://doi.org/10.1016/j.jseaes.2012.02.006

Xiao, J., Jin, Z., Wang, J., & Zhang, F. (2015). Major ion chemistry, weathering process and water quality of natural waters in the Bosten Lake catchment in an extreme arid region, NW China. *Environmental Earth Sciences*, *73*(7), 3697–3708. https://doi.org/10.1007/s12665-014-3657-z

Xu, H., Hou, Z., An, Z., Liu, X., & Dong, J. (2010). Major ion chemistry of waters in Lake Qinghai catchments, NE Qinghai-Tibet plateau, China. *Quaternary International*, *212*(1), 35–43. https://doi.org/10.1016/j.quaint.2008.11.001

Yang, Z., Zhou, Y., Wenninger, J., & Uhlenbrook, S. (2014). A multi-method approach to quantify groundwater/surface water-interactions in the semi-arid Hailiutu River basin, northwest China. *Hydrogeology Journal*, *22*(3), 527–541. https://doi.org/10.1007/s10040-013-1091-z

Yi, Y., Brock, B. E., Falcone, M. D., Wolfe, B. B., & Edwards, T. W. D. (2008). A coupled isotope tracer method to characterize input water to lakes. *Journal of Hydrology*, *350*(1–2), 1–13. https://doi.org/10.1016/j.jhydrol.2007.11.008

Yihdego, Y., & Webb, J. (2012). Modelling of seasonal and long-term trends in lake salinity in southwestern Victoria, Australia. *Journal of Environmental Management*, *112*, 149–159. https://doi.org/10.1016/j.jenvman.2012.07.002

Yihdego, Y., & Webb, J. (2016). Validation of a model with climatic and flow scenario analysis: case of Lake Burrumbeet in southeastern Australia. *Environmental Monitoring and Assessment*, *188*(5). https://doi.org/10.1007/s10661-016-5310-7

Yihdego, Y., & Webb, J. A. (2015). Use of a conceptual hydrogeological model and a time variant water budget analysis to determine controls on salinity in Lake Burrumbeet in southeast Australia. *Environmental Earth Sciences*, *73*(4), 1587–1600. https://doi.org/10.1007/s12665-014-3509-x

Yihdego, Y., Webb, J. A., & Leahy, P. (2015). Modelling of lake level under climate change conditions: Lake Purrumbete in southeastern Australia. *Environmental Earth Sciences*, *73*(7), 3855–3872. https://doi.org/10.1007/s12665-014-3669-8

Yihdego, Y., Webb, J., & Leahy, P. (2016). Modelling water and salt balances in a deep, groundwater-throughflow lake—Lake Purrumbete, southeastern Australia. *Hydrological Sciences Journal*, *61*(1), 186–199. https://doi.org/10.1080/02626667.2014.975132

Zhang, B., Zhao, D., Zhou, P., Qu, S., Liao, F., & Guangcai, W. (2020). Hydrochemical Characteristics of Groundwater and Dominant Water – Rock Interactions in the Delingha. *Water*, *12*(836), 1–16.

Zhu, B., & Yang, X. (2007). The ion chemistry of surface and ground waters in the Taklimakan Desert of Tarim Basin, western China. *Chinese Science Bulletin*, *52*(15), 2123–2129. https://doi.org/10.1007/s11434-007-0298-6

Zuber, A. (1983). On the environmental isotope method for determining the water balance components of some lakes. *Journal of Hydrology*, *61*(4), 409–427. https://doi.org/10.1016/0022-1694(83)90004-5

Supplementary data

Section 1: Lake water budget calculation

Using equation 8,

$P + Gi = E + Go$

$1.26*10^{-3}$ $m^3/s + Gi = 2.00*10^{-3}$ $m^3/s + Go$

$Gi - Go = 7.4*10^{-4}$ m^3/s……Equation I.

Application of equation 13,

$P\delta_P + Gi\delta_P = E\delta_E + Go\delta_L$

$(1.26*10^{-3}$ $m^3/s*(-2.80‰)) + (Gi*(-2.80‰)) = (2.00*10^{-3}$ m^3/s $*(-14.78‰)) + (Go*3.16‰)$

$(-3.53*10^{-3}) + (-2.80\ Gi) = (-2.96*10^{-2}) + 3.16\ Go$

$2.60*10^{-2} = 3.16\ Go + 2.80\ Gi$…….Equation II

Application of Equation I in Equation II,

$2.60*10^{-2}$ $m^3/s = 3.16\ Go + 2.80\ (7.40*10^{-4}$ $m^3/s + Go)$

$Go = 4.06*10^{-3}$ m^3/s

From Equation I,

$Gi = 4.80*10^{-3}$ m^3/s

Therefore during steady state lake water balance,

Total input = $P + Gi = 1.26*10^{-3}$ $m^3/s + 4.80*10^{-3}$ $m^3/s = 6.06*10^{-3}$ m^3/s

Total output = $E + Go = 2.00*10^{-3}$ $m^3/s + 4.06*10^{-3}$ $m^3/s = 6.06*10^{-3}$ m^3/s

Section 2: $\delta^{18}O$ and δ^2H isotope calculation for the theoretically Index lake,

Using equation 14,

For $\delta^{18}O$,

$$-2.80 = \frac{\alpha^* \delta_L - h\delta_A - \varepsilon}{1 - h + 0.001\varepsilon_K}$$

$$-2.80 = \frac{(1/1.01)^* \delta_L - (0.50 * -12.66) - 16.95}{1 - 0.50 + (0.001 * 7.09)}$$

$\delta_L = 9.29$ ‰

For δ^2H,

$$-14.40 = \frac{\left(\frac{1}{1.09}\right)^{*} \delta_L - (0.50 * -94.20) - 86.05}{1 - 0.50 + (0.001 * 6.25)}$$

$\delta_L = 34.47$ ‰

Calculations of all parameters are given in the spreadsheet-based lake models

Spreadsheet 1: Water budget calculation

Spreadsheet 2: Isotope mass balance lake model

Section 3: Comparison of precipitation data between Macarthur and Melbourne stations

In the absence of $\delta^{18}O_P$ data for Macarthur station, we compared Melbourne's $\delta^{18}O_P$ with precipitation data from both stations to determine how well they corresponded.

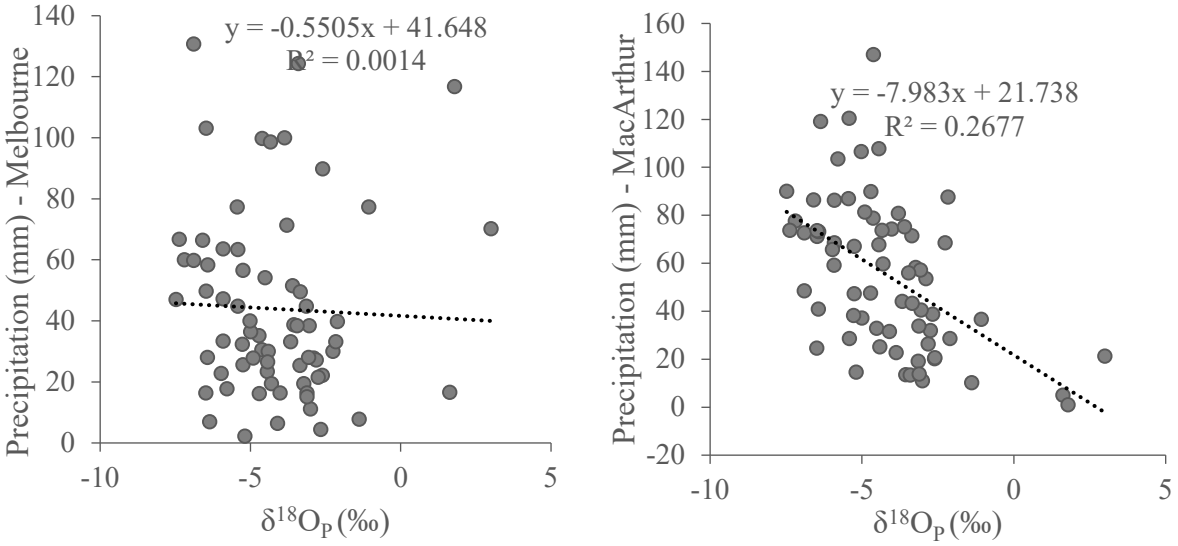

Figure I. Linear correlation between $\delta^{18}O_P$ data and precipitation amount of both weather stations.

Accordingly, a better correlation was observed between Macarthur rainfall and Melbourne isotope data compared to Melbourne isotope vs rainfall data. This is further confirmed by the opposite relationship between rainwater isotopes and precipitation as shown in figure II..

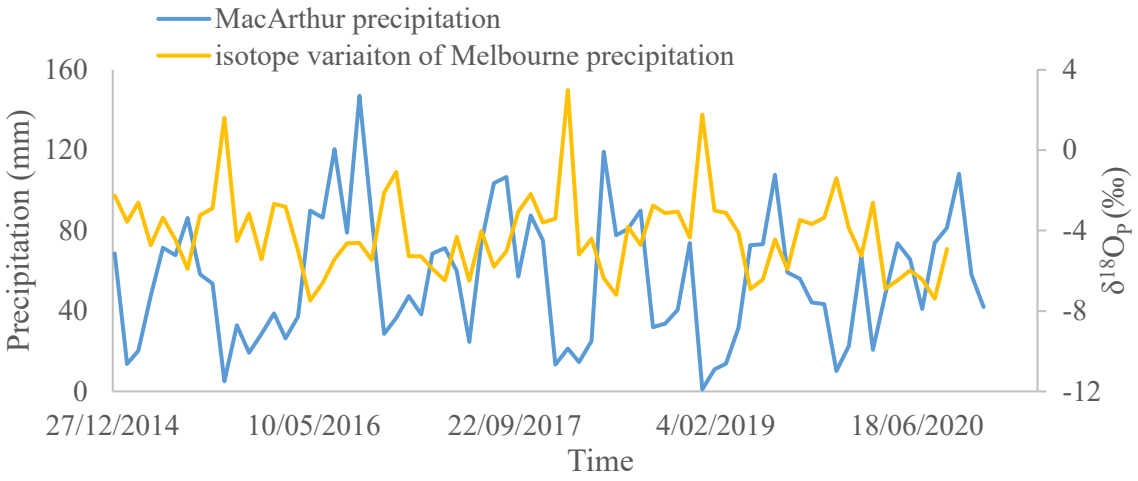

Figure II. Variation between $\delta^{18}O_P$ from Melbourne and precipitation data from Macarthur.

Section 4: OLSR calculation and regression analysis of rainfall data

Due to the presence of unexpected positive isotope values in the rainfall data obtained from the rainfall sampler, OLSR regression analysis was applied to identify any outliers in the dataset. D-excess was calculated using the linear regression equation of the original dataset, thereby, the difference between the d-excess and the original value was obtained as the residual value. Negative and positive two standard deviations of the residual data were calculated. Accordingly, the majority of the data points were concentrated within the 2-standard deviation limit. Therefore, we decided to refer to all the data points for this study.

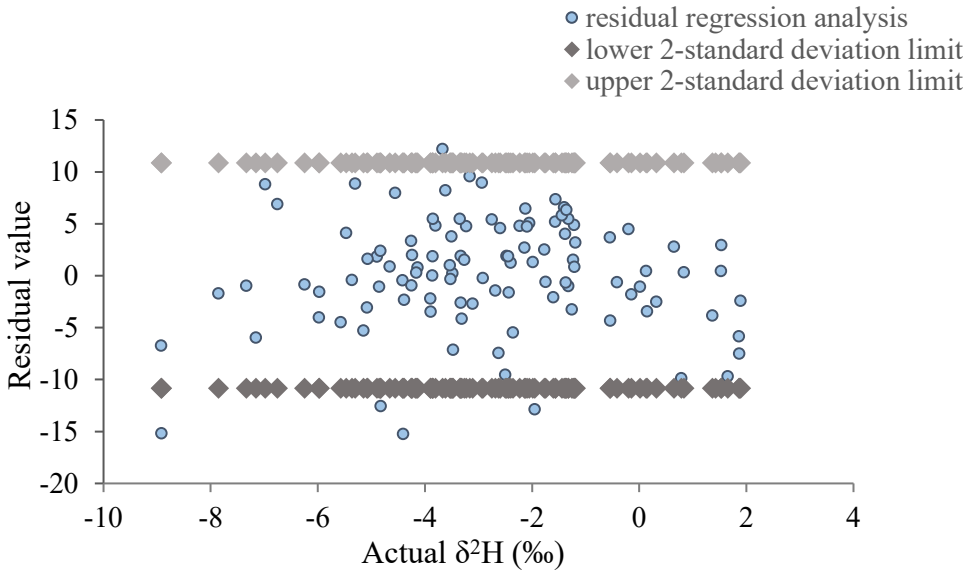

Figure III. Spatial distribution of residual regression vs actual δ^2H data.

Section 5:

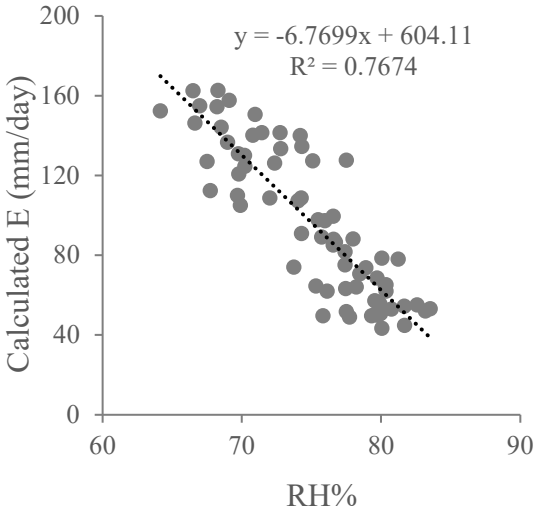

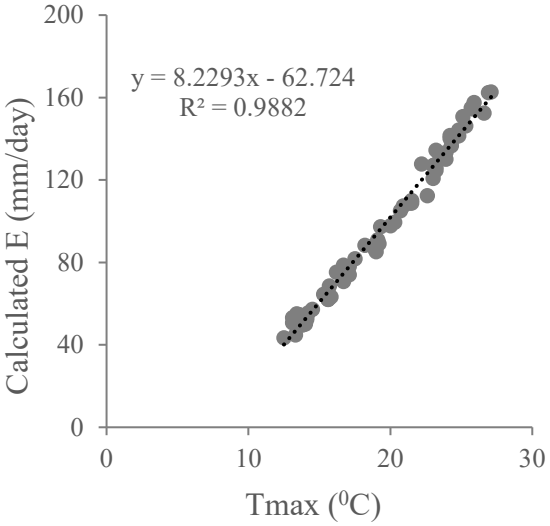

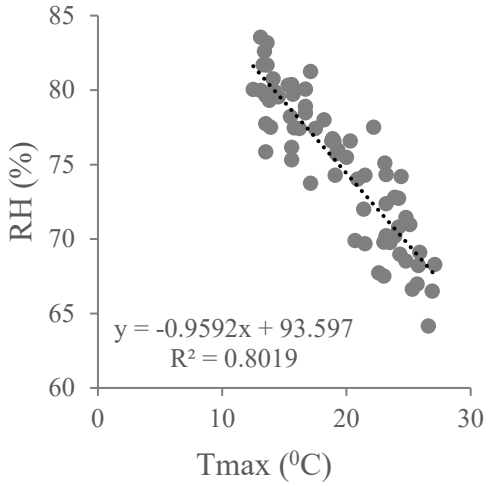

Figure IV. Linear correlation between evaporation (E), relative humidity (RH) and maximum temperature (Tmax).

CHAPTER 3

Dharmarathna, A., Tyler, J., Tibby, J., Cadd, H., Barr, C., Hua, Q., Child, D., Hotchkis, M., Zawadski, A., Francke, A., Pollen radiocarbon dating of lake sediments; a cautionary tale from Lake Surprise, Victoria, Australia.

Supplementary information concerning this chapter follows the text.

Statement of Authorship

Title of Paper	Pollen radiocarbon dating of lake sediments; a cautionary tale from Lake Surprise, Victoria, Australia.
Publication Status	☐ Published ☐ Accepted for Publication ☐ Submitted for Publication ☑ Unpublished and Unsubmitted work written manuscript style
Publication Details	Dharmarathna, A., Tyler, J., Tibby, J., Cadd, H., Barr, C., Hua, Q., Child, D., Hotchkis, M., Zawadski, A., Francke, A., Pollen radiocarbon dating of lake sediments; a cautionary tale from Lake Surprise, Victoria, Australia. *Radiocarbon,* **in prep**

Principal Author

Name of Principal Author (Candidate)	Asika Dharmarathna		
Contribution to the Paper	Field sample collection and preparation for sample analysis, Assisted in instrumental analysis, Data interpretation and modelling, Writing the manuscript and acting as the corresponding author		
Overall percentage (%)	70%		
Certification:	This paper reports on original research I conducted during the period of my Higher Degree by Research candidature and is not subject to any obligations or contractual agreements with a third party that would constrain its inclusion in this thesis. I am the primary author of this paper.		
Signature		Date	12/12/2022

Co-Author Contributions

By signing the Statement of Authorship, each author certifies that:

i. the candidate's stated contribution to the publication is accurate (as detailed above);

ii. permission is granted for the candidate in include the publication in the thesis; and

iii. The sum of all co-author contributions is equal to 100% less the candidate's stated contribution.

Name of Co-Author	Jonathan Tyler		
Contribution to the Paper	Field work assistance, Funding support, guidance in data analysis and interpretation, Manuscript evaluation and review		
Signature		Date	5/12/22

Name of Co-Author	John Tibby		
Contribution to the Paper	Field work assistance, guidance in data analysis and interpretation, Manuscript evaluation and review		
Signature		Date	1/12/2022

Name of Co-Author	Haidee Cadd		
Contribution to the Paper	Field work assistance, Acquisition of radiocarbon data of pollen samples, Assistance in data interpretation		
Signature		Date	20/11/22

Name of Co-Author	Cameron Barr		
Contribution to the Paper	Assistance with field work and sample preparation, Assistance with initial data interpretation, Provided Ca% data for comparison with radiocarbon data		
Signature		Date	2/12/2022

Name of Co-Author	Quan Hua		
Contribution to the Paper	Assistance with acquisition of radiocarbon data, Assistance with initial data interpretation, Manuscript evaluation		
Signature		Date	1 Dec 2022

Name of Co-Author	David Child		
Contribution to the Paper	Assistance with acquisition of Pu isotope data, Assistance with initial data interpretation, Manuscript evaluation		
Signature		Date	2/12/2022

Name of Co-Author	Michael Hotchkis		
Contribution to the Paper	Assistance with acquisition of Pu isotope data, Assistance with initial data interpretation, Manuscript evaluation		
Signature		Date	4/12/2022

Name of Co-Author	Atun Zawadski		
Contribution to the Paper	Assistance with acquisition of Pb-210 data, Assistance with initial data interpretation, Manuscript evaluation		
Signature		Date	6/12/2022

Name of Co-Author	Alexander Francke		
Contribution to the Paper	Assistance with acquisition and interpretation of FTIR data		
Signature		Date	23/11/2022

Name of Co-Author			
Contribution to the Paper			
Signature		Date	

Name of Co-Author			
Contribution to the Paper			
Signature		Date	

3 Pollen radiocarbon dating of lake sediments; a cautionary tale from Lake Surprise, Victoria, Australia.

Abstract

The development of reliable sediment chronologies is crucial for accurate interpretations of decadal to century-scale palaeoenvironmental changes in the late Quaternary. In this respect, the use of pollen extracts as a medium for radiocarbon dating is becoming increasingly prevalent, due to their abundance in sediments that are otherwise sparse or devoid of terrestrial plant macrofossils. Here, we used pollen radiocarbon dating, alongside a suite of macrofossil and bulk sediment dates, to develop a chronology for the Holocene sediments of Lake Surprise, an important palaeoclimate archive in western Victoria, Australia. Fourier transform infrared (FTIR) was used to screen pollen extracts for contamination. ^{210}Pb activities and Pu isotope concentrations of the recent sediment were analysed to constrain the age of the uppermost sediments, measured using alpha spectrometry and Accelerator Mass Spectrometry. Comparison of radiocarbon dates from plant macrofossils and bulk sediment revealed an age offset of 260±86 ^{14}C years. An even larger age offset of ~340 ^{14}C years was observed between radiocarbon dates for plant macrofossils and pollen extracts. The offset between pollen and plant macrofossil dates varies through time, and generally correlates with carbonate concentration within the sediment profile, although the pollen extracts themselves were not contaminated by either carbonate or charcoal. Therefore, this study infers that aquatic algal spores within the pollen extracts are a possible reason for the age offsets in pollen dates, whereby the algal spores assimilate old carbon during periods of higher groundwater influx. The offset between pollen and macrofossil dates was used to correct the pollen dates, and an age model was derived using the Bayesian *Plum* software, integrating unsupported ^{210}Pb activities, Pu data and ^{14}C dates of pollen and macrofossil samples. Our chronology suggests that the sediment cores studied have a basal age of ~10,850 yr, at 11.4 m composite depth, with a sediment accumulation rate of ~9.5 yr/cm.

3.1 Introduction

3.1.1 The need for lake sediment chronologies in south-eastern Australia

Lake sediments are important archives of past climate and environmental change given their continuity and rapid response to climate variability (Adrian et al., 2009, 2016; Tylmann et al., 2017). However, any reconstruction of environmental and climate change within a strong temporal framework requires accurate and reliable chronological control given that events are being reconstructed mostly relying on chronology (Howarth et al., 2013; Corcho-Alvarado et al., 2014; Zimmerman & Wahl, 2020; Tunno et al., 2021; Rivera-Araya et al., 2022). Among numerous dating techniques employed by palaeolimnologists, the most widely accepted methods for Holocene lacustrine sediments are radiocarbon dating of terrestrial macrofossils for the deeper (older) sediments and ^{210}Pb dating of recent sediments, however, neither method can be conducted without challenges in most instances (Appleby, 2001; Björck et al., 2001; Wolfe et al., 2004; Brenner & Kenney, 2015; Strunk et al., 2020).

Lake sediments are important archives of climate and hydrological change in southern Australia, providing context for human impacts, ecological change and climate over tens to thousands of years. However, even though south-eastern Australia has yielded an increasing number of lake sediment records, the development of detailed and accurate sediment chronologies remains a major limiting factor (Fletcher & Thomas, 2010; Wilkins et al., 2012, 2013; Gouramanis et al., 2013; Woodward et al., 2014). This study attempts to develop an age model for the Holocene sediments of Lake Surprise, which is an important palaeoclimate archive for south-eastern Australia. Previous chronologies for the Holocene sediments of Lake Surprise have used a combination of bulk sediment and pollen radiocarbon dates, as well as ^{210}Pb analyses, encountering several issues related to pollen contamination, possible groundwater effects and age reversals (Barr et al., 2014; Falster et al., 2018). Furthermore, to date, there is no continuous chronology that links the Holocene sediments to the modern day. These limitations are addressed by using a modified pollen extraction procedure (Cadd et al. 2022) and screening pollen extracts for contamination using FTIR. Further, the Bayesian *Plum* model is used to combine multiple lines of evidence to build a robust age model that more faithfully quantifies age uncertainty (Aquino-López et al., 2018).

3.1.2 ^{210}Pb dating of recent lake sediments

Atmospheric fall out of ^{210}Pb in lake sediments is used widely to obtain recent chronological information in lake sediments approximately 100 – 200 years based on its relatively lower half-life (~22.3 years) (Appleby & Oldfield, 1978; Appleby et al., 1979; Appleby, 2008; Kirchner, 2011; Aquino-López et al., 2018; Aquino-López, Ruiz-Fernández, et al., 2020; Iurian et al., 2021). ^{210}Pb is the third daughter product of the ^{238}U decay series which generates after the breakdown of ^{222}Rn in the atmosphere. ^{210}Pb is attached to aerosols and removed from the atmosphere by way of precipitation or dry deposition (Appleby, 2001). This aerosol ^{210}Pb settles in lakes and other water bodies and is absorbed into lake sediments (Appleby, 1998; 2001; Heijnis, 2001). The majority of the sediment is composed of "unsupported" or "excess" ^{210}Pb, which is the result of the atmospheric influx. However, “supported” ^{210}Pb, which is formed by in-situ decay of ^{226}Ra that has been eroded into the basin from the watershed also contributes in a lesser amount (Appleby, 2001; Heijnis, 2001). Provided that uranium-bearing minerals that are commonly found in sediments are constant sources of supported ^{210}Pb, which is likely to be in equilibrium with parent ^{226}Ra, it is possible to determine the supported ^{210}Pb activity by measuring the ^{226}Ra activity and to calculate the unsupported activity by subtracting the supported ^{210}Pb activity from the total ^{210}Pb activity (Kirchner & Ehlers, 1998; Appleby, 2001; Kirchner, 2011). Over recent decades, three models have been widely applied in defining the ^{210}Pb chronology of lake sediments: the Constant Rate of Supply (CRS) model, for lakes where the sediment accumulation rate is not uniform and the Constant Flux Constant Sedimentation (CFCS) and Constant Initial Concentration (CIC) models for lakes with constant accumulation rates (Goldberg, 1963; Krishnaswamy et al., 1971; Appleby & Oldfield, 1978; Appleby et al., 1979; Appleby, 2001; Kirchner, 2011; Sanchez-Cabeza & Ruiz-Fernández, 2012; Aquino-López et al., 2020). The CRS model permits the rate of sedimentation to change over time while assuming a constant flux of unsupported ^{210}Pb to the sediment, whereas the CFCS and CIC models assume that regardless of changes in the rate of sediment accumulation, the initial concentration of unsupported ^{210}Pb is constant at each stage of sediment accumulation (Appleby, 2001; Kirchner, 2011).

However, given that lake environments are complex and may cause variations in the vertical distribution of unsupported ^{210}Pb in the sediment, ^{210}Pb chronologies should be validated using artificial radionuclides (Appleby, 2001, 2008; Smith, 2001; Holmgren et al., 2010; Kirchner, 2011; Barsanti et al., 2020). Many artificial radionuclides (^{137}Cs, ^{239}Pu, ^{240}Pu, ^{241}Am), were produced and distributed globally during the nuclear weapon tests that occurred between 1945

and 1980 (UNCEAR, 2000; Leslie & Hancock, 2008; Hancock et al., 2011; Corcho-Alvarado et al., 2014; Harrison et al., 2021). In addition, Pu was discharged into the environment through reactor failures and satellite accidents such as Chernobyl and Fukushima events that occurred around the late 1980s and 2011 respectively (Zheng et al., 2012; Thakur et al., 2017). Recent research has focused on isotopes of Pu (^{239}Pu, ^{240}Pu and ^{241}Pu), one of the most commonly employed radionuclides, especially in the Southern Hemisphere, where atmospheric fallout is relatively low compared to the Northern Hemisphere (Leslie & Hancock, 2008; Hancock et al., 2011; Harrison et al., 2021). Accurate measurement of Pu isotopes is feasible even at low concentrations, given their higher sensitivity, particle-reactive ability in both fresh and saltwater and ability to transfer quantitatively to sediments tracking erosion and sedimentation processes in lakes (Tims et al., 2010; Pan et al., 2011; Hancock et al., 2011; Harrison et al., 2021). ^{239}Pu and ^{240}Pu with considerably long half-lives ($2.4*10^4$ and $6.5*10^3$ years respectively) make up the majority of the Pu activity linked to nuclear weapon fallout, whilst short-lived ^{238}Pu and ^{241}Pu isotopes are less common (Hancock et al., 2011). This combination of factors makes the application of Pu as a chronometer more valuable in the Southern Hemisphere than ^{137}Cs or ^{241}Am (Leslie & Hancock, 2008). It has also been noted that long-lived Pu isotopes in undisturbed lacustrine sediment sequences are good proxies for correlating the depth of deposition to the amount of nuclear fallout globally (Harrison et al., 2021). Substantially longer half-lives of Pu means that more Pu inventory is retained in sediment compared to Cs, which may have been subjected to radioactive decay sooner (Pan et al., 2011).

Given both the CFCS and CRS modelling mostly rely on assumptions or interpolations, previous studies have discussed the limitations of using these models, even with the introduction of chronological markers (Kirchner, 2011; Baskaran et al., 2014; Tylmann et al., 2016; Aquino-López et al., 2018; Abril, 2019). The most common drawbacks are inconsistencies in ages derived from different model calculations, inaccurate sediment accumulation rates and significant uncertainties in model assumptions (Tylmann et al., 2016; Aquino-López et al., 2018). It is also evident that in some cases, external or post-depositional processes such as erosion, sediment transport, and mixing were disregarded in developing ^{210}Pb chronologies (e.g. Barsanti et al., 2020). When the ^{210}Pb profile does not reach equilibrium, missing ^{210}Pb data are estimated by interpolation or extrapolation of sediment core data, which may further challenge reliable age estimates using ^{210}Pb data (Appleby, 2001; Aquino-López, Ruiz-Fernández et al., 2020).

To address many of these difficulties, Aquino-López et al., (2018) introduced the Bayesian *Plum* model as an alternative way of determining sediment age from ^{210}Pb data. The model was developed using Bayesian approaches, an advanced statistical framework for the estimation of chronological uncertainty, alongside the behaviour and fluctuation of unsupported and supported ^{210}Pb. *Plum* is an extension of the well-established Bacon-based age-depth function, which enables the incorporation of radiocarbon dates into the chronology (Blaauw & Christen, 2011; Aquino-López et al., 2018; Aquino-López, Ruiz-Fernández et al., 2020; Blaauw et al., 2020). This approach has been tested elsewhere and compared against the most widely used CRS model (Aquino-López et al., 2020b; a). This work showed that the *Plum* approach is reproducible and provides accurate measures of uncertainties and can be applied effectively in cases where the ^{210}Pb profile is not optimal such as when there are missing data in the profile, loss of the top sediment or when the ^{210}Pb activity does not reach background (Aquino-López et al., 2020b; a).

3.1.3 Radiocarbon dating of lake sediments

Radiocarbon dating (^{14}C) is largely used to determine the age of various fossil materials, based on their radioactive decay. Bayesian statistical methods of ^{14}C datasets can result in reliable chronologies with nearly decadal resolution (Björck et al., 2001; Hua, 2009; Howarth et al., 2013; Martin et al., 2019). Age control is limited to ~50,000 years, given the half-life of ^{14}C (5568 years) (Björck et al., 2001; Hua et al., 2022). In addition, radiocarbon dating has also been successfully utilised in tracing anthropogenic carbon ("post-bomb ^{14}C") derived in the atmosphere by nuclear weapon testing during 1950 – 1980 and has been also applied as a potent dating tool, which provides dating accuracies ranging from one to a few years for contemporary terrestrial materials (Hua et al., 2012, 2013, 2022). It has been identified that ^{14}C analysis of bulk sediment generates larger errors due to contributions by unknown amounts of contaminated "old" carbon, derived from geologic sources or materials synthesised from geologic carbon dissolved in groundwater (Wilkins et al., 2012; Martin et al., 2019). In some cases, material that contains "younger" carbon, such as humic acids can also contaminate bulk sediments (Björck et al., 2001; Kilian et al., 2002; Howarth et al., 2013; Strunk et al., 2020; Cadd et al., 2022).

Terrestrial macrofossils (e.g. leaves, seeds, needles and twigs) found in lake sediments produce the most accurate and reliable radiocarbon ages because they maintain an equilibrium with

atmospheric $^{14}CO_2$ until death (Olsson, 1983; Marty & Myrbo, 2014; Meng et al., 2020; Norris et al., 2020). Further, their often rapid degradation leads to short residence times in lake catchments before deposition (Howarth et al., 2013; Norris et al., 2020). However, macrofossils are not always abundant enough in depositional environments, particularly in semi-arid and high-altitude regions (Kilian et al., 2002; Fletcher et al., 2017; Cadd et al., 2022). In such cases, pollen grains that are ubiquitous and of terrestrial origin are considered a suitable substitute for ^{14}C dating (Howarth et al., 2013; Fletcher et al., 2017; Tunno et al., 2021; Cadd et al., 2022). Pollen grains are well-preserved in lake sediments due to their chemical resistance and are observed in a variety of sediment sequences (Björck et al., 2001; Fletcher et al., 2017). However, the use of pollen grains as the primary source of dating of lacustrine sediments remains uncommon (Fletcher et al., 2017). One of the major reasons for this is the complex nature of the pollen extraction procedures and many studies have focused on developing these methods over the last few decades (Long et al., 1992; Mensing & Southon, 1999; Tennant et al., 2013; Martin et al., 2019; Tunno et al., 2021; Turney et al., 2021; Cadd et al., 2022). The inclusion of reworked or anachronous pollen grains as well as extended processing times and incomplete removal of non-pollen material from the resultant pollen are significant problems that have been identified (Tennant et al., 2013; Cadd et al., 2022).

3.2 Materials and methods

3.2.1 Study site

Lake Surprise, a crater lake formed around 37000 years ago (Matchan et al., 2020) is located in the Budj Bim National Park in the volcanic plains of western Victoria, which is overlain by Cretaceous sandstone, Tertiary-quaternary marl, and limestone (Price et al., 1997; Barr et al., 2014). The lake experiences a temperate climate composed of hot dry summers and mild wet winters, with the majority of the precipitation occurring in the winter (Barr et al., 2014; Falster et al., 2018). The amalgamation of three adjacent volcanoes has formed the irregularly shaped lake surface with larger littoral habitats at each end (Timms, 1975). According to measurements obtained during fieldwork in 2019, the maximum lake water depth is ~11.5 m and it is nearly 600 m long and 200 m wide, at its longest and widest points (Appendix 1). Densely vegetated steep and high (~49 m) crater walls function as wind barriers and retain distinct boundaries during times of lake stratification (Timms, 1975; Builth et al., 2008; Barr et al., 2014; Falster et al., 2018). The lake is referred to as a "closed basin" due to the absence of any fluvial input

or output to or from the lake (Barr et al., 2014). Lake Surprise is predominantly fed by local groundwater and to some extent by precipitation (Chapter 2, section 2.4.4).

However, the lake's approximately 30,000-year history of continuous sedimentation and groundwater is anticipated to have an impact on the lake's hydrology, particularly during dry spells (Falster et al., 2018). The small and steep catchment is heavily vegetated by *Eucalyptus viminalis* ("manna gum") and *Acacia melanoxylon* ("blackwood") (Builth et al., 2008; Barr et al., 2014). Additionally, an understorey of *Pteridium esculuntum* (“bracken”), *Banksia marginanta*, Poaceae and Asteraceae. Shallow water margins are home to a diverse, though typically restricted, zone of aquatic vegetation made up primarily of emergent macrophytes and floating plants in protected open water (Tibby et al., 2006; Falster et al., 2018).

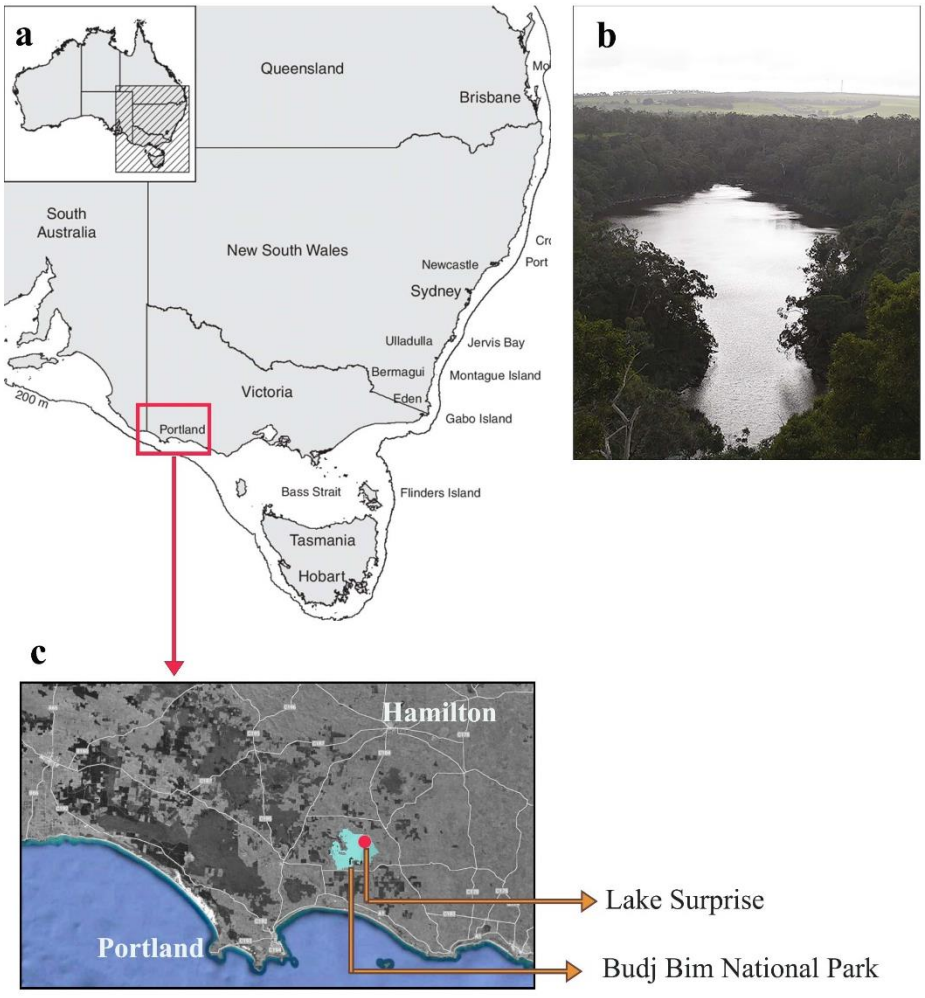

Figure 1. a) Approximate location of western Victoria b) the elongated view of Lake Surprise looking north-west from the crater rim of Mt Eccles (Falster et al., 2018) c) Zoomed-in section

of the selected region of western Victoria (from figure 1a), representing the location of Lake Surprise, the Budj Bim National Park.

3.2.2 Coring and core sampling

Three series of sediment cores were recovered from the lake (near the middle section) in October 2019, covering approximately 11.5 m of sediment depth. The upper soft sediment core (SUR-19-01), which recovered the top 1.57 m of the sediment profile was collected using a wide-diameter Perspex piston corer. Two 10 m long series of deeper sediment cores (SUR-19-02 & SUR-19-03) were collected, with SUR-19-03 overlapping at 0.5 m depth difference, were obtained as 1 m segments using a modified large-bore Bolivia corer (Wright, 1967) (Appendix 5). Because of its unconsolidated state and high water content, the SUR-19-01 core was sub-sampled in the field at a resolution of 0.5 cm, whilst the Bolivia cores were split longitudinally, photographed and sub-sampled at 0.5 cm intervals in the laboratory at the University of Adelaide. All untreated sediment samples were stored in sealed polyethylene bags at 4ºC. During the sub-sampling, macrofossil specimens (seeds, twigs, leaves, and barks) from all three cores were extracted using clean tweezers that were cleaned before being preserved in distilled water. Sediments from the SUR-19-01 core were taken for ^{210}Pb and Pu isotope measurements from samples selected from the topmost 100 cm. Wet sediments were weighed and freeze-dried (~48 hours) before being used in the sample preparation. The sample depths were selected with sufficient spacing to identify the changes in sedimentation rate.

3.2.3 Core correlation

Given that three sediment cores overlap, a composite depth was developed by comparing geochemical and visible features using the QAnalySeries v.1.5.0 software (Kotov & Paelike, 2018). The major element composition of the deeper sediments was measured using the ITRAX µ-XRF scanner at the Australian Nuclear Science and Technology Organisation (ANSTO) and soft sediments were measured using an Olympus Delta™ family handheld XRF analyser at the University of Adelaide. According to a principle components analysis of these elemental compositions, the most prominent variation in sediment composition (principle component 1; PC1) is expressed by the concentration of Ca (calcium carbonate) within the sediments (Barr et al., in preparation). Therefore, a composite depth was established by comparing the Ca content of all three cores. High-resolution sediment core images that represent stratigraphic

relationships as described in Ankor & Tyler, (2022) were used as additional tie-points (Appendix 5). Note that the depth used in this chapter refers to the corrected composite depth.

3.2.4 ^{210}Pb sediment dating method

^{210}Pb activity (half-life = 22.3 years) was measured on nine samples from the SUR-19-01 core, covering a total depth of 107.3 cm. The total ^{210}Pb was measured using ^{210}Po and supported ^{210}Pb was approximately determined by measuring ^{226}Ra activity (Harrison et al., 2003; Holmgren et al., 2010). Unsupported ^{210}Pb activities were estimated using the difference between total ^{210}Pb activity (determined from ^{210}Po) and supported ^{210}Pb activity determined from ^{226}Ra (Appleby 2002). The sample preparation and analysis were undertaken at ANSTO. Approximately 0.5 – 1 g of freeze-dried sediment from each sample was mixed with ^{209}Po and ^{133}Ba (~0.2 g) tracers of known solutions to determine the activities of ^{210}Pb and ^{226}Ra respectively. The sediment was digested using a mixture of 30% H_2O_2, concentrated HNO_3 and HCl and left overnight on a hotplate (50 – 70°C) to settle Pb/Ba/Ra precipitate. The supernatant was decanted and the precipitate was transferred to a centrifuge tube using 50% ethanol, for centrifugation at 5100 rpm for two minutes. The precipitate was dissolved by adding 5 ml of Na_5DTPA (0.2 M) and one drop of thymol blue indicator in an ultrasonic bath for 15 minutes. Methyl red indicator was added to the mixture and passed through a 0.45 μm membrane filter and 4% Na_2SO_4 was added into the filtered product, to collect the residual Na_5DTPA. The sample was mixed with 1:1 acetic acid and 1 ml of BaSO4 simultaneously for 30 minutes in the refrigerator. The solution was filtered through 1-micron filter paper with the aid of 50% ethanol and the filter paper with Ba/Ra micro-precipitate was left to air dry. A blank sample of mixed Po and Ba tracer and 0.5 mg/ml of Ba carrier was analysed along with samples to evaluate the method. The filter paper was first used in counting the Gamma spectrum (^{133}Ba) using the High Purity Germanium (HPGe) crystal gamma detector and followed by the analysis of alpha spectrometry (^{226}Ra). Independent sediment ages and mass accumulation rates were calculated using the Constant Rate of Supply (CRS) and the Constant Flux Constant Sedimentation (CFCS) models (Appleby & Oldfield, 1978).

3.2.5 Plutonium isotope measurements

Pu isotope concentrations (^{239}Pu, ^{240}Pu and ^{241}Pu) were measured in ten samples extracted at 3 cm intervals of the upper 40 cm of the SUR-19-01 core. Sample processing was carried out in a laboratory with positive-pressure HEPA-filtered air at ANSTO. Freeze-dried sediment was

(~1 g) combusted at 800℃ approximately for 30 minutes and all samples were treated with ~2 pg of NIST SRM 4334 G ^{242}Pu as the reference isotope (Child et al., 2008; Harrison et al., 2021). Ashed samples were reacted with aqua regia solution (3:1 HCl:HNO_3) at 110℃ for three hours. Samples were then dissolved in 2 M HNO_3 and processed through ion-exchange chromatography for Pu separation and purification. Pu isotopes were measured using a heavy ion beamline in the ANTARES Accelerator Mass Spectrometry (AMS) facility at ANSTO. Using a negative ion sputter source, PuO^- ions were produced and accelerated to 4 MV. After the argon gas was stripped, the Pu^{5+} charge state was used for analysis (Hotchkis et al., 2000; Child et al., 2008; Harrison et al., 2021). Synchronous high and low energy electrostatic switching was used to cycle the target plutonium isotopes (^{239}Pu, ^{240}Pu, and ^{241}Pu) into the detector and the measurements were normalised to an internal isotopic ratio standard composed of NIST SRM 4330B^{239}Pu, NIST SRM 4338a^{240}Pu, and NIST SRM 4334H^{242}Pu after being compensated for dead time losses in the detector (Harrison et al., 2021). Detailed sample preparation and the analytical procedure are described in Child et al., (2008).

3.2.6 Radiocarbon dating methods

3.2.6.1 Pollen sample preparation and analysis

The pollen processing procedure for radiocarbon samples followed a modified method of Turney et al., (2021) and Cadd et al., (2022) at the Chronos 14Carbon-cycle facility at the University of New South Wales. Samples (5 – 10 g of wet sediment) were dispersed in Milli-Q water (18 MΩ) for 1 hour and mixed with a vortex mixer before passing through a 125 µm sieve. Material >125 µm was transferred back into a vial and retained for further analysis. Dark-coloured supernatant was discarded after centrifuging the sieved samples. 1 M HCl was added to each sample and heated at 80℃ for 45 minutes. Samples were rinsed 3 times with Milli-Q water and centrifuged at 2700 rpm. Sediment samples were then sieved gently through a 70 µm sieve and material >70 µm was discarded. The fine sediment was centrifuged and 4% NaOH was added to each sample and heated for 30 minutes at 80ºC. Samples were rinsed 3 times with Milli-Q water and centrifuged at 2700 rpm. Substantial amounts of extraneous organic material were visible in the pollen samples after visual analysis. Samples were rinsed 3 times with Milli-Q water and centrifuged at 2700 rpm Samples were treated with saturated KCO_3 and concentrated HNO_3 (Schultz solution) for an hour at 60℃ to eliminate resistant organic material and algae remains. Samples were gently sieved into 50 ml glass centrifuge tubes through a 100 µm mesh sieve using Milli-Q water. Samples were centrifuged and the

supernatant was discarded. Samples were rinsed Milli-Q water and centrifuged until the supernatant was clear.

Pollen samples were density separated by adding 5 ml of sodium polytungstate (SPT) at a specific gravity of 1.8 g cm^{-1} into each sample and mixed thoroughly with vortex and centrifuged for 25 minutes at 2500 rpm. Centrifugation was carried out before the bottom of each tube was frozen in liquid nitrogen and the float decanted into a clean 50mL glass centrifuge tube. Samples were then sieved through a 20 µm sieve and the material retained on the sieve was transferred to a glass centrifuge tube. A second treatment with saturated KCO_3 and concentrated HNO_3 (Schultz solution) for an hour at 60°C was conducted, to remove any leftover organic matter from the sample. Samples were repeatedly rinsed until a clear supernatant is observed. Remains of the colonial algae, *Botryococcus*, were identified upon visual inspection even after a second Shultz solution treatment, which may have affected outcomes. 4% HCl was added to each sample and heated for 1 hour at 80ºC. Sieves were cleaned and sonicated in 4% HCl before being transferred to 30% Nitric Acid and finally Milli-Q water. All processed pollen samples were graphitised with an AGE3 system (Ionplus, Switzerland). Samples were combusted in an Elemental Analyzer before CO_2 was passed through a zeolite trap and converted to graphite using hydrogen and an iron catalyst (Wacker et al., 2010; Turney et al., 2021). ^{14}C measurements were performed on a MICADAS (Ionplus, Switzerland) Accelerator Mass Spectrometer (AMS) following Turney et al., (2021).

3.2.6.2 Macrofossil and bulk sediment sample preparation and analysis

During the sub-sampling procedure, samples of macrofossils (leaves, seeds, and twigs) were primarily extracted from SUR-19-01 and SUR-19-02, as they were absent in the SUR-19-03 core. In addition, bulk sediment was also sampled from chosen depths that corresponded with macrofossil samples. Cleaned macrofossils were stored in distilled water before being sent to ANSTO for sample preparation and radiocarbon dating. Samples were pre-treated using the standard Acid-alkali-acid (AAA) method to remove carbonates and any contaminating material from the samples (Hua et al., 2001; Norris et al., 2020). All the purified samples were then combusted to CO_2 in a sealed combustion tube, after being dried approximately for 24 hours (Hua et al., 2001; Howarth et al., 2013). Graphite was produced by the reduction of CO_2 using excess hydrogen and an iron catalyst at 600°C for 12 hours (Hua et al., 2001; Howarth et al., 2013). The graphite iron mixture was pressed into aluminium cathodes for ^{14}C analysis using the AMS facility that employs the techniques described by Fink et al., (2004). All ^{14}C readings

were normalised using the oxalic acid I NIST standard (HOxI) (Fink et al., 2004; Howarth et al., 2013). ^{14}C values were corrected for the isotope fractionation using ^{13}C measurements obtained from graphite sub-samples in the continuous flow isotope ratio mass spectrometer (CF-IRMS) and the results of ^{14}C were reported as a percentage of modern carbon (pMC) (Fink et al., 2004; Howarth et al., 2013). Radiocarbon dates were calibrated to calendar years using the revised southern hemisphere radiocarbon calibration curve, SHCal 20 for pre-bomb samples and Bomb SH 1–2 data for post-bomb samples (Hogg et al., 2020; Hua et al., 2022). The ages were reported as calendar years before the year 1950 (cal yr BP).

3.2.7 Age-model development

The composite age model for Lake Surprise was developed in R using the Bayesian *Plum* model by integrating the unsupported ^{210}Pb activities and Pu isotope concentrations with the radiocarbon data (Blaauw & Christen, 2011; Aquino-López et al., 2018). Here data from 33 pollen dates, 17 macrofossil dates, the unsupported ^{210}Pb activity profile and the maximum Pu concentration were utilised to develop the age model. The age model was run in R 4.1.3. Software (R Core Team, 2022). The measured ages were reported as conventional ^{14}C ages with 1σ errors and then converted to calibrated years during the age modelling process.

3.2.8 Contamination screening of pollen extracts using Fourier transform infrared (FTIR) analysis

Radiocarbon-dated pollen samples were screened using Fourier transform infrared spectrophotometry (Perkin Elmer Spectrum 400 FTIR) at the University of Adelaide to identify any non-pollen contaminants such as inorganic carbonate, charcoal and other organic residues. Only the samples dated above ~3 m (8 samples) were used in the analysis because the remaining material of the bottommost samples was insufficient (Supplementary data, Table IV). The transmittance (T) spectrum was converted to absorption (A), using the equation $A = 2 - \log_{10}(T)$. The values were expressed in percentage of total absorbance.

3.3 Results

3.3.1 Lake Sedimentology

The majority of the sediment profile contained fine-clay rich, blackish-grey colour texture except for the bottommost sediments (lower depths of SUR-19-02 and SUR-19-03), which are

marginally coarser-grained (Appendix 5). Undisturbed, fine carbonate laminations were observed throughout the sediment depths of SUR-19-02 and SUR-19-03 (Ankor & Tyler, 2022) (Appendix 5). However, no significant features were observed in the SUR-19-01 core, which may be due to the way the sediments were cored and extruded in the field, or it could also be in part due to the sediments being very soft in the upper 1 m. The moisture content of lake sediments is noticeably high, with SUR-19-01 sediments containing >85% water. (Chapter 4, Supplementary Figure I).

3.3.2 Results of ^{210}Pb activity measurements

The unsupported ^{210}Pb activity values that are significantly higher (5 to 901 Bq kg^{-1}) than the supported ^{210}Pb activities (3.4 to 4.8 Bq kg^{-1}), mostly contribute to the total ^{210}Pb activity profile (9 to 906 Bq kg^{-1}) (Table1.).

Table 1. ^{210}Pb activity profile (supported and excess) against sediment depth

Depth (cm)	Supported activity (Bq/kg)	Unsupported/excess activity (Bq/kg)	Total activity (Bq/kg)
0.7	4.8±1.0	901±47	906±47
9.1	3.8±0.7	715±35	719±35
17.5	4.3±0.6	249±11	253±11
25.9	5.1±0.7	164±8	170±8
41.5	3.3±0.6	32±2	35±2
54.4	3.3±0.5	15±1	18±1
66.4	2.7±0.4	15±1	17±1
87	2.3±0.3	7±1	9±1
107.4	3.4±0.5	5±1	9±1

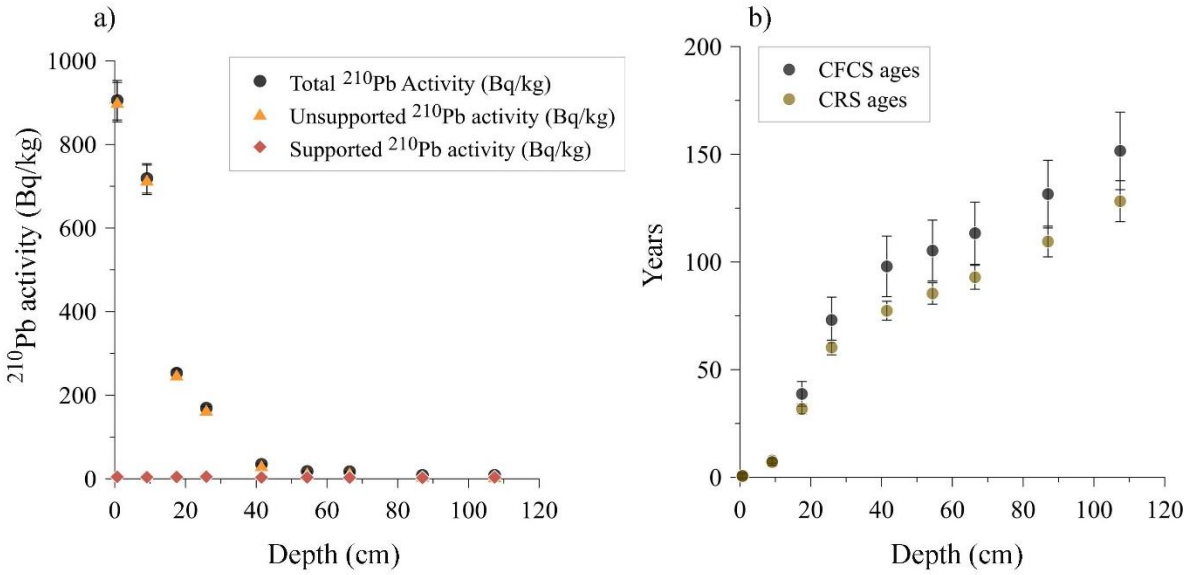

Figure 2. a) ^{210}Pb activity profile and b) calculated CFCS and CRS ages against the sediment depth.

The ^{210}Pb activity profile illustrates a downward decrease (Figure 2a) with unsupported ^{210}Pb activity reaching its measurable background at 107.4 cm (5±1 Bq kg^{-1}). The bulk density of the sediments selected for ^{210}Pb dating varies from 0.03 to 0.18 g cm^{-3}, whereas the cumulative dry mass of the sediments varies from 0.01 to 6.05 g cm^{-2} (Supplementary data, Table I). From the two age models derived using ^{210}Pb activity results, the CFCS age model is comparatively older (152±18 years) than the CRS age model (128±10 years) (Supplementary data, Table I). The CFCS age model represents two sets of constant mass accumulation rates for lower and upper zones as 0.077 and 0.0196 gcm^{-2}/ year respectively. The sediment accumulation rate is considerably higher and more variable in the CRS age model with values varying from 0.018 to 0.098 gcm^{-2}/ year. Both models show a significant rise in the accumulation rate from around 30 – 40 cm.

3.3.3 Plutonium isotope measurements

The total Pu concentration varies from 0.02 to 1.30 pg/g. Pu isotope concentration in the sediments decreases in the order of ^{239}Pu, ^{240}Pu and ^{241}Pu with values of ^{239}Pu and ^{240}Pu measured above the background level with values ranging from 0.02 – 1.11 pg/g for ^{239}Pu and 0.003 – 0.19 pg/g for ^{240}Pu (Table 2.). Two bottom samples illustrate an extremely low concentration (17.13 and 28.23 fg) with their values being approximately three orders in magnitude compared to the chemistry blanks used in measurements (0.004 and 0.016 fg).

$^{239+249}$Pu values of these sediments range from 0.07 to 4.13 mBq/g. Atomic ratios of ^{240}Pu/^{239}Pu represent relatively higher values (0.08 – 0.18) compared to the ^{241}Pu/^{239}Pu ratio in which values range from $1.33*10^{-4}$ – $8.09*10^{-4}$.

Table 2. Pu isotope concentrations against sediment depth

Depth (cm)	Total Pu concentration (pg/g)	$^{241/239}$Pu ratio	$^{240/239}$Pu ratio	$^{239+240}$Pu concentration (mBq/g)
0.7	0.1330±0.0041	4.90E-04±2.13E-04	0.166±0.006	4.20E-01±1.02E-02
4.9	0.1832±0.0042	7.32E-04±1.78E-04	0.160±0.004	5.73E-01±1.11E-02
9.1	0.3145±0.0068	5.26E-04±9.79E-05	0.130±0.003	9.42E-01±1.68E-02
13.3	0.4908±0.0111	7.89E-04±1.29E-04	0.149±0.003	1.51E-00±2.84E-02
17.5	1.2416±0.0317	7.81E-04±1.07E-04	0.151±0.003	3.84E-00±8.06E-02
21.7	1.3022±0.0268	7.54E-04±1.02E-04	0.168±0.004	4.13E-00±7.27E-02
25.9	1.1930±0.0290	8.09E-04±1.19E-04	0.179±0.004	3.84E-00±7.67E-02
29.9	0.1073±0.0023	7.79E-04±1.65E-04	0.171±0.005	3.41E-01±6.30E-02
33.8	0.0232±0.0007	5.84E-04±3.29E-04	0.168±0.007	7.36E-02±1.79E-02
37.7	0.0486±0.0011	1.33E-04±7.85E-05	0.079±0.002	1.33E-01±1.33E-02

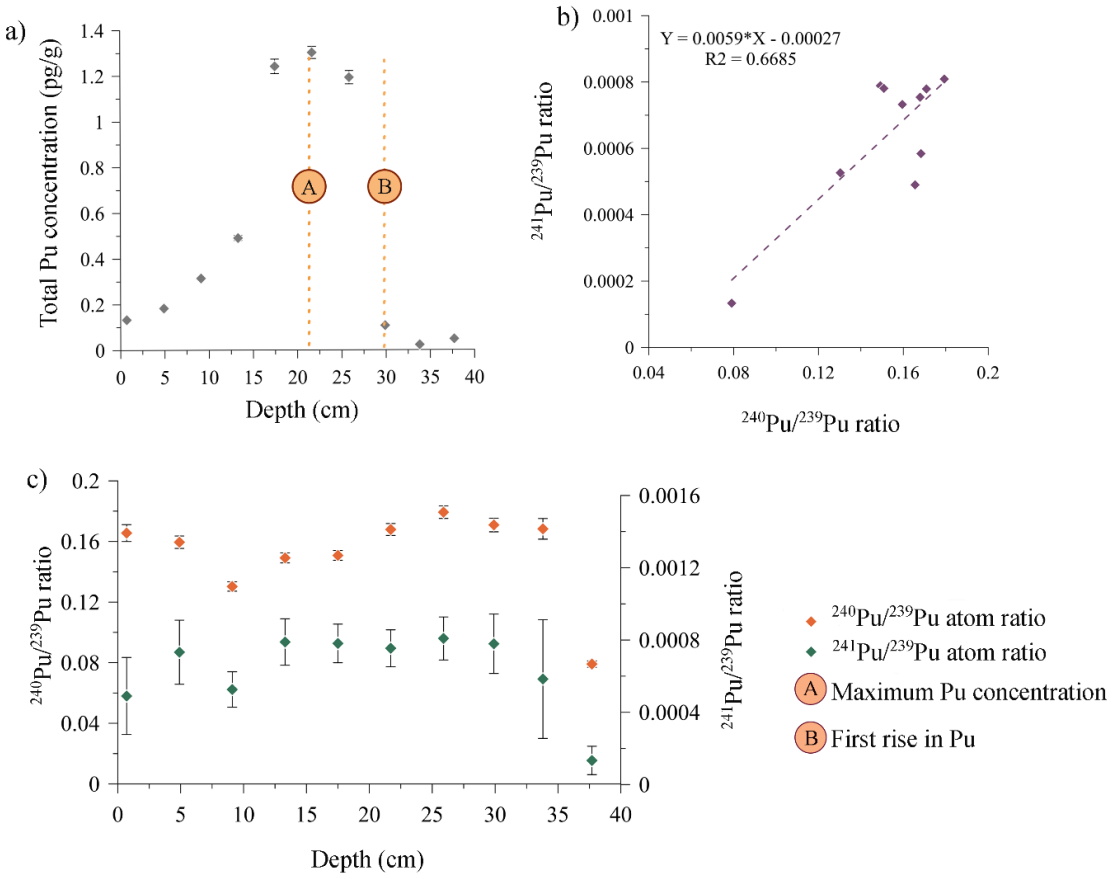

Figure 3. a) Total Pu concentration b) linear correlation between $^{240/239}$Pu and $^{241/239}$Pu atom ratios and c) representation of Pu isotope ratios against sediment depth. Note that depth refers to the corrected composite depth.

Even though the total Pu concentration illustrates a relatively broader variation, a distinct peak is observed at 21.7 cm (1.30 pg/g). The major rise in Pu content commenced at ~30 cm, and values remained high until ~20 cm, after which they progressively declined towards the surface (Figure 3a). Pu atom ratios remained within a fairly consistent range (~0.149 – 0.179) except for the bottommost (older) sample (37.7cm) which sits at a much lower value (Figure 3b). Lower depths (~20 – 34 cm) measure relatively higher atomic ratios with the highest value being recorded at 25.9 cm. Isotope ratios slightly decrease from 9 to 17 cm by approximately 0.04, although surface sediments (0 – 5 cm) show values that are comparable with the lower depths. Isotope ratios illustrate a moderate to strong linear correlation (R^2 = 0.67), with the majority of the data concentrated towards the right end of the linear regression line, except for the bottommost sample with a considerably smaller value (Figure 3b).

3.3.4 Radiocarbon dating

Table 3. List of radiocarbon analytical results of macrofossil (plant), bulk sediment and pollen samples from the sediment cores.

Material dated	Depth (cm)	Lab ID	$\delta^{13}C$ (‰PDB)	^{14}C content (pMC)		^{14}C age		Sediment-macrofossil age offset (^{14}C yr)	
				Mean	1σ	Mean	1σ	Mean	1σ
Plant	15.05	OZZ426	-28.7	135.66	0.35	-13	3		
Plant	31.55	OZZ427	-28.7	147.88	0.40	-22	3		
Pollen	41.2	UNSW-490				314	11		
Pollen	52.15	UNSW-491				375	11		
Pollen	62.15	UNSW-492				387	11		
Plant	69.15	OZZ428	-28.7	93.72	0.24	520	20		
Pollen	73.45	UNSW-493				423	11		
Pollen	77.65	UNSW-497				451	11		
Macrofossil	96.2	OZZ429	-28.6	96.89	0.24	255	20		
Pollen	97.3	UNSW-494				475	12		
Pollen	104.45	UNSW-526				565	10		
Pollen	116.65	UNSW-495				581	11		
Macrofossil	129.3	OZZ514	-25.7	94.44	0.26	460	22		
Sediment	129.3	OZZ515	-29.8	91.73	0.24	693	21	234	31
Macrofossil	136.45	OZZ430	-28.0	93.65	0.20	525	20		
Pollen	136.45	UNSW-496				865	11		
Pollen	151.51	UNSW-499				939	12		
Pollen	188	UNSW-500				1666	12		
Plant	214	OZZ516	-28.8	85.46	0.19	1262	18		
Sediment	214	OZZ517	-27.7	81.80	0.22	1614	22	352	26
Pollen	218	UNSW-501				1549	12		
Pollen	253	UNSW-502				1760	12		
Pollen	274.5	UNSW-503				2026	12		
Plant	288	OZZ518	-28.3	79.35	0.22	1858	22		
Sediment	288	OZZ519	-29.1	77.82	0.23	2014	24	156	33
Pollen	310.5	UNSW-504				2424	12		
Pollen	348.5	UNSW-505				2537	12		
Macrofossil	375.5	OZZ521	-25.3	74.81	0.20	2331	21		
Plant	379.5	OZZ520	-28.3	75.71	0.23	2235	24		
Pollen	407.5	UNSW-506				2862	12		
Pollen	450	UNSW-507				3291	12		
Pollen	479	UNSW-530				3329	12		
Plant	497	OZZ522	-29.0	68.06	0.18	3091	21		
Pollen	509.5	UNSW-510				3442	12		
Pollen	541.5	UNSW-511				3525	12		
Plant	566	OZZ524	-28.4	61.80	0.15	3866	20		
Pollen	579	UNSW-512				3976	13		
Pollen	608.5	UNSW-531				3984	13		
Macrofossil	615	OZZ523	-28.0	64.18	0.16	3562	20		
Pollen	643.5	UNSW-514				3549	12		
Pollen	717.5	UNSW-516				4785	14		
Plant	744.5	OZZ525	-27.0	55.19	0.16	4775	23		

Plant	776.5	OZZ526	-28.6	53.47	0.16	5029	24		
Macrofossil	782.5	OZZ527	-29.1	52.84	0.15	5124	23		
Pollen	809	UNSW-517				5682	14		
Pollen	854.5	UNSW-518				6625	15		
Plant	898	OZZ528	-26.4	45.66	0.14	6297	25		
Sediment	898	OZZ529	-35.3	44.32	0.14	6537	25	239	35
Pollen	924	UNSW-519				6847	15		
Pollen	956	UNSW-520				7428	16		
Pollen	982	UNSW-521				7408	15		
Pollen	1016	UNSW-522				8049	15		
Pollen	1056.5	UNSW-524				8658	17		
Pollen	1132.5	UNSW-523				10034	18		

The ^{14}C content (pMC) of the modern macrofossil samples increases upwards, with younger samples accounting for comparatively higher values than the deeper sediments that range from 44.32±0.14 to 147.88±0.40. Radiocarbon ages of macrofossil samples vary from 520±20 to 6297±25 ^{14}C years, whereas the pollen dates vary from 314±12 to 100034±18 ^{14}C years along the sediment profile (Table 3.). Macrofossil samples measured at depths of 15.05 cm and 31.55 cm illustrate a peak in ^{14}C content (pMC ≥135), with ages recorded as -13±3 and -22±3 ^{14}C years respectively.

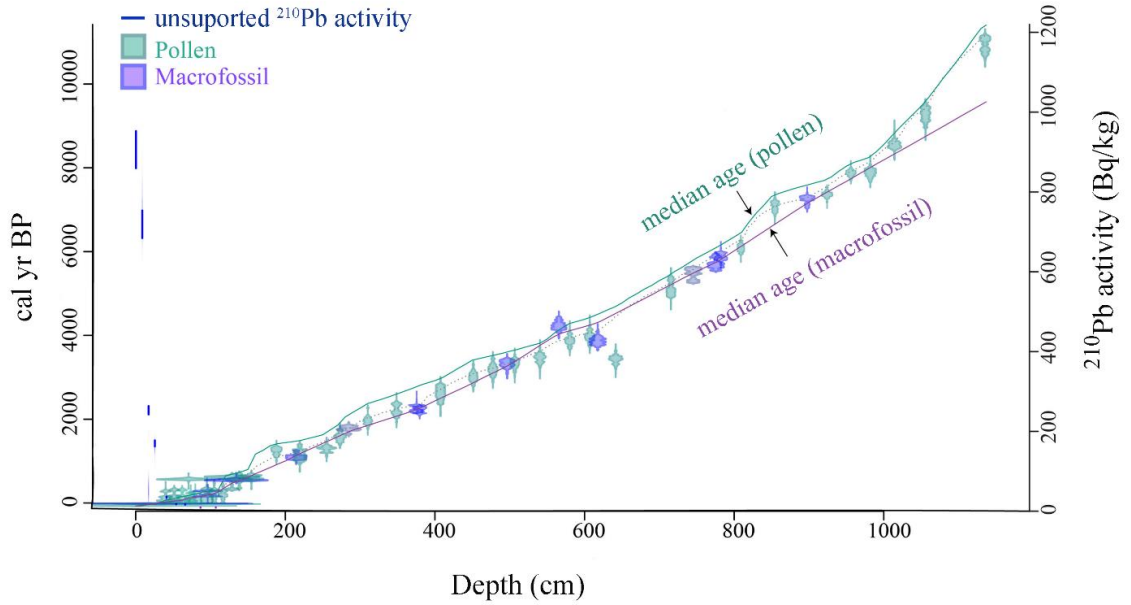

Figure 4. Representation of the age offset between radiocarbon dates of pollen and macrofossil samples vs. sediment depth.

Several noticeable age reversals are observed between pollen and macrofossil ages at around ~70 – 100 cm and ~600 cm (Table 3.). When all the radiocarbon-dated samples are compared against each other, both the bulk sediment and pollen dates remain older than the macrofossil

dates and at certain depths, bulk sediments are older than pollen ages (Supplementary data, Figure I). However, this cannot be observed deeper than 900 cm due to the scarcity of other datable materials except for pollen. The age offset between sediment and macrofossil samples for the same depth generated an old carbon effect that ranges from 156±33 to 353±26 with a weighted mean value of 260±86 ^{14}C years (Table 3). All radiocarbon ages described here are expressed with 1σ uncertainty.

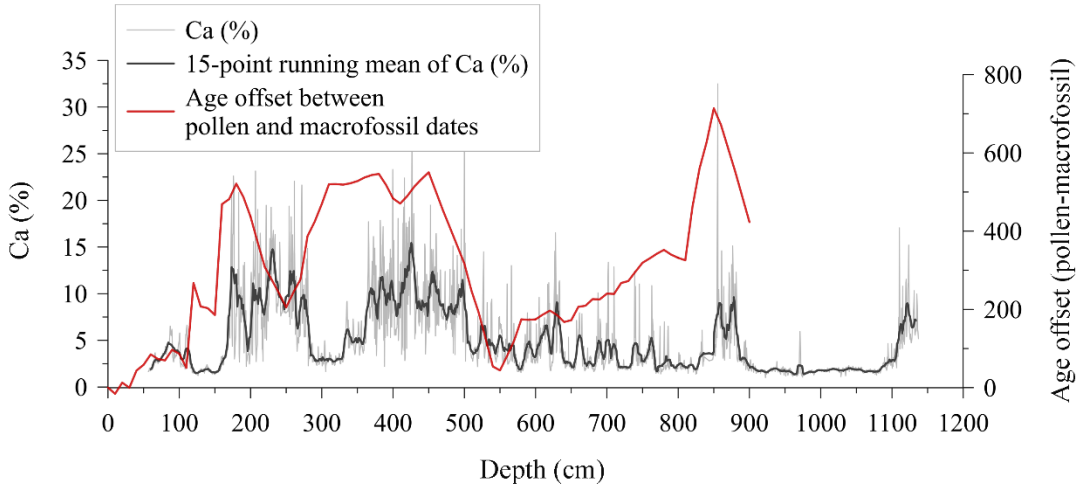

Figure 5. Comparison of age offset between pollen and macrofossil dates with measured Ca (%) through the sediment depth. Ca% data were obtained from Barr et al., in preparation.

According to the age model derived using all the radiocarbon dates, the pollen and macrofossil ages reflect two notable anomalies, with pollen ages being older than macrofossil ages (Figure 4). This is further supported by the age offset (~340 years) observed between pollen and macrofossil samples measured at the same depth (i.e. at 136.5 cm; Table 3.). However, this offset is not well represented in the bottommost section of the core (900 – 1100 cm), due to the absence of any macrofossil dates. An increase in age offset is mostly observed at depths with high Ca content, although the comparison is not perfect (Figure 5).

3.3.5 FTIR spectrum results

The major bands of absorption spectra are centred on 1000 cm^{-1}, 2800 – 3000 cm^{-1} and ~1500 – 1700 cm^{-1} along with a broader stretching band at around 3200 – 3600 cm^{-1} (Figure 6). The very strong narrow bands centred around 1000 cm^{-1} (900 – 1200 cm^{-1}) represents polysaccharide groups that are composed of various C – O and C – O – C, C – C and C – P bonds (Jebsen et al., 2012; Abdala Díaz et al., 2019; Hong et al., 2021).

Relatively strong absorption bands observed around 2800 – 3000 cm^{-1} belong to aliphatic compounds (C – H) (Jebsen et al., 2012; Liu et al., 2013). Moderate bands that spread from 1500 – 1700 cm^{-1} mainly represent protein group compounds of amide I and II that consist of N – H, C – H and C – N bonds (Mecozzi et al., 2009; Jebsen et al., 2012; Liu et al., 2013). The wider band observed after 3000 cm^{-1} indicates the hydroxyl group (O – H), which is a commonly observed compound in many proteins, lipids and carbohydrates (Kovac et al., 2005; Liu et al., 2013). Carbonate bands are not detected in the FTIR spectrum (~ 900 and ~ 1435; Figure 6). In addition, there are a few other small-moderate peaks the source of which is unidentified.

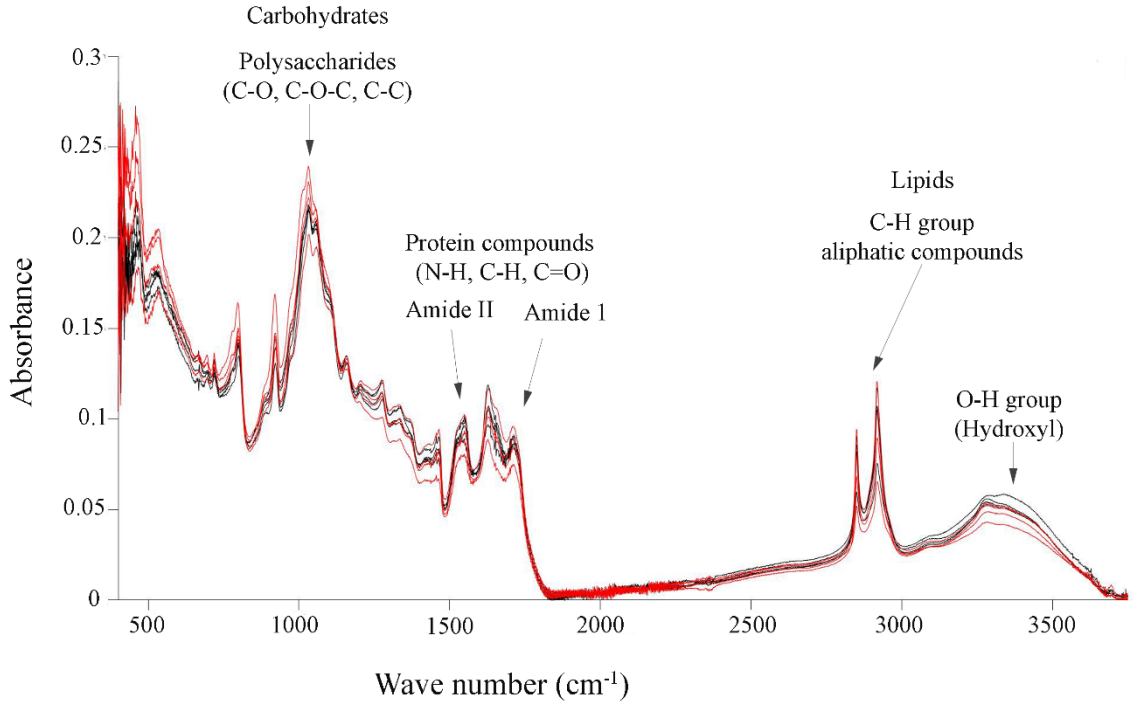

Figure 6. FTIR absorption spectrum of radiocarbon dated pollen samples. The red coloured spectra illustrate samples with higher age offset (>300 cal yr BP) and black spectra indicate samples with lower age offset (≤ 200 cal yr BP). Refer to supplementary table IV for more information.

3.4 Discussion

3.4.1 ^{210}Pb and Pu considerations for the Lake Surprise chronology

The ^{210}Pb activity profile (Figure 2a) observed along the vertical depth demonstrates a steady (monotonic) decline, suggesting that the unsupported ^{210}Pb accumulation rate in Lake Surprise sediments is most likely to be uninterrupted by external processes such as burial or removal of organic matter, sediment mixing processes and dilution of ^{210}Pb by increased rates of sediment

accumulation (Appleby, 2001; Holmgren et al., 2010) (Figure 2a). In contrast, the estimates from the CFCS model show two changes in the sediment accumulation rate (Supplementary data, Table I), suggesting that minor changes may have occurred in the sedimentation rate over time (Appleby, 2001; Heijnis, 2001; Harrison et al., 2021). However, such deviations may occur due to multiple other natural reasons such as the availability of a zone of incomplete mixing close to the surface or radioisotope migration through sediments (Benoit & Rozan, 2001; Harrison et al., 2021). Differences may also be due to artificial sources, where sediment accumulation rates tend to vary due to the mathematical framework used in CRS/CFCS modelling (Aquino-López et al., 2020a). Given the presence of Lake Surprise in a relatively sheltered national park, it is unlikely that significant anthropogenic impacts could have changed the rate of sedimentation over the last century. However, considering that the sediment samples from core SUR-19-01 contain high water content, and exhibit no visible laminations (in contrast to the deeper lake sediments) there is a chance that sediment mixing may have occurred either at the sediment-water interface or during coring.

Both hemispheres experienced nuclear testing mostly during the period between 1945 and 1980. The transport of Northern Hemisphere plutonium to the Southern Hemisphere took one to two years (Leslie & Hancock, 2008; Hancock et al., 2011). Even though the Lake Surprise data show a broader peak, the maximum Pu concentration observed at 21.7 cm can be matched with the maximum Southern Hemispheric Pu fallout recorded ~1964 following the US/former USSR nuclear tests in 1962–1963 (Hancock et al., 2011; Hirose & Povinec, 2015; Harrison et al., 2021). A relatively broader Pu profile near the maximum may be due to multiple reasons such as sediment mixing or Pu migration through sediment or due to amalgamation of different Pu sources (Harrison et al., 2021). The small and steep catchment area surrounding the lake limits soil migration through a sediment profile. Therefore, this is most likely caused by capturing several Pu sources or sediment mixing. $^{240}Pu/^{239}Pu$ atom ratio provides indications of both the global and local inputs of Pu into the sediment (Thakur et al., 2017; Harrison et al., 2021). The oldest sample (measured at 37.7 cm) with a relatively lower $^{240}Pu/^{239}Pu$ atom ratio is likely to originate from a local Pu fallout given that it deviates from all other samples, which plot within or near the value range of SH atmospheric fallout (0.185±0.014) (Figures 3b & 3c) (Kelley et al., 1999). This also disagrees with other studies that suggest sediments had a relatively high $^{240}Pu/^{239}Pu$ atom ratio during the early years (1952 – 1954) or the pre-moratorium period when US-dominated testing released more than 90% of the global fallout (Koide et al., 1982; Muramatsu et al., 2001; Harrison et al., 2021).

The second major chronological marker used in identifying Pu fallout is the period of the first detection of Pu, which refers to the year when there was enough cumulative activity in the sediment to be detected using modern measurement techniques (Leslie & Hancock, 2008). Previous studies from Australia and elsewhere have shown that detectable Pu fallout occurred for the first time ~ 1954 in the southern latitudes (30º – 40º S) (Leslie & Hancock, 2008; Hancock et al., 2011, 2014; Harrison et al., 2021). Even though all the samples measured above the detectable limit of Pu from the AMS technique, the bottommost sample illustrates an isotope ratio ($^{240}Pu/^{239}Pu$) which is lower than the global fallout range of 0.16 – 0.19 (global average = 0.18) and even below the previously recorded value range for Victoria (~ 0.12 – 0.20) (Krey et al., 1976; Tims et al., 2013; Harrison et al., 2021). Similarly, the lowering of both the total Pu concentration and $^{239+240}Pu$ atom ratio in the sample measured at 33.8 cm close to background levels further suggests that the two bottommost samples are likely to represent timing before the first detection limit of global Pu fallout. Therefore, it is likely that the first detection of fallout Pu (1954) at Lake Surprise was recorded at 29.9 cm, along with the initiation of the steep rise in Pu concentration in the sediment (Leslie & Hancock, 2008). The total Pu content in lake sediments follows the pattern of global fallout after the first detection of Pu, where Pu content remained high from the 1960s through the early 1970s and gradually declines after 1980 with a reduction of atmospheric testing (Moroney, 1979; Hancock et al., 2011; Harrison et al., 2021).

According to Antarctic ice-core records, the $^{240}Pu/^{239}Pu$ ratio of global fallout during the early 1950s was between 0.19 – 0.34 (Koide et al., 1985). Among many nuclear testings happened in Australia, the Emu Field and Maralinga nuclear testings detonated in 1953 are found to have lower atom ratios (<0.07) in the early years (Child & Hotchkis, 2013; Smith et al., 2016; Tims et al., 2016). Given that these test sites are located in South Australia, the lower atomic ratio observed in Lake Surprise may be an indication of Pu fallout from these local tests. Several other Australian records have also reported lower $^{240}Pu/^{239}Pu$ atom ratios and have proposed a similar influence (Everett et al., 2008; Tims et al., 2013; Johansen et al., 2016). Similarly, higher Pu content observed immediately before and after the maximum Pu content may represent the influence of former Soviet Union tests (1961 – 1962) and French testing in the South Pacific (1964 – 1974) in addition to United States-dominated global fallout (UNCEAR, 2000; Hirose & Aoyama, 2003). Therefore, it is apparent that Lake Surprise sediments may illustrate a combination of global and local fallout of Pu with distinctive high and low $^{240}Pu/^{239}Pu$ atom ratios in order.

3.4.2 Age offsets in bulk sediment and pollen grains

Comparison between macrofossil radiocarbon ages with pollen extracts and bulk sediments indicates old carbon effects in both pollen and bulk sediments. The old carbon effect, where the actual radiocarbon dates are mixed with relatively old carbon that is derived from ^{14}C depleted water or solid contaminants is a common feature in western Victorian lakes, given its carbonate-rich (limestone) geological setting (Price et al., 1997; Wilkins et al., 2012). Multiple other lake studies from the region have reported radiocarbon age offsets varying from approximately 200 – 670 years (Wilkins et al., 2012; Barr et al., 2014; Gouramanis et al., 2010). A previous study from Lake Surprise found an age offset between pollen grains and bulk sediment of 424±75 ^{14}C years (Barr et al., 2014), which is larger than the difference between macrofossil and bulk sediment observed in this study (~260 ^{14}C years (Table 3.). Old carbon can also be assimilated into organic matter via lacustrine algae utilising carbon derived from groundwater or dissolved carbonates (Zhang et al., 2015). In addition, reduced rates of mixing in stratified lakes may deplete the ^{14}C reservoir in water compared to atmospheric CO_2 (Philippsen, 2013; Zhou et al., 2015, 2020; Schneider et al., 2019). Previous studies from Lake Surprise have suggested this effect could be possibly due to the presence of old carbon in groundwater that flows across underlying limestone (Barr, 2010; Barr et al., 2014). Even though this explanation may be true for bulk sediment, the presence of carbonate in pollen grains is highly unlikely, given that it has been acid-treated prior to analysis. This is further strengthened by the absence of any carbonate peaks in the FTIR spectrum (Figure 6). Given that the age model for this study is solely produced using pollen and macrofossil radiocarbon dates, there is little or no influence from the bulk sediment-derived old carbon effect on the chronology.

Old carbon effects in pollen radiocarbon dates are more concerning since pollen is assumed to assimilate atmospheric CO_2 in their synthesis, equivalent to terrestrial macrofossils. However, the results of this study demonstrate that pollen radiocarbon dates are both offset from those derived from plant macrofossils, but also that the amount of offset varies down-core (Figure 4). Several previous studies have analysed pollen for radiocarbon dating and found older ages than the sediment's actual depositional age (Kilian et al., 2002; Howarth et al., 2013; Fletcher et al., 2017; Martin et al., 2019; Schiller et al., 2021) and in rare cases younger ages (Porch and Kershaw, 2010). Multiple hypotheses for the frequent occurrence of considerably older ages from pollen dating have been proposed in previous studies such as contamination of pollen grains by tracers of micro-charcoal or other organic remains (algae, spores etc.) (Martin et al.,

2019; Kilian et al., 2002; Fletcher et al., 2017), the fluvial reworking of pollen from watershed soils (Howarth et al., 2013; Schiller et al., 2021) and migration of pollen through the sediment profile due to increased catchment erosion (Li et al., 2012).

Pollen grains can be contaminated by charcoal and other organic remains including algae and spores, and are commonly observed in organic-rich sedimentary environments (Kilian et al., 2002; Martin et al., 2019). It is believed that simple laboratory techniques lead to the incomplete removal of other organic/inorganic matter from the pollen grains as the main cause of pollen contamination (Long et al., 1992; Tennant et al., 2013; Zimmerman et al., 2019; Tunno et al., 2021; Cadd et al., 2022). Although there have been many different pollen concentration techniques developed over time, total purification has been a challenge to date (Zimmerman et al., 2019; Cadd et al., 2022). Even though this study employed the most recently developed technique which combines filtering and flotation to isolate pollen concentrations (Turney et al., 2021; Cadd et al., 2022), given the organically rich environment in Lake Surprise, the organic residue may likely have retained after pollen purification. The correspondence between the pollen-macrofossil age offset and carbonate concentration (indicated by Ca%) suggests that old carbon derived from groundwater may be partly responsible, either through direct carbonate contamination or indirectly.

In this study, the contamination of pollen extracts by calcium carbonates can be largely eliminated as a potential explanation. Firstly, the pollen grains were treated in concentrated acids (HCl) for ~45 minutes, it is unlikely that calcium carbonates were retained through this treatment. This is further confirmed by FTIR analysis, which indicates an absence of any absorption bands corresponding to wave numbers of inorganic carbonate (860 – 900 cm^{-1} and 1300 – 1600 cm^{-1}) (Liu et al., 2013) (Figure 6). Several other studies have suggested that carbonates may form relatively moderate absorption bands at around 700 – 725 cm^{-1}, ~1800 cm^{-1} and 2500 cm^{-1} due to the C=O double bond (Mecozzi et al., 2001; Kovac et al., 2005; Liu et al., 2013). None of these bands is apparent in the pollen FTIR data either (Figure 6). Secondly, micro-charcoal is also commonly observed as a pollen contaminant which may contribute to the older ages, given the fire-prone environment in the region (Kershaw et al., 2002; Harris et al., 2017; Martin et al., 2019). This is another possibility for Lake Surprise sediments because fine charcoal particles were observed throughout the sediment core during the sampling procedure. However, this is not well supported by the FTIR results: charcoal particles tend to exhibit major infra-red absorption bands at 1400 cm^{-1}, 1640 cm^{-1} and stretching

bands at 3450 cm^{-1} wavelengths (El-Eswed, 2016). Even though there are absorption bands apparent corresponding to these wavelengths, a significant difference cannot be identified between these spectra to differentiate the presence of charcoal in these sediments (Figure 6). This does not exclude charcoal contamination for all pollen radiocarbon dates, however, it does suggest that charcoal contamination might be a minor problem in these samples. Additionally, the lack of clear separation absorption spectra relevant to larger and smaller age errors in the FTIR spectrum inhibits the identification of the exact contaminant in the pollen grains. In addition, pollen grains may also be stored within catchment soils and remobilised at a later date (Mensing & Southon, 1999; Li et al., 2012; Howarth et al., 2013; Neulieb et al., 2013; Fletcher et al., 2017; Schiller et al., 2021), however, the steep catchment slopes and short residence time of soils in the catchment of Lake Surprise (Timms, 1976; Barr et al., 2014; Falster et al., 2018) discounts this hypothesis for the magnitude of age offsets estimated. In addition, reworked pollen grains should be visible as broken or degraded under a light microscope, (Tweddle & Edwards, 2010; Tennant et al., 2013; Schiller et al., 2021), however, the pollen from this study exhibited clear preservation. The finely laminated nature of these sediments (Ankor & Tyler, 2022) makes the prospect of vertical migration of pollen grains equally unrealistic.

The remaining possible explanations for old radiocarbon effects in the pollen extracts, therefore, rely on old ^{14}C being included within a pollen-like matrix. One candidate in this respect is the possible presence of algal spores amongst the isolated pollen. Studies elsewhere have suggested that the isolation of aquatic algal spores from pollen grains is difficult compared to other non-pollen material (Regnéll, 1992; Fletcher et al., 2017; Steinhoff et al., 2022). Lake algae have the potential to uptake carbon from the dissolved inorganic carbon (DIC) pool that may be contaminated with "old" carbon derived from groundwater. Similarly, algae may also consume methane or CO_2 generated by the remineralisation of older sediments (Zhou et al., 2015). Even though algae (colonial algae and *Botryococcus*) were noted visually before and during sample processing, following the pollen isolation, they were clumped and dry, making it challenging to confirm their presence under a light microscope. The FTIR spectra also illustrate absorption bands relevant to carbohydrates, proteins and lipids, which could also be derived from algal remains (Jebsen et al., 2012; Liu et al., 2013) (Figure 6). Alternative explanations include the saturation of the pollen grains by groundwater containing highly processed ancient organic matter that may have survived the pollen pre-treatment. Overall, considering both the FTIR analytical results and the correspondence between age-offset and carbonate concentration, it appears that contamination of the pollen extracts by algal spores,

which in turn were partially synthesised using groundwater-derived inorganic carbon, is the most likely explanation for pollen-macrofossil ^{14}C age offsets in the Holocene sediments of Lake Surprise.

3.4.3 Radiocarbon chronology for Holocene sediments at Lake Surprise

Considering our observation of an age offset for pollen radiocarbon dates, which concurs with previous work (e.g. Martin et al., 2019), the measured radiocarbon dates of pollen extracts were corrected using a mean age offset of 340±50 years, input as Delta.R and Delta.STD in *Plum*. The final age model was developed by incorporating these corrected radiocarbon dates of pollen and macrofossil samples along with the ^{210}Pb unsupported activities and the year of maximum Pu concentration. The surface depth which is equivalent to the date of sampling (~2019.5) was taken as the uppermost chronological control point. To balance the chronological precision, the model was run in R with relatively higher (8000) iterations and 8 cm thickness while other settings remained as default.

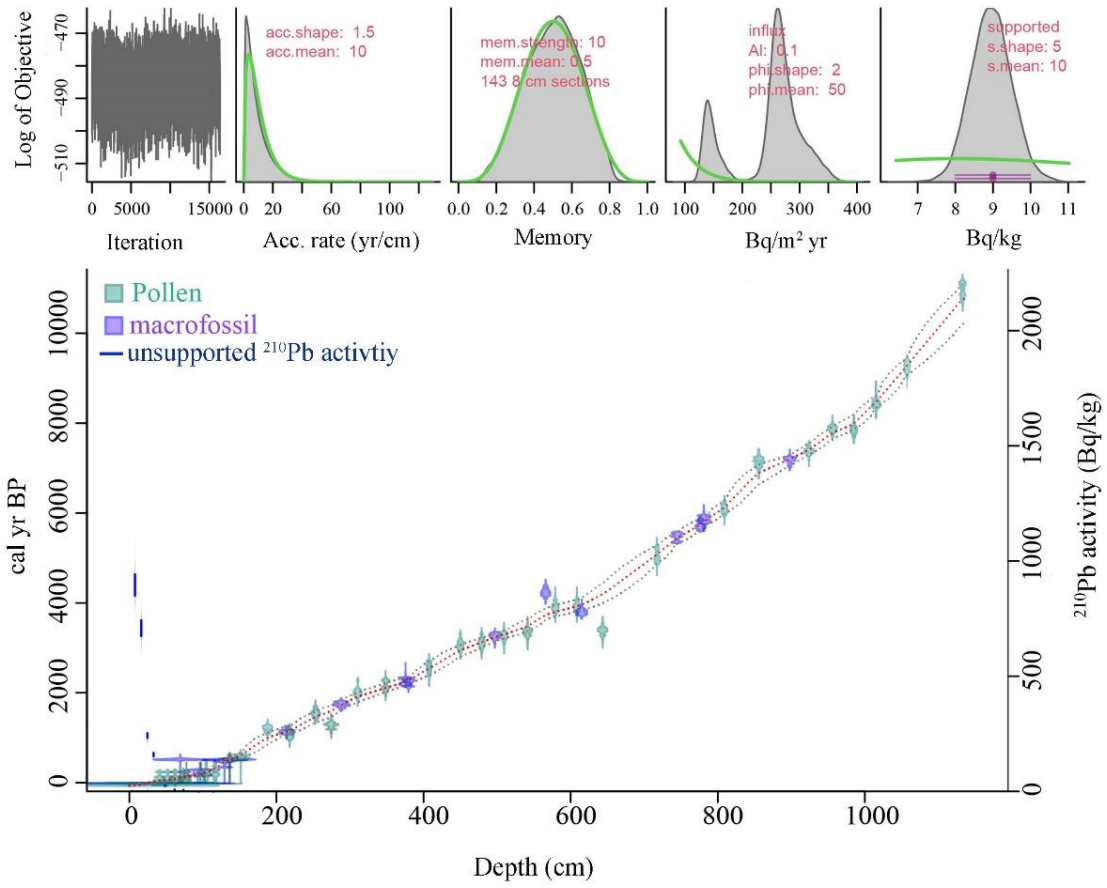

Figure 7. Lake Surprise age model derived using radiocarbon ages of pollen and macrofossil samples, ^{210}Pb activities and Pu concentration in the *Plum* package in R 4.1.3 software (R Core Team 2022). All ^{14}C dates were calibrated to SHCal20 (Hogg et al., 2020).

The final age model was then evaluated using the modern chronological markers obtained from Barr et al., (2014), such as an age estimate from the *Pinus* pollen arrival at Lake Surprise (75±20 cal yr BP) and the date of the previous sediment coring (core LSFS) at Lake Surprise (-54±2 cal yr BP; 2004 CE), which was identified by comparing the corresponding depths of diatom species composition data counted at 4 cm resolution from SUR-19-01 with the diatom record in Barr et al., (2014) (Supplementary data, Figure II). Accordingly, the top of the LSFS core was estimated to be equivalent to approximately 5 cm depth in SUR-19-01. These modern chronomarkers were plotted considering the 5 cm offset. In addition, ages corresponding to the first detection of Pu and the year of maximum Pu concentration, post-bomb radiocarbon dates and CRS and CFCS age models obtained from this study were plotted in the same diagram to assess their applicability.

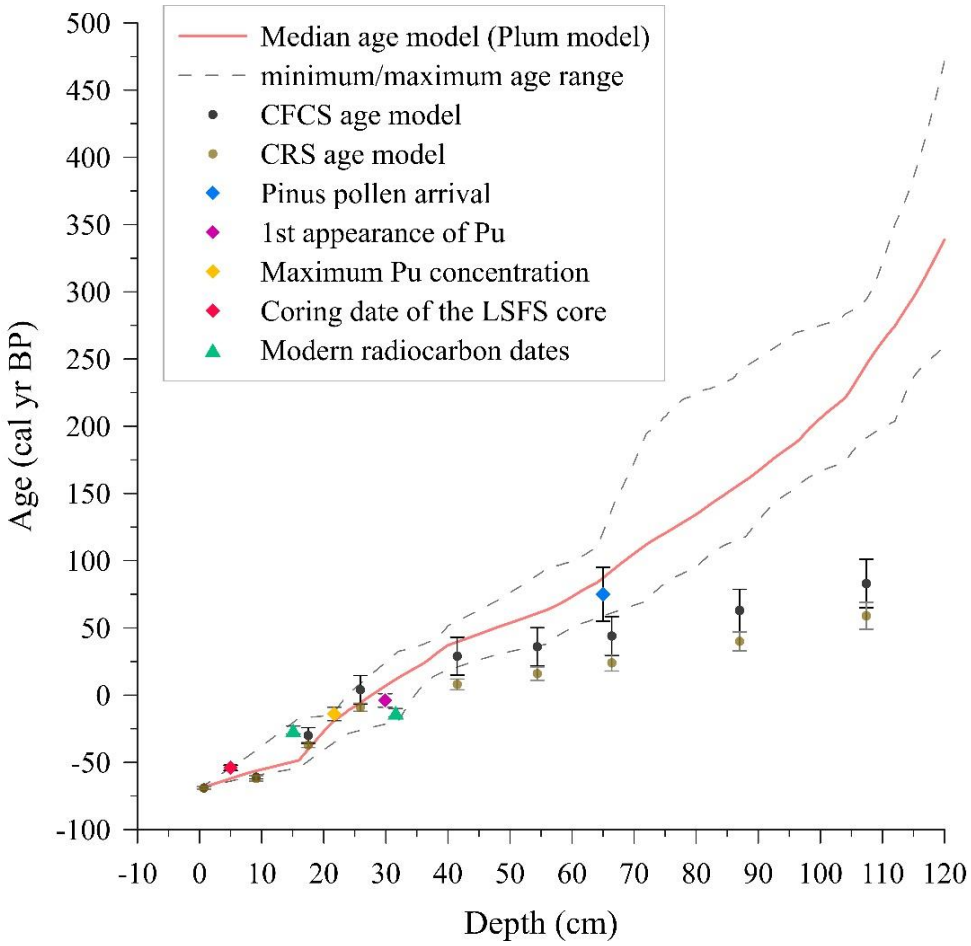

Figure 8. Representation of modern sediment markers in the top 120 cm of the age model illustrated in the figure. Note that the coring date of the previous sediment core (LSFS) and *Pinus* pollen arrivals dates were taken from Barr et al., (2014). Maximum Pu concentration and the first appearance of Pu are illustrated as A and B in Figure 3a (Supplementary data, Table III).

According to the model representation in Figure 8, the majority of age markers plot within the 95% confidence interval of the modelled ages indicating that the final model is acceptable within the given age limits. However, both CFCS and CRS models deviate from the *Plum* model towards older ages with increasing rates of age uncertainties. This deviation is much greater for the CRS model where the deviation was initiated about 20 cm earlier than in the CFCS model. Previous records have explained this behaviour as an artificial increase in the sedimentation rate that occurs as a result of the mathematical structure and differing interpolations used in the model, where the age function tends to reach infinity, as a response to the decreasing ^{210}Pb activity (Aquino-López et al., 2020a; b; Barsanti et al., 2020).

Given their higher uncertainties, it has been recommended that CFCS and CRS-derived ^{210}Pb ages older than ~100 years be presented as extrapolations instead of directly measured ages (Barsanti et al., 2020). However, provided that the *Plum* model is based only on the existing data and developed using an independent age-depth function, it is unlikely to indicate any artificial increase in the sedimentation rate (Aquino-López et al., 2020a). The CRS/CFCS models and *Plum* model comparison in this study suggest that *Plum* has a higher potential to capture true ages, which has also been suggested previously by Aquino-López et al., (2020b). The shift in sedimentation observed at around 54 cm in this study may serve as an indication of consequences of modelling, rather than any natural causes due to the disagreement between CFCS/CRS modelled ages and the final age model and due to the lack of any evidence of related to sedimentation change throughout this period.

According to the median of the modelled age estimates, the entire sediment profile (~11.4 m) extends to ~10,846 cal yr BP with a mean sedimentation rate of approximately ~9.5 yr/cm. A past study from Lake Surprise indicates average sedimentation of <10 yr/cm in the upper 3 m of a previously recovered sediment core, however, the chronological control of this core was developed using CRS modelling of ^{210}Pb ages and very few radiocarbon dates, where linear interpolations had to be used in estimating the basal ages (Barr, 2010; Barr et al., 2014). However, the relatively high rates of sedimentation found in our chronology agree with several other studies, which illustrate continuous and nearly consistent sedimentation of roughly 30,000 cal yr BP that was obtained from 30 pollen-derived radiocarbon dates of an ~18 m thick sediment sequence at Lake Surprise (Builth et al., 2008; Falster et al., 2018). Even though it is recommended that lake sedimentation should be at least 1m/1000 years to allow a sampling routine that would, typically, offer a sub-decadal scale temporal resolution per sample, the

majority of Australian lakes generally illustrate a lower sedimentation rate, at least in the period before landscape clearance by European settlers (Harle et al., 2005). However, our interpretation along with previous studies has demonstrated that Lake Surprise has a suitable rate of sedimentation across longer periods (Barr, 2010; Falster et al., 2018).

3.5 Conclusion

In this study, a well-constrained chronology was developed for the Holocene Epoch at Lake Surprise using both radionuclide and radiocarbon techniques. The monotonic behaviour of the ^{210}Pb profile and the well-resolved structure of the Pu concentration illustrate that sediment mixing or any other physical processes are highly unlikely. The ^{240}Pu/^{239}Pu isotope ratio varies from 0.08 – 0.18 with values in the early 1950s being even smaller indicating that Pu from Australian nuclear testing may have influenced the site in addition to global fallout. This is further supported by the broader fallout peak and relatively smaller value (0.152±0.004) of ^{240}Pu/^{239}Pu ratio compared to the global fallout average. AMS ^{14}C dates were analysed in multiple datable proxies and to obtain the most reliable chronology here we utilised only the pollen and macrofossil radiocarbon ages in the age model. In the pre-historical sediments, the majority of the chronology is based on pollen ages, given the scarcity of sufficient macrofossils from the sediment. An old carbon effect in this study has been estimated using bulk sediment and macrofossil ages and exhibits comparatively lower values compared to previous studies from the lake. Bulk sediment ^{14}C may have been effected by old carbon derived from groundwater flux as previously suggested and evidenced in groundwater-dominated lakes with carbonaceous bedrock.

The systematic age offset between the pollen and macrofossil indicates that pollen ages are ~340 ^{14}C years older than desired ages. Further experimental analysis suggests that this is most likely due to the admixture of pollen grains and aquatic algae. The final age model derived using the Bayesian *Plum* model for corrected pollen dates and macrofossils along with ^{210}Pb activity and Pu dates, explains approximately 10846 cal yr BP from an 11.4 m long composite sediment depth. The age model agrees with the majority of the recent chronomarkers demonstrating accuracy and reliability. Given that this age model well explains most of the issues that were not addressed in previous studies and its consistency and minimal uncertainties, demonstrate its potential in robust climate interpretations.

3.6 List of references cited

Abdala Díaz, R. T., Casas Arrojo, V., Arrojo Agudo, M. A., Cárdenas, C., Dobretsov, S., & Figueroa, F. L. (2019). Immunomodulatory and Antioxidant Activities of Sulfated Polysaccharides from Laminaria ochroleuca, Porphyra umbilicalis, and Gelidium corneum. *Marine Biotechnology*, *21*(4), 577–587. https://doi.org/10.1007/s10126-019-09905-x

Abril, J. M. (2019). Radiometric dating of recent sediments: On the performance of 210Pb-based CRS chronologies under varying rates of supply. *Quaternary Geochronology*, *51*(November 2018), 1–14. https://doi.org/10.1016/j.quageo.2018.12.003

Adrian, R., O'Reilly, C. M., Zagarese, H., Baines, S. B., Hessen, D. O., Keller, W., Livingstone, D. M., Sommaruga, R., Straile, D., Van Donk, E., Weyhenmeyer, G. A., & Winder, M. (2009). Lakes as sentinels of climate change. *Limnology and Oceanography*, *54*(6 PART 2), 2283–2297. https://doi.org/10.4319/lo.2009.54.6_part_2.2283

Ankor, M. J., & Tyler, J. J. (2022). A computational method for rapid orthographic photography of lake sediment cores. *Journal of Paleolimnology*, *0123456789*. https://doi.org/10.1007/s10933-022-00241-0

Appleby, P. G. (2001). *in Recent Sediments*. *1*, 171–172.

Appleby, P. G. (2008). Three decades of dating recent sediments by fallout radionuclides: A review. *Holocene*, *18*(1), 83–93. https://doi.org/10.1177/0959683607085598

Appleby, P. G., & Oldfield, F. (1978). The calculation of lead-210 dates assuming a constant rate of supply of unsupported 210Pb to the sediment. *Catena*, *5*(1), 1–8. https://doi.org/10.1016/S0341-8162(78)80002-2

Appleby, P. G., Oldfield, F., Thompson, R., Huttunen, P., & Tolonen, K. (1979). 210Pb dating of annually laminated lake sediments from Finland [10]. *Nature*, *280*(5717), 53–55. https://doi.org/10.1038/280053a0

Aquino-López, M. A., Blaauw, M., Christen, J. A., & Sanderson, N. K. (2018). Bayesian Analysis of 210 Pb Dating. *Journal of Agricultural, Biological, and Environmental Statistics*, *23*(3), 317–333. https://doi.org/10.1007/s13253-018-0328-7

Aquino-López, M. A., Ruiz-Fernández, A. C., Blaauw, M., & Sanchez-Cabeza, J. A. (2020a). Comparing classical and Bayesian 210Pb dating models in human-impacted aquatic environments. *Quaternary Geochronology*, *60*(November 2019). https://doi.org/10.1016/j.quageo.2020.101106

Aquino-López, M. A., Sanderson, N. K., Blaauw, M., Sanchez-Cabeza, J.-A., Ruiz-Fernandez, A. C., Aquino-López, J. A. C. M. A., Sanderson, N. K., Blaauw, M., Sanchez-Cabeza, J.-A., Ruiz-Fernandez, A. C., & Christen, J. A. (2020b). *A simulation study to compare 210Pb dating data analyses*. 1–21. http://arxiv.org/abs/2012.06819

Barr, C., Tibby, J., Gell, P., Tyler, J., Zawadzki, A., & Jacobsen, G. E. (2014). Climate variability in south-eastern Australia over the last 1500 years inferred from the high-

resolution diatom records of two crater lakes. *Quaternary Science Reviews*, *95*, 115–131. https://doi.org/10.1016/j.quascirev.2014.05.001

Barsanti, M., Garcia-Tenorio, R., Schirone, A., Rozmaric, M., Ruiz-Fernández, A. C., Sanchez-Cabeza, J. A., Delbono, I., Conte, F., De Oliveira Godoy, J. M., Heijnis, H., Eriksson, M., Hatje, V., Laissaoui, A., Nguyen, H. Q., Okuku, E., Al-Rousan, S. A., Uddin, S., Yii, M. W., & Osvath, I. (2020). Challenges and limitations of the 210Pb sediment dating method: Results from an IAEA modelling interlaboratory comparison exercise. *Quaternary Geochronology*, *59*(April). https://doi.org/10.1016/j.quageo.2020.101093

Baskaran, M., Nix, J., Kuyper, C., & Karunakara, N. (2014). Problems with the dating of sediment core using excess 210Pb in a freshwater system impacted by large scale watershed changes. *Journal of Environmental Radioactivity*, *138*, 355–363. https://doi.org/10.1016/j.jenvrad.2014.07.006

Beasley, T. M., Carpenter, R., & Jennings, C. D. (1982). Plutonium, 241Am and 137Cs ratios, inventories and vertical profiles in Washington and Oregon continental shelf sediments. *Geochimica et Cosmochimica Acta*, *46*(10), 1931–1946. https://doi.org/10.1016/0016-7037(82)90131-4

Benoit, G., & Rozan, T. F. (2001). 210Pb and 137Cs dating methods in lakes: A retrospective study. *Journal of Paleolimnology*, *25*(4), 455–465. https://doi.org/10.1023/A:1011179318352

Björck, S., Wohlfarth, B., & Wohlfarth@geol, B. L. (2001). *1.10.Dvi*. *1*(1955).

Blaauw, M., & Christen, J. A. (2011). *Bacon manual – v 2.3.9.1*. 1–15.

Blaauw, M., Christen, J. A., & Aquino-López, M. A. (2020). A Review of Statistics in Palaeoenvironmental Research. *Journal of Agricultural, Biological, and Environmental Statistics*, *25*(1), 17–31. https://doi.org/10.1007/s13253-019-00374-2

Blaauw, M., & Christeny, J. A. (2011). Flexible paleoclimate age-depth models using an autoregressive gamma process. *Bayesian Analysis*, *6*(3), 457–474. https://doi.org/10.1214/11-BA618

Brenner, M., & Kenney, W. F. (2015). Dating wetland sediment cores. *Methods in Biogeochemistry of Wetlands*, *September 2016*, 879–900. https://doi.org/10.2136/sssabookser10.c45

Builth, H., Kershaw, A. P., White, C., Roach, A., Hartney, L., McKenzie, M., Lewis, T., & Jacobsen, G. (2008). Environmental and cultural change on the Mt Eccles lava-flow landscapes of southwest Victoria, Australia. *Holocene*, *18*(3), 413–424. https://doi.org/10.1177/0959683607087931

Cadd, H., Sherborne-Higgins, B., Becerra-Valdivia, L., Tibby, J., Barr, C., Forbes, M., Cohen, T. J., Tyler, J., Vandergoes, M., Francke, A., Lewis, R., Arnold, L. J., Jacobsen, G., Marjo, C., & Turney, C. (2022). the Application of Pollen Radiocarbon Dating and

Bayesian Age-Depth Modeling for Developing Robust Geochronological Frameworks of Wetland Archives. *Radiocarbon*, *64*(2), 213–235. https://doi.org/10.1017/RDC.2022.29

Child, D. P., & Hotchkis, M. A. C. (2013). Nuclear Instruments and Methods in Physics Research B Plutonium and uranium contamination in soils from former nuclear weapon test sites in Australia. *Nuclear Inst. and Methods in Physics Research, B*, *294*, 642–646. https://doi.org/10.1016/j.nimb.2012.05.018

Child, D. P., Hotchkis, M. A. C., & Williams, M. L. (2008). High sensitivity analysis of plutonium isotopes in environmental samples using accelerator mass spectrometry (AMS). *Journal of Analytical Atomic Spectrometry*, *23*(5), 765–768. https://doi.org/10.1039/b715788f

Corcho-Alvarado, J. A., Diaz-Asencio, M., Froidevaux, P., Bochud, F., Alonso-Hernández, C. M., & Sanchez-Cabeza, J. A. (2014). Dating young Holocene coastal sediments in tropical regions: Use of fallout 239,240Pu as alternative chronostratigraphic marker. *Quaternary Geochronology*, *22*, 1–10. https://doi.org/10.1016/j.quageo.2014.02.001

El-Eswed, B. (2016). Effect of basicity and hydrophobicity of amines on their adsorption onto charcoal. *Desalination and Water Treatment*, *57*(41), 19227–19238. https://doi.org/10.1080/19443994.2015.1101622

Everett, S. E., Tims, S. G., Hancock, G. J., Bartley, R., & Fifield, L. K. (2008). *Comparison of Pu and 137 Cs as tracers of soil and sediment transport in a terrestrial environment*. *99*, 383–393. https://doi.org/10.1016/j.jenvrad.2007.10.019

Falster, G., Tyler, J., Grant, K., Tibby, J., Turney, C., Löhr, S., Jacobsen, G., & Kershaw, A. P. (2018). Millennial-scale variability in south-east Australian hydroclimate between 30,000 and 10,000 years ago. *Quaternary Science Reviews*, *192*, 106–122. https://doi.org/10.1016/j.quascirev.2018.05.031

Fink, D., Hotchkis, M., Hua, Q., Jacobsen, G., Smith, A. M., Zoppi, U., Child, D., Mifsud, C., Van Der Gaast, H., Williams, A., & Williams, M. (2004). The ANTARES AMS facility at ANSTO. *Nuclear Instruments and Methods in Physics Research, Section B: Beam Interactions with Materials and Atoms*, *223–224*(SPEC. ISS.), 109–115. https://doi.org/10.1016/j.nimb.2004.04.025

Fletcher, M. S., & Thomas, I. (2010). A quantitative Late Quaternary temperature reconstruction from western Tasmania, Australia. *Quaternary Science Reviews*, *29*(17–18), 2351–2361. https://doi.org/10.1016/j.quascirev.2010.06.012

Fletcher, W. J., Zielhofer, C., Mischke, S., Bryant, C., Xu, X., & Fink, D. (2017). AMS radiocarbon dating of pollen concentrates in a karstic lake system. *Quaternary Geochronology*, *39*, 112–123. https://doi.org/10.1016/j.quageo.2017.02.006

Gouramanis, C., Deckker, P. De, Switzer, A. D., & Wilkins, D. (2013). Earth-Science Reviews Cross-continent comparison of high-resolution Holocene climate records from southern Australia — Deciphering the impacts of far- fi eld teleconnections Austra l

Winte r ITCZ today mer I ral Sum TCZ to Approx . position of today. *Earth Science Reviews*, *121*, 55–72. https://doi.org/10.1016/j.earscirev.2013.02.006

Hancock, G. J., Leslie, C., Everett, S. E., Tims, S. G., Brunskill, G. J., & Haese, R. (2011). Plutonium as a chronomarker in Australian and New Zealand sediments: A comparison with 137Cs. *Journal of Environmental Radioactivity*, *102*(10), 919–929. https://doi.org/10.1016/j.jenvrad.2009.09.008

Hancock, G. J., Tims, S. G., Fifield, L. K., & Webster, I. T. (2014). The release and persistence of radioactive anthropogenic nuclides. *Geological Society Special Publication*, *395*(1), 265–281. https://doi.org/10.1144/SP395.15

Harris, S., Mills, G., & Brown, T. (2017). Variability and drivers of extreme fire weather in fire-prone areas of south-eastern Australia. *International Journal of Wildland Fire*, *26*(3), 177–190. https://doi.org/10.1071/WF16118

Harrison, J., Heijnis, H., & Caprarelli, G. (2003). Historical pollution variability from abandoned mine sites, Greater Blue Mountains World Heritage Area, New South Wales, Australia. *Environmental Geology*, *43*(6), 680–687. https://doi.org/10.1007/s00254-002-0687-8

Harrison, J. J., Saunders, K. M., Child, D. P., & Hotchkis, M. A. C. (2021). A record of fallout 239Pu and 240Pu at World Heritage Bathurst Harbour, Tasmania, Australia. *Journal of Environmental Radioactivity*, *237*(June). https://doi.org/10.1016/j.jenvrad.2021.106679

Hirose, K., & Aoyama, M. (2003). Present background levels of surface 137Cs and 239,240Pu concentrations in the Pacific. *Journal of Environmental Radioactivity*, *69*(1–2), 53–60. https://doi.org/10.1016/S0265-931X(03)00086-9

Hirose, K., & Povinec, P. P. (2015). Sources of plutonium in the atmosphere and stratosphere-troposphere mixing. *Scientific Reports*, *5*, 1–9. https://doi.org/10.1038/srep15707

Hogg, A. G., Heaton, T. J., Hua, Q., Palmer, J. G., Turney, C. S. M., Southon, J., Bayliss, A., Blackwell, P. G., Boswijk, G., Bronk Ramsey, C., Pearson, C., Petchey, F., Reimer, P., Reimer, R., & Wacker, L. (2020). SHCal20 Southern Hemisphere Calibration, 0-55,000 Years cal BP. *Radiocarbon*, *62*(4), 759–778. https://doi.org/10.1017/RDC.2020.59

Holmgren, S. U., Bigler, C., Ingólfsson, Ó., & Wolfe, A. P. (2010). The Holocene-Anthropocene transition in lakes of western spitsbergen, Svalbard (Norwegian high arctic): Climate change and nitrogen deposition. *Journal of Paleolimnology*, *43*(2), 393–412. https://doi.org/10.1007/s10933-009-9338-3

Hong, T., Yin, J. Y., Nie, S. P., & Xie, M. Y. (2021). Applications of infrared spectroscopy in polysaccharide structural analysis: Progress, challenge and perspective. *Food Chemistry: X*, *12*(November), 100168. https://doi.org/10.1016/j.fochx.2021.100168

Hotchkis, M. A. C., Child, D., Fink, D., Jacobsen, G. E., Lee, P. J., Mino, N., Smith, A. M.,

& Tuniz, C. (2000). Measurement of 236U in environmental media. *Nuclear Instruments and Methods in Physics Research, Section B: Beam Interactions with Materials and Atoms*, *172*(1–4), 659–665. https://doi.org/10.1016/S0168-583X(00)00146-4

Howarth, J. D., Fitzsimons, S. J., Jacobsen, G. E., Vandergoes, M. J., & Norris, R. J. (2013). Identifying a reliable target fraction for radiocarbon dating sedimentary records from lakes. *Quaternary Geochronology*, *17*, 68–80. https://doi.org/10.1016/j.quageo.2013.02.001

Hua, Q. (2009). Radiocarbon: A chronological tool for the recent past. *Quaternary Geochronology*, *4*(5), 378–390. https://doi.org/10.1016/j.quageo.2009.03.006

Hua, Q., Barbetti, M., Levchenko, V. A., D'Arrigo, R. D., Buckley, B. M., & Smith, A. M. (2012). Monsoonal influence on Southern Hemisphere 14CO2. *Geophysical Research Letters*, *39*(19), 1–5. https://doi.org/10.1029/2012GL052971

Hua, Q., Barbetti, M., & Rakowski, A. Z. (2013). Atmospheric Radiocarbon for the Period 1950–2010. *Radiocarbon*, *55*(4), 2059–2072. https://doi.org/10.2458/azu_js_rc.v55i2.16177

Hua, Q., Jacobsen, G. E., Zoppi, U., Lawson, E. M., Williams, A. A., Smith, A. M., & McGann, M. J. (2001). Progress in radiocarbon target preparation at the ANTARES AMS centre. *Radiocarbon*, *43*(2 PART I), 275–282. https://doi.org/10.1017/s003382220003811x

Hua, Q., Turnbull, J. C., Santos, G. M., Rakowski, A. Z., Ancapichún, S., De Pol-Holz, R., Hammer, S., Lehman, S. J., Levin, I., Miller, J. B., Palmer, J. G., & Turney, C. S. M. (2022). Atmospheric Radiocarbon for the Period 1950-2019. *Radiocarbon*, *64*(4), 723–745. https://doi.org/10.1017/RDC.2021.95

Iurian, A. R., Millward, G., Blake, W., & Abril Hernández, J. M. (2021). Fine-tuning of 210Pb-based methods for dating vegetated saltmarsh sediments. *Quaternary Geochronology*, *62*(April 2020). https://doi.org/10.1016/j.quageo.2021.101153

Jebsen, C., Norici, A., Wagner, H., Palmucci, M., Giordano, M., & Wilhelm, C. (2012). FTIR spectra of algal species can be used as physiological fingerprints to assess their actual growth potential. *Physiologia Plantarum*, *146*(4), 427–438. https://doi.org/10.1111/j.1399-3054.2012.01636.x

Johansen, M. P., Child, D. P., Caffrey, E. A., Davis, E., Harrison, J. J., Hotchkis, M. A. C., Payne, T. E., Ikeda-ohno, A., Thiruvoth, S., Twining, J. R., & Beresford, N. A. (2016). Accumulation of plutonium in mammalian wildlife tissues following dispersal by accidental-release tests. *Journal of Environmental Radioactivity*, *151*, 387–394. https://doi.org/10.1016/j.jenvrad.2015.03.031

Kelley, J. M., Bond, L. A., & Beasley, T. M. (1999). Global distribution of Pu isotopes and 237Np. *Science of the Total Environment*, *237–238*, 483–500. https://doi.org/10.1016/S0048-9697(99)00160-6

Kilian, M. R., Van Der Plicht, J., Van Geel, B., & Goslar, T. (2002). Problematic 14C-AMS dates of pollen concentrates from Lake Gosciaz (Poland). *Quaternary International*, *88*(1), 21–26. https://doi.org/10.1016/S1040-6182(01)00070-2

Kirchner, G. (2011). 210Pb as a tool for establishing sediment chronologies: Examples of potentials and limitations of conventional dating models. *Journal of Environmental Radioactivity*, *102*(5), 490–494. https://doi.org/10.1016/j.jenvrad.2010.11.010

Kirchner, G., & Ehlers, H. (1998). Sediment geochronology in changing coastal environments: Potentials and limitations of the 137Cs and 210Pb methods. *Journal of Coastal Research*, *14*(2), 483–492.

Koide, M., Bertine, K. K., Chow, T. J., & Goldberg, E. D. (1985). *The 240Pu/239Pu ratio , a potential geochronometer*. *72*, 1–8.

Koide, M., Michel, R., & Goldberg, E. D. (1982). : *j*. *296*(April), 544–547.

Leslie, C., & Hancock, G. J. (2008). Estimating the date corresponding to the horizon of the first detection of 137Cs and 239+240Pu in sediment cores. *Journal of Environmental Radioactivity*, *99*(3), 483–490. https://doi.org/10.1016/j.jenvrad.2007.08.016

Li, Y., Wang, N. A., Li, Z. L., Zhang, C. Q., & Zhou, X. H. (2012). Reworking effects in the Holocene Zhuye Lake sediments: A case study by pollen concentrates AMS 14C dating. *Science China Earth Sciences*, *55*(10), 1669–1678. https://doi.org/10.1007/s11430-012-4482-4

Liu, X., Colman, S. M., Brown, E. T., Minor, E. C., & Li, H. (2013). Estimation of carbonate, total organic carbon, and biogenic silica content by FTIR and XRF techniques in lacustrine sediments. *Journal of Paleolimnology*, *50*(3), 387–398. https://doi.org/10.1007/s10933-013-9733-7

Long, A., Davis, O. K., & De Lanois, J. (1992). Separation and 14C dating of pure pollen from lake sediments: nanofossil AMS dating. *Radiocarbon*, *34*(3), 557–560. https://doi.org/10.1017/S0033822200063827

Martin, L., Goff, J., Jacobsen, G., & Mooney, S. (2019). The radiocarbon ages of different organic components in the mires of Eastern Australia. *Radiocarbon*, *61*(1), 173–184. https://doi.org/10.1017/RDC.2018.118

Marty, J., & Myrbo, A. (2014). Radiocarbon dating suitability of aquatic plant macrofossils. *Journal of Paleolimnology*, *52*(4), 435–443. https://doi.org/10.1007/s10933-014-9796-0

Matchan, E. L., Phillips, D., Jourdan, F., & Oostingh, K. (2020). Early human occupation of southeastern Australia: Newinsights from 40Ar/39Ar dating of young volcanoes. *Geology*, *48*(4), 390–394. https://doi.org/10.1130/G47166.1

Mecozzi, M., Pietrantonio, E., Amici, M., & Romanelli, G. (2001). Determination of carbonate in marine solid samples by FTIR-ATR spectroscopy. *Analyst*, *126*(2), 144–146. https://doi.org/10.1039/b009031j

Mecozzi, M., Pietrantonio, E., & Pietroletti, M. (2009). The roles of carbohydrates, proteins and lipids in the process of aggregation of natural marine organic matter investigated by means of 2D correlation spectroscopy applied to infrared spectra. *Spectrochimica Acta - Part A: Molecular and Biomolecular Spectroscopy*, *71*(5), 1877–1884. https://doi.org/10.1016/j.saa.2008.07.015

Meng, B., Zhou, A., Zhang, Y., Song, M., Liu, W., Xie, Z., Li, S., & Liu, Z. (2020). Downcore variations of carbon reservoir ages linked to lake level changes in northwest China. *Quaternary Geochronology*, *60*(October 2019), 101105. https://doi.org/10.1016/j.quageo.2020.101105

Mensing, S. A., & Southon, J. R. (1999). A simple method to separate pollen for AMS radiocarbon dating and its application to lacustrine and marine sediments. *Radiocarbon*, *41*(1), 1–8. https://doi.org/10.1017/S0033822200019287

Moss, P. T., Tibby, J., Petherick, L., McGowan, H., & Barr, C. (2013). Late Quaternary vegetation history of North Stradbroke Island, Queensland, eastern Australia. *Quaternary Science Reviews*, *74*, 257–272. https://doi.org/10.1016/j.quascirev.2013.02.019

Muramatsu, Y., Hamilton, T., Uchida, S., Tagami, K., & Yoshida, S. (2001). *Measurement of 240 Pu r 239 Pu isotopic ratios in soils from the Marshall Islands using ICP-MS*. 151–159.

Neulieb, T., Levac, E., Southon, J., Lewis, M., Pendea, I. F., & Chmura, G. L. (2013). Potential Pitfalls of Pollen Dating. *Radiocarbon*, *55*(3), 1142–1155. https://doi.org/10.1017/s0033822200048050

Norris, M. W., Turnbull, J. C., Howarth, J. D., & Vandergoes, M. J. (2020). Pretreatment of Terrestrial Macrofossils. *Radiocarbon*, *62*(2), 349–360. https://doi.org/10.1017/RDC.2020.8

Pan, S. M., Tims, S. G., Liu, X. Y., & Fifield, L. K. (2011). 137Cs, 239+240Pu concentrations and the 240Pu/ 239Pu atom ratio in a sediment core from the sub-aqueous delta of Yangtze River estuary. *Journal of Environmental Radioactivity*, *102*(10), 930–936. https://doi.org/10.1016/j.jenvrad.2010.05.012

Philippsen, B. (2013). The freshwater reservoir effect in radiocarbon dating. *Heritage Science*, *1*(1), 1–19. https://doi.org/10.1186/2050-7445-1-24

Price, R. C., Gray, C. M., & Frey, F. A. (1997). Strontium isotopic and trace element heterogeneity in the plains basalts of the Newer Volcanic Province, Victoria, Australia. *Geochimica et Cosmochimica Acta*, *61*(1), 171–192. https://doi.org/10.1016/S0016-7037(96)00318-3

Regnell, J. (1992). Preparing pollen concentrates for AMS dating – a methodological study from a hard-water lake in southern Sweden. *Boreas*, *21*(4), 373–377. https://doi.org/10.1111/j.1502-3885.1992.tb00042.x

Rivera-Araya, M., Rowe, C., Levchenko, V., Ulm, S., & Bird, M. I. (2022). A radiocarbon chronology for Sanamere Lagoon, Cape York Peninsula, using multiple organic fractions. *Quaternary Geochronology*, *70*(March), 101273. https://doi.org/10.1016/j.quageo.2022.101273

Sanchez-Cabeza, J. A., & Ruiz-Fernández, A. C. (2012). 210Pb sediment radiochronology: An integrated formulation and classification of dating models. *Geochimica et Cosmochimica Acta*, *82*, 183–200. https://doi.org/10.1016/j.gca.2010.12.024

Schiller, C. M., Whitlock, C., Elder, K. L., Iverson, N. A., & Abbott, M. B. (2021). Erroneously old radiocarbon ages from terrestrial pollen concentrates in yellowstone lake, wyoming, usa. *Radiocarbon*, *63*(1), 321–342. https://doi.org/10.1017/RDC.2020.118

Schneider, L., Pain, C. F., Haberle, S., Blong, R., Alloway, B. V, Fallon, S. J., Hope, G., & Zawadzki, A. (2019). *1,2*. *61*(1), 287–308. https://doi.org/10.1017/RDC.2018.49

Smith, B. S., Child, D. P., Fierro, D., Harrison, J. J., Heijnis, H., Hotchkis, M. A. C., Johansen, M. P., Marx, S., Payne, T. E., & Zawadzki, A. (2016). Measurement of fallout radionuclides , 239 , 240 Pu and creek sediment : Sydney Basin , Australia Cs , in soil and. *Journal of Environmental Radioactivity*, *151*, 579–586. https://doi.org/10.1016/j.jenvrad.2015.06.015

Smith, J. N. (2001). Why should we believe ^{210}Pb sediment geochronologies? *Journal of Environmental Radioactivity*, *55*(2), 121–123. https://doi.org/10.1016/S0265-931X(00)00152-1

Steinhoff, C., Pickarski, N., Litt, T., Hajdas, I., Welte, C., Wurst, P., Kühne, D., Dolf, A., Germer, M., & Kallmeyer, J. (2022). New Approach To Separate and Date Small Spores and Pollen From Lake Sediments in Semi-Arid Climates. *Radiocarbon*, *64*(5), 1–17. https://doi.org/10.1017/rdc.2022.34

Strunk, A., Olsen, J., Sanei, H., Rudra, A., & Larsen, N. K. (2020). Improving the reliability of bulk sediment radiocarbon dating. *Quaternary Science Reviews*, *242*, 106442. https://doi.org/10.1016/j.quascirev.2020.106442

Tennant, R. K., Jones, R. T., Brock, F., Cook, C., Turney, C. S. M., Love, J., & Lee, R. (2013). A new flow cytometry method enabling rapid purification of fossil pollen from terrestrial sediments for AMS radiocarbon dating. *Journal of Quaternary Science*, *28*(3), 229–236. https://doi.org/10.1002/jqs.2606

Thakur, P., Khaing, H., & Salminen-Paatero, S. (2017). Plutonium in the atmosphere: A global perspective. *Journal of Environmental Radioactivity*, *175–176*, 39–51. https://doi.org/10.1016/j.jenvrad.2017.04.008

Tibby, J., Penny, D., Leahy, P., & Kershaw, A. P. (2012). Vegetation and water quality responses to Holocene climate variability in Lake Purrumbete, western Victoria. *Peopled Landscapes: Archaeological and Biogeographic Approaches to Landscapes*, *May*. https://doi.org/10.22459/ta34.01.2012.17

Timms, B. V. (1976). A Comparative Study of the Limnology of Three Maar Lakes in Western Victoria. I. physiography and physicochemical features. *Marine and Freshwater Research*, *27*(1), 35–60. https://doi.org/10.1071/MF9760035

Tims, S. G., Fifield, L. K., Hancock, G. J., Lal, R. R., & Hoo, W. T. (2013). Nuclear Instruments and Methods in Physics Research B Plutonium isotope measurements from across continental Australia. *Nuclear Inst. and Methods in Physics Research, B*, *294*, 636–641. https://doi.org/10.1016/j.nimb.2012.07.010

Tims, S. G., Froehlich, M. B., Fi, L. K., Wallner, A., & Cesare, M. De. (2016). *U and 239 , 240 Pu ratios from soils around an Australian nuclear weapons test site*. *151*, 563–567. https://doi.org/10.1016/j.jenvrad.2015.06.020

Tunno, I., Zimmerman, S. R. H., Brown, T. A., & Hassel, C. A. (2021). An Improved Method for Extracting, Sorting, and AMS Dating of Pollen Concentrates From Lake Sediment. *Frontiers in Ecology and Evolution*, *9*(May). https://doi.org/10.3389/fevo.2021.668676

Turney, C., Becerra-Valdivia, L., Sookdeo, A., Thomas, Z. A., Palmer, J., Haines, H. A., Cadd, H., Wacker, L., Baker, A., Andersen, M. S., Jacobsen, G., Meredith, K., Chinu, K., Bollhalder, S., & Marjo, C. (2021). Radiocarbon Protocols and First Intercomparison results from the CHRONOS 14Carbon-Cycle Facility, University of New South Wales, Sydney, Australia. *Radiocarbon*, *63*(3), 1003–1023. https://doi.org/10.1017/RDC.2021.23

Tweddle, J. C., & Edwards, K. J. (2010). Pollen preservation zones as an interpretative tool in Holocene palynology. *Review of Palaeobotany and Palynology*, *161*(1–2), 59–76. https://doi.org/10.1016/j.revpalbo.2010.03.004

Tylmann, W., Bonk, A., Goslar, T., Wulf, S., & Grosjean, M. (2016). Calibrating 210Pb dating results with varve chronology and independent chronostratigraphic markers: Problems and implications. *Quaternary Geochronology*, *32*, 1–10. https://doi.org/10.1016/j.quageo.2015.11.004

Tylmann, W., Głowacka, P., & Szczerba, A. (2017). Tracking climate signals in varved lake sediments: research strategy and key sites for comprehensive process studies in the Masurian Lakeland. *Limnological Review*, *17*(3), 159–166. https://doi.org/10.1515/limre-2017-0015

Wacker, L., Němec, M., & Bourquin, J. (2010). A revolutionary graphitisation system: Fully automated, compact and simple. *Nuclear Instruments and Methods in Physics Research, Section B: Beam Interactions with Materials and Atoms*, *268*(7–8), 931–934. https://doi.org/10.1016/j.nimb.2009.10.067

Wilkins, D., De Deckker, P., Fifield, L. K., Gouramanis, C., & Olley, J. (2012). Comparative optical and radiocarbon dating of laminated Holocene sediments in two maar lakes: Lake Keilambete and Lake Gnotuk, south-western Victoria, Australia. *Quaternary Geochronology*, *9*, 3–15. https://doi.org/10.1016/j.quageo.2012.01.008

Wolfe, A. P., Smith, I. R. O. D., & Miller, G. H. (2004). *Department of Earth and*

Atmospheric Sciences University of Alberta Edmonton, Alberta T6G 2E3, Canada. 19–52.

Woodward, C., Shulmeister, J., Bell, D., Haworth, R., Jacobsen, G., & Zawadzki, A. (2014). A Holocene record of climate and hydrological changes from Little Llangothlin Lagoon, south eastern Australia. *Holocene*, *24*(12), 1665–1674. https://doi.org/10.1177/0959683614551218

Wright, H. E. (1967). A square-rod piston sampler for lake sediments. *Journal of Sedimentary Research*, *37*(3), 975–976. https://doi.org/10.1306/74d71807-2b21-11d7-8648000102c1865d

Zhang, Y., Wu, Z., Liu, M., He, J., Shi, K., Zhou, Y., Wang, M., & Liu, X. (2015). Dissolved oxygen stratification and response to thermal structure and long-term climate change in a large and deep subtropical reservoir (Lake Qiandaohu, China). *Water Research*, *75*, 249–258. https://doi.org/10.1016/j.watres.2015.02.052

Zheng, J., Tagami, K., Watanabe, Y., Uchida, S., Aono, T., Ishii, N., Yoshida, S., Kubota, Y., Fuma, S., & Ihara, S. (2012). Isotopic evidence of plutonium release into the environment from the Fukushima DNPP accident. *Scientific Reports*, *2*, 1–8. https://doi.org/10.1038/srep00304

Zhou, A., He, Y., Wu, D., Zhang, X., Zhang, C., Liu, Z., & Yu, J. (2015). Changes in the radiocarbon reservoir age in Lake Xingyun, Southwestern China during the holocene. *PLoS ONE*, *10*(3), 1–12. https://doi.org/10.1371/journal.pone.0121532

Zhou, K., Xu, H., Lan, J., Yan, D., Sheng, E., Yu, K., & Meyers, P. A. (2020). *Variable Late Holocene 14 C Reservoir Ages in Lake Bosten , Northwestern*. *7*(January), 1–11. https://doi.org/10.3389/feart.2019.00328

Zimmerman, S. R. H., Brown, T. A., Hassel, C., & Heck, J. (2019). Testing pollen sorted by flow cytometry as the basis for high-resolution lacustrine chronologies. *Radiocarbon*, *61*(1), 359–374. https://doi.org/10.1017/RDC.2018.89

Zimmerman, S. R. H., & Wahl, D. B. (2020). Holocene paleoclimate change in the western US: The importance of chronology in discerning patterns and drivers. *Quaternary Science Reviews*, *246*, 106487. https://doi.org/10.1016/j.quascirev.2020.106487

Supplementary data

Section 1: Results of ^{210}Pb analysis

Table I. CFCS and CRS age model calculations

Laboratory code	Sample depth (cm)	Dry bulk density (g/cm^3)	Cumulative dry mass (g/cm^2)	Calculated CFCS ages (years)	Mass accumulation (g/cm^2/year)	Calculated CRS ages (years)	Mass accumulation (g/cm^2/year)
W557	0.7	0.03	0.01±0.01	1±1	0.0196±0.003	1±1	0.021±0.001
W558	9.1	0.02	0.15±0.01	8±1		7±2	0.022±0.001
W559	17.5	0.18	0.76±0.03	39±6		32±2	0.029±0.002
W560	25.9	0.04	1.43±0.04	73±11		60±3	0.018±0.002
W561	41.6	0.04	1.92±0.03	98±14		77±4	0.055±0.008
W562	54.5	0.05	2.48±0.03	105±14	0.077±0.016	85±5	0.093±0.015
W563	66.5	0.05	3.11±0.03	113±14		93±6	0.074±0.013
W564	87	0.11	4.50±0.03	132±16		109±7	0.098±0.022
W565	107.5	0.07	6.05±0.03	152±18		128±10	0.068±0.020

Section 2: Results of ^{14}C analysis

Table II. List of radiocarbon ages (pollen and macrofossil) corrected for the age-offset and recent sediment dates used in the age-model of Lake Surprise sediment profile.

Material dated	Depth (cm)	Lab ID	^{14}C age		Delta.R	Delta.STD
			Mean	1σ		
Core surface	0	-	-69	3	0	0
Plant	15.05	OZZ426	-13	3	0	0
Pu peak	21.7	-	-14	3	0	0
Plant	31.55	OZZ427	-22	3	0	0
Pollen	41.2	UNSW-490	314	11	340	50
Pollen	52.15	UNSW-491	375	11`	340	50
Pollen	62.15	UNSW-492	387	11	340	50
Plant	69.15	OZZ428	520	20	0	0
Pollen	73.45	UNSW-493	423	11	340	50
Pollen	77.65	UNSW-497	451	11	340	50
Macrofossil	96.2	OZZ429	255	20	0	0
Pollen	97.3	UNSW-494	475	12	340	50
Pollen	104.45	UNSW-526	565	10	340	50
Pollen	116.65	UNSW-495	581	11	340	50
Macrofossil	129.3	OZZ514	460	22	0	0
Macrofossil	**136.45**	**OZZ430**	**525**	**20**	**0**	**0**
Pollen	**136.45**	**UNSW-496**	**865**	**11**	**340**	**50**
Pollen	151.51	UNSW-499	939	12	340	50
Pollen	188	UNSW-500	1666	12	340	50
Plant	214	OZZ516	1262	18	0	0
Pollen	218	UNSW-501	1549	12	340	50
Pollen	253	UNSW-502	1760	12	340	50
Pollen	274.5	UNSW-503	2026	12	340	50
Plant	288	OZZ518	1858	22	0	0
Pollen	310.5	UNSW-504	2424	12	340	50
Pollen	348.5	UNSW-505	2537	12	340	50
Macrofossil	375.5	OZZ521	2331	21	0	0
Plant	379.5	OZZ520	2235	24	0	0
Pollen	407.5	UNSW-506	2862	12	340	50
Pollen	450	UNSW-507	3291	12	340	50
Pollen	479	UNSW-530	3329	12	340	50
Plant	497	OZZ522	3091	21	0	0
Pollen	509.5	UNSW-510	3442	12	340	50
Pollen	541.5	UNSW-511	3525	12	340	50
Plant	566	OZZ524	3866	20	0	0
Pollen	579	UNSW-512	3976	13	340	50
Pollen	608.5	UNSW-531	3984	13	340	50
Macrofossil	615	OZZ523	3562	20		0
Pollen	643.5	UNSW-514	3549	12	340	50

Pollen	717.5	UNSW-516	4785	14	340	50
Plant	744.5	OZZ525	4775	23	0	0
Plant	776.5	OZZ526	5029	24	0	0
Macrofossil	782.5	OZZ527	5124	23	0	0
Pollen	809	UNSW-517	5682	14	340	50
Pollen	854.5	UNSW-518	6625	15	340	50
Plant	898	OZZ528	6297	25	0	0
Pollen	924	UNSW-519	6847	15	340	50
Pollen	956	UNSW-520	7428	16	340	50
Pollen	982	UNSW-521	7408	15	340	50
Pollen	1016	UNSW-522	8049	15	340	50
Pollen	1056.5	UNSW-524	8658	17	340	50
Pollen	1132.5	UNSW-523	10034	18	340	50

Table III. Modern age markers used in Figure 8 (for CFCS/CRS see Table I)

Sample	Depth (cm)	Age (CE)	Age error	Age (cal yr BP)
Pinus (LSFS core)	65.0	1875.0	20	75.0
modern C	15.1	1976.0	3	-26.0
modern C	31.6	1963.0	3	-13.0
Pu peak	21.7	1964.0	5	-14.0
Pu appearance	29.9	1954.0	-	-4.0
LSFS coring age	5.0	2004.0	2	-54.0

Section 3: FTIR analysis

Table IV. Radiocarbon dated pollen samples analysed for the FTIR spectrum

Sample ID	Composite depth (cm) of the sample	Age- offset (pollen-macrofossil) cal yr BP
UNSW-494	97.3	49.1
UNSW-495	116.65	187
UNSW-496	136.45	213
UNSW-500	188	456
UNSW-501	218	339
UNSW-502	253	386
UNSW-503	274.5	407
UNSW-504	310.5	522

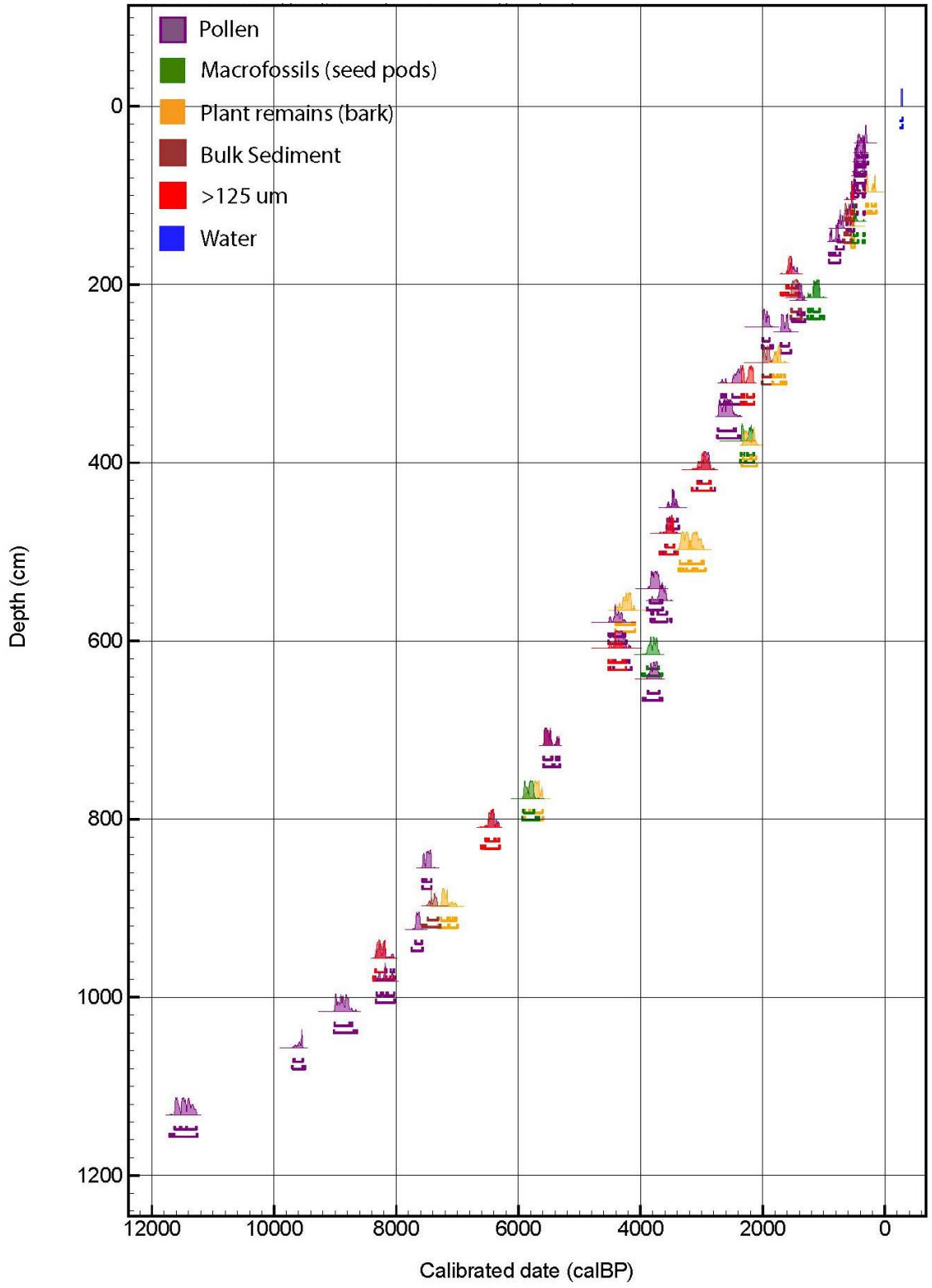

Figure I. Representation of age uncertainty among all measured radiocarbon dates against the composite sediment depth

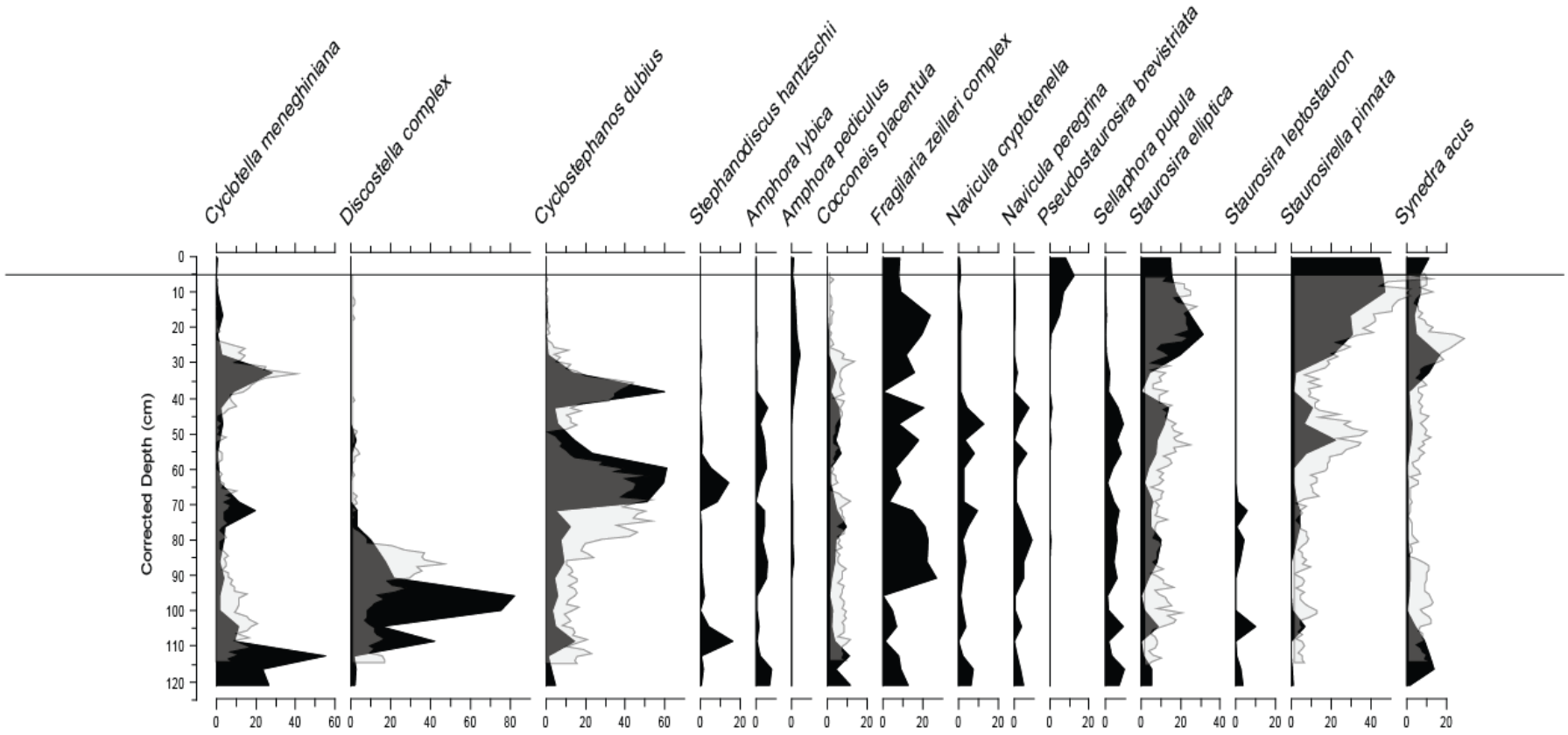

Figure II. Comparison of diatom data from SUR-19-01 (Black-shaded) and previous sediment core (LSFS) recovered in 2004 (Barr et al., 2014) (White-shaded). Black horizontal line corresponds with the 5 cm depth.

It appears that the top of LSFS is around about at 5 cm depth of SUR19-1 (+/- 1-2 cm perhaps), giving this depth an age of 15 years from our coring date (2019) and a sedimentation rate of 5 yr/cm, which is certainly within the realms of possibility.

CHAPTER 4

Dharmarathna, A., Tyler, J., Barr, C., Cadd, H., Tibby, J., Klaebe, R., Hall, T., Hua, Q., Child, D., Hotchkis, M., Zawadski, A., Validating lake sediment proxies against instrumental climate records; isotope and major element data from Lake Surprise, Victoria, Australia.

Supplementary information concerning this chapter follows the text. Data tables concerning this chapter are provided in Appendix 3 and 4.

Statement of Authorship

Title of Paper	Validating lake sediment palaeoclimate proxies against instrumental climate records: isotope and major element data from Lake Surprise, Victoria, Australia
Publication Status	☐ Published ☐ Accepted for Publication ☐ Submitted for Publication ☑ Unpublished and Unsubmitted work written manuscript style
Publication Details	Dharmarathna, A., Tyler, J., Barr, C., Cadd, H., Tibby, J., Klaebe, R., Hall, T., Hua, Q., Child, D., Hotchkis, M., Zawadski, A., Validating lake sediment proxies against instrumental climate records; isotope and major element data from Lake Surprise, Victoria, Australia. *Journal of Paleolimnology*. **in prep**

Principal Author

Name of Principal Author (Candidate)	Asika Dharmarathna		
Contribution to the Paper	Field sample collection, Laboratory sample preparation and analysis (cellulose oxygen isotopes, stable carbon and nitrogen isotopes) Assisted in instrumental analysis, Data analysis and interpretation Writing the manuscript and acting as the corresponding author		
Overall percentage (%)	80%		
Certification:	This paper reports on original research I conducted during the period of my Higher Degree by Research candidature and is not subject to any obligations or contractual agreements with a third party that would constrain its inclusion in this thesis. I am the primary author of this paper.		
Signature		Date	12/12/2022

Co-Author Contributions

By signing the Statement of Authorship, each author certifies that:

i. the candidate's stated contribution to the publication is accurate (as detailed above);

ii. permission is granted for the candidate in include the publication in the thesis; and

iii. The sum of all co-author contributions is equal to 100% less the candidate's stated contribution.

Name of Co-Author	Jonathan Tyler		
Contribution to the Paper	Field work assistance, Funding support, guidance in data analysis and interpretation, Manuscript evaluation and review		
Signature		Date	5/12/22

Name of Co-Author	Cameron Barr		
Contribution to the Paper	Field work assistance, assistance in sample preparation, core correlation calculations, Assistance in data interpretation		
Signature		Date	23/11/2022

Name of Co-Author	Haidee Cadd		
Contribution to the Paper	Field work assistance, Acquisition of radiocarbon data of pollen samples, Assistance in data interpretation		
Signature		Date	20/11/22

Name of Co-Author	John Tibby		
Contribution to the Paper	Field work assistance, guidance in data analysis and interpretation, Manuscript evaluation and review		
Signature		Date	1/12/2022

Name of Co-Author	Robert Klaebe		
Contribution to the Paper	Assistance with analysis of oxygen isotopes of cellulose		
Signature		Date	2/12/2022

Name of Co-Author	Tony Hall		
Contribution to the Paper	Assistance with analysis of stable carbon and nitrogen isotope data		
Signature		Date	22/11/2022

Name of Co-Author	Quan Hua		
Contribution to the Paper	Acquisition of radiocarbon data of macrofossil samples		
Signature		Date	23/11/2022

Name of Co-Author	David Child		
Contribution to the Paper	Assistance with acquisition of Pu isotope data		
Signature		Date	2/12/2022

Name of Co-Author	Michael Hotchkis		
Contribution to the Paper	Assistance with acquisition of Pu isotope data		
Signature		Date	4/12/2022

Name of Co-Author	Atun Zawadski		
Contribution to the Paper	Assistance with acquisition of Pb-210 data		
Signature		Date	6/12/2022

4 Validating lake sediment palaeoclimate proxies against instrumental climate records; isotope and major element data from Lake Surprise, Victoria, Australia.

Abstract

Independent validation of sediment proxy data against instrumental climate records is an important, yet uncommon step in achieving rigorous palaeoclimate reconstructions. To this end, this study analysed a 1.57 m long sediment core recovered from the uppermost soft sediments of Lake Surprise, Victoria, Australia. A combination of ^{210}Pb, Pu concentration, ^{14}C and recent historical markers indicates that the instrumental period (1890 – 2019 CE) is captured by the upper 0.5 m of sediment. Major elemental composition, bulk organic geochemistry and oxygen isotope ratios of aquatic cellulose were validated as proxies of past hydroclimate through comparison with instrumental climate records from the nearby town of Macarthur. Oxygen isotope ratios of cellulose and carbon isotope ratios of bulk organic matter exhibited a positive correlation with mean annual maximum air temperature (Tmax), and evaporation, and a negative correlation with the precipitation minus evaporation deficit (P-E) and precipitation to evaporation (P/E) ratio. The sediment carbonate concentration, inferred from Ca was negatively correlated with the Tmax and evaporation. Variations in oxygen and carbon isotopes conform to expected patterns of heavy isotope enrichment in response to increased rates of evaporation and increased productivity during spring and summer intervals. Carbon isotopes and C/N ratios provided evidence that algal sources dominate the organic composition of the sediments. The carbonate deposition in Lake Surprise contradicts the generally utilised palaeoclimate assumption of evaporative enrichment. Major hypotheses used to explain the enhanced carbonate deposition during wetter climate at Lake Surprise are: (1) Authigenic carbonate production may increase during periods of increased groundwater inflow during rainy seasons; (2) productivity-driven carbonate deposition may have been enhanced during wet periods, associated with deeper lake mixing and nutrient influx; (3) carbonate dissolution by anoxic decomposition may have occurred during periods of thermal stratification under warm, dry climates. Reconstruction of the pre-instrumental period climate based on the sediment proxy-climate relationships identified relatively wet climates around 1680 – 1700 CE and 1710 – 1790 CE, whereas dry periods were detected from 1700 – 1745 CE and 1300 – 1680 CE. These observations suggest that oxygen isotope analysis of aquatic cellulose is a valid, potentially quantitative tracer of past hydroclimate variability from

sediments of Lake Surprise. Carbonate deposition, as inferred by Ca concentration, also appears to be climatically sensitive. However, it is necessary to better understand the mechanism of carbonate deposition which is beyond the scope of this study. Overall, this work highlights the significance of understanding the proxy-climate relationship to validate long-used assumptions applied to interpret past climates.

4.1 Introduction

Lake sediments provide important archives of past climate change on every continent (Cohen, 2003). Lakes respond directly and indirectly to climate change and incorporate climate impacts within the catchment, lake and sediments (Adrian et al., 2009, 2016; Battarbee et al., 2002, 2012; Li et al., 2020). Climate change directly or indirectly influences the biological, chemical and physical properties of lake ecosystems, such as lake water level fluctuations, seasonal mixing and stratification regimes, nutrient enrichment and algal blooms, carbonate deposition, bacterial degradation and changes in biogeochemical cycles (Battarbee et al. 2012; Wilkins et al. 2013; Jeppesen et al. 2014; Havens and Jeppesen 2018). Lake sediments preserve these signals of past climate change, particularly variability in surface hydrology (Jones et al., 2006; Tylmann et al., 2017; Zhang et al., 2021). However, despite the clear links between climate variability and lake systems, there remains a need to validate the understanding of these processes in order to develop rigorous reconstructions of past climates.

Among many of the palaeoclimate proxies in lake sediments, major element composition, carbon isotopes of organic matter and archives of lake water oxygen isotopes are commonly used tools to infer past climate, landscape and aquatic ecosystem changes (Leng & Marshall, 2004; Davies et al., 2015). Importantly, inferred changes in lake water oxygen isotopes have long been used to reconstruct hydrological response to climate variability given their capability to capture changes in precipitation, evaporation and atmospheric circulation (Craig, 1961; Gat, 1995; Leng & Marshall, 2004; Heikkilä et al., 2010; Steinman et al., 2010). Lake water stable oxygen isotope ratios are recorded in sediments in a range of carbonate, silicate and organic remains (Eto, 2001; Wolfe et al., 2001, 2007; Rozanski et al., 2010; van Hardenbroek et al., 2018). Aquatic cellulose offers particular promise as a proxy for past lake water $\delta^{18}O$, free of the effects of temperature (Wolfe et al. 2001; Street-Perrot et al. 2018). The use of cellulose $\delta^{18}O$ usually relies on the assumption that the fine-grained (<150 μm) lake sediment cellulose is predominantly aquatic and that the isotope fractionation ($\alpha^{18}O_{cell\text{-}lw}$) between cellulose and

lake water is constant, at 1.028 ± 0.003 ‰ (Edwards & McAndrews, 1989; Street-Perrott et al., 2018). However, there is little to no evidence of previous research based on sedimentary cellulose in the lakes of south-east Australia. Furthermore, stable carbon isotopes of organic matter provide insights into aquatic and terrestrial ecosystem change (Meyers & Teranes, 2002; Meyers, 2003; Leng & Marshall, 2004) which also reflect changes in past climate (Battarbee 2002).

Inorganic geochemical analysis of lake sediments has become increasingly common since the invention of X-Ray fluorescence core scanners, which rapidly generate non-destructive, high-resolution geochemical data at spatial resolutions of less than 100 µm (Löwemark et al., 2011; Martín-Puertas et al., 2011; Davies et al., 2015; Chawchai et al., 2016). However, in most cases, the elemental and stable isotope composition of lake sediments provide, at best, a qualitative proxy for past environmental change, beset by multiple and complex driving factors coupled with a poor understanding of the contemporary processes which lead to sedimentation (Leng & Marshall, 2004; Davies et al., 2015; Jones et al., 2016). This study addresses uncertainties regarding the interplay between climate and sediment geochemical proxies through the analysis of recent lake sediments that have accumulated rapidly over the recent centuries in Lake Surprise, a volcanic crater lake in south-east Australia.

Lake sediment composition varies in response to changing climate and anthropogenic activities. To some extent, lakes are controlled by tectonic and geomorphological settings (Battarbee et al. 2002, 2012; Fritz 2008; Barr et al. 2013; Petherick et al. 2013; Nomosatryo et al. 2021). Here we focus on climate-driven lake mechanisms such as primary productivity, redox changes and organic and inorganic carbon cycling that can modify the sediment geochemistry and stable isotope composition overtime. During dry climate episodes, evaporative enrichment and lake stratification enhance the concentration of redox-sensitive elements (Fe, Mn and S) (Naeher et al., 2013; Davies et al., 2015; Otte et al., 2018) and evaporative elements (Ca and Sr) in the sediment (Gierlowski-Kordesch, 2010; Brown, 2011; Karami et al., 2019; McCormack et al., 2019; Francke et al., 2021). Similarly, aquatic productivity associated with the enhanced nutrient influx and lake water mixing during wet periods and increased light energy during spring/summer times is expected to alter the sedimentary carbon isotope composition (Meyers, 1997; Leng & Marshall, 2004). With preferential uptake of ^{12}C by aquatic plants during photosynthesis, organic $\delta^{13}C$ values in the

lake enriched with increasing productivity (Meyers, 1997; Meyers & Lallier-Vergès, 1999; Leng & Marshall, 2004).

Globally, a limited number of studies have attempted to validate the sensitivity of lake sediment proxies against instrumental records of recent climate (Battarbee et al., 2002; Cameron et al., 2002; Larocque et al., 2009; Axford et al., 2011; Tian et al., 2011). In part, such an approach can be limited by a shortage of long, reliable instrumental climate records (Teranes & Mckenzie, 2001; Jones et al., 2005, 2006; Shanahan et al., 2008; Vegas-Vilarrúbia et al., 2022). More frequently, unpicking the effects of climate versus non-climatic human impacts on lake systems can heavily undermine attempts to calibrate or validate lake sediment interpretations against recent instrumental time series. Furthermore, rigorous comparison between lake sediments and instrumental data requires sediments which have accumulated quickly, with minimal disturbance, alongside detailed sediment dating (Battarbee et al., 2002).

In this study, sediments obtained from Lake Surprise in the western Victorian volcanic plains were analysed for their potency to represent the past local climate. Due to the sheltered, vegetated catchment, the lake has likely been free of major human-induced catchment disturbance (Barr et al., 2014). Before European colonisation, the lake was completely isolated from the region's most popular industry; eel aquaculture, suggesting that changes in the lake hydrology are mostly responses to changing climate (Builth et al., 2008). A combination of oxygen isotopes in aquatic cellulose, bulk organic C and N isotopes and major element concentrations (Ca, Sr, Fe, S, Si and Cl) were analysed and compared with instrumental climate records, in order to assess their potential for reconstructing past climate variability. In doing so, a foundation can be laid for the interpretation of Holocene and Pleistocene sediments from Lake Surprise, as well as similar systems worldwide.

4.2 Site description

4.2.1 Geological and climate setting,

Lake Surprise is located in the Budj Bim-Mt Eccles crater complex in the newer volcanic province of western Victoria in south-eastern Australia. The western Victorian plain is overlain by Cretaceous sandstone, Tertiary limestone, marl and thin layers of basalts in many localities (Price et al., 1997; Boyce, 2013; Barr et al., 2014; Matchan et al., 2020). $^{40}Ar/^{39}Ar$ dating of the Tyrendarra lava flow, a nepheline-normative hawaiite that originates from Mt Eccles

indicates an eruption age of 36.9±3.1 ka (Matchan et al., 2020). This is considered to be a dormant volcanic plain since the mid-Holocene which has given rise to over 400 eruption centres of simple and complex magmatic features (Boyce, 2013; Barr et al., 2014). According to archaeological evidence, Indigenous activities were likely in place before the eruption of Mt Eccles (Dawson, 1881; O'Connell & Allen, 2015). The Budj Bim ("Mt Eccles") National Park was included on the United Nations Educational Scientific and Cultural Organization (UNESCO)'s World Heritage list due to its cultural, natural and geological significance (Bell & Johnston, 2008; Smith et al., 2019).

The western Victorian plains experience a temperate climate (Tweed et al., 2009; Barr et al., 2014) and according to the instrumental monitoring data from the Bureau of Meteorology (BOM), the mean annual precipitation ranges from 500mm to 1500mm, with 60% of rainfall occurring mainly in winter and spring months (Australian Bureau of Meteorology, 2022). The majority of the winter-dominated rainfall is modulated by latitudinal shifts of prevailing westerly and south-westerly winds that are generated in the Southern Ocean (Risbey et al., 2009). The strength of these westerlies is influenced by the Southern Annular Mode (SAM), an important driver of rainfall variability in southern Australia (Abram et al., 2014; Barr et al., 2014). According to the meteorological data available in the BOM database, annual average evaporation, and minimum and maximum air temperatures range from 1100mm to 1500mm, 17℃ to 20℃ and 7℃ to 9℃ respectively (BOM, 2022). The regional climate variability is also influenced by large-scale climate systems including the Indian Ocean Dipole (IOD), the El-Niño Southern Oscillation (ENSO) and the Interdecadal Pacific Oscillation (IPO) (Cai et al., 2011b; a; Cleverly et al., 2016; Dey et al., 2019).

4.2.2 Lake features, hydrology and limnology,

Lake Surprise was formed by adjoining three craters of different sizes (Timms, 1975), leading to an elongated lake of approximately 600 m of maximum length and 200 m of maximum width as inferred by the most recent lake bathymetry developed in 2019 (Figure 1b and Appendix 1). The densely vegetated and high crater walls (~49 m) protect the lake from wind-blown turbulence, inhibiting lake water mixing (Timms 1975; Barr et al. 2014). The funnel-shaped lake floor was ~11.5 m deep at the time of coring in September 2019 with sharp boundaries of horizontal isotherms, indicating thermal stratification (Chapter 2, Section 2.2). Previous studies have identified evidence of minor fluctuations in water depth in response to regional climate

change, for instance, measured water depths were ~13 m in 1971 and 10.4 m in 2004 (Timms, 1975; Barr et al., 2014).

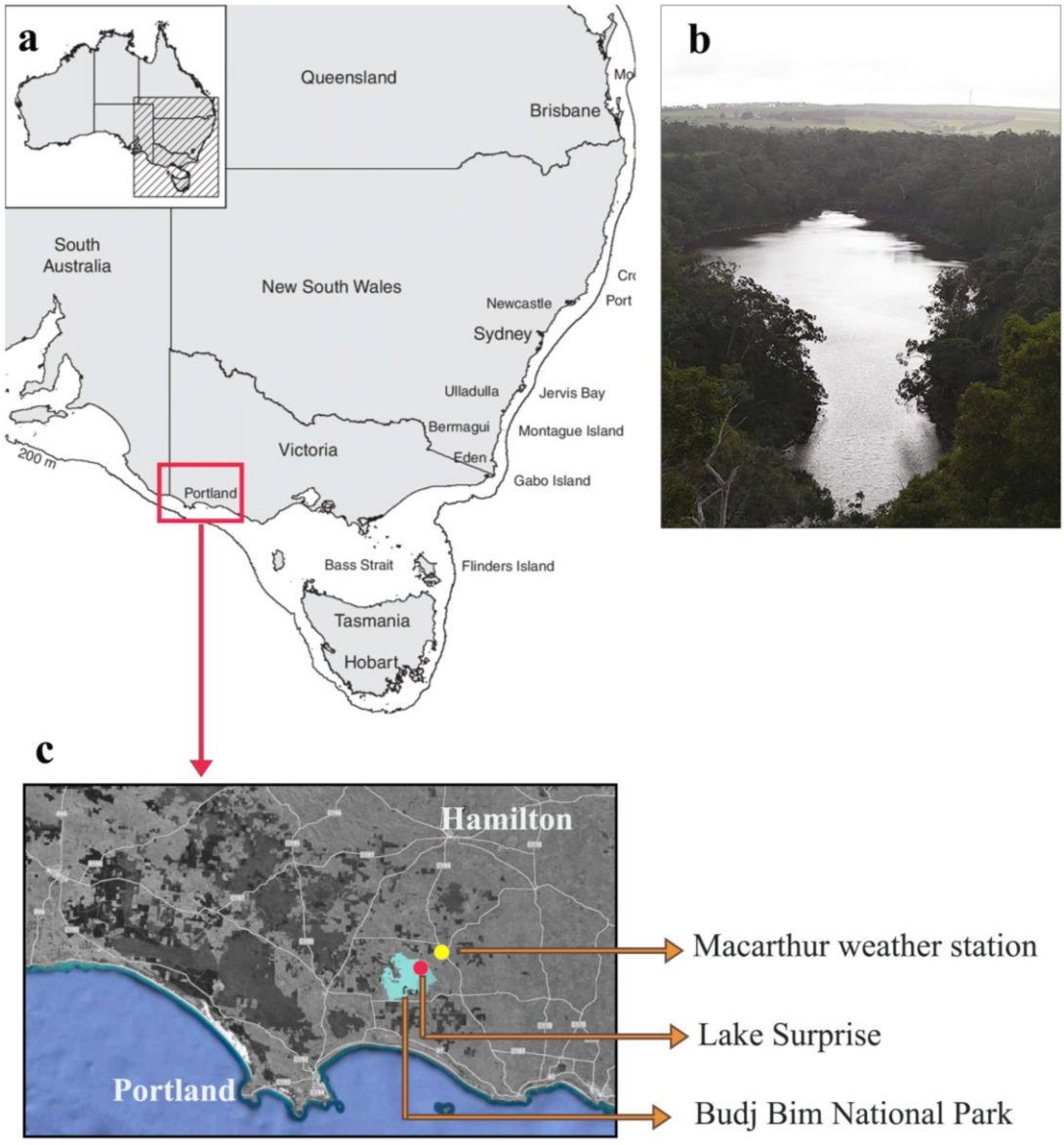

Figure 1. a) Approximate location of western Victoria b) elongated view of Lake Surprise looking north-west from the crater rim of Mt Eccles (Falster et al., 2018) c) Zoomed-in section of the selected region of western Victoria (from figure 1a), representing the location of Lake Surprise, the Budj Bim National park and Macarthur weather station where climate data were measured since 1890 CE.

Continuous sedimentation of approximately 30,000 years (Falster et al. 2018) indicates that groundwater is likely to be an important component of lake hydrology (Chapter 2, Section 2.4.4), particularly during arid periods such as the last glacial maximum and the Millennium Drought (Builth et al., 2008; Barr et al., 2014; Falster et al., 2018). The lake is characterised as a "freshwater" lake with alkaline pH values (~ 7 – 9) and relatively high concentrations of Na^+ and HCO_3^- or CO_3^{2-} ions (Timms, 1975; Ankor, 2020; Chapter 2 of this thesis). The vegetation within the crater is dominated by *Eucalyptus viminalis* ("Manna gum"), *Acacia melanoxylum* ("Blackwood") and a ground cover of *Pteridium esculentum* ("bracken'') (Tibby et al., 2006; Builth et al., 2008; Falster et al., 2018).

4.3 Materials and methods,

4.3.1 Sediment core acquisition,

In October 2019, a 1.57 m long sediment core (SUR-19-01) was collected from a coring platform located over the deepest point of the lake, using a wide-diameter Perspex piston corer. To minimise any disturbance to the sediment profile, the core was extruded at 0.5 cm intervals on-site, keeping the sediment core in an upright position. All sediment samples were sealed in Zip-lock bags and were stored in cold storage at 4°C. Before the preparation of samples for analysis, the moisture content was estimated by measuring the wet weight which was subtracted from the weight after freeze-drying.

4.3.2 Geochronology

The chronology of the sediments was defined by ^{210}Pb dates obtained from freeze-dried sediments of the upper 100 cm, and Pu isotope measurements (^{239}Pu, ^{240}Pu and ^{241}Pu) of the top 50 cm of the core. Of these samples, total and "supported" ^{210}Pb activities were measured on nine samples using ^{210}Po and ^{226}Ra activity, respectively (Appleby, 2001; Harrison et al., 2003; Holmgren et al., 2010). The measured activity difference was used to determine the unsupported activity. ^{210}Po was analysed with a High Purity Germanium (HPGe) crystal gamma detector and the ^{226}Ra was measured by alpha spectrometry. Sample preparation and analyses were undertaken at the Australian Nuclear Science and Technology Organisation (ANSTO) in Lucas Heights, New South Wales. Sample preparation for Pu isotope analysis was carried out in a laboratory with positive pressure HEPA-filtered air that was carefully ventilated at ANSTO and samples were analysed at the ANTARES Accelerator Mass Spectrometry

(AMS) facility at ANSTO (Child et al., 2008). Pu isotope measurements were used to validate the age model via independent chronological markers such as the period of maximum atmospheric fallout and the first detection of Pu in the atmosphere (Leslie & Hancock, 2008; Hancock et al., 2011; Harrison et al., 2021). A detailed methodology used in sediment dating is explained in Chapter 3 of this thesis (Section 3.2).

Radiocarbon dating was performed in both the pollen and macrofossil samples extracted across the entire sediment profile. 33 pollen samples were treated following the modified method by Turney et al., (2021) and Cadd et al., (2022) at the Chronos 14Carbon-cycle facility at the University of New South Wales. ^{14}C measurements of pollen were performed on a MICADAS (Ionplus, Switzerland) Accelerator Mass Spectrometer (AMS) following Turney et al., (2021). 17 macrofossil samples were pre-treated using the standard AAA method to remove carbonates and any contaminating material from the samples (Hua et al., 2001; Norris et al., 2020) and followed the method explained in Hua et al., (2001) for further treatment. A detailed method is given in Chapter 3 of this thesis. ^{14}C analysis of macrofossil samples was performed using the AMS facility at ANSTO (Fink et al., 2004). The oxalic acid I NIST standard (HOxI) was used to normalise ^{14}C readings. Using ^{13}C measurements from graphite sub-samples in the continuous flow isotope ratio mass spectrometer (CF-IRMS), ^{14}C values were adjusted for isotope fractionation, and the results of ^{14}C were presented as a percentage of modern carbon (pMC) (Fink et al., 2004; Howarth et al., 2013).

Radiocarbon dates were calibrated to calendar years using the revised southern hemisphere radiocarbon calibration curve, SHCal 20 for pre-bomb samples and Bomb SH 1–2 data for post-bomb samples (Hogg et al., 2020; Hua et al., 2022). The ages were reported as calendar years before the year 1950 (cal yr BP). The final age model was established using the Bayesian *Plum* model (Aquino-López et al., 2018), in the R programming environment (version 4.1.3) (R Core Team, 2022).

4.3.3 XRF element analysis

Major elemental concentrations of the sediments (Ca, Sr, Fe, S, Si and Cl) were obtained at 0.5 cm resolution, using an Olympus Delta^{TM} handheld XRF (X-ray fluorescence) analyser. Previous studies that analysed the element concentrations of lake sediment using the handheld XRF analyser also suggested that the XRF results are in good agreement with the ITRAX

element variation (Rodysill et al., 2012). Sediments were analysed through thin Zip-lock bags to prevent any contamination. A calibration check was followed by three internal standard measurements of SiO_2, NIST2710a and NIST2711a were performed after every 20 samples to maintain the precision and accuracy of the instrumental results.

4.3.4 Stable isotope analysis

4.3.4.1 Stable carbon isotopes and C/N measurements

Stable carbon isotopes ($\delta^{13}C$), total organic carbon (TOC) and C/N ratios were determined on freeze-dried sediment that was crushed and powdered using a Retsch MM400 ball mill. Samples for the carbon isotope analysis were selected at 2 cm intervals across the entire sediment depth. However, because of the increased moisture, a small amount of material remained for analytical purposes (<2 mg), following the freeze-drying step. $\delta^{13}C$ analysis and TOC concentrations were prepared using the acid fumigation method (Harris et al., 2001). About 1 – 2 mg of powdered dry sediment was weighed into silver capsules and after adding ~25 µl of deionised water, the capsules were acidified for nearly 4 hours in concentrated hydrochloric acid vapour to remove inorganic carbon from the sediment before being dried overnight at 60ºC. The capsules were placed inside larger tin capsules and crimped before the analyses. All the samples were analysed by Elemental Analyser/Isotope Ratio Mass Spectrometry (EA/IRMS) using a EuroVector EuroEA coupled to a Nu Instruments Horizon IRMS at the University of Adelaide. Three in-house standards namely, Glycerine ($\delta^{13}C$:-31.2, $\delta^{15}N$: +1.32, C/N: 2), Glutamic acid ($\delta^{13}C$: -16.7, $\delta^{15}N$: -6.18, C/N: 5) and a quality control (QC) standard TPA (triphenylamine $\delta^{13}C$: -29.2, $\delta^{15}N$: -0.54, C/N: 18) were used to calibrate carbon isotopes. $\delta^{13}C$ isotope values were reported in per mille (‰) units relative to the Vienna Pee Dee Belemnite. Total nitrogen and organic carbon contents in the sample were also measured acquired during the same analytical procedure and reported as a percentage (%) values.

4.3.4.2 Oxygen isotopes in cellulose

Sediments were sampled at 5 cm intervals for oxygen isotope analysis of cellulose. Cellulose extraction was achieved using the dissolution and precipitation method described by Wissel et al. (2008). For each analysis, ~ 5 – 10 g of wet sediment was needed for the extraction procedure. Fine sediment was retained by sieving (250 µm) and settling overnight. This process

minimises the incorporation of terrestrial material and coarse organic residue including macro-charcoal (Edwards and McAndrews 1989; Rozanski et al. 2010; Street-Perrott et al. 2018). Then fine sediment was reacted with 7% sodium chlorite acidified to a pH of 4 – 5 with concentrated acetic acid (98%) and left to oxidise at 60°C for 10 hours. Treated sediment was rinsed three times with hot deionised water (70°C) and freeze-dried. The cellulose dissolution process was followed by reacting dried sediment with cuprammonium solution. The solution was prepared by mixing 15 g of copper hydroxide, 900 ml of ammonium hydroxide (25%) and 100 ml of deionised water and the resultant solution was stirred overnight at room temperature. The sediment solution mixture was left to react in the end-over-end shaker for 6 hours and then for another 10 hours for the complete dissolution of cellulose. The cellulose precipitation step was initiated by treating the supernatant cellulose solution with 3 ml of 20% H_2SO_4 until the precipitate turned white. Extracted cellulose was rinsed and freeze-dried before sample preparation for analysis. Afterwards, 100 µg of dry cellulose were weighed into Ag capsules and were crimped. As the cuprammonium treatment of cellulose tends to extend its hygroscopic character, Ag capsules were stored at 40°C in the oven after weighing and immediately before analysis, the oven temperature was ramped to 100°C overnight (Wissel et al., 2008).

Cellulose oxygen isotopes were measured using a HEKAtech HT Oxygen analyser coupled with a EuroVector EuroEA Elemental analyser. Samples were reacted at 1500°C and measured as CO using a Nu Instruments Perspective IRMS in continuous flow mode. Results were calibrated against the standard NBS127 and compared to internal analytical standards such as cellulose ($\delta^{18}O$ = 35.48±0.27 ‰), sucrose ($\delta^{18}O$ = 30.24±0.17 ‰) and certified elemental microanalysis silver phosphate (Ag_3PO_4) ($\delta^{18}O$ = +21.7±0.3 ‰). In addition, Pinewood and cellulose powder were processed in each batch alongside sediment samples as a means to monitor the replicability of the extraction method. Repeated measurements of internal standards taken throughout each sample run yielded an analytical accuracy of ±0.3 ‰. Results are reported relative to Vienna Standard Mean Ocean Water (VSMOW) and expressed in per mille (‰) units.

Cellulose-water isotope fractionation was expressed as follows (Edwards & McAndrews, 1989),

$$1.028 = \left[\frac{\delta^{18}O_{cellulose}+1000}{\delta^{18}O_{Lake\ water}+1000}\right] \quad \text{Equation 1}$$

The oxygen isotope composition of palaeo-lake water ($\delta^{18}O_{LW}$) was estimated using the following equation expressed by Rozanski et al., (2010) by re-arranging the terms in Equation 1 (Edwards & McAndrews, 1989)

$$\delta^{18}O_{LW} = 0.973\ \delta^{18}O_{cellulose} - 27.2 \qquad \text{Equation 2}$$

The cellulose isotope record obtained from SUR-19-01 overlaps with a longer sediment profile (SUR-19-02) used in the detailed reconstruction of the Holocene period (Chapter 5). Isotope records from both sediment cores for the overlapping period were compared to assess the accuracy of data measurements and to select the most reasonable record (Supplementary Figure II). Therefore this study represents cellulose oxygen isotope records from both the SUR-19-01 (0 – 46.7 cm) and SUR-19-02 (52 – 156 cm) cores.

4.3.5 Meteorological data acquisition

Meteorological data were obtained from the nearest weather station, which is located at Macarthur (station number 090055), approximately 10 km northeast of Lake Surprise. Climate data at this station was recorded since 1889 and is now archived by the Australian Bureau of Meteorology (BOM). However, gaps and erroneous values exist in these records due to failures in the equipment, observers being unavailable or events that produce controversial data. Therefore, here we used post-processed instrumental data from the Scientific Information for Land Owners (SILO) database (https://www.longpaddock.qld.gov.au/silo/) that includes raw observational data from the Bureau of Meteorology (BOM) and other providers. In the SILO database, missing values or erroneous values in the observational record are corrected by using interpolation, providing a complete dataset from 1889 to the present day (Jeffrey et al., 2001).

4.3.6 Statistical analysis

The comparison between climate data and sediment proxy data is challenging, given the timing disparities between the two records. Climate data are regularly spaced in daily, monthly or annual scales, whilst sediment proxy scales vary over time, depending on sediment thickness, rates of sedimentation and multiple other factors including the location, analytical techniques etc. Given that simple linear regression or correlation is impossible without equally distributed data, the climate data were averaged corresponding to the estimated period represented by each

sediment proxy data point. Thereby, Pearson correlation was used in R ("rstatix" package) (v0.7.0, Kassambara A., 2021), to determine proxy-climate correlation for the instrumental period (1889 – 2019). Major sediment proxies of Ca%, which is the most prominent inorganic element in the lake sediment data, $\delta^{18}O_{LW}$ and $\delta^{13}C_{org}$ were correlated with mean annual precipitation, evaporation and air temperature separately, due to the differences in their sampling resolution.

4.4 Results

4.4.1 Sediment lithology and chronology

The entire sediment profile consisted of very fine-grained clay and was dominated by organic-rich (20 – 45%) blackish-grey sediment. The moisture content of these sediments was over 85% (Supplementary Figure I), thus retaining a very small amount of material after freeze-drying for sample analysis. Laminations or any other distinctive features were not identified from this sediment core, although this may be the result of coring and sediment extrusion.

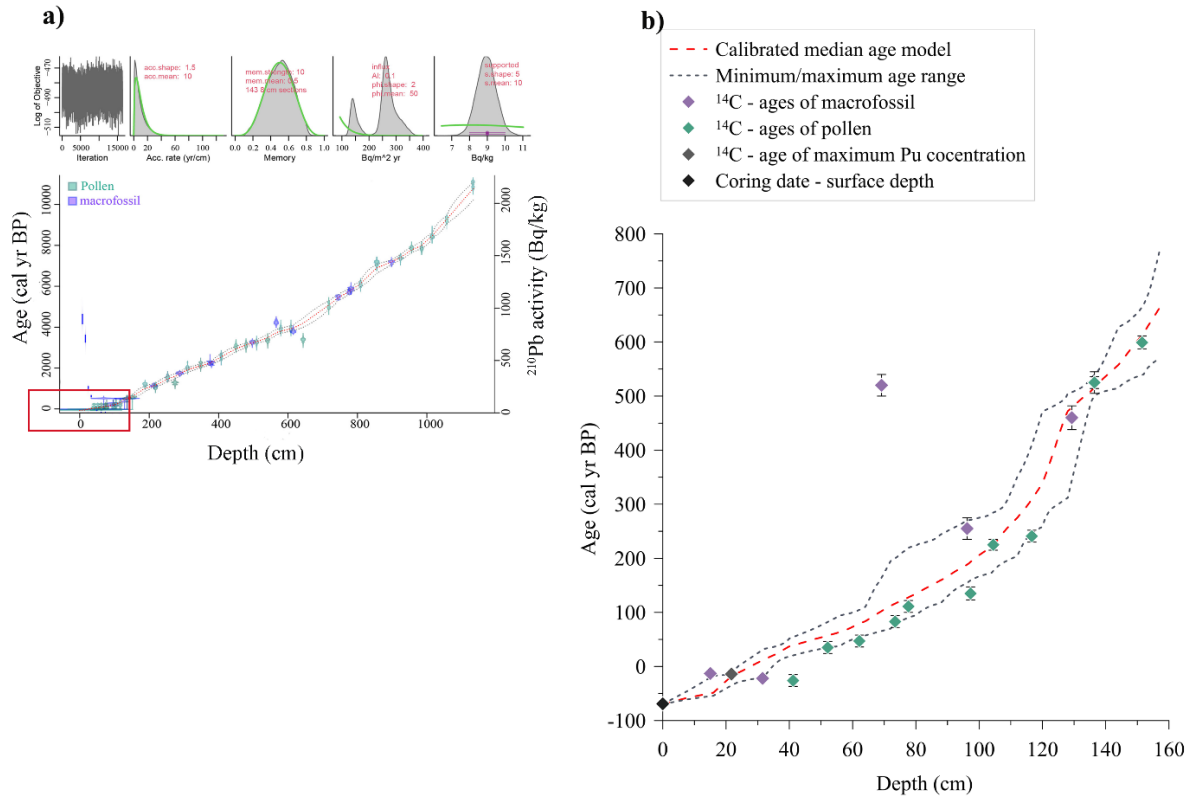

Figure 2. (a) The age model developed for the full Holocene sediment package at Lake Surprise. (b) Zoomed in section of the top 160 cm (core SUR-19-1) from the composite age model. All pollen radiocarbon ages are corrected with a Delta.R of 340 and Delta.STD of 50 years.

The total ^{210}Pb activity profile varied from 9 – 906 Bq kg^{-1}, with activity reaching the measurable background at ~107.4 cm. The unsupported/excess ^{210}Pb activity is significantly higher compared to the supported ^{210}Pb activity profile (Chapter 3, Section 3.3.2). The maximum Pu isotope concentration, relevant to the year 1964 was observed at 21.7 cm, followed by a steep rise in values from 29.9 cm (Hancock et al., 2011; Harrison et al., 2021). Detailed information related to Pu isotope concentration in these sediments can be found in Chapter 3 (Section 3.3.3) of this thesis. The majority of radiocarbon dates of pollen samples illustrate an age offset of approximately 340±50 ^{14}C years, with pollen dates being older than macrofossil ages. Therefore, Delta.R and Delta.STD value of 340±50 was used as an age correction to all the pollen radiocarbon dates before being modelled (Chapter 3, Section 3.4.2). According to the final age model, the SUR-19-01 core has a basal age of approximately 660 cal yr BP. For detailed chronological control of Lake Surprise sediments, refer to Chapter 3 of this thesis.

4.4.2 Geochemistry of the lake Sediment

Among multiple elements measured by the Handheld XRF analyser, major element oxides including Ca, Sr, Fe, S, Si and Cl were identified in detectable amounts. Additionally, extremely small quantities of Mn, Cu, Cr, and P were observed and the concentrations of the remaining elements were found below the lower detection limit (0.001%). The interpretable elements of Ca, Sr, Fe, S, Si, and Cl were primarily found below 2% because the light element content in the wet sediment (C, H, and O) was greater than 95 % (Appendix 3, Table I).

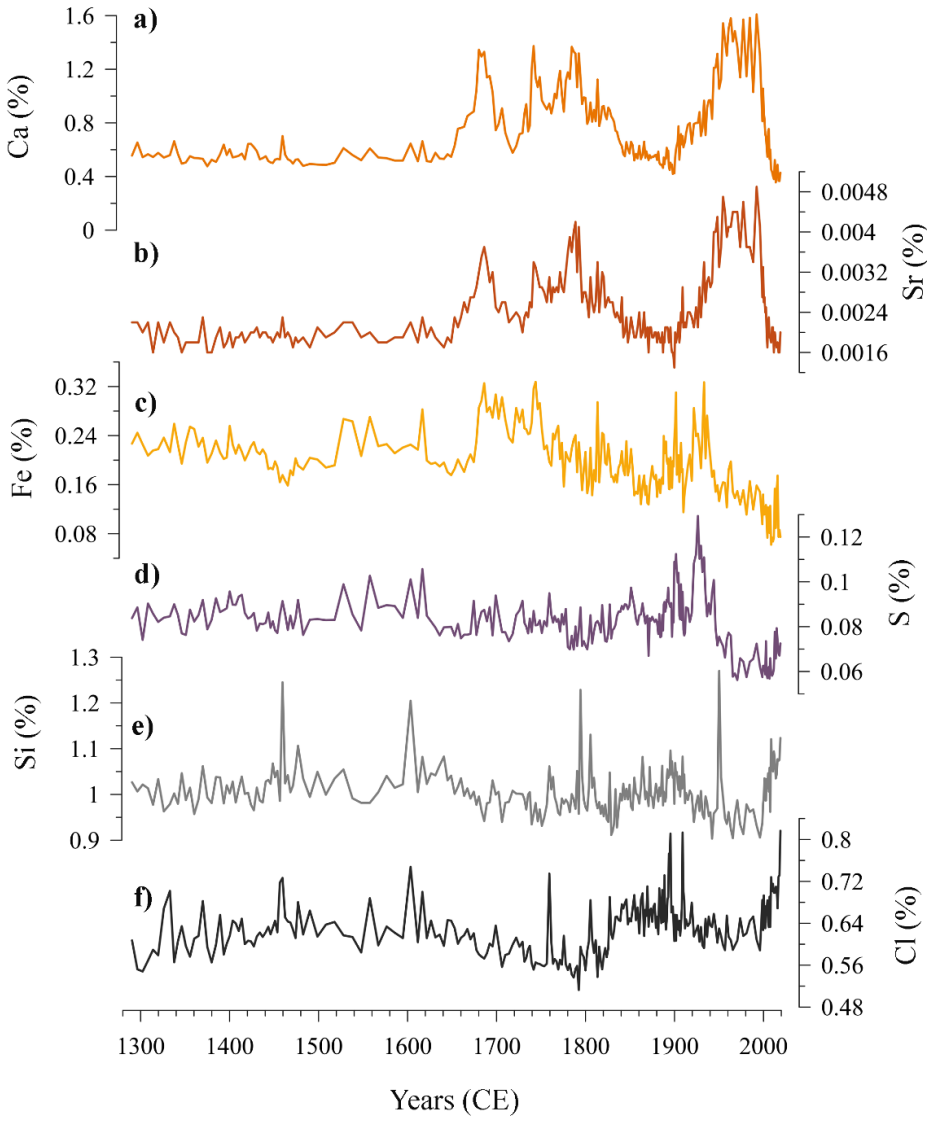

Figure 3. Major elements of a) Ca b) Sr c) Fe d) S e) Si and f) Cl distribution against the sediment age.

Among interpretable elements, Ca is the most abundant inorganic element with concentration varying from 0.36±0.003 – 1.61±0.012% and illustrating identical down–core variation to Sr (Figure 3) with minor concentrations of 0.0013±0.0001 – 0.0049±0.0001% (R^2 = 0.95, p-value <0.0001) (Supplementary section, table V). Si, which is the second most abundant element ranges from 0.90±0.01 – 1.27±0.02% and Cl varies from 0.51±0.004 – 0.82±0.007%. Similarly, Fe and S concentrations exhibit approximately similar variation along the sediment profile, with values varying from 0.06±0.006 – 0.33±0.009% for Fe and 0.06±0.002 – 0.13±0.002% for S, respectively (R^2 = 0.57, p-value <0.0001) (Supplementary section, table V). The elemental percentages illustrate relatively high variation from around late 1600 CE to the present day, whereas the concentrations before 1600 CE remain nearly consistent except for Si

and Cl. Ca (Sr) concentrations represent an opposite trend to Fe (S), roughly from ~1750 – 2019 CE. This is consistent with the relatively low levels of Ca and Sr that correspond to a gradual rise in the concentrations of Fe and S in the early years (1280 – 1700 CE). However, this is not true for the period of ~1680 – 1740 CE, where both Ca and Fe concentrations seem to increase or decrease simultaneously, whilst S remains low throughout this period. Since around 1800 CE, even though, both Si and Cl ions illustrate relatively high fluctuations across the sediment depth, with roughly both Si and Cl content seem to vary in a similar pattern (R^2 = 0.46, p-value <0.0001) towards younger sediment (Supplementary section, table V).

4.4.3 Stable isotope results

4.4.3.1 Stable carbon isotope and C/N results

Sedimentary $\delta^{13}C_{org}$ values illustrate relatively low values that range from -27.3 to -29.7‰, whereas the TOC content varies from 21.6 to 42.5% (Appendix 4, Table II). Both proxies exhibit a similar pattern of variation along the sediment profile, with a sharp drop in values from ~1940 – 1960 CE. TOC content and TN in the sediment show a moderate, positive linear correlation (R^2 = 0.40). The C/N ratio in the sediment shows less variation with values clustered within the range of 7.15 – 13.20 (Figure 4c; Appendix 4, Table II).

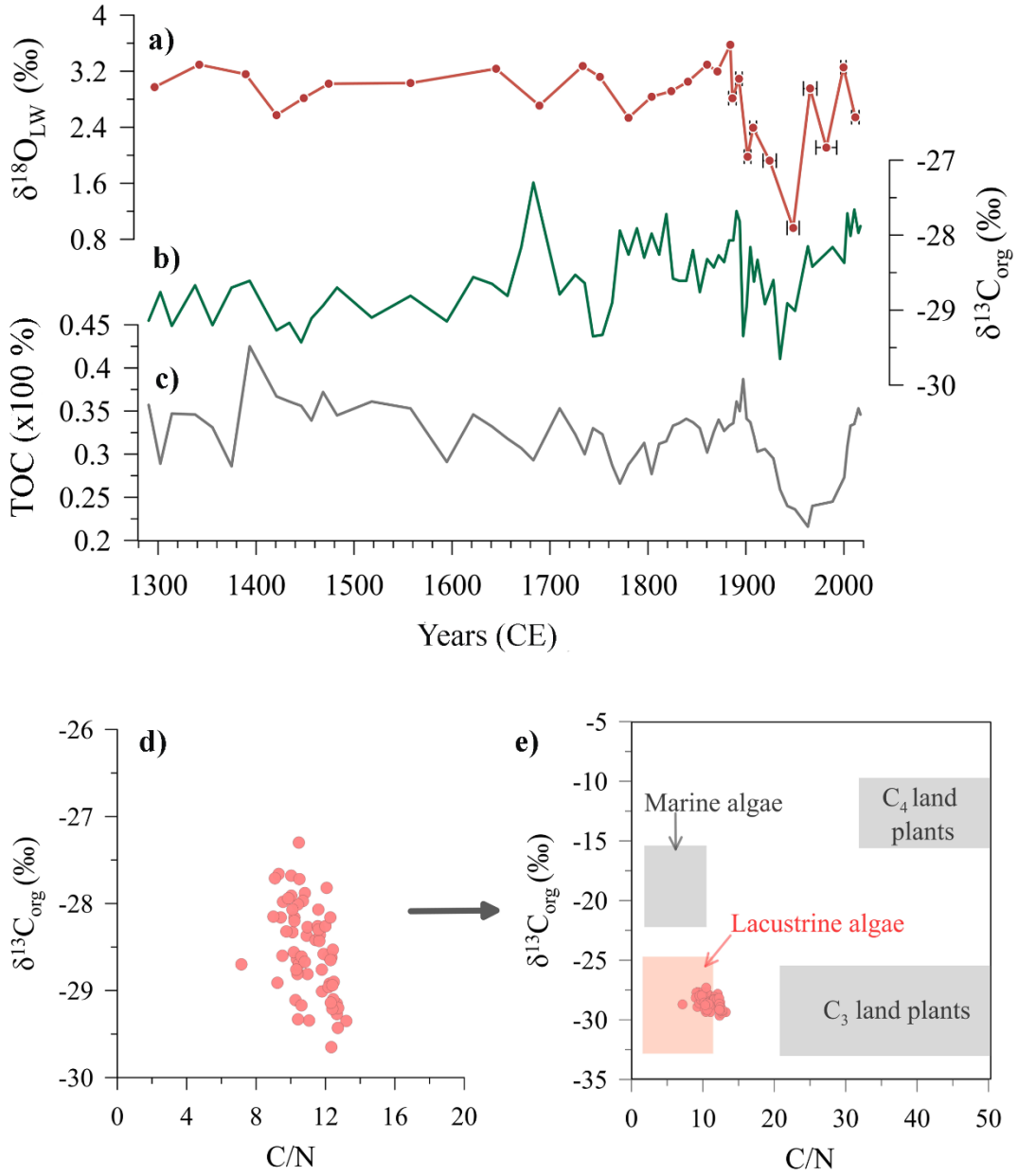

Figure 4. a) Cellulose-inferred water oxygen isotopes ($\delta^{18}O_{LW}$ ‰) b) organic carbon isotopes ($\delta^{13}C_{org}$ ‰) c) total organic carbon (TOC) against sediment age; d) bi-plot of $\delta^{13}C_{org}$ vs total organic carbon to total nitrogen ratio (C/N); e) distribution of Lake Surprise C/N vs $\delta^{13}C$ data within the reference ranges established by Meyers (1997).

4.4.3.2 Cellulose inferred oxygen isotope results

$\delta^{18}O$ analyses from cellulose range approximately from 29 – 32‰ (Supplementary data, Table 1). $\delta^{18}O_{cell}$ in pinewood illustrate relatively smaller deviation (±0.4) with values varying from 28.99 – 30.18‰. However, cellulose powder illustrates considerable bias between different batches (27.17 – 29.84‰) (Chapter 5, Supplementary Section 1). Cellulose inferred $\delta^{18}O_{LW}$ values (obtained by applying Equation 2) range from 0.96 – 3.58‰, with a period of relatively

enriched values between 1300 – 1750 CE, punctuated by occasionally depleted values at ~1400, ~1690 and ~1790 CE (Figure 4). From 1790 to 1890, $\delta^{18}O_{LW}$ increased by 2.4 – 3.6‰, before exhibiting a clear period of decreasing $\delta^{18}O_{LW}$ between 1890 and 1940 CE. The four values younger than 1950 suggest a return to higher $\delta^{18}O_{LW}$ leading towards present data (Figure 4), following a pattern resembling that of $\delta^{13}C_{org}$ and TOC. A larger amount of sediment (~5-7 cm of sediment section) was required for cellulose extraction used from the upper 30 cm of the core due to the high water content. As a result, the oxygen isotope values of younger material were given an age bracket ranging from 2.7–10.6 CE, which corresponds to the thickness of each sediment sample.

4.4.4 Instrumental climate vs. sediment proxy data correlation

Ca content shows a moderate, yet negative correlation to both evaporation and annual maximum temperature (Tmax) (-0.48 and -0.56 respectively), whilst a positive correlation with precipitation, effective precipitation (P-E) and the P/E ratio (0.33, 0.48 and 0.44 respectively) (Table 1). The correlation between climate variables is generally stronger (R >0.7) compared to the climate-Ca correlation. However, average precipitation has a relatively moderate negative relationship with both evaporation and maximum temperature (R<0.4) and interestingly minimum temperature (Tmin) lacks any correlation to Ca% or the majority of other climate variables.

Table 1. Correlation matrix of Ca% vs climate data averaged to each data point based on the sediment thickness (age uncertainty). The number of data points used in the correlation (covering the instrumental period) = 81 and the p-values corresponding to climate-proxy correlation are given in Supplementary data, (Table II).

(P = precipitation, E = evaporation, P-E = effective precipitation, Tmax = maximum air temperature, Tmin = minimum air temperature).

	Ca	P	E	P-E	P/E	Tmax	Tmin
Ca	1						
P	0.33	1					
E	-0.48	-0.42	1				
P-E	0.48	0.85	-0.84	1			
P/E	0.44	0.92	-0.73	0.98	1		
Tmax	-0.56	-0.3	0.78	-0.64	-0.56	1	
Tmin	-0.1	-0.52	0.23	-0.44	-0.47	0.15	1

Table 2. Correlation matrix of $\delta^{13}C_{org}$ vs climate data averaged to each data point based on the sediment thickness (age uncertainty). The number of data points used in the correlation (covering the instrumental period) = 21 and the p-values corresponding to climate-proxy correlation are given in Supplementary data, (Table III).

	$\delta^{13}C_{org}$	P	E	P-E	P/E	Tmax	Tmin
$\delta^{13}C_{org}$	1.00						
P	-0.07	1.00					
E	0.39	-0.34	1.00				
P-E	-0.29	0.80	-0.84	1.00			
P/E	-0.22	0.90	-0.70	0.97	1.00		
Tmax	0.53	-0.13	0.71	-0.53	-0.44	1.00	
Tmin	0.32	-0.68	0.36	-0.62	-0.66	0.18	1.00

Table 3. Correlation matrix of $\delta^{18}O_{LW}$ vs climate data averaged to each data point based on the sediment thickness (age uncertainty). The number of data points used in the correlation (covering the instrumental period) = 9 and the p-values corresponding to climate-proxy correlation are given in Supplementary data, (Table IV).

	$\delta^{18}O_{LW}$	P	E	P-E	P/E	Tmax	Tmin
$\delta^{18}O_{LW}$	1						
P	-0.4	1					
E	0.72	-0.29	1				
P-E	-0.68	0.84	-0.77	1			
P/E	-0.67	0.91	-0.66	0.99	1		
Tmax	0.74	-0.23	0.95	-0.7	-0.6	1	
Tmin	0.33	-0.54	0.07	-0.4	-0.47	0.05	1

$\delta^{13}C_{org}$ positively correlates with Tmax and evaporation but with poor-moderate strength (R = 0.3 – 0.5). The correlation with precipitation, P-E and P/E ratio is negative but with a lower strength ($R \leq 0.3$) compared to previous correlations. $\delta^{18}O_{LW}$ illustrates a strong positive correlation to both Tmax and evaporation ($R > 0.7$), whilst a negative correlation to both P-E and P/E ratio with a moderate-strong potency ($R \sim 0.68$). The correlation between $\delta^{18}O_{LW}$ and precipitation remain relatively poor (R = -4). As observed in the Ca% correlation results, Tmin illustrates a very poor correlation between sediment proxies and climate variables. Overall, all three sediment proxies strongly correlate with temperature maximum and annual evaporation compared to annual precipitation.

4.5 Discussion

4.5.1 Interpretation of major elements

Among many measurable elements, Ca, Sr, K, Ti, Al, Si, Fe and S have been commonly used to infer in-lake dynamics (Davies et al., 2015). Previous studies have used a wide variety of assumptions and competing hypotheses in interpreting these elements. For instance, Ca concentration in freshwater lakes has been used to interpret authigenic carbonate deposition, which is generally associated with evaporative enrichment and reflects a low precipitation to evaporation (P/E) ratio during drier conditions (Leng and Marshall, 2004; Scholz et al., 2007; Gierlowski-Kordesch, 2010; Wilkins et al., 2013; Barr et al., 2014). In contrast, few studies have identified high Ca concentration in the sediment during wet periods as a result of groundwater throughflow that saturates the carbonate concentration in the water column and lessens the effect of evaporation (Teller & Last, 1990; Herczeg et al., 2003; Shapley et al., 2005) and increasing primary productivity that stimulates authigenic carbonate deposition by recycling organic carbon in the sediment-water interface (Dean, 1999; Karami et al., 2019; Sun et al., 2019). Sr is also used as a measure of inorganic carbonate deposition in lacustrine environments, given its closer association with the +2 oxidation state in CaO, (Blaschko et al., 2018). Sr is commonly used as a palaeoclimate proxy due to its increased mobility, some studies have used the Sr/Ca ratio in freshwater environments as a measure of authigenic and biogenic carbonate deposition (Gouramanis et al., 2010; Wilkins et al., 2013; Burn & Palmer, 2014). The abundance of $CaCO_3$ and $SrCO_3$ in the Lake Surprise deposits, as well as their identical variability, imply that the main driver of inorganic carbonate deposition is a similar source.

Fe and S distribution in lake sediments is mainly an indication of redox conditions (Wetzel, 2001a; Naeher et al., 2013), and sometimes may represent the aeolian-flux into lakes, particularly in environments with Fe-rich soils (De Deckker, 2019; Perron et al., 2020). Previous research and current monitoring data from Lake Surprise have identified distinct layers of stratification in Lake Surprise (Timms, 1975; Chapter 2 of this thesis). With the co-occurrence of increased drying and lake stratification, Fe and S reduce in the anoxic hypolimnion to form pyrite (FeS) (Wetzel, 2001a). Si concentration in lake sediments may represent either biogenic Si (diatom assemblages) or inorganic Si mainly from erosion and aeolian influx (Peinerud, 2000; Wetzel, 2001a; Martín-Puertas et al., 2011; Falster et al., 2018). The possibility of the inorganic contribution of Si to Lake Surprise has been discussed by

Falster et al., (2018). However, it is difficult to use Si as a palaeoclimate proxy since it is not possible to differentiate between biogenic and inorganic Si using only XRF analysis. Even though, chloride ions may concentrate in lakes with evaporative enrichment and with increased salinity (Harriss, 1966; Guo et al., 2018; Han et al., 2022), it is uncommon to assess climate change using Cl concentration in lake sediments due to its high mobility and solubility (Dugan et al., 2017). Further, Cl ions are likely preserved in pore waters compared to actual sediment. To lay the foundation for the interpretation of elemental and isotope distribution across the studied period, the relationship between sediment proxy and climate is first discussed.

4.5.2 Relationship between sediment proxy data and instrumental climate variables

The concentration of calcium carbonate and the stable oxygen and carbon isotope composition of lake sedimentary materials are commonly used palaeoclimate proxies. However, the underlying interpretation of these proxies is rarely supported by objective validation prior to their use in long-term climate reconstructions, which may eventually lead to erroneous or uncertain representations of the past climate (Tian et al., 2011; Dolman et al., 2021). Therefore, in this study these three data types are compared across the instrumental period (1780 – 2019 CE), to test these hypotheses and determine if they accurately reflect local climate conditions.

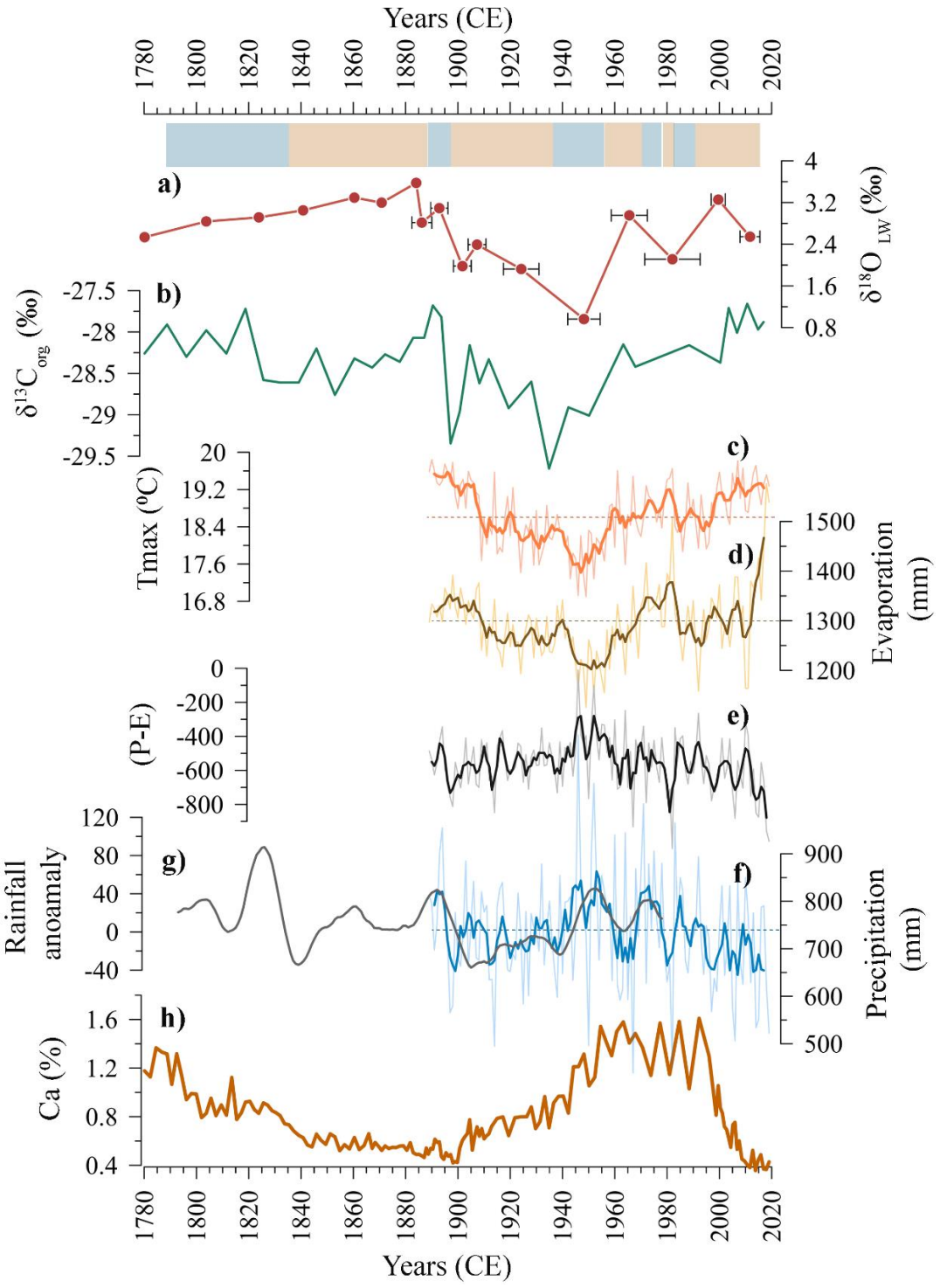

Figure 5. Comparison of sediment proxy data a) lake water oxygen isotopes ($\delta^{18}O_{LW}$‰) b) organic carbon isotopes ($\delta^{13}C_{org}$‰) & h) Ca (%) with instrumental climate data of c) annual maximum air temperature d) annual evaporation e) effective precipitation (P-E) f) annual precipitation & g) reconstructed rainfall anomaly (Gergis et al., 2012). Blue-shaded bars illustrate wet periods and brown-shaded regions illustrate dry periods. Horizontal dotted lines in c, d & f represent their average values for the instrumental period. In Figure a) the error bars illustrate the time interval covered by the sediments used in each sample.

4.5.2.1 Correlation between lake water oxygen isotopes and climate variability

The oxygen isotope composition of lake waters ($\delta^{18}O_{LW}$) is an important tracer of contemporary and past climate and environmental change (Leng & Marshall, 2004; Steinman et al., 2010; Wu et al., 2015; Tyler et al., 2022). With the preferential loss of lighter isotopes during evaporation, lake waters obtain higher $\delta^{18}O_{LW}$ values, particularly in closed (or nearly closed) lakes where the majority of water loss occurs through evaporation (Craig & Gordon, 1965; Leng & Marshall, 2004; Horton et al., 2016; Shi et al., 2017). The balance between precipitation and evaporation, or the P/E ratio, is a common framework used to interpret past climate conditions from inferred $\delta^{18}O_{LW}$ (Abbott et al., 2000; Wolfe et al., 2001; Brahney et al., 2010; Heikkilä et al., 2010; Rozanski et al., 2010; Heyng et al., 2014; Wu et al., 2015; Jones et al., 2016). The $\delta^{18}O_{LW}$ record in this study agrees well with the above hypothesis, with a strong positive correlation between $\delta^{18}O_{LW}$, evaporation and Tmax. Even though the $\delta^{18}O_{LW}$ record is low resolution, low $\delta^{18}O_{LW}$ values are concentrated at or near wet periods of 1935 – 1955 CE and ~1970 – 1990 CE. Similarly, elevated $\delta^{18}O_{LW}$ values are mostly associated with dry episodes (1900 – 1935 CE, 1955 – 1970 CE and 1990 – 2020 CE). While the amount of precipitation does not seem to reflect a distinctive trend through time, both evaporation and Tmax have, and these appear to have had a greater influence over changes in $\delta^{18}O_{LW}$. Therefore, when evaluating palaeoclimate data, it's critical to focus on the role of evaporation and the way it relates to temperature, rather than interpreting oxygen variation as solely a precipitation-sensitive record. Overall, $\delta^{18}O_{LW}$ values can be utilised to interpret long-term climate variability in the region.

4.5.2.2 Correlation between carbon isotopes in organic matter and climate variability

Stable carbon isotope composition ($\delta^{13}C_{org}$) along with the C/N ratio in lacustrine organic matter is mainly used to trace biological sources, carbon burial and to differentiate between the aquatic and terrestrial origin of organic matter (Meyers, 1997; Meyers, 2003; Leng & Marshall, 2004; Zhang et al., 2015; Liu et al., 2019). $\delta^{13}C_{org}$ is also used as a proxy for palaeoproductivity in lakes, thus interpretation of $\delta^{13}C_{org}$ is difficult, due to the complex nature of carbon cycling in freshwater environments (Meyers & Lallier-Vergès, 1999; Torres et al., 2012; Barr et al., 2017; Guiry, 2019). The $\delta^{13}C_{org}$ signature in aquatic organic carbon may vary with changes in the dissolved inorganic carbon (DIC) pool (Meyers & Lallier-Vergès, 1999), effects from microbial reworking (Meyers & Lallier-Vergès, 1999; Hollander & Smith, 2001; Thompson et al., 2018), post-burial diagenesis (Meyers & Teranes, 2002), changes in terrestrial ^{13}C influence

(Falster et al., 2018) and also with anthropogenic effects (Rosenmeier et al., 2004; Thevenon et al., 2012; Fiskal et al., 2019).

Relatively low $\delta^{13}C_{org}$ values in Lake Surprise indicate a predominance of C_3 plant-derived productivity either from land plants or phytoplankton (Meyers & Ishiwatari, 1993; Meyers, 1997; Meyers & Lallier-Vergès, 1999; Torres et al., 2012). Relatively low C/N ratios (6 – 12) provide evidence of dominant sources of algal or bacterial contribution to sediment organic matter, however, provided that the values from Lake Surprise sediment are slightly above the expected range of algal sources (>10), the sediment organic matter may have been influenced by a minor terrestrial source. It has also been identified that higher C/N ratios may be observed as a result of nitrogen-limited environments and sometimes due to selective diagenesis in lakes, which speed up the breakdown of N-bearing fractions relative to C-rich fractions (Talbot, 2001; Olsen et al., 2013; Brahney et al., 2014; Cadd et al., 2018). Consequently, $\delta^{13}C_{org}$ and C/N values in this study predominantly demonstrate aquatic algae dominant productivity in the lake (Figures 4d and 4e). The TOC content mainly represents the organic matter abundance in the sediment (Meyers & Teranes, 2002; Das et al., 2008; Liu et al., 2019) and in some studies, this has been used to interpret the past climate with the assumption that TOC content lowers with the decreasing photosynthesis during cold or dry environments, whereas TOC content is expected to increase under warm/humid conditions (Meyers & Lallier-Vergès, 1999; Lücke, 2003; Liu et al., 2019). Accordingly, comparable variations in both the TOC and $\delta^{13}C_{org}$ record in the lake sediment (Figure 4b&c) demonstrate that changes in $\delta^{13}C_{org}$ are most likely to be influenced by primary productivity (Liu et al., 2019). In lakes where terrestrial influx is possible, this assumption may vary accordingly (Zhu et al., 2008), Even though there is a potential for terrestrial input into Lake Surprise due to its steep and densely vegetated slopes, $\delta^{13}C_{org}$ and C/N values suggest that any terrestrial input is a minor effect, and instead, the highly productive lake contributed a high amount of organic matter.

Even though the correlation of $\delta^{13}C_{org}$ to climate variables in Lake Surprise is comparatively weaker compared to other sediment proxies, it correlates with Tmax and to a minor extent with evaporation. The $\delta^{13}C_{org}$ record also suggests, at first glance, a similar trend to the $\delta^{18}O_{LW}$ record (Figure 5), with broadly lower $\delta^{13}C$ values during wetter intervals and higher values during dry periods. However, this comparison might be misleading due to the differences in sample resolution, since a comparison between $\delta^{13}C_{org}$ and $\delta^{18}O_{LW}$ for the same samples highlights some discrepancies, including periods where depleted $\delta^{18}O_{LW}$ corresponds with

higher $\delta^{13}C_{org}$ (~1890 CE). Similarly, an increasing trend in $\delta^{13}C_{org}$ is observed during the wet period that existed from 1935 – 1955 CE. These comparisons highlight the complexity when interpreting $\delta^{13}C_{org}$ variability. If higher $\delta^{13}C_{org}$ values correspond with periods of high productivity due to ^{12}C depletion with increased uptake (Hollander & Smith, 2001; Torres et al., 2012), then the observations presented here could imply that lake productivity peaks during both wet and dry periods. In general, the lake's productivity should increase during late spring and early summer time (Dean, 1999; Kragh & Sand-Jensen, 2018; Tonetta & Petrucio, 2020). However, given the higher eutrophic nature of Lake Surprise, it is arguable that even during periods of heavy rainfall (winter and autumn), due to the increased nutrient influx lake may reflect a considerable amount of productivity.

Seasonal variation in lake waters may also affect the $\delta^{13}C_{org}$ value, during summer stratification, ^{12}C taken by algae for photosynthesis is transferred to the hypolimnion by algal detritus, where it is oxidised and returns as ^{12}C to the DIC pool, yet remains beneath the thermocline until winter overturn (Dean, 1999). However, when the hypolimnion reaches oxygen-depleted condition, anaerobic methane oxidation may introduce ^{13}C-depleted CO_2 to the DIC pool, resulting in lower $\delta^{13}C_{org}$ values (Torres et al., 2012; Liu et al., 2019; Forbes et al., 2021). This has been commonly observed in lacustrine environments with long-term or permanent stratification (Hollander & Smith, 2001). Therefore, considering all these challenges, it is clear that $\delta^{13}C_{org}$ variability in lake sediments does indeed integrate changes in lake productivity and carbon burial, however, the climatic controls over those processes are still uncertain and require further detailed studies of modern environments. It is possible to lessen uncertainties in $\delta^{13}C_{org}$ -based palaeoclimate interpretations by combining them with other proxies or with a clear understanding of the contemporary lake system (Meyers, 2003).

4.5.2.3 Controls over carbonate deposition at Lake Surprise

Carbonate, which is the major inorganic carbon sink in lake sediments can be precipitated biogenically or inorganically within the lake water column, or it can be introduced externally via erosion or aeolian supply (Gierlowski-Kordesch, 2010; Li et al., 2013; Karami et al., 2019). A common interpretation of climatic controls over carbonate deposition is that evaporation of lake water causes both Ca and CO_3^{2-} ions to become increasingly saturated, causing the precipitation of $CaCO_3$ (Kelts & Hsü, 1978; Ito, E., 2002; Leng & Marshall, 2004; Deocampo, 2010; Gierlowski-Kordesch, 2010). This assumption has been used globally to interpret both

long-term and contemporary climate variability as a reflection of decreased P/E ratio in a wide range of lake settings (Rosen et al., 1996; Scholz et al., 2011; Jouve et al., 2013; Rodríguez-Ramírez et al., 2015; Hou et al., 2017). At two more saline crater lakes in western Victoria (Lakes Keilambete and Gnotuk), Wilkins et al. (2013) interpret the occurrence of carbonate-rich (aragonite) laminae to reflect salinity increase as a response to precipitation decline.

The concentration of carbonate in the Lake Surprise sediments, as reflected by Ca%, presents a contrasting scenario to the evaporative enrichment hypothesis. The presence of carbonate rocks in the catchment precludes detrital carbonate flux as being a factor in this instance. Generally speaking, Ca% is highest during periods of relatively high rainfall and low evaporation over the instrumental period (Figure 5h). This is well-represented by periods of increased Ca concentration from ~1790 – 1835 CE and from ~ 1935 to late 1990 CE, which corresponds to more frequent wet intervals. By contrast, Ca concentrations were low during periods of higher evaporation and maximum temperature around 1900 – 1935 CE, ~ 1980 CE and 1990 – 2020 CE. Similarly, an inferred dry interval from ~ 1835 – 1900 CE, based on higher $\delta^{18}O_{LW}$ values, also corresponds with the lower Ca content in the sediment. However, the relationship between Ca% and climate does not appear to be consistent through time. During the short dry period that existed from 1955 – 1970 CE, there is no discernible link between either wet or dry conditions and carbonate concentration in the sediments. This may be either caused by the lagged relationship with climate or human activities. The Budj Bim national park was opened for public access in 1960 CE (Parks Victoria, 1996). Further, Ca content seems to show a lagged relationship with stable isotope variation. This may be due to the comparatively low resolution in other proxies. In addition to evaporative concentration, other natural factors such as biological productivity, microbial activities, groundwater flux (Dean, 1999; Leng & Marshall, 2004; Karami et al., 2019; Sun et al., 2019) and anthropogenic activities may also induce the authigenic carbonate deposition in freshwater lakes (Sun et al., 2019).

Given that it is highly unlikely that evaporation contributed to the carbonate accumulation in Lake Surprise, two potential hypotheses are presented for the carbonate deposition during wet intervals. A groundwater influence on Lake Surprise has been suggested by previous authors (Barr et al., 2014) and this has been reinforced by contemporary geochemical monitoring and modelling, which suggests that groundwater input accounts for ~ 80% of the total lake water influx (Chapter 2, Section 2.4.4). Groundwater inflow passes through both basaltic and

limestone rocks (Barr et al., 2014; Falster et al., 2018; Ankor, 2020), therefore providing Ca^{2+} and HCO_3^- ions to the lake water (Chapter 2, Section 2.5.1). It is proposed that during climatically humid periods, water infiltration increases and elevates the groundwater table, resulting in a greater hydraulic gradient towards the lake. When aquifer recharge is enhanced, calcium flux into the lake increases as a result of greater weathering rates (Teller & Last, 1990; Shapley et al., 2005). With high alkalinity and elevated pH values, Ca has the ability to precipitate as $CaCO_3$ in the lacustrine sediment, potentially explaining the elevated carbonate concentration in the sediments at these times (Shapley et al., 2005; Karami et al., 2019). This increased calcium flux from groundwater recharge during wet periods has been observed elsewhere. Shapley et al., (2005) tested this correlation using both freshwater and saline lakes from Montana, USA and observed groundwater-influenced elevated carbonate flux during climatically humid periods.

Another important factor in the precipitation of calcium carbonates in lakes is the uptake of CO_2 and associated pH changes during primary productivity, which is commonly observed to result in carbonate deposition events in eutrophic lakes (Andersen et al., 2019; Ryves et al., 2020). Given the favourable characteristics such as high pH, high alkalinity and nutrient concentration in Lake Surprise, it is likely that microbial activity is also a contributing factor behind carbonate deposition. Periods of higher precipitation feasibly result in an increased contribution of nutrients to the lake, via runoff and throughflow. Furthermore, wetter years tend to be associated with a deeper lake overturn, which can recycle nutrients from the hypolimnion, although no data exist to support this interpretation for Lake Surprise. Furthermore, the photosynthetic process may also accelerate with a rise in temperature and light energy during the late spring/summer seasons, enhancing the productivity of the lake (Dean, 1999; Pueyo et al., 2011; Karami et al., 2019; Sun et al., 2019). During times of reduced rainfall, it is probable that lake stratification is increased as a counterbalance to enhanced primary output producing greater carbonate deposition (Dean, 1999; Wetzel, 2001c; Boehrer and Schultze, 2008). High organic matter content produced by photosynthesis, exposes to bacterial decomposition in the anoxic hypolimnion, which releases organic acids lowering the pH in the water column (Dean, 1999). These organic acids trigger $CaCO_3$ dissolution in the hypolimnion and sediment-water interface (Dean, 1999). Therefore, it is likely that productivity and summer stratification may also have influenced the authigenic carbonate deposition in the lake sediment. According to previous literature, photosynthetic activity and the pH are potential drivers of authigenic carbonate deposition in freshwater lakes with high

productivity (Dean, 1999; Li et al., 2013; Karami et al., 2019; Sun et al., 2019; Vegas-Vilarrúbia et al., 2022).

The possibility of groundwater-influenced carbonate deposition in Lake Surprise has been discussed previously by Barr, C., (2010). However, he suggested that that lake water level decline, as a consequence of lower P/E, may lead to increased groundwater flux into the lake relative to surface runoff. As per Barr, C., (2010), Lake Surprise can assume to be heavily groundwater-influenced during relatively dry climates. It is feasible that both hypotheses can be true. Under those scenarios, short-term periods of increased rainfall transport carbonate ions to the lake and contribute to enhanced carbonate precipitation. However, under centennial-scale periods of elevated rainfall, and hence greater surface runoff contribution to lake water balance, it is also feasible that groundwater inflow to the lake could be diminished, resulting in reduced carbonate deposition. However, to use authigenic carbonate deposition as a palaeoclimate proxy, it is crucial to have a clear knowledge of these mechanisms. Deeper sediments from Lake Surprise consist of finely yet distinct laminations (Ankor & Tyler, 2022) (Appendix 5). However, this is not obvious in this sediment core (top 1.57 m) which might be due to the sediment coring and extruding method or due to the sediments being very soft in the upper section.

4.5.3 Palaeoclimate reconstruction

Past climates were reconstructed to the base of SUR-19-01 (~1300 CE), based on the climate-proxy correlation. Even though the $\delta^{18}O_{LW}$ variability has a lower resolution, it is employed as the primary climate indicator since it is more reliable than other sediment proxies. Enrichment of $\delta^{18}O_{LW}$ and $\delta^{13}C_{org}$ values agree well with the climatically arid period that existed from around 1990 – 2019 AD and this is further confirmed by the steady rise in TOC content, which suggests enhanced productivity and organic matter abundance (Figure 5) (Hollander & Smith, 2001; Meyers & Teranes, 2002). This is consistent with the lowering of inorganic carbonate deposition as illustrated by a gradual decline in both Ca and Sr ions. In contrast, pyrite formation is not apparent during this period. Microbial influence is highly likely given the lake's eutrophic and stratified nature. It is evident that highly eutrophic freshwater environments produce nitrate-reducing Fe(II) oxidizing bacteria that grow in the upper anoxic sediment layer in thermally stratified lakes (Hauck et al., 2001; Melton et al., 2012; Otte et al., 2018; Lueder et al., 2020). These bacteria have the ability to oxidise by re-dissolving Fe^{2+} ions

deposited in the sediment-water interface (Melton et al., 2012; Otte et al., 2018; Lueder et al., 2020). This may deplete the pyrite content in the lake sediment (Melton et al., 2012). This extreme dry period corresponds with the elevated levels of diatom-inferred (DI) conductivity values observed in a previous study from Lake Surprise by Barr et al., (2014), who suggested Lake Surprise sediments may reflect the period of "Millennium Drought (~1997 – 2010 CE).

Despite a very short interval of reduction in rainfall ~ 1980 CE, the period from 1970 – 1990 CE is mostly characterised by frequent wet intervals. This wet period is consistent with elevated levels of carbonate and depletion of $\delta^{18}O_{LW}$ and $\delta^{13}C_{org}$ values that indicate decreasing evaporation and productivity. Relatively lower concentrations of Fe and S that reflect the absence of a redox environment provide solid evidence for climatically wet conditions. Sediment proxies illustrate a similar pattern of variation during the wet period that existed from ~1935 – 1955 CE. In contrast, these wet periods are not well-defined in Barr et al., (2014), given the steady rise in DI-conductivity values since early 1900. However, conductivity values remain lower from ~1900 – 1970 CE, compared to the period after 1970 CE. The dry period that existed from ~1955 – 1970 CE correspondent with enriched $\delta^{18}O_{LW}$ and $\delta^{13}C_{org}$ values, whilst Ca (Sr) content remains high suggesting elevated levels of carbonate accumulation in the lake. Similarly, relatively low Fe and S concentrations disagree with this dry climate. This may be due to the microbial influence by Fe(II) reducing bacteria as explained in the dry period that existed after 1990 CE. Enrichment in $\delta^{18}O_{LW}$ values that indicates an evaporative environment is in agreement with the prolonged drying condition that existed from around 1900 – 1935 CE. This is further strengthened by the enrichment of $\delta^{13}C_{org}$ along with TOC content which suggests enhanced lake productivity. Further, lake drying is illustrated by a decrease in carbonate deposition (Ca and Sr) and a considerable increase in redox conditions (Fe and S).

According to the reconstructed rainfall anomaly (Gergis et al., 2012), a climatically arid period existed between 1835 – 1890 CE, with a minor increase in rainfall towards the end of the period. This is consistent with the considerable increase in $\delta^{18}O_{LW}$, which shows an evaporative environment. According to the enrichment of $\delta^{18}O_{LW}$ values at around 1885 AD, the lake sediments represent relatively high drying conditions at least for the last 700 years. Similarly, $\delta^{13}C_{org}$ and TOC content also remained at higher levels suggesting an increase in productivity. Ca and Sr content remained lower indicating lesser carbonate deposition during this period. Both Fe and S concentrations demarcate increased variability and smaller concentration,

resulting in a discrepancy with the climate variables. This arid phase corresponds with the previous drying observed in Lake Surprise and other lakes in the region (Wilkins et al., 2013; Barr et al., 2014). Western Victoria is considered to have experienced the beginning of European settlement after the mid-nineteenth century (~1850 AD) (Barr et al., 2014; Jones, 2014)**.** Therefore, increased aridity after 1850 CE may have been triggered by both climate and human intervention. Potentially the combined effect of increased eutrophication after 1850 CE and lake stratification activated Fe (II) oxidizing bacteria causing frequent reduction of Fe during arid intervals, which occurred after 1850 CE (~1955 – 1970 CE and ~1990 – 2019 CE).

Elevated carbonate levels correspond well with the relatively high rainfall from ~1790 – 1835 CE (Gergis et al., 2012). However, consistent and high $\delta^{18}O_{LW}$ variability contrasts with this wet period, which may be the consequence of the very low resolution in which only two data points are available for this period. Similarly, enriched values of $\delta^{13}C_{org}$ and TOC content also disagree with this period suggesting enhanced productivity. This may have been caused by increased amounts of nutrient inflow due to higher rainfall events. Even though S concentration remained lower throughout this period, increasing variability in Fe disagrees with the interpretation.

Using isotope and element data, it is possible to reconstruct the climate that existed between 1300 and 1790 CE, according to the inferences from climate-proxy correlation. $\delta^{18}O_{LW}$ values remained consistent at approximately 3‰ throughout this period although this may be a product of the low resolution in this part of the record (Figure 4a). Similarly, relatively more depleted $\delta^{13}C_{org}$ and high TOC content varied at minor scales except for the spike in $\delta^{13}C_{org}$ at ~1690 CE and lowering in TOC content before 1390 CE (Figure 4b & 4c). Therefore, reconstruction of climate using only isotope data is challenging for this period. Considering the XRF data (Figure 3), elevated levels of Ca and Sr ~1750 – 1790 CE and 1680 – 1700 CE may indicate increased carbonate deposition associated with periods of high rainfall. This is further strengthened relatively low Fe and S contents in the later period which exhibit a reduction in pyrite formation. Lowering of carbonate deposition and increased amounts of Fe content in between these two wet periods (~1700 – 1740 CE) provides evidence for lake drying. This period is not well illustrated in isotope data due to the lower resolution. However, $\delta^{18}O_{LW}$ values show an increasing trend suggesting an evaporative environment, whilst $\delta^{13}C_{org}$ and TOC represent a declining trend suggesting a lowering in productivity that contrasts with the interpretation. This might be due to a lower resolution, where changes in isotope data may not

have been captured by a few data points, or there is also a higher likelihood that carbon isotopes may have been altered by other external factors, such as methanotrophic bacteria, which caused a decrease in $\delta^{13}C_{org}$ values (Torres et al., 2012).

Ca and Sr variation from ~1300 – 1680 CE infer more consistent and reduced levels of carbonate deposition, which may correspond to a prolonged drier climate. Although using $\delta^{18}O_{LW}$ variability for this period is challenging, enhanced isotope values most likely reflect lake drying as illustrated by XRF data. Although the amounts of Fe and S do not consistently increase through time, there are frequent intervals of elevated concentrations, particularly in the later years (~1500–1600 CE), which may indicate a redox state. Even though TOC content agrees with predominant lake drying, $\delta^{13}C_{org}$ remained relatively lower conflicting with the palaeoproductivity interpretation. Long-term depletion in $\delta^{13}C_{org}$ might indicate methane production due to anaerobic decomposition by methanotrophic microbes (Hollander & Smith, 2001; Torres et al., 2012).

Notably, this interpretation conflicts with a previous study by Barr et al., (2014), which provides evidence of a prolonged wet period that is comparable to the Little Ice Age (LIA), which lasted from around 1400 to 1880 CE. The LIA events might not have been captured due to the lower resolution in this study. Albeit, wet periods observed from ~1680 – 1700 CE and ~1750 – 1835 CE in this study, coincide with the period of LIA. Further, Barr et al. (2014) have identified a decrease in inter-decadal variability, which is analogous to minor fluctuations in this study. Even though Barr et al. (2014) identified the period between 1400 and 1880 CE as a general wet phase, relatively high DI-conductivity measurements that are almost as intense as the Millennium Drought occurred around 1545 CE, which may correspond with the arid intervals discussed in this study. Further, by increasing the resolution of the proxy data, limitations observed during numerical analysis and palaeoclimate reconstruction can be minimised in future studies. However, given that the main goal of this work is to evaluate palaeoclimate assumptions by comparing sediment proxy data against climate variables, a detailed palaeoclimate reconstruction for the Holocene is conducted in the following chapter (Chapter 5) using more reliable sediment proxy data (cellulose inferred lake water isotopes) at decadal to centennial-scale resolution as demonstrated in this study.

4.6 Conclusion

The validity of palaeoclimate inferences commonly applied in lake studies was evaluated in this study by comparing sediment proxy data obtained from Lake Surprise against instrumental climate data. Correlation of $\delta^{18}O_{LW}$, $\delta^{13}C_{org}$ and Ca% with multiple climate variables over the instrumental period (1889 – 2019 CE), shows that both the $\delta^{18}O_{LW}$ and Ca% appear to reflect the local climate variability. Even though $\delta^{13}C_{org}$, TOC and $\delta^{18}O_{LW}$ show some similarity with climate variables, the palaeoclimate interpretation of $\delta^{13}C_{org}$ and TOC is more complicated due to the complexities of likely mechanisms that affect these proxies. As expected, the $\delta^{18}O_{LW}$ record negatively correlates with the effective water balance (precipitation–evaporation) which, in turn, varies mostly as a function of changes in evaporation, thus the evaporation is governed mainly by temperature, a higher correlation is observed with Tmax (Table 3). This observation agrees with the assumed link between $\delta^{18}O_{LW}$ and heavy isotope enrichment during periods of high E/P ratio. A negative correlation between Ca%, Tmax and evaporation indicates that inorganic carbonate deposition was predominantly higher during wet periods. This suggests that rather than being driven by evaporative enrichment, carbonate deposition is instead driven by increased rates of groundwater flux during periods of high rainfall as well as photosynthetic uptake of CO_2. Aquatic algae-dominant productivity is well illustrated by depleted $\delta^{13}C_{org}$ values and lower C/N ratios. However, considering the disagreements between $\delta^{13}C_{org}$ values and climate variables, it is likely that other processes such as anoxic methane production, and nutrient influx may have altered the $\delta^{13}C_{org}$ variability in the lake.

Based upon the sediment-proxy climate relationship, in the pre-instrumental period (~1300 – 1790 CE) there were relatively dry intervals from around 1300 – 1680 CE and 1700 – 1745 CE and relatively wet periods from ~1680 – 1700 CE and 1710 – 1790 CE. A clear representation of these wet or dry intervals is limited by the lower resolution of stable isotope data and by microbial influence (Fe and S contents, $\delta^{13}C_{org}$ values and TOC content). Evidence for the LIA is not visible in this study as suggested in previous records from Lake Surprise (Barr et al., 2014). Overall this study demonstrates the significance of understanding the climate-proxy correlation to make reliable palaeoclimate reconstructions. Findings from this study indicate, for Lake Surprise, the $\delta^{18}O_{LW}$ record is a more reliable and accurate measure of palaeoclimate variability at least for the instrumental period. Even though it is plausible to utilise carbonate deposition as a palaeoclimate proxy for Lake Surprise, it is essential to have a detailed understanding of the carbonate accumulation in the lake.

4.7 List of references cited

Abbott, M. B., Wolfe, B. B., Aravena, R., Wolfe, A. P., & Seltzer, G. O. (2000). Holocene hydrological reconstructions from stable isotopes and paleolimnology, Cordillera Real, Bolivia. *Quaternary Science Reviews*, *19*(17–18), 1801–1820. https://doi.org/10.1016/S0277-3791(00)00078-0

Abram, N. J., Mulvaney, R., Vimeux, F., Phipps, S. J., Turner, J., & England, M. H. (2014). Evolution of the Southern Annular Mode during the past millennium. *Nature Climate Change*, *4*(7), 564–569. https://doi.org/10.1038/nclimate2235

Adrian, R., O'Reilly, C. M., Zagarese, H., Baines, S. B., Hessen, D. O., Keller, W., Livingstone, D. M., Sommaruga, R., Straile, D., Van Donk, E., Weyhenmeyer, G. A., & Winder, M. (2009). Lakes as sentinels of climate change. *Limnology and Oceanography*, *54*(6 PART 2), 2283–2297. https://doi.org/10.4319/lo.2009.54.6_part_2.2283

Andersen, M. R., Kragh, T., Martinsen, K. T., Kristensen, E., & Sand-Jensen, K. (2019). The carbon pump supports high primary production in a shallow lake. *Aquatic Sciences*, *81*(2), 1–11. https://doi.org/10.1007/s00027-019-0622-7

Andreas, L. (2003). *A Lateglacial and Holocene organic carbon isotope record of lacustrine palaeoproductivity and climatic change derived from varved lake sediments of Lake Holzmaar , Germany*. *22*, 569–580.

Ankor, M. J. (2020). *Hydrologic and Isotopic Lake Modelling for Palaeoclimate Research*. *January*.

Ankor, M. J., & Tyler, J. J. (2022). A computational method for rapid orthographic photography of lake sediment cores. *Journal of Paleolimnology*, *0123456789*. https://doi.org/10.1007/s10933-022-00241-0

Appleby, P. G. (2001). *in Recent Sediments*. *1*, 171–172.

Aquino-López, M. A., Blaauw, M., Christen, J. A., & Sanderson, N. K. (2018). Bayesian Analysis of 210 Pb Dating. *Journal of Agricultural, Biological, and Environmental Statistics*, *23*(3), 317–333. https://doi.org/10.1007/s13253-018-0328-7

Axford, Y., Andresen, C. S., Andrews, J. T., Belt, S. T., Geirsdóttir, Á., Massé, G., Miller, G. H., Ólafsdóttir, S., & Vare, L. L. (2011). Do paleoclimate proxies agree? A test comparing 19 late Holocene climate and sea-ice reconstructions from Icelandic marine and lake sediments. *Journal of Quaternary Science*, *26*(6), 645–656. https://doi.org/10.1002/jqs.1487

Barr, C., Tibby, J., Gell, P., Tyler, J., Zawadzki, A., & Jacobsen, G. E. (2014). Climate variability in south-eastern Australia over the last 1500 years inferred from the high-resolution diatom records of two crater lakes. *Quaternary Science Reviews*, *95*, 115–131. https://doi.org/10.1016/j.quascirev.2014.05.001

Barr, C., Tibby, J., Marshall, J. C., Mcgregor, G. B., Moss, P. T., Halverson, G. P., & Fluin, J. (2013). Combining monitoring, models and palaeolimnology to assess ecosystem

response to environmental change at monthly to millennial timescales: The stability of Blue Lake, North Stradbroke Island, Australia. *Freshwater Biology*, *58*(8), 1614–1630. https://doi.org/10.1111/fwb.12154

Barr, C., Tibby, J., Moss, P. T., Halverson, G. P., Marshall, J. C., McGregor, G. B., & Stirling, E. (2017). A 25,000-year record of environmental change from Welsby Lagoon, North Stradbroke Island, in the Australian subtropics. *Quaternary International*, *449*, 106–118. https://doi.org/10.1016/j.quaint.2017.04.011

Battarbee, R. W., Anderson, N. J., Bennion, H., & Simpson, G. L. (2012). Combining limnological and palaeolimnological data to disentangle the effects of nutrient pollution and climate change on lake ecosystems: Problems and potential. *Freshwater Biology*, *57*(10), 2091–2106. https://doi.org/10.1111/j.1365-2427.2012.02860.x

Battarbee, R. W., Grytnes, J. A., Thompson, R., Appleby, P. G., Catalan, J., Korhola, A., Birks, H. J. B., Heegaard, E., & Lami, A. (2002). Comparing palaeolimnological and instrumental evidence of climate change for remote mountain lakes over the last 200 years. *Journal of Paleolimnology*, *28*(1), 161–179. https://doi.org/10.1023/A:1020384204940

Bell, D., & Johnston, C. (2008). Budj Bim; Caring for the spirit and the people. *Finding the Spirit of Place : Between Tangible and Intangible Heritage. (16th ICOMOS General Assembly and International Scientific Symposium, Quebec, 2008)*, 213-224. http://openarchive.icomos.org/12/%5Cnhttp://openarchive.icomos.org/12/1/77-7xnf-104.pdf

Boehrer, B., & Schultze, M. (2008). Stratification of lakes. *Reviews of Geophysics*, *46*(2), 1–27. https://doi.org/10.1029/2006RG000210

Boyce, J. (2013). The Newer Volcanics Province of southeastern Australia: A new classification scheme and distribution map for eruption centres. *Australian Journal of Earth Sciences*, *60*(4), 449–462. https://doi.org/10.1080/08120099.2013.806954

Brahney, J., Clague, J. J., Edwards, T. W. D., & Menounos, B. (2010). Late Holocene paleohydrology of Kluane Lake, Yukon Territory, Canada. *Journal of Paleolimnology*, *44*(3), 873–885. https://doi.org/10.1007/s10933-010-9459-8

Brown, E. T. (2011). Lake Malawi's response to "megadrought" terminations: Sedimentary records of flooding, weathering and erosion. *Palaeogeography, Palaeoclimatology, Palaeoecology*, *303*(1–4), 120–125. https://doi.org/10.1016/j.palaeo.2010.01.038

Builth, H., Kershaw, A. P., White, C., Roach, A., Hartney, L., McKenzie, M., Lewis, T., & Jacobsen, G. (2008). Environmental and cultural change on the Mt Eccles lava-flow landscapes of southwest Victoria, Australia. *Holocene*, *18*(3), 413–424. https://doi.org/10.1177/0959683607087931

Burn, M. J., & Palmer, S. E. (2014). Solar forcing of Caribbean drought events during the last millennium. *Journal of Quaternary Science*, *29*(8), 827–836. https://doi.org/10.1002/jqs.2660

Cadd, H. R., Tibby, J., Barr, C., Tyler, J., Unger, L., Leng, M. J., Marshall, J. C., McGregor, G., Lewis, R., Arnold, L. J., Lewis, T., & Baldock, J. (2018). Development of a southern hemisphere subtropical wetland (Welsby Lagoon, south-east Queensland, Australia) through the last glacial cycle. *Quaternary Science Reviews*, *202*, 53–65. https://doi.org/10.1016/j.quascirev.2018.09.010

Cadd, H., Sherborne-Higgins, B., Becerra-Valdivia, L., Tibby, J., Barr, C., Forbes, M., Cohen, T. J., Tyler, J., Vandergoes, M., Francke, A., Lewis, R., Arnold, L. J., Jacobsen, G., Marjo, C., & Turney, C. (2022). the Application of Pollen Radiocarbon Dating and Bayesian Age-Depth Modeling for Developing Robust Geochronological Frameworks of Wetland Archives. *Radiocarbon*, *64*(2), 213–235. https://doi.org/10.1017/RDC.2022.29

Cai, W., Sullivan, A., & Cowan, T. (2011a). Interactions of ENSO, the IOD, and the SAM in CMIP3 models. *Journal of Climate*, *24*(6), 1688–1704. https://doi.org/10.1175/2010JCLI3744.1

Cai, W., van Rensch, P., Cowan, T., & Hendon, H. H. (2011b). Teleconnection pathways of ENSO and the IOD and the mechanisms for impacts on Australian rainfall. *Journal of Climate*, *24*(15), 3910–3923. https://doi.org/10.1175/2011JCLI4129.1

Cameron, N. G., Schnell, A., Rautio, M. L., Lami, A., Livingstone, D. M., Appleby, P. G., Dearing, J. A., & Rose, N. L. (2002). High-resolution analyses of recent sediments from a Norwegian mountain lake and comparison with instrumental records of climate. *Journal of Paleolimnology*, *28*(1), 79–93. https://doi.org/10.1023/A:1020324019052

Chawchai, S., Kylander, M. E., Chabangborn, A., Löwemark, L., & Wohlfarth, B. (2016). Testing commonly used X-ray fluorescence core scanning-based proxies for organic-rich lake sediments and peat. *Boreas*, *45*(1), 180–189. https://doi.org/10.1111/bor.12145

Child, D. P., Hotchkis, M. A. C., & Williams, M. L. (2008). High sensitivity analysis of plutonium isotopes in environmental samples using accelerator mass spectrometry (AMS). *Journal of Analytical Atomic Spectrometry*, *23*(5), 765–768. https://doi.org/10.1039/b715788f

Cleverly, J., Eamus, D., Luo, Q., Coupe, N. R., Kljun, N., Ma, X., Ewenz, C., Li, L., Yu, Q., & Huete, A. (2016). The importance of interacting climate modes on Australia's contribution to global carbon cycle extremes. *Scientific Reports*, *6*(November 2015), 1–10. https://doi.org/10.1038/srep23113

Das, S. K., Routh, J., Roychoudhury, A. N., & Klump, J. V. (2008). Elemental (C, N, H and P) and stable isotope (δ15N and δ13C) signatures in sediments from Zeekoevlei, South Africa: A record of human intervention in the lake. *Journal of Paleolimnology*, *39*(3), 349–360. https://doi.org/10.1007/s10933-007-9110-5

Davies, S. J., Lamb, H. F., & Roberts, S. J. (2015). *Micro-XRF Core Scanning in Palaeolimnology: Recent Developments*. https://doi.org/10.1007/978-94-017-9849-5_7

De Deckker, P. (2019). An evaluation of Australia as a major source of dust. *Earth-Science*

Reviews, *194*(June 2018), 536–567. https://doi.org/10.1016/j.earscirev.2019.01.008

Dean Jr., W. E. (1999). The carbon cycle and biogeochemical dynamics in lake sediments. *Journal of Paleolimnology*, *21*(1997), 375–393.

Deocampo, D. M. (2010). Chapter 1 The Geochemistry of Continental Carbonates. In *Developments in Sedimentology* (Vol. 62, Issue C). Elsevier. https://doi.org/10.1016/S0070-4571(09)06201-3

Dey, R., Lewis, S. C., Arblaster, J. M., & Abram, N. J. (2019). A review of past and projected changes in Australia's rainfall. *Wiley Interdisciplinary Reviews: Climate Change*, *10*(3), 1–23. https://doi.org/10.1002/wcc.577

Dodson, J. (1974). Calcium carbonate formation by Enteromorpha nana algae in a hypersaline volcanic crater lake. *Hydrobiologia*, *44*(2–3), 247–255. https://doi.org/10.1007/BF00187274

Dolman, A. M., Kunz, T., Groeneveld, J., & Laepple, T. (2021). A spectral approach to estimating the timescale-dependent uncertainty of paleoclimate records - Part 2: Application and interpretation. *Climate of the Past*, *17*(2), 825–841. https://doi.org/10.5194/cp-17-825-2021

Dugan, H. A., Bartlett, S. L., Burke, S. M., Doubek, J. P., Krivak-Tetley, F. E., Skaff, N. K., Summers, J. C., Farrell, K. J., McCullough, I. M., Morales-Williams, A. M., Roberts, D. C., Ouyang, Z., Scordo, F., Hanson, P. C., & Weathers, K. C. (2017). Salting our freshwater lakes. *Proceedings of the National Academy of Sciences of the United States of America*, *114*(17), 4453–4458. https://doi.org/10.1073/pnas.1620211114

Edwards, T. W. D., & McAndrews, J. H. (1989). Paleohydrology of a Canadian Shield land inferred from 18O in sediment cellulose. *Canadian Journal of Earth Sciences*, *26*(9), 1850–1859. https://doi.org/10.1139/e89-158

Falster, G., Tyler, J., Grant, K., Tibby, J., Turney, C., Löhr, S., Jacobsen, G., & Kershaw, A. P. (2018). Millennial-scale variability in south-east Australian hydroclimate between 30,000 and 10,000 years ago. *Quaternary Science Reviews*, *192*, 106–122. https://doi.org/10.1016/j.quascirev.2018.05.031

Fink, D., Hotchkis, M., Hua, Q., Jacobsen, G., Smith, A. M., Zoppi, U., Child, D., Mifsud, C., Van Der Gaast, H., Williams, A., & Williams, M. (2004). The ANTARES AMS facility at ANSTO. *Nuclear Instruments and Methods in Physics Research, Section B: Beam Interactions with Materials and Atoms*, *223–224*(SPEC. ISS.), 109–115. https://doi.org/10.1016/j.nimb.2004.04.025

Fiskal, A., Deng, L., Michel, A., Eickenbusch, P., Han, X., Lagostina, L., Zhu, R., Sander, M., Schroth, M. H., Bernasconi, S. M., Dubois, N., & Lever, M. A. (2019). Effects of eutrophication on sedimentary organic carbon cycling in five temperate lakes. *Biogeosciences*, *16*(19), 3725–3746. https://doi.org/10.5194/bg-16-3725-2019

Forbes, M., Cohen, T., Jacobs, Z., Marx, S., Barber, E., Dodson, J., Zamora, A., Cadd, H.,

Francke, A., Constantine, M., Mooney, S., Short, J., Tibby, J., Parker, A., Cendón, D., Peterson, M., Tyler, J., Swallow, E., Haines, H., … Woodward, C. (2021). Comparing interglacials in eastern Australia: A multi-proxy investigation of a new sedimentary record. *Quaternary Science Reviews*, *252*. https://doi.org/10.1016/j.quascirev.2020.106750

Francke, A., Lacey, J. H., Marchegiano, M., Wagner, B., Ariztegui, D., Zanchetta, G., Kusch, S., Ufer, K., Baneschi, I., & Knödgen, K. (2021). Last Glacial central Mediterranean hydrology inferred from Lake Trasimeno's (Italy) calcium carbonate geochemistry. *Boreas*. https://doi.org/10.1111/bor.12552

Fritz, S. C. (2008). Deciphering climatic history from lake sediments. *Journal of Paleolimnology*, *39*(1), 5–16. https://doi.org/10.1007/s10933-007-9134-x

Gergis, J., Gallant, A. J. E., Braganza, K., Karoly, D. J., Allen, K., Cullen, L., D'Arrigo, R., Goodwin, I., Grierson, P., & McGregor, S. (2012). On the long-term context of the 1997-2009 "Big Dry" in South-Eastern Australia: Insights from a 206-year multi-proxy rainfall reconstruction. *Climatic Change*, *111*(3), 923–944. https://doi.org/10.1007/s10584-011-0263-x

Gierlowski-Kordesch, E. H. (2010). Chapter 1 Lacustrine Carbonates. *Developments in Sedimentology*, *61*(C), 1–101. https://doi.org/10.1016/S0070-4571(09)06101-9

Gouramanis, C., Deckker, P. De, Switzer, A. D., & Wilkins, D. (2013). Earth-Science Reviews Cross-continent comparison of high-resolution Holocene climate records from southern Australia — Deciphering the impacts of far- fi eld teleconnections Austra l Winte r ITCZ today mer I ral Sum TCZ to Approx . position of today. *Earth Science Reviews*, *121*, 55–72. https://doi.org/10.1016/j.earscirev.2013.02.006

Gouramanis, C., Wilkins, D., & De Deckker, P. (2010). 6000years of environmental changes recorded in Blue Lake, South Australia, based on ostracod ecology and valve chemistry. *Palaeogeography, Palaeoclimatology, Palaeoecology*, *297*(1), 223–237. https://doi.org/10.1016/j.palaeo.2010.08.005

Guiry, E. (2019). Complexities of stable carbon and nitrogen isotope biogeochemistry in ancient freshwater ecosystems: Implications for the study of past subsistence and environmental change. *Frontiers in Ecology and Evolution*, *7*(AUG). https://doi.org/10.3389/fevo.2019.00313

Guo, P., Liu, C., Huang, L., Yu, M., Wang, P., & Zhang, G. (2018). Palaeohydrological evolution of the late Cenozoic saline lake in the Qaidam Basin , NE Tibetan Plateau : Tectonic vs . climatic control. *Global and Planetary Change*, *165*(March), 44–61. https://doi.org/10.1016/j.gloplacha.2018.03.012

Han, L., Li, Y., Zou, Y., Gao, X., Gu, Y., & Wang, L. (2022). Science of the Total Environment Relationship between lake salinity and the climatic gradient in northeastern China and its implications for studying climate change. *Science of the Total Environment*, *805*, 150403. https://doi.org/10.1016/j.scitotenv.2021.150403

Hancock, G. J., Leslie, C., Everett, S. E., Tims, S. G., Brunskill, G. J., & Haese, R. (2011). Plutonium as a chronomarker in Australian and New Zealand sediments: A comparison with 137Cs. *Journal of Environmental Radioactivity*, *102*(10), 919–929. https://doi.org/10.1016/j.jenvrad.2009.09.008

Harris, D., Horwáth, W. R., & Van Kessel, C. (2001). Acid fumigation of soils to remove carbonates prior to total organic carbon or carbon-13 isotopic analysis. *Soil Science Society of America Journal*, *65*(6), 1853–1856. https://doi.org/10.2136/sssaj2001.1853

Harrison, J., Heijnis, H., & Caprarelli, G. (2003). Historical pollution variability from abandoned mine sites, Greater Blue Mountains World Heritage Area, New South Wales, Australia. *Environmental Geology*, *43*(6), 680–687. https://doi.org/10.1007/s00254-002-0687-8

Harrison, J. J., Saunders, K. M., Child, D. P., & Hotchkis, M. A. C. (2021). A record of fallout 239Pu and 240Pu at World Heritage Bathurst Harbour, Tasmania, Australia. *Journal of Environmental Radioactivity*, *237*(June). https://doi.org/10.1016/j.jenvrad.2021.106679

Harriss, R. C. (1966). *and chloride in interstitial*. 8–12.

Hauck, S., Benz, M., Brune, A., & Schink, B. (2001). Ferrous iron oxidation by denitrifying bacteria in profundal sediments of a deep lake (Lake Constance). *FEMS Microbiology Ecology*, *37*(2), 127–134. https://doi.org/10.1016/S0168-6496(01)00153-2

Havens, K., & Jeppesen, E. (2018). Ecological responses of lakes to climate change. *Water (Switzerland)*, *10*(7), 1–9. https://doi.org/10.3390/w10070917

Heikkilä, M., Edwards, T. W. D., Seppä, H., & Sonninen, E. (2010). Sediment isotope tracers from Lake Saarikko, Finland, and implications for Holocene hydroclimatology. *Quaternary Science Reviews*, *29*(17–18), 2146–2160. https://doi.org/10.1016/j.quascirev.2010.05.010

Herczeg, A. L., Leaney, F. W., Dighton, J. C., Lamontagne, S., Schiff, S. L., Telfer, A. L., & English, M. C. (2003). A modern isotope record of changes in water and carbon budgets in a groundwater-fed lake: Blue Lake, South Australia. *Limnology and Oceanography*, *48*(6), 2093–2105. https://doi.org/10.4319/lo.2003.48.6.2093

Heyng, A. M., Mayr, C., Lücke, A., Wissel, H., & Striewski, B. (2014). Late Holocene hydrologic changes in northern New Zealand inferred from stable isotope values of aquatic cellulose in sediments from Lake Pupuke. *Journal of Paleolimnology*, *51*(4), 485–497. https://doi.org/10.1007/s10933-014-9769-3

Hogg, A. G., Heaton, T. J., Hua, Q., Palmer, J. G., Turney, C. S. M., Southon, J., Bayliss, A., Blackwell, P. G., Boswijk, G., Bronk Ramsey, C., Pearson, C., Petchey, F., Reimer, P., Reimer, R., & Wacker, L. (2020). SHCal20 Southern Hemisphere Calibration, 0-55,000 Years cal BP. *Radiocarbon*, *62*(4), 759–778. https://doi.org/10.1017/RDC.2020.59

Holmgren, S. U., Bigler, C., Ingólfsson, Ó., & Wolfe, A. P. (2010). The Holocene-

Anthropocene transition in lakes of western spitsbergen, Svalbard (Norwegian high arctic): Climate change and nitrogen deposition. *Journal of Paleolimnology*, *43*(2), 393–412. https://doi.org/10.1007/s10933-009-9338-3

Horton, T. W., Defliese, W. F., Tripati, A. K., & Oze, C. (2016). Evaporation induced 18O and 13C enrichment in lake systems: A global perspective on hydrologic balance effects. *Quaternary Science Reviews*, *131*, 365–379. https://doi.org/10.1016/j.quascirev.2015.06.030

Hou, J., Tian, Q., Liang, J., Wang, M., & He, Y. (2017). Climatic implications of hydrologic changes in two lake catchments on the central Tibetan Plateau since the last glacial. *Journal of Paleolimnology*, *58*(2), 257–273. https://doi.org/10.1007/s10933-017-9976-9

Howarth, J. D., Fitzsimons, S. J., Jacobsen, G. E., Vandergoes, M. J., & Norris, R. J. (2013). Identifying a reliable target fraction for radiocarbon dating sedimentary records from lakes. *Quaternary Geochronology*, *17*, 68–80. https://doi.org/10.1016/j.quageo.2013.02.001

Hua, Q., Jacobsen, G. E., Zoppi, U., Lawson, E. M., Williams, A. A., Smith, A. M., & McGann, M. J. (2001). Progress in radiocarbon target preparation at the ANTARES AMS centre. *Radiocarbon*, *43*(2 PART I), 275–282. https://doi.org/10.1017/s003382220003811x

Hua, Q., Turnbull, J. C., Santos, G. M., Rakowski, A. Z., Ancapichún, S., De Pol-Holz, R., Hammer, S., Lehman, S. J., Levin, I., Miller, J. B., Palmer, J. G., & Turney, C. S. M. (2022). Atmospheric Radiocarbon for the Period 1950-2019. *Radiocarbon*, *64*(4), 723–745. https://doi.org/10.1017/RDC.2021.95

Jeffrey, S. J., Carter, J. O., Moodie, K. B., & Beswick, A. R. (2001). *Using spatial interpolation to construct a comprehensive archive of Australian climate data*. *16*, 309–330.

Jeppesen, E., Meerhoff, M., Davidson, T. A., Trolle, D., Søndergaard, M., Lauridsen, T. L., Beklioğlu, M., Brucet, S., Volta, P., González-Bergonzoni, I., & Nielsen, A. (2014). Climate change impacts on lakes: An integrated ecological perspective based on a multi-faceted approach, with special focus on shallow lakes. *Journal of Limnology*, *73*(1 SUPPL), 88–111. https://doi.org/10.4081/jlimnol.2014.844

Jones, M. D., Cuthbert, M. O., Leng, M. J., Mcgowan, S., Mariethoz, G., Arrowsmith, C., Sloane, H. J., Humphrey, K. K., & Cross, I. (2016a). Comparisons of observed and modelled lake d 18 O variability. *JQSR*, *131*, 329–340. https://doi.org/10.1016/j.quascirev.2015.09.012

Jones, M. D., Cuthbert, M. O., Leng, M. J., McGowan, S., Mariethoz, G., Arrowsmith, C., Sloane, H. J., Humphrey, K. K., & Cross, I. (2016b). Comparisons of observed and modelled lake δ18O variability. *Quaternary Science Reviews*, *131*, 329–340. https://doi.org/10.1016/j.quascirev.2015.09.012

Jones, M. D., Leng, M. J., Roberts, C. N., & Tu, M. (2005). *A coupled calibration and*

modelling approach to the understanding of dry-land lake oxygen isotope records. 391–411. https://doi.org/10.1007/s10933-005-6743-0

Jones, M. D., Roberts, C. N., Leng, M. J., & Türkeş, M. (2006). A high-resolution late Holocene lake isotope record from Turkey and links to North Atlantic and monsoon climate. *Geology*, *34*(5), 361–364. https://doi.org/10.1130/G22407.1

Jones, R. (2014). *Natural and Human Influences on the Distribution and Extent of Victorian Lowland Grasslands*. *January 1999*.

Jones, R. N., McMahon, T. A., & Bowler, J. M. (2001). Modelling historical lake levels and recent climate change at three closed lakes, Western Victoria, Australia (c.1840-1990). *Journal of Hydrology*, *246*(1–4), 159–180. https://doi.org/10.1016/S0022-1694(01)00369-9

Jouve, G., Francus, P., Lamoureux, S., Provencher-Nolet, L., Hahn, A., Haberzettl, T., Fortin, D., & Nuttin, L. (2013). Microsedimentological characterization using image analysis and μ-XRF as indicators of sedimentary processes and climate changes during Lateglacial at Laguna Potrok Aike, Santa Cruz, Argentina. *Quaternary Science Reviews*, *71*, 191–204. https://doi.org/10.1016/j.quascirev.2012.06.003

Karami, F., Balci, N., & Guven, B. (2019). A modeling approach for calcium carbonate precipitation in a hypersaline environment: A case study from a shallow, alkaline lake. *Ecological Complexity*, *39*(July), 100774. https://doi.org/10.1016/j.ecocom.2019.100774

Kelts, K., & Hsü, K. J. (1978). Freshwater Carbonate Sedimentation. *Lakes*, 295–323. https://doi.org/10.1007/978-1-4757-1152-3_9

Kragh, T., & Sand-Jensen, K. (2018). Carbon limitation of lake productivity. *Proceedings of the Royal Society B: Biological Sciences*, *285*(1891). https://doi.org/10.1098/rspb.2018.1415

Larocque, I., Grosjean, M., Heiri, O., Bigler, C., & Blass, A. (2009). Comparison between chironomid-inferred July temperatures and meteorological data AD 1850-2001 from varved Lake Silvaplana, Switzerland. *Journal of Paleolimnology*, *41*(2), 329–342. https://doi.org/10.1007/s10933-008-9228-0

Leng, M. J., & Marshall, J. D. (2004). Palaeoclimate interpretation of stable isotope data from lake sediment archives. *Quaternary Science Reviews*, *23*(7–8), 811–831. https://doi.org/10.1016/j.quascirev.2003.06.012

Leslie, C., & Hancock, G. J. (2008). Estimating the date corresponding to the horizon of the first detection of 137Cs and 239+240Pu in sediment cores. *Journal of Environmental Radioactivity*, *99*(3), 483–490. https://doi.org/10.1016/j.jenvrad.2007.08.016

Li, H., Liu, X., Tripati, A., Feng, S., Elliott, B., Whicker, C., Arnold, A., & Kelley, A. M. (2020). Factors controlling the oxygen isotopic composition of lacustrine authigenic carbonates in Western China: implications for paleoclimate reconstructions. *Scientific Reports*, *10*(1), 1–17. https://doi.org/10.1038/s41598-020-73422-4

Li, Y., Wang, N., Li, Z., Zhou, X., Zhang, C., & Wang, Y. (2013). Carbonate formation and water level changes in a paleo-lake and its implication for carbon cycle and climate change, arid China. *Frontiers of Earth Science*, *7*(4), 487–500. https://doi.org/10.1007/s11707-013-0392-9

Liu, W., Li, X., Wang, Z., Wang, H., Liu, H., Zhang, B., & Zhang, H. (2019). Carbon isotope and environmental changes in lakes in arid Northwest China. *Science China Earth Sciences*, *62*(8), 1193–1206. https://doi.org/10.1007/s11430-018-9232-4

Löwemark, L., Chen, H. F., Yang, T. N., Kylander, M., Yu, E. F., Hsu, Y. W., Lee, T. Q., Song, S. R., & Jarvis, S. (2011). Normalizing XRF-scanner data: A cautionary note on the interpretation of high-resolution records from organic-rich lakes. *Journal of Asian Earth Sciences*, *40*(6), 1250–1256. https://doi.org/10.1016/j.jseaes.2010.06.002

Lueder, U., Jørgensen, B. B., Kappler, A., & Schmidt, C. (2020). Fe(III) Photoreduction Producing Feaq2+ in Oxic Freshwater Sediment. *Environmental Science and Technology*, *54*(2), 862–869. https://doi.org/10.1021/acs.est.9b05682

Martín-Puertas, C., Valero-Garcés, B. L., Mata, M. P., Moreno, A., Giralt, S., Martínez-Ruiz, F., & Jiménez-Espejo, F. (2011). Geochemical processes in a Mediterranean Lake: A high-resolution study of the last 4,000 years in Zoñar Lake, southern Spain. *Journal of Paleolimnology*, *46*(3), 405–421. https://doi.org/10.1007/s10933-009-9373-0

Matchan, E. L., Phillips, D., Jourdan, F., & Oostingh, K. (2020). Early human occupation of southeastern Australia: Newinsights from 40Ar/39Ar dating of young volcanoes. *Geology*, *48*(4), 390–394. https://doi.org/10.1130/G47166.1

McCormack, J., Nehrke, G., Jöns, N., Immenhauser, A., & Kwiecien, O. (2019). Refining the interpretation of lacustrine carbonate isotope records: Implications of a mineralogy-specific Lake Van case study. *Chemical Geology*, *513*(March), 167–183. https://doi.org/10.1016/j.chemgeo.2019.03.014

Melton, E. D., Schmidt, C., & Kappler, A. (2012). Microbial iron(II) oxidation in littoral freshwater lake sediment: The potential for competition between phototrophic vs. nitrate-reducing iron(II)-oxidizers. *Frontiers in Microbiology*, *3*(MAY), 1–12. https://doi.org/10.3389/fmicb.2012.00197

Meyers, P. A. (1997). Organic geochemical proxies of paleoceanographic, paleolimnologic, and paleoclimatic processes. *Organic Geochemistry*, *27*(5–6), 213–250. https://doi.org/10.1016/S0146-6380(97)00049-1

Meyers, P. A., & Arbor, A. (2001). Sediment Organic Matter. *Tracking Environmental Change Using Lake Sediments. Volume 2: Physical and Geochemical Methods*, *2*(1999), 239–269.

Meyers, P. A., & Ishiwatari, R. (1993). Lacustrine organic geochemistry-an overview of indicators of organic matter sources and diagenesis in lake sediments. *Organic Geochemistry*, *20*(7), 867–900. https://doi.org/10.1016/0146-6380(93)90100-P

Meyers, P. A., & Lallier-Vergès, E. (1999). Lacustrine sedimentary organic matter records of Late Quaternary paleoclimates. *Journal of Paleolimnology*, *21*(3), 345–372. https://doi.org/10.1023/A:1008073732192

Naeher, S., Gilli, A., North, R. P., Hamann, Y., & Schubert, C. J. (2013). Tracing bottom water oxygenation with sedimentary Mn/Fe ratios in Lake Zurich, Switzerland. *Chemical Geology*, *352*, 125–133. https://doi.org/10.1016/j.chemgeo.2013.06.006

Nomosatryo, S., Tjallingii, R., Schleicher, A. M., Boli, P., Henny, C., Wagner, D., & Kallmeyer, J. (2021). Geochemical Characteristics of Sediment in Tropical Lake Sentani, Indonesia, Are Influenced by Spatial Differences in Catchment Geology and Water Column Stratification. *Frontiers in Earth Science*, *9*(May), 1–16. https://doi.org/10.3389/feart.2021.671642

Norris, M. W., Turnbull, J. C., Howarth, J. D., & Vandergoes, M. J. (2020). Pretreatment of Terrestrial Macrofossils. *Radiocarbon*, *62*(2), 349–360. https://doi.org/10.1017/RDC.2020.8

O'Connell, J. F., & Allen, J. (2015). The process, biotic impact, and global implications of the human colonization of Sahul about 47,000 years ago. *Journal of Archaeological Science*, *56*, 73–84. https://doi.org/10.1016/j.jas.2015.02.020

Olsen, J., Anderson, N. J., & Leng, M. J. (2013). Limnological controls on stable isotope records of late-Holocene palaeoenvironment change in SW Greenland : a paired lake study. *Quaternary Science Reviews*, *66*, 85–95. https://doi.org/10.1016/j.quascirev.2012.10.043

Otte, J. M., Harter, J., Laufer, K., Blackwell, N., Straub, D., Kappler, A., & Kleindienst, S. (2018). The distribution of active iron-cycling bacteria in marine and freshwater sediments is decoupled from geochemical gradients. *Environmental Microbiology*, *20*(7), 2483–2499. https://doi.org/10.1111/1462-2920.14260

P.A. Meyers. (2003). Application of organic geochemistry to paleolimnological reconstruction: a summary of examples from the Laurention Great Lakes. *Organic Geochemistry*, *34*(2), 261–289.

Parks Victoria. (1996). *Mount Eccles National park and Mount Napier state park; Management plan*.

Peinerud, E. K. (2000). Interpretation of Si concentrations in lake sediments: Three case studies. *Environmental Geology*, *40*(1–2), 64–72. https://doi.org/10.1007/PL00013330

Perron, M. M. G., Proemse, B. C., Strzelec, M., Gault-Ringold, M., Boyd, P. W., Rodriguez, E. S., Paull, B., & Bowie, A. R. (2020). Origin, transport and deposition of aerosol iron to Australian coastal waters. *Atmospheric Environment*, *228*(October 2019), 117432. https://doi.org/10.1016/j.atmosenv.2020.117432

Petherick, L., Bostock, H., Cohen, T. J., Fitzsimmons, K., Tibby, J., Fletcher, M. S., Moss, P., Reeves, J., Mooney, S., Barrows, T., Kemp, J., Jansen, J., Nanson, G., & Dosseto, A.

(2013). Climatic records over the past 30ka from temperate Australia - a synthesis from the Oz-INTIMATE workgroup. *Quaternary Science Reviews*, *74*, 58–77. https://doi.org/10.1016/j.quascirev.2012.12.012

Price, R. C., Gray, C. M., & Frey, F. A. (1997). Strontium isotopic and trace element heterogeneity in the plains basalts of the Newer Volcanic Province, Victoria, Australia. *Geochimica et Cosmochimica Acta*, *61*(1), 171–192. https://doi.org/10.1016/S0016-7037(96)00318-3

Pueyo, J. J., Sáez, A., Giralt, S., Valero-Garcés, B. L., Moreno, A., Bao, R., Schwalb, A., Herrera, C., Klosowska, B., & Taberner, C. (2011). Carbonate and organic matter sedimentation and isotopic signatures in Lake Chungará, Chilean Altiplano, during the last 12.3kyr. *Palaeogeography, Palaeoclimatology, Palaeoecology*, *307*(1–4), 339–355. https://doi.org/10.1016/j.palaeo.2011.05.036

Risbey, J. S., Pook, M. J., McIntosh, P. C., Wheeler, M. C., & Hendon, H. H. (2009). On the remote drivers of rainfall variability in Australia. *Monthly Weather Review*, *137*(10), 3233–3253. https://doi.org/10.1175/2009MWR2861.1

Rodríguez-Ramírez, A., Caballero, M., Roy, P., Ortega, B., Vázquez-Castro, G., & Lozano-García, S. (2015). Climatic variability and human impact during the last 2000 years in western Mesoamerica: Evidence of late Classic (AD 600-900) and Little Ice Age drought events. *Climate of the Past*, *11*(9), 1239–1248. https://doi.org/10.5194/cp-11-1239-2015

Rodysill, J. R., Russell, J. M., Bijaksana, S., Brown, E. T., Safiuddin, L. O., & Eggermont, H. (2012). A paleolimnological record of rainfall and drought from East Java, Indonesia during the last 1,400 years. *Journal of Paleolimnology*, *47*(1), 125–139. https://doi.org/10.1007/s10933-011-9564-3

Rosen, M. R., Coshell, L., Turner, J. V., & Woodbury, R. J. (1996). Hydrochemistry and nutrient cycling in Yalgorup National Park, Western Australia. In *Journal of Hydrology* (Vol. 185, Issues 1–4). https://doi.org/10.1016/0022-1694(95)02981-8

Rosenmeier, M. F., Brenner, M., Kenney, W. F., Whitmore, T. J., & Taylor, C. M. (2004). Recent eutrophication in the Southern Basin of Lake Petén Itzá, Guatemala: Human impact on a large tropical lake. *Hydrobiologia*, *511*, 161–172. https://doi.org/10.1023/B:HYDR.0000014038.64403.4d

Rozanski, K., Klisch, M. A., Wachniew, P., Gorczyca, Z., Goslar, T., Edwards, T. W. D., & Shemesh, A. (2010). Oxygen-isotope geothermometers in lacustrine sediments: New insights through combined δ18O analyses of aquatic cellulose, authigenic calcite and biogenic silica in Lake Gościaz, central Poland. *Geochimica et Cosmochimica Acta*, *74*(10), 2957–2969. https://doi.org/10.1016/j.gca.2010.02.026

Ryves, D. B., Leng, M. J., Barker, P. A., Snelling, A. M., Sloane, H. J., Arrowsmith, C., Tyler, J. J., Scott, D. R., Radbourne, A. D., & Anderson, N. J. (2020). Understanding the transfer of contemporary temperature signals into lake sediments via paired oxygen

isotope ratios in carbonates and diatom silica: Problems and potential. *Chemical Geology*, *552*(June), 119705. https://doi.org/10.1016/j.chemgeo.2020.119705

Scholz, C. A., Cohen, A. S., Johnson, T. C., King, J., Talbot, M. R., & Brown, E. T. (2011). Scientific drilling in the Great Rift Valley: The 2005 Lake Malawi Scientific Drilling Project - An overview of the past 145,000years of climate variability in Southern Hemisphere East Africa. *Palaeogeography, Palaeoclimatology, Palaeoecology*, *303*(1–4), 3–19. https://doi.org/10.1016/j.palaeo.2010.10.030

Scholz, C. A., Johnson, T. C., Cohen, A. S., King, J. W., Peck, J. A., Overpeck, J. T., Talbot, M. R., Brown, E. T., Kalindekafe, L., Amoako, P. Y. O., Lyons, R. P., Shanahan, T. M., Castañeda, I. S., Heil, C. W., Forman, S. L., McHargue, L. R., Beuning, K. R., Gomez, J., & Pierson, J. (2007). East African megadroughts between 135 and 75 thousand years ago and bearing on early-modern human origins. *Proceedings of the National Academy of Sciences of the United States of America*, *104*(42), 16416–16421. https://doi.org/10.1073/pnas.0703874104

Shanahan, T. M., Overpeck, J. T., Beck, J. W., Wheeler, C. W., Peck, J. A., King, J. W., & Scholz, C. A. (2008). The formation of biogeochemical laminations in Lake Bosumtwi, Ghana, and their usefulness as indicators of past environmental changes. *Journal of Paleolimnology*, *40*(1), 339–355. https://doi.org/10.1007/s10933-007-9164-4

Shapley, M. D., Ito, E., & Donovan, J. J. (2005). Authigenic calcium carbonate flux in groundwater-controlled lakes: Implications for lacustrine paleoclimate records. *Geochimica et Cosmochimica Acta*, *69*(10), 2517–2533. https://doi.org/10.1016/j.gca.2004.12.001

Shi, X., Pu, T., He, Y., Qi, C., Zhang, G., & Xia, D. (2017). Variability of stable isotope in lakewater and its hydrological processes identification in Mt. Yulong region. *Water (Switzerland)*, *9*(9). https://doi.org/10.3390/w9090711

Smith, A., McNiven, I. J., Rose, D., Brown, S., Johnston, C., & Crocker, S. (2019). Indigenous Knowledge and Resource Management as World Heritage Values: Budj Bim Cultural Landscape, Australia. *Archaeologies*, *15*(2), 285–313. https://doi.org/10.1007/s11759-019-09368-5

Steinman, B. A., Rosenmeier, M. F., Abbott, M. B., & Bain, D. J. (2010). The isotopic and hydrologic response of small, closed-basin lakes to climate forcing from predictive models: Application to paleoclimate studies in the upper Columbia River basin. *Limnology and Oceanography*, *55*(6), 2231–2245. https://doi.org/10.4319/lo.2010.55.6.2231

Street-Perrott, F. A., Holmes, J. A., Robertson, I., Ficken, K. J., Koff, T., Loader, N. J., Marshall, J. D., & Martma, T. (2018). The Holocene isotopic record of aquatic cellulose from Lake Äntu Sinijärv, Estonia: Influence of changing climate and organic-matter sources. *Quaternary Science Reviews*, *193*, 68–83. https://doi.org/10.1016/j.quascirev.2018.05.010

Sun, D., He, Y., Wu, J., Liu, W., & Sun, Y. (2019). Hydrological and Ecological Controls on Autochthonous Carbonate Deposition in Lake Systems: A Case Study From Lake Wuliangsu and the Global Perspective. *Geophysical Research Letters*, *46*(12), 6583–6593. https://doi.org/10.1029/2019GL082224

Talbot, M. R. (2001). *15 . Nitrogen isotopes in palaeolimnology*. *2*, 401–402.

Teller, J. T., & Last, W. M. (1990). Paleohydrological indicators in playas and salt lakes, with examples from Canada, Australia, and Africa. *Palaeogeography, Palaeoclimatology, Palaeoecology*, *76*(3–4), 215–240. https://doi.org/10.1016/0031-0182(90)90114-M

Teranes, J. L., & Mckenzie, J. A. (2001). Lacustrine oxygen isotope record of 20th-century climate change in central Europe: Evaluation of climatic controls on oxygen isotopes in precipitation. *Journal of Paleolimnology*, *26*(2), 131–146. https://doi.org/10.1023/A:1011175701502

Thevenon, F., Adatte, T., Spangenberg, J. E., & Anselmetti, F. S. (2012). Elemental (C/N ratios) and isotopic (δ15Norg, δ13Corg) compositions of sedimentary organic matter from a high-altitude mountain lake (Meidsee, 2661 m a.s.l., Switzerland): Implications for Lateglacial and Holocene Alpine landscape evolution. *Holocene*, *22*(10), 1135–1142. https://doi.org/10.1177/0959683612441841

Tian, J., Nelson, D. M., & Hu, F. S. (2011). How well do sediment indicators record past climate? An evaluation using annually laminated sediments. *Journal of Paleolimnology*, *45*(1), 73–84. https://doi.org/10.1007/s10933-010-9481-x

Timms, B. V. (1976). A Comparative Study of the Limnology of Three Maar Lakes in Western Victoria. I. physiography and physicochemical features. *Marine and Freshwater Research*, *27*(1), 35–60. https://doi.org/10.1071/MF9760035

Tonetta, D., & Petrucio, M. M. (2020). Seasonal changes in primary production and respiration in a subtropical lake undergoing eutrophication. *Environmental Monitoring and Assessment*, *192*(9). https://doi.org/10.1007/s10661-020-08525-6

Torres, I. C., Inglett, P. W., Brenner, M., Kenney, W. F., & Reddy, K. R. (2012). Stable isotope (δ 13C and δ 15N) values of sediment organic matter in subtropical lakes of different trophic status. *Journal of Paleolimnology*, *47*(4), 693–706. https://doi.org/10.1007/s10933-012-9593-6

Turney, C., Becerra-Valdivia, L., Sookdeo, A., Thomas, Z. A., Palmer, J., Haines, H. A., Cadd, H., Wacker, L., Baker, A., Andersen, M. S., Jacobsen, G., Meredith, K., Chinu, K., Bollhalder, S., & Marjo, C. (2021). Radiocarbon protocols and first intercomparison results from the CHRONOS 14Carbon-Cycle facility, University of New South Wales, Sydney, Australia. *Radiocarbon*, *63*(3), 1003–1023. https://doi.org/10.1017/RDC.2021.23

Tweed, S., Leblanc, M., & Cartwright, I. (2009). Groundwater-surface water interaction and the impact of a multi-year drought on lakes conditions in South-East Australia. *Journal of Hydrology*, *379*(1–2), 41–53. https://doi.org/10.1016/j.jhydrol.2009.09.043

Tyler, J. J., Marshall, J. C., Schulz, C., Barr, C., Hofmann, H., Blessing, J. J., Mccoy, K., Mcgregor, G. B., & Tibby, J. (2022). *Hydrological and Isotopic Variability of Perched Wetlands on North Stradbroke Island (Minjerribah), Australia : Implications for Understanding the Effects of Past and Future Climate Change*. *10*(July), 1–21. https://doi.org/10.3389/fenvs.2022.868114

Tylmann, W., Głowacka, P., & Szczerba, A. (2017). Tracking climate signals in varved lake sediments: research strategy and key sites for comprehensive process studies in the Masurian Lakeland. *Limnological Review*, *17*(3), 159–166. https://doi.org/10.1515/limre-2017-0015

Vegas-Vilarrúbia, T., Corella, J. P., Sigró, J., Rull, V., Dorado-Liñan, I., Valero-Garcés, B., & Gutiérrez-Merino, E. (2022). Regional precipitation trends since 1500 CE reconstructed from calcite sublayers of a varved Mediterranean lake record (Central Pyrenees). *Science of the Total Environment*, *826*. https://doi.org/10.1016/j.scitotenv.2022.153773

Wetzel, R. G. (2001a). Iron, Sulfur, and Silica Cycles. *Limnology*, 289–330. https://doi.org/10.1016/b978-0-08-057439-4.50018-6

Wetzel, R. G. (2001b). the Inorganic Carbon Complex. *Limnology*, 187–204. https://doi.org/10.1016/b978-0-08-057439-4.50015-0

Wilkins, D., Gouramanis, C., de Deckker, P., Fifield, L. K., & Olley, J. (2013). Holocene lake-level fluctuations in Lakes Keilambete and Gnotuk, southwestern Victoria, Australia. *Holocene*, *23*(6), 784–795. https://doi.org/10.1177/0959683612471983

Wissel, H., Mayr, C., & Lücke, A. (2008). A new approach for the isolation of cellulose from aquatic plant tissue and freshwater sediments for stable isotope analysis. *Organic Geochemistry*, *39*(11), 1545–1561. https://doi.org/10.1016/j.orggeochem.2008.07.014

Wolfe, B. B., Aravena, R., Abbott, M. B., Seltzer, G. O., & Gibson, J. J. (2001). Reconstruction of paleohydrology and paleohumidity from oxygen isotope records in the Bolivian Andes. *Palaeogeography, Palaeoclimatology, Palaeoecology*, *176*(1–4), 177–192. https://doi.org/10.1016/S0031-0182(01)00337-6

Wolfe, B. B., Falcone, M. D., Clogg-Wright, K. P., Mongeon, C. L., Yi, Y., Brock, B. E., Amour, N. A. S., Mark, W. A., & Edwards, T. W. D. (2007). Progress in isotope paleohydrology using lake sediment cellulose. *Journal of Paleolimnology*, *37*(2), 221–231. https://doi.org/10.1007/s10933-006-9015-8

Wu, H., Li, X., Li, J., Jiang, Z., Li, G., & Liu, L. (2015). Evaporative enrichment of stable isotopes (δ18o and δd) in lake water and the relation to lake-level change of lake qinghai, northeast tibetan plateau of China. *Journal of Arid Land*, *7*(5), 623–635. https://doi.org/10.1007/s40333-015-0048-6

Zhang, Y., Jones, M., Zhang, J., McGowan, S., & Metcalfe, S. (2021). Can δ18O help indicate the causes of recent lake area expansion on the western Tibetan Plateau? A case study from Aweng Co. *Journal of Paleolimnology*, *65*(1), 169–180.

https://doi.org/10.1007/s10933-020-00158-6

Zhang, Y., Wu, Z., Liu, M., He, J., Shi, K., Zhou, Y., Wang, M., & Liu, X. (2015). Dissolved oxygen stratification and response to thermal structure and long-term climate change in a large and deep subtropical reservoir (Lake Qiandaohu, China). *Water Research, 75*, 249–258. https://doi.org/10.1016/j.watres.2015.02.052

Zhu, L., Wu, Y., Wang, J., Lin, X., Ju, J., Xie, M., Li, M., Mäusbacher, R., Schwalb, A., & Daut, G. (2008). Environmental changes since 8.4 ka reflected in the lacustrine core sediments from Nam Co, central Tibetan Plateau, China. *Holocene, 18*(5), 831–839. https://doi.org/10.1177/0959683608091801.

Supplementary data

Section 1: Moisture content of SUR-19-01 sediments

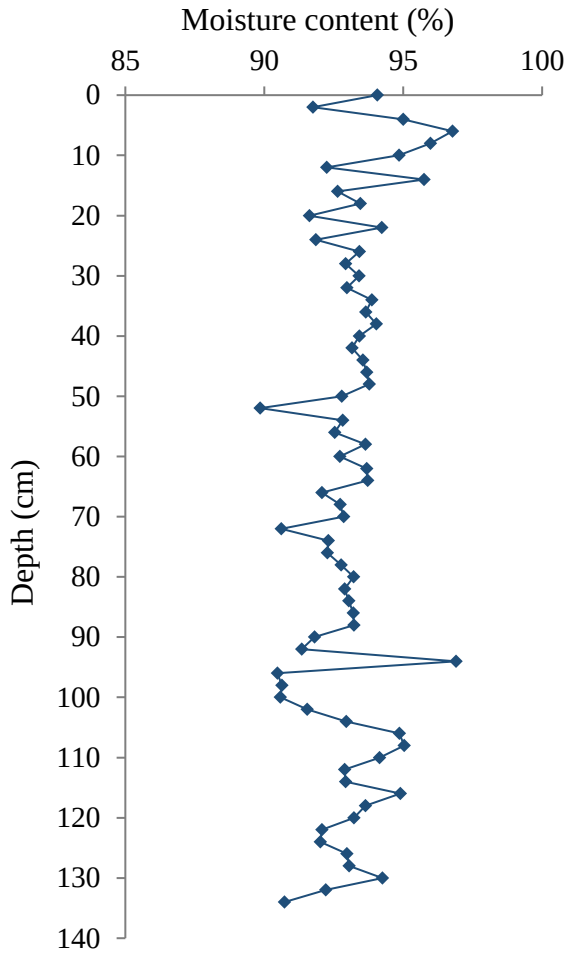

Figure I. A plot of moisture content variation measured at 0.5 cm intervals along the sediment profile.

Section 2: Cellulose oxygen isotopes

Here we compared the lake water isotopes obtained from SUR-19-01 with the overlapping section of SUR-19-02. Note that from 0 – 30 cm only one set of measurements is available. Even though, both records illustrate similar variation, numerical values are different from each other. Here we exclude the SUR-19-01 data set (lower values), because we assume increased moisture in these sediments may have influenced the water isotope measurements. Similarly, given that SUR-19-01 samples were first to be extracted, methodological errors were possible. Later in the process several methodological developments were employed for effective

cellulose extraction (increase in sample drying temperature to confirm that samples no longer contain in moisture).

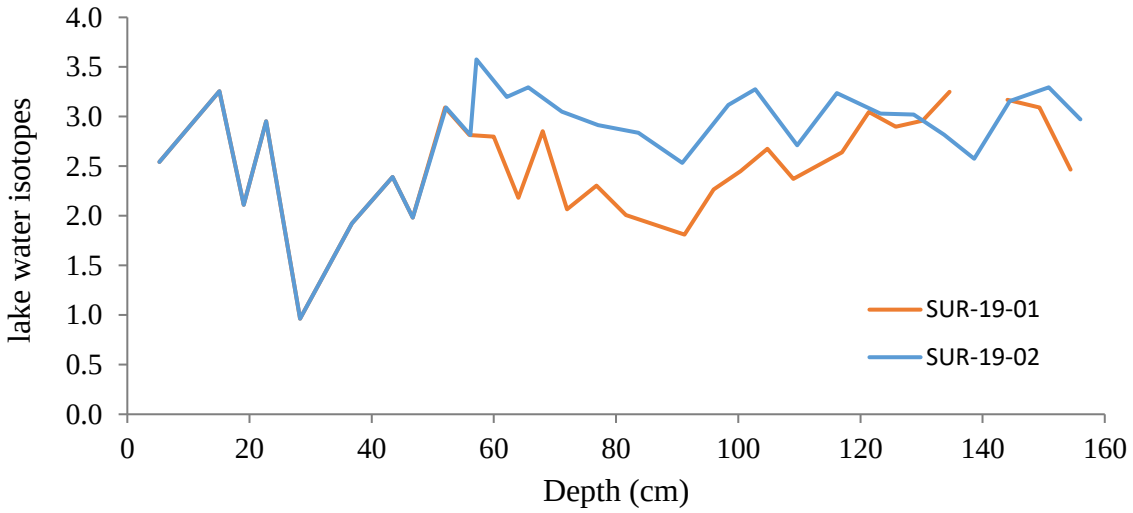

Supplementary figure II. Comparison of lake water isotopes between SUR-19-01 and SUR-19-02 for the sediment depth 0 – 154 cm. sediment core overlapping initiates from ~52 cm.

Table I. $\delta^{18}O$ values of cellulose from both SUR-19-01 (0 – 46.7 cm) and SUR-19-2 (52 – 156 cm) cores relevant to the basal depth of SUR-19-01 along with calculated age-errors

Composite depth	Age	Age	Calculated age error	$\delta^{18}O_{Cellulose}$	$\delta^{18}O_{LW}$
cm	cal yr BP	CE		‰	‰
5.25	-61.7	2011.7	3.8	30.57	2.54
15.05	-49.55	1999.55	2.7	31.30	3.26
19.05	-32.05	1982.05	10.6	30.12	2.11
22.75	-15.55	1965.55	6.9	30.99	2.95
28.3	1.8	1948.2	6.2	28.94	0.96
36.75	25.8	1924.2	6.8	29.93	1.92
43.4	42.7	1907.3	3.4	30.41	2.39
46.7	48.3	1901.7	3.4	29.99	1.98
52.15	57.1	1892.9	3.3	31.13	3.09
56.15	63.8	1886.2	3.8	30.85	2.81
57.15	65.95	1884.05	0	31.63	3.58
62.15	79.15	1870.85	0	31.24	3.20
65.65	89.6	1860.4	0	31.34	3.29
71.15	109.2	1840.8	0	31.09	3.05
77.05	126.15	1823.85	0	30.95	2.91
83.65	146.25	1803.75	0	30.87	2.84
90.85	169.85	1780.15	0	30.56	2.53

98.4	199.1	1750.9	0	31.16	3.12
102.8	216.6	1733.4	0	31.32	3.27
109.65	260.8	1689.2	0	30.74	2.71
116.15	305.05	1644.95	0	31.28	3.24
123.25	392.35	1557.65	0	31.07	3.03
128.75	475.85	1474.15	0	31.06	3.02
133.7	501.4	1448.6	0	30.85	2.82
138.65	529.2	1420.8	0	30.6	2.57
144.44	560.68	1389.32	0	31.2	3.16
150.86	608.06	1341.94	0	31.34	3.29
156.01	653.6	1296.4	0	31.01	2.97

Section 3: Correlation matrix statistics

Table II. p-values corresponding to the correlation matrix of Ca% vs climate variables. (P = precipitation, E = evaporation, P-E = effective precipitation, P/E = precipitation to evaporation ratio, Tmax = temperature maximum, Tmin = temperature minimum).

	Ca	P	E	P-E	P/E	Tmax	Tmin
Ca	1						
P	0.0285	1					
E	5.14E-06	0.0001	1				
P-E	6.01E-06	1.97E-23	2.3E-22	1			
P/E	3.60E-05	1.61E-34	1.69E-14	5.43E-58	1		
Tmax	5.40E-08	0.00619	9.31E-18	1.51E-10	6.42E-08	1	
Tmin	0.365	8.69E-07	0.0396	3.23E-05	1.09E-05	0.174	1

Table III. p-values corresponding to the correlation matrix of $\delta^{13}C_{org}$ vs climate variables

	$\delta^{13}C_{org}$	P	E	P-E	P/E	Tmax	Tmin
$\delta^{13}C_{org}$	1.00						
P	0.748	1.00					
E	0.0816	0.136	1.00				
P-E	0.197	1.63E-5	2.07E-6	1.00			
P/E	0.332	2.28E-8	0.00042	1.97E-13	1.00		
Tmax	0.0128	0.585	0.00032	0.0136	0.0469	1.00	
Tmin	0.161	0.0007	0.109	0.00246	0.00109	0.422	1.00

Table IV. p-values corresponding to the correlation matrix of $\delta^{18}O_{LW}$ vs climate variables.

	$\delta^{18}O_{LW}$	P	E	P-E	P/E	Tmax	Tmin
$\delta^{18}O_{LW}$	1						
P	0.283	1					
E	0.030	0.448	1				
P-E	0.045	0.004	0.016	1			
P/E	0.049	0.0007	0.0513	8.45E-7	1		
Tmax	0.022	0.553	6.61E-5	0.0362	0.0902	1	
Tmin	0.283	0.136	0.851	0.283	0.204	0.904	1

Section 4: correlation matrix between XRF elements (p values <0.0001)

Table V. Pearson correlation statistics between XRF element percentages

	Ca	Sr	Fe	S	Si	Cl
Ca	1					
Sr	0.95	1				
Fe	0.19	0.098	1			
S	-0.22	-0.25	0.57	1		
Si	-0.42	-0.37	-0.21	0.094	1	
Cl	-0.49	-0.38	-0.52	0.069	0.46	1

CHAPTER 5

Dharmarathna, A., Tyler, J., Tibby, J., Barr, C., Cadd, H., Ankor, M., Klaebe, R., Hall, T., Hua, Q., Child, D., Hotchkis, M., Zawadski, A., Holocene climate variability in south-eastern Australia; inferred from oxygen isotopes in sedimentary cellulose at Lake Surprise, Victoria, Australia.

Supplementary information concerning this chapter follows the text. Data tables concerning this chapter are provided in Appendix 4.

Statement of Authorship

Title of Paper	Holocene climate variability in south-eastern Australia inferred from oxygen isotopes in sedimentary cellulose at Lake Surprise, Victoria.
Publication Status	☐ Published ☐ Accepted for Publication ☐ Submitted for Publication ☑ Unpublished and Unsubmitted work written manuscript style
Publication Details	Dharmarathna, A., Tyler, J., Tibby, J., Barr, C., Cadd, H., Ankor, M., Klaebe, R., Hall, T., Hua, Q., Child, D., Hotchkis, M., Zawadski, A., Holocene climate variability in south-eastern Australia; inferred from oxygen isotopes in sedimentary cellulose at Lake Surprise, *Quaternary Science Reviews*. **in prep**

Principal Author

Name of Principal Author (Candidate)	Asika Dharmarathna		
Contribution to the Paper	Field sample collection, Laboratory sample preparation and analysis (cellulose oxygen isotopes, stable carbon and nitrogen isotopes) Assisted in instrumental analysis, Data analysis and interpretation Writing the manuscript and acting as the corresponding author		
Overall percentage (%)	80%		
Certification:	This paper reports on original research I conducted during the period of my Higher Degree by Research candidature and is not subject to any obligations or contractual agreements with a third party that would constrain its inclusion in this thesis. I am the primary author of this paper.		
Signature		Date	12/12/2022

Co-Author Contributions

By signing the Statement of Authorship, each author certifies that:

i. the candidate's stated contribution to the publication is accurate (as detailed above);

ii. permission is granted for the candidate in include the publication in the thesis; and

iii. The sum of all co-author contributions is equal to 100% less the candidate's stated contribution.

Name of Co-Author	Jonathan Tyler		
Contribution to the Paper	Field work assistance, Funding support, guidance in data analysis and interpretation, Manuscript evaluation and review		
Signature		Date	5/12/22

Name of Co-Author	John Tibby		
Contribution to the Paper	Field work assistance, guidance in data analysis and interpretation, Manuscript evaluation and review		
Signature		Date	1/12/2022

Name of Co-Author	Cameron Barr		
Contribution to the Paper	Field work assistance, assistance in sample preparation, core correlation calculations, Assistance in data interpretation		
Signature		Date	22/11/2022

Name of Co-Author	Haidee Cadd		
Contribution to the Paper	Field work assistance, Acquisition of radiocarbon data of pollen samples, Assistance in data interpretation		
Signature		Date	20/11/22

Name of Co-Author	Martin Ankor		
Contribution to the Paper	Preparation of 3D printed sediment trap and rainfall sampler for modern sample collection,		
Signature		Date	

Name of Co-Author	Robert Klaebe		
Contribution to the Paper	Assistance with acquisition of stable oxygen isotope data from cellulose		
Signature		Date	2/11/2022

Name of Co-Author	Tony Hall		
Contribution to the Paper	Assistance with acquisition of stable carbon and nitrogen isotope data		
Signature		Date	22/11/2022

Name of Co-Author	Quan Hua		
Contribution to the Paper	Assistance with acquisition of radiocarbon data of macrofossil samples		
Signature		Date	23/11/2022

Name of Co-Author	David Child		
Contribution to the Paper	Assistance with acquisition of Pu isotope data		
Signature		Date	23/11/22

Name of Co-Author	Michael Hotchkis		
Contribution to the Paper	Assistance with acquisition of Pu isotope data		
Signature		Date	4/12/2022

Name of Co-Author	Atun Zawadski		
Contribution to the Paper	Assistance with acquisition of Pb-210 data		
Signature		Date	6/12/2022

5 Holocene climate variability in south-eastern Australia; inferred from oxygen isotopes in sedimentary cellulose at Lake Surprise, Victoria, Australia.

Abstract

During the Holocene, south-east Australia has endured extreme climate conditions varying from extended droughts and devastating floods (Head et al., 2014; King et al., 2020). However, knowledge of the frequency and intensity of such episodes is restricted due to the scarcity of quantitative, high-resolution climate records from the region. It is assumed that when conditions are possible, oxygen isotopes preserved in lake sediments are a useful tool for retracing the past climatic and environment. This study presents a well-dated, highly resolved Holocene hydroclimate record based on $\delta^{18}O$ values of aquatic cellulose, alongside stable organic carbon isotopes and carbon/nitrogen ratios from a 10.5 m sediment core. Lake Surprise in western Victoria. Our interpretation of the palaeo-data is supported by monitoring of water and sediment accumulation to understand the hydrology of the lake. The cellulose record indicates a trend of gradually increasing aridity towards the present day, with notable extreme wet periods prevailing from 10850 – 10000 cal yr BP, ca. 7400 – 7000 cal yr BP and 5600 – 4500 cal yr BP and a significant climate transition towards prolonged aridity at ~4500 cal yr BP. The overall pattern in the Lake Surprise record is consistent with that in other records from western Victorian lakes. However, excessive wet intervals observed in this study are not well defined in previous records.

This study demonstrates a strong coherence with Southern Western Wind variability suggesting that Southern Ocean processes were the dominant controls of Holocene climate change in the study area. The increasing frequency of El-Niño Southern Oscillation corresponds with the late Holocene drying. Correlation between the oxygen isotope record and the Indian Ocean Dipole remains weaker at least until the last millennium. The Lake Surprise record further exhibits a similar pattern of variation to solar forcing variability implying an influence of solar intensity on regional climate. However, detailed analyses focused on solar activity and climate modes are required to understand teleconnections among these climate drivers and their mechanisms.

5.1 Introduction

Australia, the driest inhabited continent on Earth, experiences adverse impacts of multi-decadal to multi-centennial extreme climate variability which can result in severe agricultural losses with far-reaching socio-economic and environmental impacts, particularly in the south east, which is Australia's most densely populated and intensively farmed region (Hughes, 2003; Ummenhofer et al., 2009; CSIRO, 2018; King et al., 2020). Instrumental records provide evidence of historical droughts that occurred throughout the last century, including the Federation Drought (1895 – 1902), the World War II Drought (1937 – 1945) and the Millennium Drought (1997 – 2010), more than a decade of low rainfall that severely affected south-eastern Australia (Tweed et al., 2009; Gergis et al., 2012; Barr et al., 2014; Scroxton et al., 2020). A sudden occurrence of heavy rainfall events around 2010 – 2012 caused damaging floods mostly in the eastern regions (Flack et al., 2020; King et al., 2020). Widespread bush fires and heat waves from 2019 to 2020 are more recent occurrences that particularly threaten wildlife and the entirety of temperate forests in south-eastern Australia (Abram et al., 2021; Reddy et al., 2022b).

Future climate projections suggest these climate occurrences will become longer and more severe, however, given that short-term instrumental evidence (~120 years) is not indicative of the full range of climate variability, such projections remain highly uncertain (Kiem et al., 2016, 2020; Kirono et al., 2020). As a consequence, there remains a demand for robust records of long-term hydroclimate variability to both validate models and interrogate the major drivers of multi-decadal to centennial climatic change (Murphy and Timbal 2008; Grant et al., 2013). To date, several Australian hydroclimate reconstructions have been developed using palaeoclimate records which are distal from the region of interest, such as Antarctic ice cores (Delmonte et al., 2002; Masson-Delmotte et al., 2004; Stenni et al., 2010; Thomas et al., 2019), tropical corals (Gagan et al., 2000, 2004; Abram et al., 2009, 2020b) and New Zealand tree rings (Cook et al., 2002; Fowler et al., 2012; Pauly et al., 2021). These records often exhibit relatively poor predictive ability for Australian rainfall and are predominantly focused on recent millennia, and as such also potentially fail to capture the long-term natural variability.

Being a continent surrounded by three major oceans, the rainfall patterns of Australia are highly variable compared to other regions elsewhere in the world (Nicholls et al., 1997). Large-scale climate drivers that govern Australia's precipitation include Southern Annular Mode (SAM), the El Niño Southern Oscillation (ENSO) in the tropical Pacific Ocean and the Indian Ocean

Dipole (IOD) in the Indian Ocean (Abram et al., 2007, 2008, 2020b; Evans et al., 2009; Ummenhofer et al., 2009; Cai et al., 2011a; Henley et al., 2015; Vance et al., 2015; Cleverly et al., 2016; Beck et al., 2017; Jones et al., 2018; Barr et al., 2019). While potential teleconnections have been identified between ENSO, SAM and the IOD and modern rainfall in south-east Australia, the effects of these processes over decades to centuries remain poorly understood (Cai et al., 2011a, b, c, 2012; Gouramanis et al., 2013; Cleverly et al., 2016).

Lake chemistry and biology are strongly influenced by regional climate and their responses are assimilated in the sedimentary record. The continuity and widespread nature of these sediments provide well-established tools for studying past climate conditions. Multi-proxy sediment records from western Victorian maar crater lakes have been increasingly used in climate reconstructions over the years, given their ability to act as "rain gauges" (Kemp et al., 2012; Gouramanis et al., 2013). These records consist of a diverse range of sediment proxies such as grain size, ostracod valve chemistry, diatoms, bulk sediment geochemistry, pollen and charcoal (Bowler and Hamada, 1971; Edney et al., 1990; Gell et al., 1994; Gell, 1997; Jones et al., 1998; Builth et al., 2008; Gouramanis et al., 2010, 2013; Kemp et al., 2012; Tibby et al., 2012; Wilkins et al., 2013; Falster et al., 2018). Whilst hydroclimate records have been developed at sites located in south-eastern Australia, many of these are undermined by a lack of temporal resolution, chronological precision or lack a proxy which is mechanistically linked to climate variability (Neukom & Gergis, 2012; Tyler et al., 2015; Dixon et al., 2017).

The lake level reconstruction based on sediment grain size from Lake Keilambete (supported by that from Lake Gnotuk) has been the cornerstone of hydrological inferences from Western Victoria and south-east Australia for almost 50 years. This work, originated by Bowler (1970, 1981) has been supported and updated by a number of authors (Dodson 1974a,b; De Deckker, 1982; Chivas et al., 1985, 1993; Mooney, 1997; Jones et al, 1998; Jones et al., 2001; Kirono et al., 2009; Wilkins et al., 2013). Several authors have also demonstrated that this lake level reconstruction, at least at a coarse scale, corresponds to patterns of hydrological change observed over the south-east of Australia (e.g. Gingele et al., 2007). However, as highlighted in the analysis of other run-off-climate interactions, the relationship between grain size and climate in Lake Keilambete is strongly non-linear (Wilkins et al., 2013; Emile-Geay & Tingley, 2016). In particular, this raises the challenge that the lake level records are relatively insensitive to changes during at least in humid phases. Indeed, a change in lake level from ~15 m to the lake full (representing a 25 m change in lake level and a much greater proportional change in

volume) is inferred from a change in grain size in the range of 0 – 5% (Wilkins et al., 2013). A similar issue exists with the Lake Gnotuk record which has even fewer constraints in terms of the lake level vs grain size relationship (Wilkins et al., 2013).

Stable isotope records of lake sediments add a physically-based insight into lake hydrological balance (Leng & Marshall, 2004; Jonsson et al., 2010; Rozanski et al., 2010; Gibson et al., 2016; Zhang et al., 2021). Lake water isotope composition ($^{18}O/^{16}O$, $^{2}H/^{1}H$) responds directly to hydroclimate variability including changes in precipitation, evaporation and atmospheric circulation patterns (Leng & Marshall, 2004; Heikkilä et al., 2010; Steinman et al., 2010). Lakes are either fed directly by rainwater and runoff, or indirectly by groundwater, and shifts in the $\delta^{18}O_{LW}$ reflect changes in the source, pathway and intensity of rainfall (Barras & Simmonds, 2009; Crawford et al., 2013; Hughes & Crawford, 2013; Treble et al., 2021). However, lake waters also undergo evaporation, which can markedly alter the $\delta^{18}O$ signal, subject to lake water residence time, surface area and evaporation rate (Gibson & Edwards, 2002; Gibson et al., 2008, 2016). Therefore, prior to using $\delta^{18}O$ as a palaeoclimate proxy, it is necessary to understand the underlying controls over lake water $\delta^{18}O$ at the site in question.

Aquatic cellulose preserved in organic-rich sediment was first used as a tracer of past lake water $\delta^{18}O$ by Edwards & McAndrews, (1989). Since then oxygen isotopes in lacustrine cellulose have been incorporated in palaeolimnological studies in many parts of the world to resolve past hydrological, hydroecological and hydroclimatic questions (Abbott et al., 2000; Wolfe et al., 2000, 2001, 2007; Beuning et al., 2002; Wissel et al., 2008; Mayr et al., 2009; Brahney et al., 2010; Heikkilä et al., 2010; Rozanski et al., 2010; Buhay et al., 2012; Heyng et al., 2014; Street-Perrott et al., 2018). The use of cellulose $\delta^{18}O$ usually relies on the assumption that the fine-grained (<150 μm) lake sediment cellulose is predominantly aquatic and that the isotope fractionation ($\alpha^{18}O_{cell\text{-}lw}$) between cellulose and lake water is constant, at 1.028 ± 0.003 ‰ (Edwards & McAndrews, 1989; Street-Perrott et al., 2018). Unlike carbonates and diatom silica, the cellulose-water oxygen isotope fractionation is temperature and species-independent and enriched by 27 – 28 ‰ relative to the source water (Sternberg, 1989; Abbott et al., 2000; Wolfe et al., 2001, 2007; Street-Perrott et al., 2018). Several studies have identified a slight lowering in $\alpha^{18}O_{cell\text{-}lw}$ value (1.025 ± 0.003 ‰) in different environmental settings (Wolfe et al., 2001; Beuning et al., 2002; Street-Perrott et al., 2018; Savage et al., 2021). Savage et al., (2021) explored this question by calculating $\alpha^{18}O_{cell\text{-}lw}$ in 52 lakes in western central Canada

and suggested that slight differences that fall within the range of 1.028 ± 0.003 are acceptable. The seasonal timing of cellulose synthesis and contamination by minerogenic residue may potentially explain the observed variability in estimated $\alpha^{18}O_{cell\text{-}lw}$ in other studies (Savage et al., 2021).

This study presents a high-resolution, cellulose oxygen isotope record which spans the Holocene from the sediments of Lake Surprise, a crater lake in western Victoria. Reconstruction of lake water oxygen isotope variability, which in turn is interpreted as a record of lake hydrological balance, is supported by modern monitoring data. Results of this study refine the regional perspective of hydroclimate variability in mainland south-eastern Australia, highlighting a decline in effective moisture along with reduced climate variability after 4500 cal years BP.

5.2 Site description

5.2.1 Regional climate

Lake Surprise is located in the newer volcanic province of western Victoria, in south-east Australia, with a "Mediterranean-like" climate, composed of hot, dry summers and cool, wet winters (Barr et al., 2014; Gouramanis et al., 2013). Mean annual temperature ranges between 8ºC to 22ºC and mean annual evaporation varies between 1100 mm to 1500 mm (The Bureau of Meteorology & CSIRO, 2020). Modern mean annual rainfall of the region varies from 500 mm to 1500 mm, with evidence of marked declines in rainfall since the late 1990s (The Bureau of Meteorology & CSIRO, 2020). The majority of the rainfall is received during the winter months (June to August) and is mainly controlled by the position and strength of the Southern Westerly Wind belt (SWW), which brings moist air from the Southern Ocean over southern Victoria (Murphy and Timbal, 2008; Risbey et al., 2009). Variability in the strength and position of the SWW are reflected in the Southern Annular Mode (SAM) index, which is correlated to rainfall variability in southern Australia (Murphy and Timbal, 2008; Saunders et al., 2012; Abram et al., 2014; Barr et al., 2014; Gergis and Henley, 2017). Air temperature in the region has increased steadily since 1950 reaching more than 1°C increase by the time of the "Millennium Drought" which prevailed from 1997 – 2007 (Ummenhofer et al., 2009; CSIRO, 2020). Extreme heatwaves and more frequent warmer months were in place since 2013, making 2019 the warmest and driest year on record (CSIRO, 2020). Evaporation has also increased in recent decades, due to high vapour pressure deficits that developed with increasing air temperature (Stephens et al., 2018). Continuous increases in air temperature and

evaporation, and rainfall decline have largely contributed to the growing severity of recent droughts (Nicholls, 2004; Ummenhofer et al., 2009).

5.2.2 Study site (Lake Surprise)

Lake Surprise is a crater lake formed approximately around 37000 years ago (Matchan et al., 2020) at an elevation of ~78 m AHD (38ºS, 141.55ºE) within the Budj Bim National Park (formerly known as "Mt. Eccles"') (Timms, 1975; Barr et al., 2014; Matchan et al., 2020), a UNESCO World Heritage Cultural Landscape (Bell & Johnston, 2008).

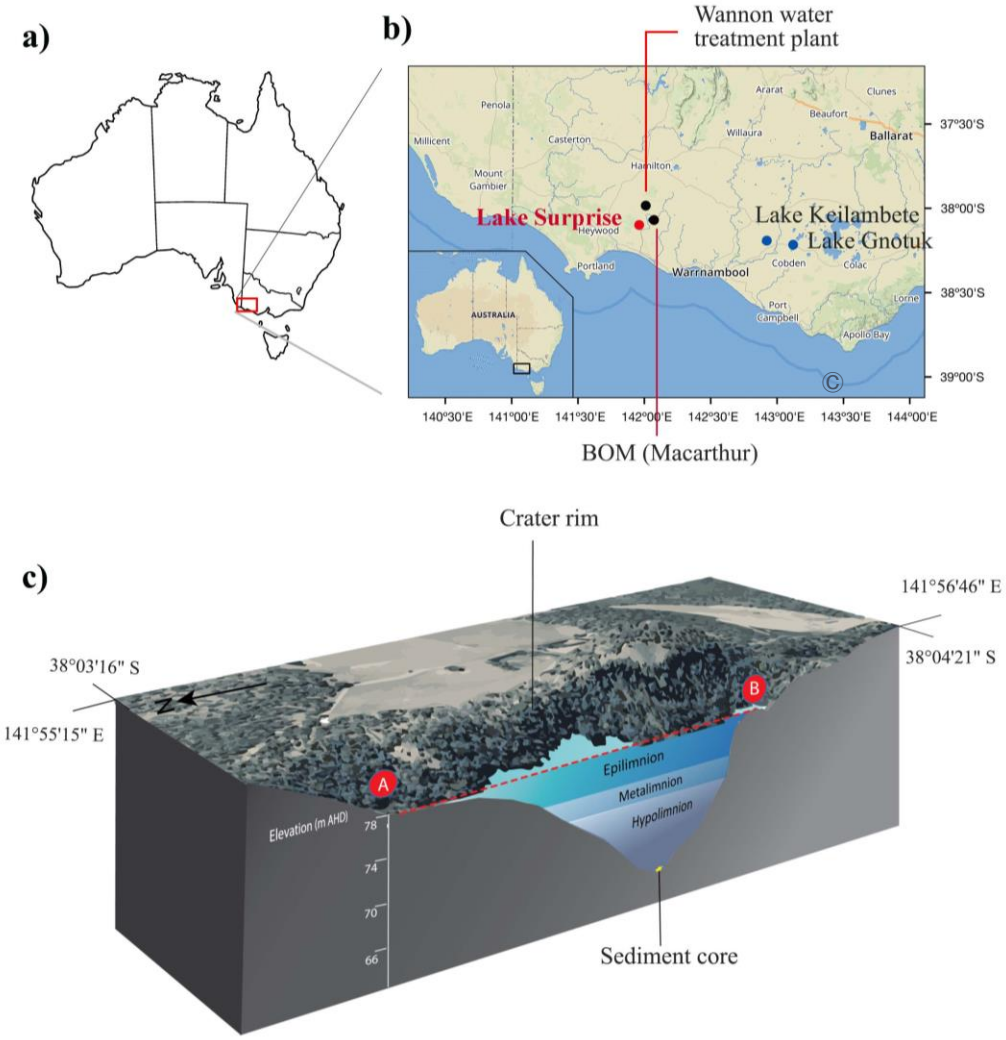

Figure 1. a) Approximate location of the study region b) Zoom-in map section (rectangular box) representing the approximate locations of Lake Surprise, lakes Keilambete and Gnotuk (discussed in this chapter) Macarthur Bureau of Meteorology (BOM) weather station and Wannon Water treatment plant; the site of rainfall collection for isotope monitoring (Ankor, 2020) c) three-dimensional view of the Lake relative to the lake bathymetry developed in 2019 (Appendix 1).

Lake bathymetry developed by Timms (1975) suggests that the amalgamation of three overlapping volcanic craters created the irregularly shaped lake with larger littoral areas at each end. According to the lake bathymetry developed at the time of coring in 2019, the water depth was ~11.5 m and the maximum length and width were ~600 m and ~200 m respectively (Figure 1c). Steep and high crater walls act as wind barriers that limit deep mixing and maintain sharp boundaries during lake stratification periods (Timms, 1975; Falster et al., 2018). The surrounding catchment is densely vegetated by *Eucalyptus viminalis* ("manna gum") and *Acacia melanoxylon* ("blackwood") (Tibby et al., 2006; Builth et al., 2008). Additionally, the ground cover is enriched with Poaceae, Asteraceae, bracken and bands of aquatic vegetation along the shallow water margins (Tibby et al., 2006). Further, previous studies suggest that relatively smaller lake area and larger littoral habitat that varies with lake level may be likely to respond to climate change (Barr et al., 2014). Theoretically, the lake is a "closed" basin, with no fluvial input or output. According to previous studies hydrological balance of the lake is likely to be mainly controlled by precipitation and evaporation (Barr et al., 2014; Falster et al., 2018). These studies further mentioned possible groundwater influence, particularly during extreme arid periods (Barr et al., 2014). This hypothesis was tested in this thesis (Chapter 2, Section 2.4) using stable isotope and major ions concentrations in lake water. Accordingly, Lake Surprise is most likely fed by local groundwater sources. Unlike many crater lakes in the western Victorian plains, Lake Surprise has been free of major catchment disturbances and preserves the natural climate signal in sediments (Barr et al., 2014).

5.3 Materials and methods

5.3.1 Modern water and sediment monitoring

In order to understand the modern controls on lake water isotope variability and seasonal variability in sediment accumulation, a modern monitoring program was conducted by collecting lake water, rainwater and sediment samples. For this project, monthly lake water samples were collected from 30th October 2019 until 14th April 2022, using high-quality HDPE bottles, initially rinsed three times with lake water. Samples were taken from just below the water surface at the centre of the lake and the bottles were filled entirely to minimise isotope exchange with the atmosphere. Additional data were acquired from Ankor, (2020), in which the sample collection extended back to 23rd May 2015 and continued until 11th September 2018 at varying sampling intervals. Lake water sampling was not performed at certain periods in the isotope dataset obtained from Ankor, (2020), especially before August 2016 and from October

2018 to October 2019. Rainwater samples were collected during the monitoring period using an autonomous rainfall sampler which collects both daily and monthly rainfall samples (Ankor et al., 2019). The sampler was installed at the Wannon Water treatment plant at Macarthur, about 10 km north of the lake. A simple sediment trap was deployed at the lowest point of the lake using an anchor attached to the lake bed. This collects two sediment columns of 125ml, in the plastic containers attached under the funnels (Supplementary section 3). Sample collection and replacement of the sediment trap and the rainwater sampler were initially planned to be repeated at quarterly intervals (every three months). However covid related interruptions (e.g. health risks and Interstate travel restrictions) caused intermittent and delayed sampling events. Therefore, only 4 sediment collections were done over the sampling period from 2020 – 2022.

Bureau of Meteorology (BOM) climate data at Macarthur (monthly mean values of air temperature and precipitation data), the nearest weather station to Lake Surprise were used to evaluate data obtained from the monitoring program. The BOM data were acquired from the Scientific Information for Land Owners (SILO) database, post-processed data that can be utilised in scientific applications (https://www.longpaddock.qld.gov.au/). Given that $\delta^{18}O$ values in precipitation are not available for the Macarthur weather station (BOM) and measured rainfall isotopes extend from 2019 – 2021, $\delta^{18}O$ values of monthly precipitation of Global Network of Isotopes in Precipitation (GNIP) data from 2015 – 2022 at Melbourne were used. A comparison of precipitation amount and $\delta^{18}O$ values in precipitation between Macarthur and Melbourne weather stations was performed to evaluate the applicability of $\delta^{18}O$ values for Lake Surprise data (Chapter 2, Supplementary data, Section 3).

5.3.2 Water isotope analysis

Water samples were analysed for stable oxygen and hydrogen isotopes using Piccaro Cavity Ring-Down Spectrometers at the Flinders analytical laboratory and Australian Nuclear Science and Technology Organization (ANSTO), Lucas Heights, New South Wales. The sample analysis at Flinders analytical was performed using two internal standards (DESAL and EVIAN) alongside a QC check against the internal RAIN standard. Samples in the glass vials were injected seven times with the first three injections being discarded to minimise the memory effect. Similarly, at ANSTO three in-house standards (AILS-006, AILS-012 and AILS-013) were calibrated against three separate standards used in the QC check (AILS-008, AILS-009 and AILS-014) and samples were injected 20 times with the first eight being

discarded. All the water isotopes were measured with reference to the Vienna Standard Mean Ocean Water (VSMOW) and the delta notation is recorded in per mille (‰) units. Results were reported as accurate to ±0.15‰ for $\delta^{18}O$ and ±1‰ for $\delta^{2}H$ at ANSTO and ±0.07 for $\delta^{18}O$‰ and ±0.58 for $\delta^{2}H$‰ at Flinders Analytical.

5.3.3 Sediment coring and sampling

Sediments were recovered from Lake Surprise in 2019 using a wide-diameter Perspex piston corer for the upper soft sediments and a modified large-bore Bolivia corer for deeper sediments (Wright, 1967). The complete Holocene record was obtained by merging the 1.57 m long soft sediment core (SUR-19-1) and two 10 m long overlapping cores (SUR-19-2 and SUR-19-3) with a 0.5 m depth difference that capture the entire sediment sequence. These cores were recovered as 1m segments and stored in PVC pipes, at 4°C in the cold room. The soft sediment core was extruded and sub-sampled at 0.5 cm resolution in the field due to its high water content and unconsolidated nature. All three sediment cores were sub-sampled before analysis at 0.5 cm intervals and stored in sealed Zip-lock bags at 4°C.

5.3.4 Core photography

Photographs of core sections of SUR-19-02 and SUR-19-03 were taken using an Olympus E-M1 II camera, with a resolution of 5184 × 3888 pixels before the sub-sampling and analysis. Structure from Motion-Multi-View Stereo (SFM-MVS) photogrammetric technique which generates 3D photogrammetric models was applied in this study (Ankor & Tyler, 2022). A pole was hooked into 2 tripods placed 1.5 m apart, where the camera can slide along facing downward. After setting the core section on the flat surface in between tripods, the camera was moved along the pole taking a photo at every ~7 cm, to ensure that the entire core was photographed. The core surface was scraped using a clean blade to remove any moisture and diminish the highlighting and glare of the photo. Post-processing of original photos was completed using the computation photogrammetry software “Agisoft Metashape Pro 1.6” as described in Ankor & Tyler, (2022) (Appendix 5).

5.3.5 Core correlation and construction of the composite depth

A single composite depth was developed by comparing the quantitative Ca records from all three sediment cores using the QAnalySeries v.1.5.0 software (Kotove and Palike, 2018) and guided by the stratigraphic correlations evident in high-resolution images of the sediment cores (Ankor & Tyler, 2022). Soft sediments were analysed for Ca using the Olympus Delta^{TM} handheld XRF (X-ray fluorescence) analyser and deeper sediments were analysed using the ITRAX μ-XRF scanner at ANSTO. The PC1 of these elemental compositions exhibits a high correlation with the Ca content, according to the principle components analysis (Supplementary section 4) (Barr et al., in preparation). Therefore, a composite core was developed by overlapping sediment core sections that have comparable Ca variability. Further, a 5 cm section from the top and bottom of each drive (~1m) of all three cores was eliminated for compaction correction. Note that the depth used in this study refers to the corrected composite depth.

5.3.6 Sediment Geochronology

The chronology of the Lake Surprise composite depth was developed using radiocarbon dates of 17 macrofossil samples and 33 pollen samples alongside ^{210}Pb dating of recent sediments (9 samples) from the top 100 cm of the soft sediment core. ^{210}Pb dates were assessed using evidence of previous atmospheric nuclear testing information from ^{239}Pu and ^{240}Pu concentrations of the top 50 cm of the same core (10 samples) (Hancock et al., 2011; Yang et al., 2015). Radiocarbon sample preparation and analysis of macrofossil samples were carried out at the Australian Nuclear Sciences and Technology Organization (ANSTO). Sample preparation and analysis of pollen were conducted at the Chronos 14Carbon-cycle facility at the University of New South Wales (Cadd et al., 2022; Turney et al., 2021). Samples for ^{210}Pb and Pu isotopes were prepared and analysed at the ANSTO using alpha spectrometry and Accelerator Mass Spectrometry respectively. For the detailed methodology of ^{210}Pb, Pu and radiocarbon sample analysis refer to Chapter 3 of this thesis (Section 3.2). Measured radiocarbon dates of pollen samples were relatively older than the macrofossil samples, therefore, an age correction equivalent to the age offset (340 ± 50 ^{14}Cyears) was included in the age model. The Bayesian *Plum* model approach was used to develop the age model by integrating ^{14}C years of pollen and macrofossil samples, ^{210}Pb activity data and Pu concentration (Aquino-López et al., 2018, 2020) in the R programming environment (version 4.1.3) (R Core Team 2022).

5.3.7 Stable isotope analysis of sediments

5.3.7.1 Carbon isotopes in organic matter

Core sediments were sampled at 10 cm intervals for stable carbon isotope analysis, total organic carbon (TOC) concentration and carbon/nitrogen C/N ratios of organic matter in the lake sediment. The sample processing for isotope analysis was completed following the "acid fumigation method" (Harris et al., 2001; Falster et al., 2018). Approximately 1 – 2 mg freeze-dried, powdered sediment was weighed into silver (Ag) capsules and was followed by the addition of 25 µl of deionized water. The capsules were then acidified for 3 – 4 hours in concentrated hydrochloric acid vapour and were dried overnight at 60°C in the oven. Dry capsules were positioned inside large Tin (Sn) capsules and crimped and left in the oven at 40°C to ensure that samples were anhydrous before analysis. All capsules were analysed for $\delta^{13}C_{org}$, total carbon and nitrogen concentration using the Elemental Analyser/Isotope Ratio Mass Spectrometer (EA/IRMS) at the University of Adelaide. Samples were calibrated against three internal standards Glycerine (C:-31.2, N: +1.32, C/N: 2), Glutamic acid (C: -16.7, N: -6.18, C/N: 5) and a QC standard TPA (triphenylamine C: -29.2, N: -0.54, C/N: 18). Isotope values were expressed on the delta scale to per mille (‰) units with reference to Vienna Pee Dee Belemnite (VPDB) international standard. Given that nitrogen content in deeper sediments is considerably lower (<3.5%) compared to carbon content (17 – 43%), $\delta^{15}N$ isotope analysis was not performed due to the deficiency of enough sample size for measurements. Isotope values obtained from smaller sample sizes generate larger errors.

5.3.7.2 Oxygen isotopes in cellulose

Cellulose from lake sediment was extracted following the dissolution and precipitation method in Wissel et al., 2008. Initially, sub-sampled 0.5 cm samples over a 1.5 cm depth were integrated in order to obtain 5 – 10 g of sediment, at sampling intervals of 5 cm. Fine sediment was retained by sieving (250 µm) and settling overnight. This process minimises the incorporation of terrestrial material and coarse organic residue including macro-charcoal (Edwards and McAndrews 1989; Rozanski et al., 2010; Street-Perrott et al., 2018). Then fine sediment was reacted with 7% sodium chlorite acidified to a pH of 4 – 5 with concentrated acetic acid (98%) and left to oxidise at 60°C for 10 hours. Treated sediment was rinsed three times with hot deionized water (70°C) and freeze-dried. The cellulose dissolution process was followed by reacting dried sediment with cuprammonium solution. The solution was prepared by mixing 15 g of copper hydroxide, 900 ml of ammonium hydroxide (25%) and 100 ml of

deionized water and the resultant solution was stirred overnight at room temperature. The sediment solution mixture was left to react in the end-over-end shaker for 6 hours and then for another 10 hours for the complete dissolution of cellulose. The cellulose precipitation step was initiated by treating the supernatant cellulose solution with 3 ml of 20% H_2SO_4 until the precipitate turned white. Extracted cellulose was rinsed and freeze-dried before sample preparation for analysis. 100 µg of dry cellulose were weighed into Ag capsules and crimped. As the cuprammonium treatment of cellulose tends to extend its hygroscopic character, Ag capsules were stored at 40°C in the oven after weighing and immediately before analysis the oven temperature was ramped to 100°C overnight (Wissel et al., 2008).

Cellulose was extracted using the same method from modern sediment collected from the sediment trap. Oxygen isotopes of cellulose were measured using a HEKAtech HT Oxygen analyser coupled with a EuroVector EuroEA Elemental analyser. Samples were reacted at 1500 degrees and measured as CO using a Nu instruments Perspective IRMS in continuous flow mode. Results were expressed in per mille (‰) units with reference to the Vienna Standard Mean Ocean Water (VSMOW) standard. Pinewood and cellulose powder were used as external standards and were processed for cellulose in each batch of sedimentary cellulose extraction to reassure the accuracy and consistency of the method of extraction and sample analysis (Supplementary data, Section 1). Results were normalised to NBS127 and checked against elemental microanalysis silver phosphate (Ag_3PO_4) which is not certified and in-house analytical standards cellulose ($\delta^{18}O$ = 35.48±0.27 ‰), sucrose ($\delta^{18}O$ = 30.24±0.17 ‰). The analytical precision was reported by repeated measurements of internal standards in each sample run with ±0.3 ‰.

5.3.7.3 Calculations used in the cellulose isotope analysis

Equation 1 is used as described in Edwards & McAndrews, (1989) and Rozanski et al., (2010) to convert of $\delta^{18}O_{cell}$ into $\delta^{18}O_{LW}$ values.

$$\delta^{18}O_{LW} = 0.973\ \delta^{18}O_{cell} - 27.2 \quad \text{.....Equation 1}$$

Isotope fractionation between cellulose and lake water ($\alpha^{18}O_{cell\text{-}lw}$) was calculated using equation 2 (Edwards & McAndrews, 1989).

$$\alpha_{cell-lw} = \left[\frac{\delta^{18}O_{cell}+1000}{\delta^{18}O_{LW}+1000}\right] \quad \text{.....Equation 2}$$

5.4 Results

5.4.1 Modern hydroclimatology and sediment geochemistry

Modern hydroclimate variability (2015 – 2021) in the Lake Surprise region is illustrated in Figure 2. Seasonal monthly precipitation at Macarthur and Melbourne is highly concentrated in late autumn and winter months (April to July) and lower precipitation is recorded during the summer months. The seasonal cyclic pattern of average air temperature in both Melbourne and Macarthur records is nearly consistent through time (Figure 2d). Considering the annual average precipitation values in Macarthur, 2016 and 2017 were the two wettest years (784 mm, and 790 mm respectively) and 2019 was the driest year (522 mm) at least for the monitoring period (2015 – 2022). In Melbourne, 2016 recorded the highest rainfall (615 mm) during the monitoring period, whilst 2017 recorded relatively average precipitation (525 mm). In comparable with the Macarthur data, 2019 was the driest year (354 mm) in Melbourne.

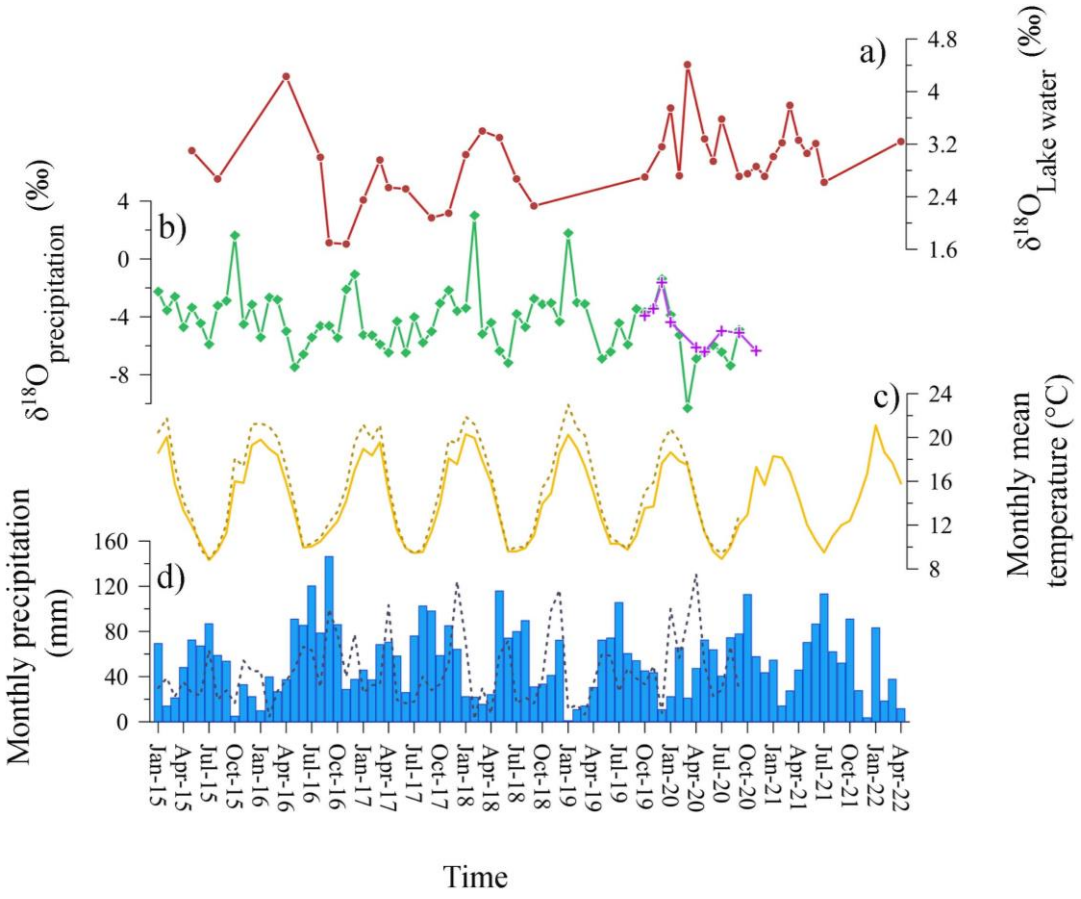

Figure 2. Modern climate and hydrology of Lake Surprise. a) Time-series of monthly $\delta^{18}O$ values in lake water; b) $\delta^{18}O$ values in monthly precipitation obtained from GNIP data at Melbourne (green diamonds) and monthly weighted mean of precipitation samples collected at Wannon Water treatment plant in Macarthur (purple cross); c) Monthly mean temperature values obtained from the Australian Bureau of Meteorology (SILO database) at Macarthur (solid line) and GNIP database at Melbourne (dotted line); d) Monthly precipitation (SILO database) at Macarthur (blue bars) and GNIP database at Melbourne (dotted line).

Despite these similarities, contrasting rainfall events have also been recorded between these weather stations, for instance, from June to August 2018 and July 2019 where Melbourne data recorded much higher rainfall compared to Macarthur data. Similarly in early 2020, BOM recorded lower rainfall at Macarthur compared to Melbourne data. However, these discrepancies are relatively minor compared to the overall seasonal variability observed between Macarthur and Melbourne (Figure 2c&d). As a result, there is a good possibility that both locations may experience precipitation with nearly comparable isotope variability. This is further clarified by the proximity between Macarthur and Melbourne isotope variability since October 2019 (Figure 2b). Therefore, the modern rainfall isotope record was extended by plotting Melbourne $\delta^{18}O$ in precipitation (GNIP data) alongside measured $\delta^{18}O$ values of rainfall at Macarthur (Figure 2b). (Appendix 2, Table IV).

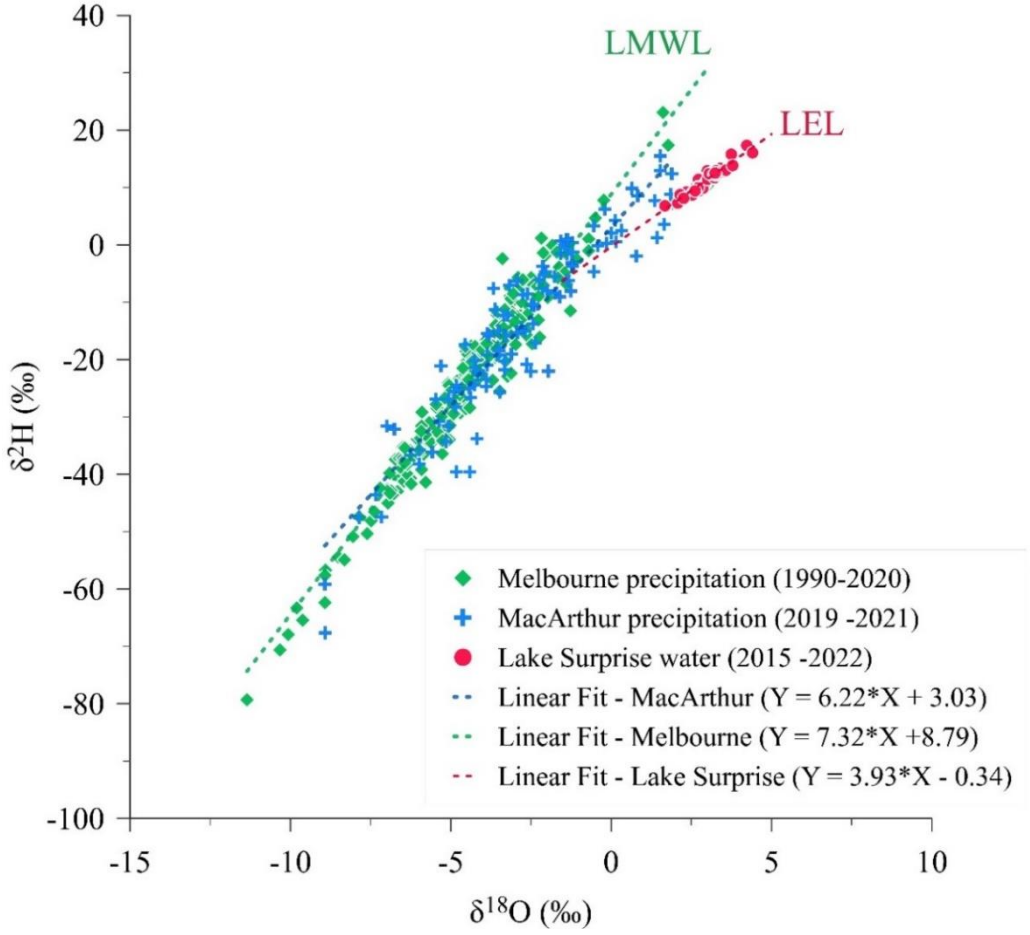

Figure 3. $\delta^{18}O$ vs $\delta^{2}H$ in modern lake waters and daily precipitation collected during the monitoring period (2015 – 2022) with monthly precipitation isotope data from the Melbourne GNIP station over the last 30 years. LMWL (Local Meteoric Water Line) and LEL (Local Evaporation Line) were developed with respect to Melbourne precipitation and Lake Surprise water isotopes.

Lake response to seasonal climate variability can be identified by comparing $\delta^{18}O$ in lake water ($\delta^{18}O_{LW}$) against $\delta^{18}O$ values in precipitation in the same time series. $\delta^{18}O_{LW}$ varies from 1.7 – 4.4‰, representing more negative values during cooler (winter) months and positive values during warmer (summer) months (Appendix 2, Table II). Overall, $\delta^{18}O_{LW}$ exhibits an upward linear trend towards the present day, especially since September 2020. $\delta^{18}O_P$ samples collected near Lake Surprise (October 2019-November 2020) are approximately similar to the concurrent GNIP values at Melbourne (Figure 2b). $\delta^{18}O_P$ values vary from -10.3 to 3‰ with lower values occurring after January 2020. The linear relationship between $\delta^{18}O$ and $\delta^{2}H$ defines both the local meteoric water line (precipitation) and local evaporation line (lake water) (Figure 3). The local meteoric water line is similar to the Global Meteoric Water Line (GMWL) defined by the equation $\delta^{2}H = 8(\delta^{18}O) +10$ (Craig, 1961). Isotope values of precipitation from the GNIP data at Melbourne represent the Local Meteoric Water Line (LMWL), with a slope of 7.32 and an R^2 value of 0.95. Likewise, a majority of the isotope values of daily rainwater samples collected near the lake site plots along the LMWL, albeit with a slightly lower slope and R^2 value (m =6.22, $R^2 = 0.88$) in the linear trend. This slight deviation in precipitation isotope data could be an effect of evaporation due to instrumental failures or during sampling procedures or may be due to isotope fractionation that occurred during transferring samples between containers for analysis (Chapter 2, Section 2.5.2). More positive lake water isotope values cluster along the Local Evaporation Line (LEL) with a slope of 3.97 ($R^2 = 0.92$) consistent with the effect of kinetic isotope fractionation during evaporation (Gibson et al., 2008, 2016).

Table 1: Modern lake water and cellulose oxygen isotope measurements and calculations of cellulose isotope enrichment ($\varepsilon_{cell\text{-}lw}$) and isotope fractionation factor ($\alpha^{18}O_{cell\text{-}lw}$) between cellulose and lake water (calculations are based on Equation 2)

Period of sample collection	Sample type	$\delta^{18}O_{cell}$	$\delta^{18}O_{LW}$	$\alpha^{18}O_{cell\text{-}lw}$	$\varepsilon_{cell\text{-}lw}$
Nov 2019 –Feb 2019	sediment	29.55	3.17	1.026	26.38
Feb 2020 – Jun 2020	sediment	30.51	3.5	1.027	27.01
Jun 2020 – Dec 2020	sediment	31.16	2.87	1.028	28.29
Jan 2021 – Mar 2021	sediment	28.53	3.33	1.025	25.20

$\delta^{18}O_{cell}$ values of modern sediments vary from 28.5 to 31.2‰ (Table 1). Seasonal isotope variation is lacking in the dataset due to the limited number of sample analyses and inconsistent

sample collection, due to the delays caused by the covid situation. For the validation of isotope enrichment in cellulose and fractionation, the average $\delta^{18}O_{LW}$ values measured within the modern sediment accumulation period are used. $\delta^{18}O_{LW}$ values vary from 2.87 to 3.5‰. Calculated $\alpha^{18}O_{cell\text{-}lw}$ and $\varepsilon_{cell\text{-}lw}$ values remained in the range of 1.025 to 1.028 and 25.2 to 28.3‰ respectively.

5.4.2 Sediment texture and chronology

Sediments in Lake Surprise are mainly blackish-grey in colour and are dominated by fine-grained clay-rich sediment. Except for the SUR-19-01 core (surface core), the entire sediment depth is enriched with relatively light-coloured fine laminations (~1 – 2 mm in thickness) (Ankor & Tyler, 2022).

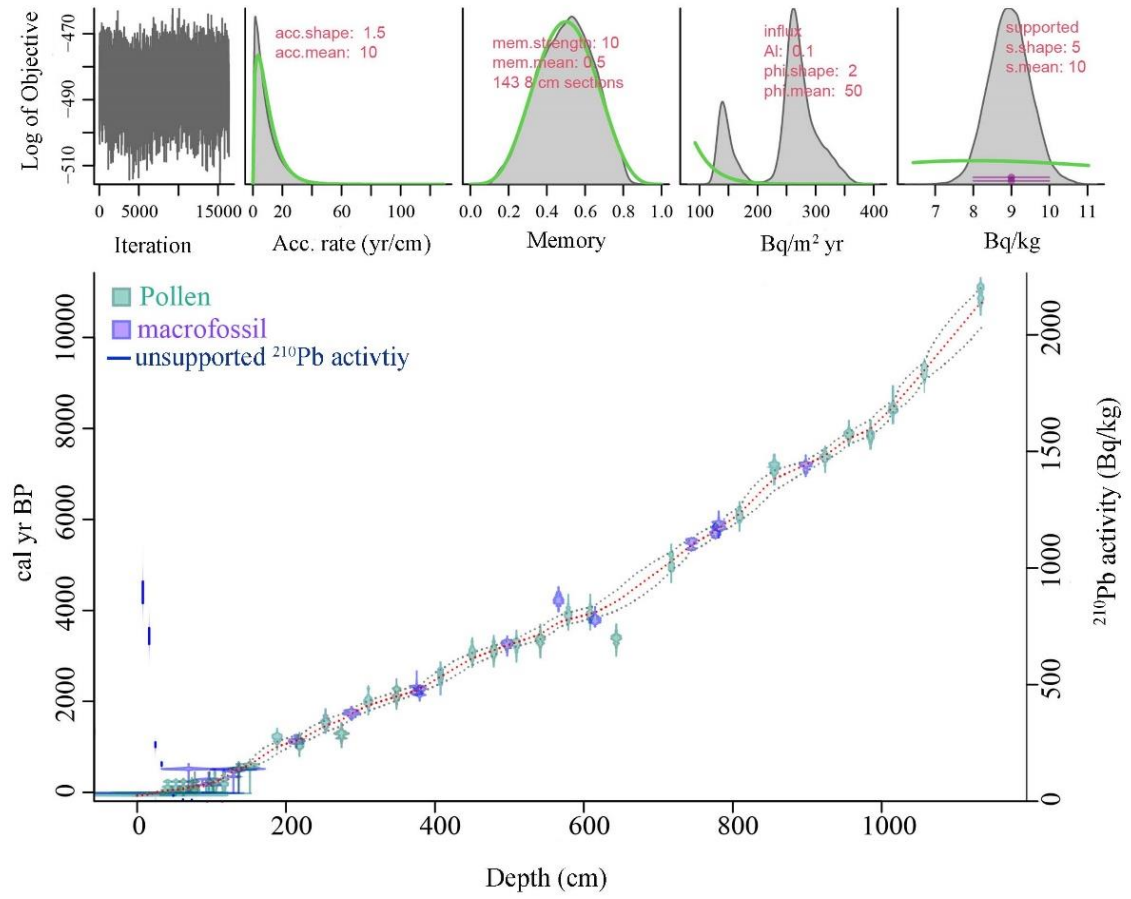

Figure 4. Age depth model developed for the Lake Surprise sediments using radiocarbon ages of pollen and macrofossil samples, unsupported ^{210}Pb activity measurements and Pu concentration in the "plum" package in R software

A detailed discussion of the age model development of Lake Surprise sediments can be found in Chapter 3 of this thesis. Considerably high unsupported/excess ^{210}Pb activity profile ranges from 901±47 Bq kg^{-1} at the surface to 5±1 Bq kg^{-1} at 107.4 cm reaching its background level (Chapter 3, Table 1). The total Pu concentration varies from 0.02 to 1.30 pg/g and the Pu isotope profile indicates maximum concentration, which is correspondent with the period of atmospheric nuclear fallout in the Southern Hemisphere (~1964) at around 21.7 cm (Chapter 3, Table 2) (Hancock et al., 2011; Harrison et al., 2021). Radiocarbon ages obtained from pollen and plant and macrofossil samples for the sediment record range from -13±3 to 10034±18 cal yr BP (Chapter 3, Supplementary data, Table 2.1). The final age model for the 1137 cm sediment depth profile indicates a median age of 10846 cal year BP with an approximate accumulation rate of 9.5 years/cm (Figure 4).

5.4.3 Carbon isotopes and C/N ratio of lake sediment

$\delta^{13}C_{org}$ values of organic matter of the composite record are concentrated within a range of -27.30 to – 32.4‰ (Appendix 4, Table II), indicating that organic carbon isotopes in Lake Surprise sediment remained depleted through Holocene. Carbon isotopes in modern sediments (collected from February 2020 until March 2021) vary between -24.8 to -27.7‰, indicating slight enrichment in $\delta^{13}C_{org}$ compared to the sediment core. The C/N ratio of sediment core samples varies between 7.1 and 14.5. Modern sediment exhibits a significant drop in the C/N ratio with values ranging from 5.4 – 6.1. In addition, these sediments represent a noticeably higher TOC content (18.3 – 42.5%) compared to TN (1.6 – 3.5 %) (Appendix 4, Table II). However, the nitrogen content is higher in modern sediment from around (4.6 – 6.6%), whereas carbon content remains nearly the same (Appendix 4, Table II). The majority of lake sediments from both SUR-19-01 and SUR-19-02 concentrate within or near the lacustrine algae dominant region in the $\delta^{13}C_{org}$ and C/N bi-plot (Figure 5).

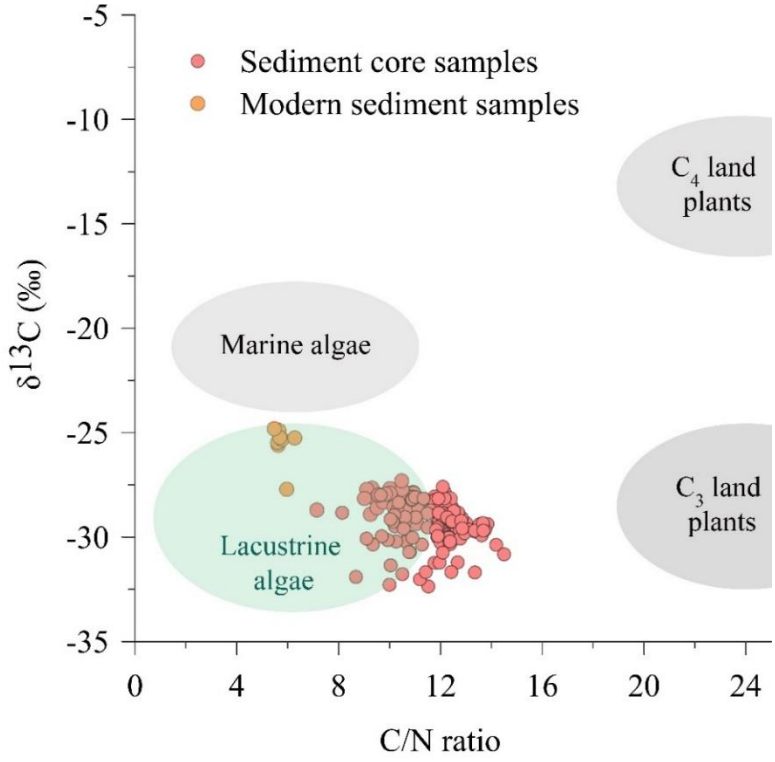

Figure 5. Distribution of $\delta^{13}C_{org}$ vs total organic carbon to total nitrogen ratio (C/N) of Lake Surprise sediments against the reference ranges established by Meyers, (1997).

5.4.4 Oxygen isotopes in lake sediment.

Cellulose $\delta^{18}O$ values ($\delta^{18}O_{cell}$) in the sediment record range from 26.87 to 31.66‰ from approximately -61 to 10849 cal yr BP, equivalent to lake water oxygen isotope values ranging from -1.96 to 3.61‰ (Appendix 4, Table I). The majority of negative $\delta^{18}O_{LW}$ values occurred prior to 5000 cal yr BP and more enriched values towards the late Holocene (Figure 6a). $\delta^{18}O_{cell}$ in Pinewood illustrate relatively smaller deviation (±0.4) with values varying from 28.99 – 30.18‰. However, cellulose powder illustrates considerable bias between different batches (27.17 – 29.84‰) (Supplementary data, Section 1) A notable decrease in $\delta^{18}O_{LW}$ values are observed in periods approximately from 10850 – 10000, 7400 – 7000 and 5600 – 4500 cal yr BP, dropping approximately by 2‰ compared to the Holocene average of 2.24±0.87‰. Except for minor depletions(≤0.8‰) recorded approximately ~9800 – 9200 cal yr BP and 8500 cal yr BP, other periods illustrated an enrichment $\delta^{18}O_{LW}$ isotopes with the majority of data fluctuating within the Holocene average value (Figure 6a).

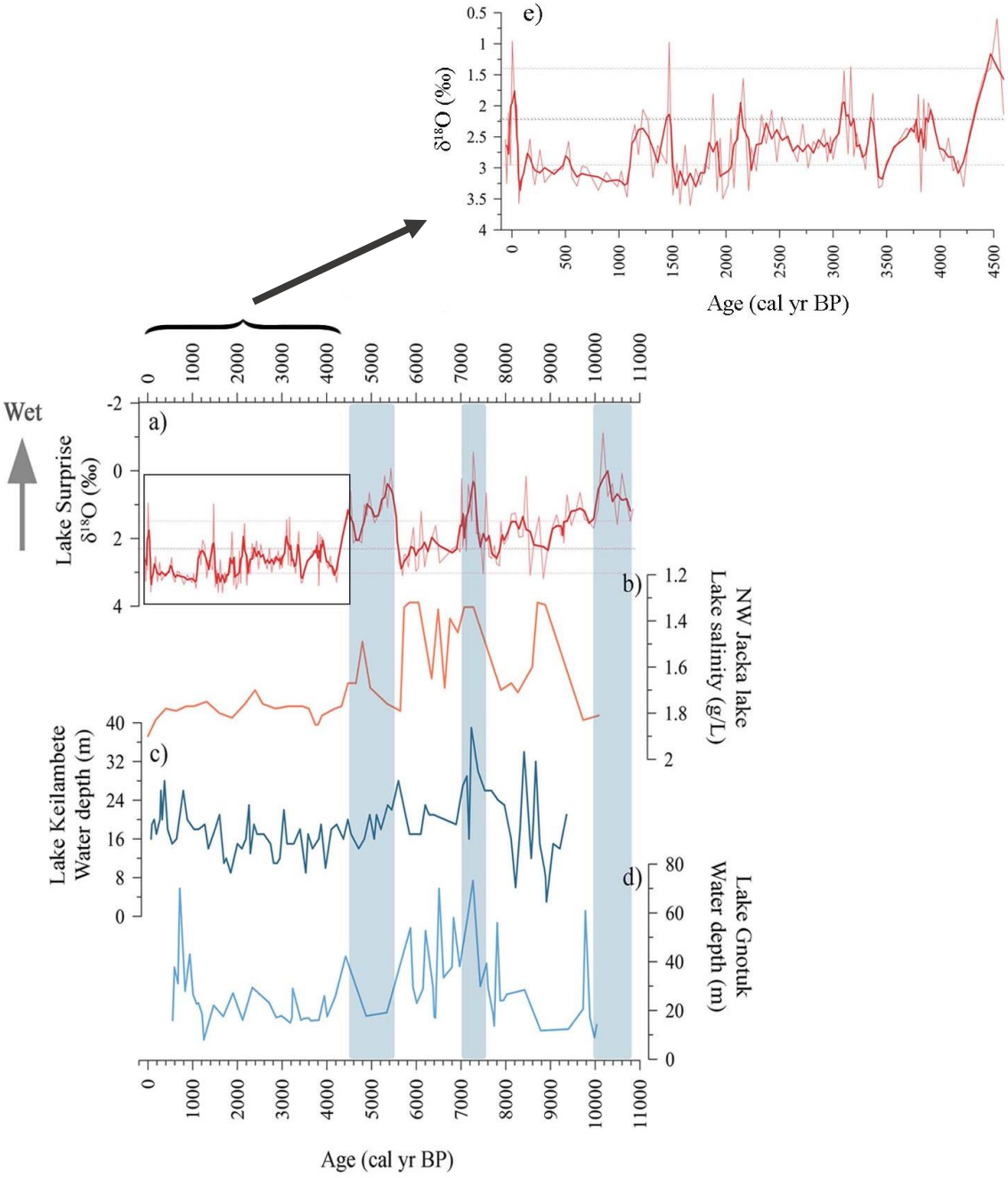

Figure 6. Comparison of Lake Surprise record with previously published records from western Victoria a) cellulose inferred lake water $\delta^{18}O$ at Lake Surprise (running mean of 3). b) Reconstructed lake water salinity (TDS) inferred from ostracod taxonomic assemblages at NW Jacka Lake (Kemp et al., 2012). c) Grain size inferred lake water depth at Lake Keilambete and d) Lake Gnotuk (Wilkins et al., 2013). e). Zoomed-in section of the Lake Surprise $\delta^{18}O$ record from the present day to 4500 cal yr BP. The y-axis of figures a) and b) are reversed to represent wetter periods in all the records upward. Three lines in figures a) and e) represent the range of Holocene average of $\delta^{18}O$ values at Lake Surprise (2.24 ±0.88).

$\delta^{18}O_{LW}$ values started to shift above the Holocene average around 4500 cal yr BP and remained high throughout the last 4500 years. Within two hundred years (4530 – 4220 cal yr BP), lake water isotopes represent their highest transition with a significant increase by ~2.7‰. Thenceforward, a minor decrease in $\delta^{18}O_{LW}$ values prevailed until around 2100 cal yr BP, along with intervals of higher $\delta^{18}O$ values observed around 3900, 3500 and near 2400 cal yr BP, however, these depletions are relatively minor events compared to the depletions observed during early-mid Holocene. The highest rise in $\delta^{18}O_{LW}$ values (approximately by 1‰) is mainly constrained around 2000 – 1700 cal yr BP (Figure 6e). Following the depletion of isotope values from ~ 1500 – 1000 cal yr BP, $\delta^{18}O_{LW}$ variability remained high and nearly consistent throughout the last millennium, except for a few years around 3.4 cal yr BP (~1946 CE) (Figure 6e).

5.5 Discussion

5.5.1 Modern hydrology of the Lake Surprise

Oxygen isotope composition of lakes varies as a function of multiple factors including changes in $\delta^{18}O$ inflowing water (precipitation, surface water and groundwater) and the subsequent evaporation of lake water (Leng and Marshall, 2004; Jones and Imbers, 2010; Steinman et al., 2010; Wu et al., 2015b; Lacey and Jones, 2018; Li et al., 2020). In closed lakes, where an effective outflow stream is absent, evaporative water loss tends to dominate both the hydrology and isotope geochemistry of lake waters (Henderson and Shuman, 2009; Horton et al., 2016; Tyler et al., 2022). Enrichment of $\delta^{18}O$ in lake water bodies, due to the progressive removal of lighter molecules during evaporation leads to relatively higher $\delta^{18}O_{LW}$ measurements. This is common in closed lakes in arid and semi-arid regions where water loss happens through evaporation (Leng and Marshall, 2004; Gat, 2010; Jones et al., 2016; Shi et al., 2017). Over six years of monitoring (2015 – 2022), $\delta^{18}O_{LW}$ at Lake Surprise consistently exceeded concurrent $\delta^{18}O_P$ by >3‰, clearly indicating that evaporation is an important driver of the isotope composition of the lake (Figure 3). Periods of high $\delta^{18}O_{LW}$ and $\delta^{18}O_P$ values correspond with relatively dry, summer months demonstrating the importance of the precipitation/evaporation (P/E) ratio on the lake water isotope mass balance (Jones et al., 2005; Dean et al., 2014). This is further highlighted by the characteristic local evaporation line (LEL) in $\delta^{18}O$ vs. $\delta^{2}H$ space (Figure 4) when compared to a local meteoric water line (LMWL) which is characteristic of both local and rainfall (Figure 4) (Leng et al., 1999; Leng & Marshall, 2004; Wu et al., 2015; Gibson et al., 2016; Jones et al., 2016; Hua et al., 2019). As a consequence, it is realistic to

interpret long-term changes in $\delta^{18}O_{LW}$ as being predominantly driven by changes in P/E, although changes in $\delta^{18}O_P$ may also have an effect.

5.5.2 Sources of organic matter to the sediments of Lake Surprise

Prior to the application of oxygen isotopes in cellulose as a palaeo-hydrological proxy, it is necessary to understand the origins of the organic matter preserved within the sediments. To this end, the ^{13}C isotope composition of lake sediment organic matter ($\delta^{13}C_{org}$) and the organic C/N elemental ratio have long been used to differentiate between terrestrial and lacustrine-derived productivity in the lake basin (Meyers & Ishiwatari, 1993; Hassan et al., 1997; Meyers, 1997; Meyers & Lallier-Vergès, 1999; Leng & Marshall, 2004; Torres et al., 2012). Higher $\delta^{13}C_{org}$ values indicate enhanced productivity in the lake basin due to the preferential uptake of ^{12}C by aquatic photoautotrophs. However, lower $\delta^{13}C_{org}$ can also reflect the higher influx of C_3 plant-derived terrestrial organic matter from the surrounding watershed (Hassan et al., 1997; Meyers & Lallier-Vergès, 1999). C/N ratios provide an additional line of evidence. Although there are some exceptions in nitrogen-limited environments (Cadd et al., 2018; Maxson et al., 2021), low C/N ratios (<20) are usually indicative of a dominant algal or bacterial contribution to sediment organic matter, due to the higher relative abundance of nitrogen-rich proteins, amino acids and pigments in simple algae and heterotrophs, whereas higher vascular plants tend to produce tissue enriched in carbon-bearing cellulose or lignin (Meyers, 1997; Meyers and Lallier-Vergès, 1999; Meyers and Terranes, 2002; Leng et al., 2006). Consequently, the $\delta^{13}C$ and C/N of Lake Surprise sediments imply a dominant aquatic algal source of organic carbon.

The lake sediment values differ slightly from modern sediment trap samples, possibly indicating enhanced lake productivity in recent years compared to pre-colonial conditions (Barr et al., 2014). This is supported by the significant increase in nitrogen content (average of 5.4%) in modern sediments compared to the sediment core (average of 2.5 – 3%), further suggesting increased nutrient input, although a shift away from aquatic plant contributions, or the preferential loss of N during sediment diagenesis could also explain this trend (Lehmann et al., 2002). Nevertheless, the $\delta^{13}C$ and C/N ratios of the sediment core samples consistently point to a dominant aquatic source of organic matter in the Holocene sediments, with a relatively small contribution of terrestrial organic matter. This contrasts with data from the last glacial-

interglacial transition (30-10 ka) at Lake Surprise, where (Falster et al., 2018) report higher C/N ratios, indicative of a greater terrestrial contribution at that time.

5.5.3 Oxygen isotope fractionation into modern cellulose in Lake Surprise

Several studies have investigated the oxygen isotope fractionation between water and cellulose, in both higher plants and algae. In the majority of cases, a virtually consistent isotope fractionation factor has been identified, namely alpha (α) = 1.028±0.003 (Sternberg et al., 1984; Wolfe et al., 2001; Street-Perrott et al., 2018; Savage et al., 2021). Evaluation of the seasonal variability of $\alpha^{18}O_{cell\text{-}lw}$ values using modern sediment and lake water measurements correspond well with the commonly applied value range of 1.028±0.003 (Table 1), suggesting that cellulose-water isotope fractionation in Lake Surprise remained nearly consistent throughout the monitoring period, with an oxygen isotope enrichment in cellulose ($\varepsilon_{cell\text{-}lw}$) approximately between 25 – 28‰ (Table 1). Previous studies have suggested that lower values of $\varepsilon_{cell\text{-}lw}$ from the accepted value range might indicate contamination by minerogenic material (clay, silicates) within the extracted cellulose since this has the potential to introduce oxygen from mineral hydration water (Savage et al., 2021). However, given the highly organic nature of the samples studied here, as well as their collection in the centre of the lake, the chances of substantial silicate contamination should be relatively low. In addition, the extraction method used here involves centrifugation for 25 – 30 minutes, which should have been more than sufficient to separate any suspended particles from the cuprammonium before the precipitation of the cellulose. Therefore, the small deviation from the expected $\varepsilon_{cell\text{-}lw}$ observed here is unlikely to be a consequence of silica contamination.

5.5.4 Holocene hydroclimate change in Lake Surprise

The Lake Surprise lake water isotope record derived using cellulose oxygen isotopes resolves hydroclimate variability at approximately 50-year resolution and exhibits a clear trend through the Holocene, in particular by defining two distinct episodes of hydroclimate change: a more variable period of generally wetter climates in the early-mid Holocene (~10,850 – 4500 cal yr BP) and a drier and less variable period from ~ 4500 cal yr BP to present-day.

5.5.4.1 Early-Mid Holocene (~10850 – 4500 cal yr BP)

Most notable in the Lake Surprise $\delta^{18}O_{LW}$ record are three periods of distinctly low $\delta^{18}O_{LW}$ between ~10850 – 4500 cal yr BP suggestive of centennial-scale periods of above average P/E compared to modern climate (Figure 6a). Several previous studies have suggested that the early Holocene (the period before 6000 cal yr BP) in south-eastern Australia was relatively wet compared to the late Holocene (Gingele et al., 2007; Donders et al., 2008; Fitzsimmons & Barrows, 2010; Kemp et al., 2012; Petherick et al., 2013). Unlike most of those studies, however, the Lake Surprise record suggests that the early Holocene consisted of three distinct multi-decadal to centennial-scale periods of wet climate, interspersed with periods not dissimilar to modern hydroclimate (Figure 6a). The earliest wet phase is recorded from ~10850 to 10000 cal yr BP with $\delta^{18}O_{LW}$ reaching its lowest value at ~10200 cal yr BP. Unfortunately, the comparison of this period remained challenging given that this period is not well captured in majority of the western Victorian studies.

A moisture decrease is suggested by increasing $\delta^{18}O_{LW}$ values until ~7500 cal yr BP, but with relatively short periods of lower $\delta^{18}O_{LW}$ approximately between 9800 to 9400 cal yr BP and at ~8500 cal yr BP, suggesting the occurrence of brief wet intervals (Figure 6a). Even though, this warming phase is not well explained in other lake hydroclimate records from western Victoria, certain similarities can be seen, especially related to short wet intervals, albeit with varying resolution and chronological precision (Figure 6). The sediments of Lakes Gnotuk and Keilambete, approximately 100 km to the east of Lake Surprise, were used to infer lake level high stands at around 9780 cal yr BP and ~8700 cal yr BP, respectively, based on changes in sediment grain size, calibrated against recent observations (Wilkins et al., 2013). The sediments of NW Jacka Lake, approximately 170 km north-west of Lake Surprise illustrated a decrease in salinity (~1.8 to 1.3 g L^{-1}) from ~8800 and 8700 cal yr BP and also suggestive of an increase in P/E at that time (Kemp et al., 2012), which is not apparent in Lake Surprise record. Yet, the Lake Surprise warming is associated with the significant salinity increase observed ~8600 – 8200 cal yr BP in NW Jacka lake and water level decline in Lake Gnotuk from ~9600 – 8500 cal yr BP (Kemp et al., 2012; Wilkins et al., 2013). The relative wet period that existed before 9000 cal yr BP, is also evident from modelled water depths in western Victorian crater lakes (Lakes Keilambete, Gnotuk and Bullenmerri) (Jones et al., 1998).

Considering the broader south-east Australian region, studies from Lynds Cave in Tasmania recorded a relatively unstable climate with increased effective precipitation existing from

~9000 – 8600 cal yr BP (Xia et al., 2001). similarly, a cold phase existed from 9500 – 7500 cal yr BP as evidenced by previous studies based on the sediment cores obtained from the Murray Canyon site (MD-2611) (Gingele et al., 2007; Moros et al., 2009). Similarly, Lake George, further inland from Lake Surprise is also illustrated permanent lake conditions prevailed from ~10000 – 8000 cal yr BP (Fitzsimmons & Barrows, 2010). Another consistent warming phase or a period of decreasing P/E is identified from around 7000 cal yr BP to 5600 cal yr BP. Similarly, this period is also poorly represented in other regional studies (Wilkins et al., 2013). Increased water depth and salinity in both Lakes Gnotuk and NW Jacka Lake are suggestive of ongoing wet climates during this period. However, Lake Keilambete does record a decrease in water depth during this period (Jones, 1998; Wilkins et al., 2013). Few studies from elsewhere in the region have identified that climate was more variable during this period based on multiple climate proxies (grain size variation, speleothem records, lake salinity etc.) (Harrison, 1993; Gell, 1998; Xia et al., 2001; Stanley and De Deckker, 2002; Gingele et al., 2007; Gouramanis et al., 2013).

Many of these records have likely identified the early-mid Holocene period in south-east Australia as a typically wet period. Previous studies suggested that these discrepancies between regional comparisons are mainly due to the obvious lower resolution and chronological uncertainties in these records (De Deckker, 2022). However, the most recent study from off-shore southern Australia demonstrated the existence of a period of relatively warm and wet that expanded from ~8200 – 5500 cal yr BP, which is named the "Holocene Hypsithermal" or a period when the temperatures were warmer than today (De Deckker, 2022). Enrichment of lake water isotopes in Lake Surprise from around 9000 – 5500 cal yr BP, appeared to align with this warming phase. However, $\delta^{18}O_{LW}$ composition alone cannot provide sufficient evidence for a strong interpretation. Even though this is not reflected in many western Victorian studies, this period corresponds with the warmest and wettest period recorded in Lynds Cave, Tasmania (Xia et al., 2001). This is further supported by several other distal records (e.g. Antarctica) that infer a relatively warm/wet environment (Atahan et al., 2015; Parrenin et al., 2013).

The second wettest period is recorded in Lake Surprise between 7400 to 7000 cal yr BP, along with relative depletion of $\delta^{18}O_{LW}$. This period of relatively high inferred P/E is in agreement with evidence that lakes Gnotuk and Keilambete reached their maximum water depth at ~7200 cal yr BP and with another notable decrease in ostracod-inferred salinity at NW Jacka Lake (Bowler and Hamada, 1971; Bowler, 1981; Jones et al., 1998; Kemp et al., 2012; Wilkins et al.,

2013). This is further illustrated by Jones et al., (1998), who suggested that Lakes Bullenmerri and Gnotuk were overflowing at least by 7000 cal yr BP. Concurrent evidence of a steady increase in precipitation and lower mean annual temperature is provided from Lynds Cave Tasmania based on isotopes and the growth rate of stalagmites (7400 – 7000 cal yr BP) (Xia et al., 2001). Similarly, this wet phase is supported by the low occurrence of palaeo-fires and an increase in moisture-induced vegetation elsewhere in the region (Hope et al., 2004; Fletcher & Moreno, 2011; Stahle et al., 2016; Mariani & Fletcher, 2017).

The final wet phase at Lake Surprise initiated ~5600 cal yr BP and remained wet until 4800 cal yr BP, followed by a short wet event that occurred around 4500 cal yr BP. this wet phase was longer than earlier wet intervals. This distinct wet period is not well-defined in western Victorian records, where Lakes Keilambete and Gnotuk suggest that the lake levels had already declined by this point. At NW Jacka Lake, a brief period of lower salinity is inferred for around 4800 cal yr BP, which broadly corresponds with the much longer wetter period inferred for Lake Surprise (Figure 6). However, this interpretation is supported by evidence of decreased fire intensity and increased effective precipitation from studies in Tasmania since 6000 cal yr BP (Mooney et al., 2011; Gliganic et al., 2014; Mariani and Fletcher, 2017). Few records suggested a lowering in both temperature and precipitation leading to a warm and wet climate during this period (Xia et al., 2001; Moros et al., 2009). Many terrestrial records have not captured this brief cooling phase, which is most likely a result of low resolution and poor chronology. Instead, a range of studies from the region has recorded the sharp transition from a relatively wetter environment to progressive drying around 5000 cal yr BP (Fletcher and Moreno, 2012; Kemp et al., 2012; Gouramanis et al., 2013; Wilkins et al., 2013; Mariani and Fletcher, 2017). However recent data on the planktonic foraminifer assemblage and alkenone-derived sea surface temperatures (SST) from offshore Southern Australia suggested the occurrence of a La-Niña-like ENSO event corresponding with this wet period (5000 – 4500 cal yr BP) (Perner et al., 2018).

5.5.4.2 Mid-Late Holocene (4500 cal yr BP – present day)

Over the last 4500 years, higher than average $\delta^{18}O_{LW}$ values at Lake Surprise suggest an overall period of prolonged drier and less variable climate (Figure 6). While several studies have suggested that this period was generally drier in south-eastern Australia, many of those records have also implied that the late Holocene was more variable, particularly with the intensification

and high amplitude changes in ENSO events (Dodson, 1974; Mckenzie and Kershaw, 1997; Calvo et al., 2007; Gingele et al., 2007; Kemp et al., 2012; Saunders et al., 2012; Gouramanis et al., 2013; Wilkins et al., 2013; Barr et al., 2019). Even though, increased aridity at Lake Surprise corresponds with the ENSO variability, a more stable climate may indicate that the influence of ENSO was masked by SWW/IOD changes (poleward shift of SWW and more positive IOD events). Identification of episodic dry/wet periods is complicated due to the lesser fluctuations in $\delta^{18}O_{LW}$ compared to the period before 5000 cal yr BP. Therefore, an enlarged section of the last 4800 years (Figure 6e) is shown for a clear representation of isotope variability.

With a steady rise in $\delta^{18}O_{LW}$ values from ~4500 to 4250 cal yr BP, the prolonged dry phase in Lake Surprise commenced around 4500 cal yr BP (Figure 6e). This increase in $\delta^{18}O_{LW}$ at Lake Surprise is coincident with the water level decline at Lake Gnotuk and the start of an extended period of high salinity at NW Jacka Lake from ~4600 cal yr BP, alongside driest conditions around 4200 cal yr BP. (Kemp et al., 2012). The onset of drier conditions during this period is in agreement with lake-level depression at Lakes Gnotuk, Bullenmerri and evidence of aragonite to dolomite transition in sediments at Lake Keilambete (~4300 – 4200 cal yr BP) that relate to a long-term decline in P/E ratio (Jones et al., 1998). By contrast, the onset of drying occurred much earlier at Lake Keilambete at ~5600 cal yr BP, continuing through to 4200 cal yr BP (Kemp et al., 2012; Wilkins et al., 2013). Several records from the broader region have identified intense aeolian activity after 4000 cal yr BP and reduced river discharge with the onset of drier conditions (Stanley & De Deckker, 2002; Cohen & Nanson, 2007; Gingele et al., 2007). Similarly, a series of studies from Tasmania recorded evidence of increased fires and reduced wet, rainforest vegetation from around 4500 cal yr BP (Fletcher et al., 2014; Stahle et al., 2016, 2017; Beck et al., 2017; Mariani & Fletcher, 2017; Mariani et al., 2019).

After ~4200 cal yr BP, lake water values shifted towards the Holocene average, indicating a relatively moderate to dry climate that persisted until ~2000 cal yr BP, with the exception of extreme dry events observed around 3800 and 3500 cal yr BP respectively. However, identification of these periods is difficult in other studies (figures 6b-6d), due to the scarcity of temporal sampling resolution, for instance, NW Jacka lake exhibits nearly constant salinity through this period with a slight reduction in salinity near 2400 cal yr BP (Kemp et al., 2012). The relatively lower water level is illustrated in both the Lakes Keilambete and Gnotuk with lake level minima observed at ~3500 cal yr BP at Lake Keilambete and ~3600 cal yr BP at

Lake Gnotuk (Wilkins et al., 2013). This moderate to dry period is further supported by previous studies from western Victorian lakes that recorded reasonably average lake levels alongside fluctuating salinity conditions (Bowler, 1970, 1981; De Decker, 1982; Chivas, 1985, 1993; Jones et al., 1998; Gouramanis et al., 2010). Reasonably moist conditions that prevailed during this period are supported by several studies elsewhere in the region that suggests increased precipitation coupled with cooler summer temperatures (Saunders et al., 2012; Thomas et al., 2022). Further, increased aeolian activity recorded in Blue Lake sediments around 3500 cal yr BP, along with moderate climate conditions observed until ~2500 cal yr BP agrees with the Lake surprise isotope record (Stanley & De Deckker, 2002).

More extensive dry intervals are recorded in Lake Surprise between 2000 – 1500 cal yr BP, with a considerable increase in lake water $\delta^{18}O$ at around 2100 cal yr BP and from 1700 – 1600 cal yr BP. Lakes Keilambete and Gnotuk recorded late Holocene lake level minimums of ~1800 and 1300 cal yr BP correspondingly. It is also evident that during this period trees were present along the lower margins of the catchment areas of Lakes Keilambete and Gnotuk (Bowler and Hamada, 1971; Bowler, 1981; Jones et al., 1998, 2001; Gouramanis et al., 2013). However, this extensive drying is not evident in the NW Jacka lake salinity record (Kemp et al., 2012). In addition, lowering of water depth recorded in Lake George between 2400 – 900 cal yr BP, reduction in wind strength (2300 – 1800 cal yr BP) over Blue Lake in south-east NSW and gradual precipitation decline in Rebecca Lagoon in Tasmania are consistent with Lake Surprise drying (Stanley & De Deckker, 2002; Fitzsimmons & Barrows, 2010; Saunders et al., 2012). Lake Surprise experienced a short period of moisture increase with subsequent depletion of lake water values between 1500 – 1100 cal yr BP. Even though Lake Keilambete exhibits a marginal increase in water depth, Lake Gnotuk reaches a lake level minimum of ~1250 cal yr BP (Wilkins et al., 2013). Further, NW Jacka lake represents a steady increase in salinity since ~1300 cal yr BP, demonstrating synchronous drying (Kemp et al., 2012). However, the depletion of the $Sr/Ca_{(lake\ water)}$ ratio and $\delta^{18}O$ in ostracods in Lake Keilambete indicates a lack of ostracod preservation in accordance with this interpretation (Wilkins et al., 2013). Positive moisture balance existed before 1300 cal yr BP was recognised by low diatom-inferred conductivity measurements recorded at Lakes Surprise and Elingamite (Barr et al., 2014). Similarly, (Cook et al., 2000) recorded that the climate was stable and cooler during this period.

According to lake water oxygen isotopes, the lake experienced a relatively drier, more stable climate over the last millennium compared to previous periods. The sharp increase in Lake

Gnotuk's water depth during this period is mainly due to inflow from Lake Bullenmerri (Jones et al., 1998; Wilkins et al., 2013). A slower rise in water depth and the presence of aragonite laminae in Lake Keilambete illustrate warm and wet climate prevailed at the beginning of the Last millennium (Wilkins et al., 2013). However, the gradual salinity increase in NW Jacka Lake indicates extended drying in the region throughout the last millennium (Kemp et al., 2012). Similarly, multiple late Holocene climate reconstructions available for the region explained the gradual increase in aridity through the last millennium. According to Gergis et al., (2016), 800 – 600 cal yr BP, was the warmest period over the last millennium before the post-European period. Increased laminae deposition in lakes Keilambete and Gnotuk, precipitation variability recorded in Rebecca lagoon and aeolian deposition from Blue lake indicate a generally warm and wet climate existed during the early years of the last millennium (Stanley & De Deckker, 2002; Saunders et al., 2012; Wilkins et al., 2013). Increased climate variability recorded in Lake Surprise, during this period was recognised for the more frequent occurrence of extreme droughts than experienced in the historical period (Barr et al., 2014). Further, this study agrees with elevated temperatures documented in Tasmania before 500 cal yr BP (Cook et al., 2000; Saunders et al., 2013; Thomas et al., 2022). According to previous studies from the region, the period between 500 – 200 cal yr BP corresponds with the timing of the Little Ice Age (LIA) (Cook et al., 2000; Yan et al., 2011; Saunders et al., 2012, 2013; Barr et al., 2014; Gergis et al., 2016; Dixon et al., 2019). Even though our record does not highlight LIA clearly, (Barr et al., 2014) have identified corresponding evidence from Lake Surprise during 500 – 70 cal yr BP. This corresponds with the water level rise at Lake Keilambete from ~500 to late 200 cal yr BP (Wilkins et al., 2013). The absence of data from Lake Gnotuk and lower sampling resolution from NW Jacka Lake limit any detailed comparison for this period.

In the period between 100 cal yr BP and the present day, Lake Surprise exhibits an interval of increased aridity and a subtle transition to a considerable wet period around the early 20th century followed by gradual drying towards the present day. Even though there are discrepancies related to increased moisture phase ~45 – 25 cal yr BP (1900 -1926 CE), lake drying recorded at the beginning and the end the of last 100 years coincide with decadal-scale major historical droughts that occurred from 1895 – 1902 CE (Federation Drought) and 1997 – 2010 CE (Millennium Drought) (Barr et al., 2014; Scroxton et al., 2020). Further, a generally drier climate existed during this period agrees with nearby crater lakes that indicate a lowering in P/E ratio, an increase in salinity, gradual decline in lake level since 110 cal yr BP (Jones et

al., 1998; Jones et al., 2001; Kemp et al., 2012; Wilkins et al., 2013). Similarly, increased drying over the last century is evident in other studies elsewhere in the region (Fitzsimmons & Barrows, 2010; Saunders et al., 2012; Dixon et al., 2019; Scroxton et al., 2020). Intervals of increased moisture are nearly consistent with high precipitation events recorded from the early to mid-20th century, particularly around 1945 CE (Australian Bureau of Meteorology, 2021; Gergis et al., 2012; Scroxton et al., 2020). Lake drying was intensified in western Victoria by the anthropogenic influence after European settlement (Tibby et al., 2006; Leahy et al., 2010; Barr et al., 2014). As a consequence, most of the climate-related lake responses were undermined in previous studies due to the impacts of vegetation and landscape clearance (Wilkins et al., 2013). However, Lake Surprise lacks any evidence of human settlement due to its geographical location and geomorphological features. Besides, the lake water oxygen isotope record for the last century shows a close relationship with the instrumental climate data at the nearest rain gauge station (Macarthur). As recorded in Barr, (2010), the disappearance of diatom species, *Discostella pseudostelligera* suggests lake level decline soon after 80 cal yr BP (1870 CE) and dominance of diatom species *Cysclostephanos dubius* and *Cyclotella meneghiniana* after 10 cal yr BP (after 1940 CE), correspond with the increase in rainfall anomaly. Such indications may demonstrate the Lake's response to regional climate over the last century.

5.5.4.3 Influence of major climate drivers in the western Victorian hydroclimate variability

To elucidate the potential drivers of climate variability in Lake Surprise, the oxygen isotope record was compared with long-term climate reconstructions that exhibit the behaviour of ENSO, IOD, SWW and solar variability through the Holocene. To infer the comparison with SWW variability, a record of SWW intensity developed using diatom-inferred salinity (DI conductivity) and minerogenic input into Emerald lake Macquarie Island, which directly lies within the southern westerly wind belt was utilised (Saunders et al., 2018). This was further supported by SWW reconstruction using planktonic foraminifer assemblages from offshore southern Australia (Murray Canyons) (Moros et al., 2009). ENSO variability was implied using the most commonly cited record of Holocene ENSO events at Laguna Pallcacocha from southern Ecuador (Moy et al., 2002), which generally corresponds with the lake level and precipitation reconstruction at the El Junco Lake, Galapagos Islands and also with the record of rainfall variability from North Stradbroke Island, south-eastern Queensland all of which are considered to be highly sensitive to Pacific Ocean driven ENSO variability (Conroy et al.,

2008; Barr et al., 2019). Previous work on the IOD has mostly concentrated on its current behaviour, and little is known about its historical variability outside of the observational record (Kwiatkowski et al., 2015). Therefore, Lake Surprise $\delta^{18}O_{LW}$ record was correlated with the Sea surface temperature (SST) anomaly reconstruction based on fossil coral Sr/Ca ratio and precipitation record derived from δD and $\delta^{13}C$ of plant wax from north-west Sumatra, which is among very few long-term records available for the region (Abram et al., 2009; Niedermeyer et al., 2014). To understand the influence of solar activity, the total solar irradiance (TSI) reconstruction derived from the cosmogenic isotope ^{14}C was applied in this study (Vieira et al., 2011).

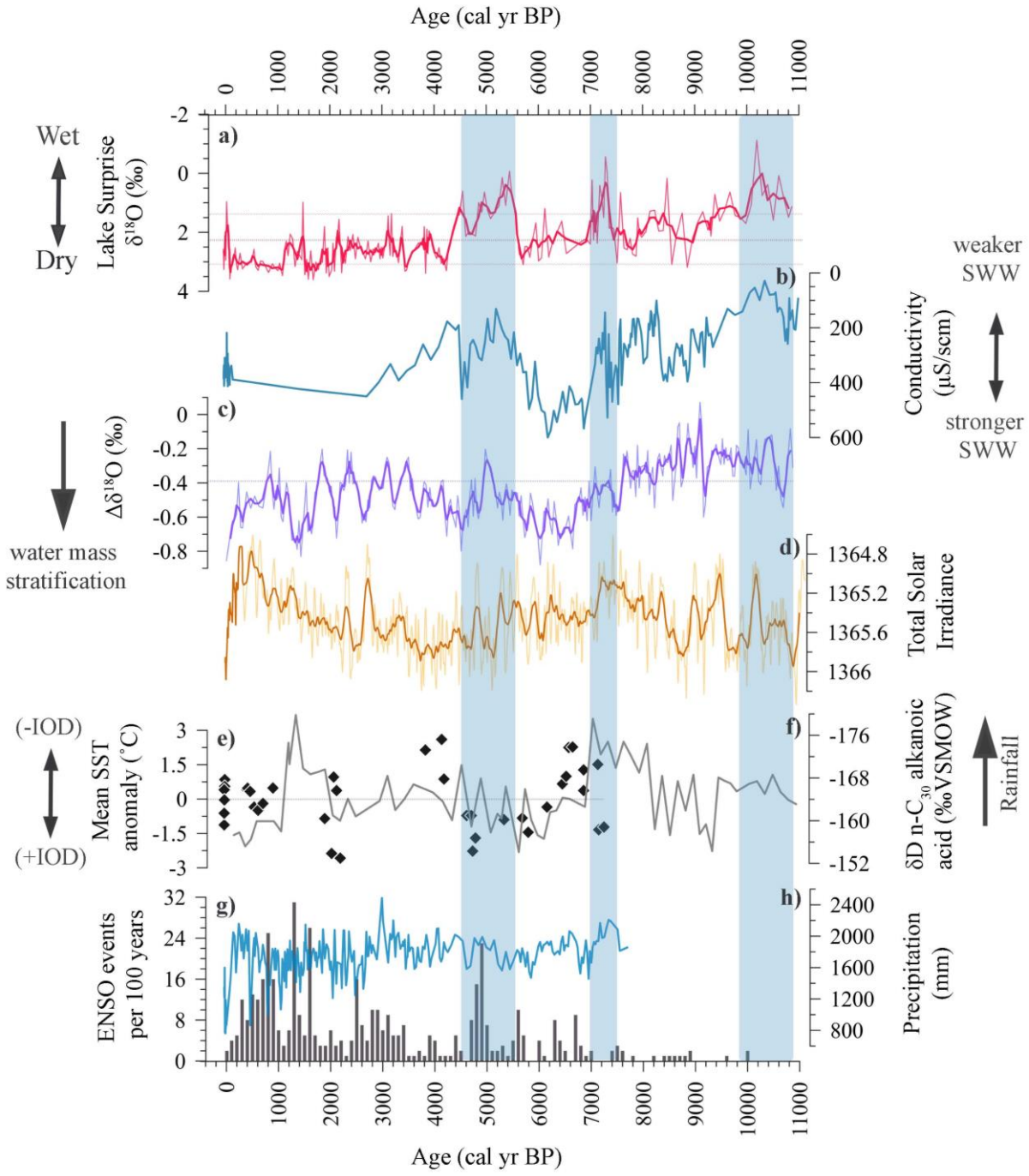

Figure 7. Comparison of a) cellulose inferred lake water $\delta^{18}O$ at Lake Surprise with b). Diatom-inferred conductivity reconstruction at Lake Emerald, Macquarie Island (Saunders et al., 2018). c). Water mass stratification developed using the difference between $\delta^{18}O$ values of planktonic foraminifer species in Murray Canyon sediments, offshore South Australia (core MD03-2611). The line across (-0.42) represents the Holocene average. (Moros et al., 2009). d). Reconstruction of the TSI for the Holocene (Vieira et al., 2011). e). Mean Sea Surface Temperature (SST) reconstruction based on Sr/Ca analyses of fossil corals from Sumatra, Indonesia (Abram et al., 2009). f) δD record of the n-C_{30} alkanoic acids extracted from plant waxes at the Nias basin off NW Sumatra (Niedermeyer et al., 2014). g). ENSO event

reconstrcution at Laguna Pallcacocha (Moy et al., 2002). h). Precipitation reconstruction derived using carbon isotopes of fossil leaves at Swallow lagoon, south-eastern Queensland (Barr et al., 2019). The y-axis of figures c and e are reversed to represent wet periods of all records downward. Three lines in figure a represent the Holocene average range of $\delta^{18}O$ values at Lake Surprise (2.24 ±0.88).

In particular, the Lake Surprise $\delta^{18}O_{LW}$ record exhibits marked similarity to the changes in SWW intensity as recorded in Saunders et al., (2018), particularly during the distinct wet intervals recorded at Lake Surprise. It has been suggested that the relative abundance of tropical planktonic foraminifer assemblages, well-stratified water column and increased SST are reflective of relatively weaker westerlies and La-Niña-like-state (Perner et al., 2018). The Lake Emerald record indicates multi-centennial periods of SWW weakening between 11200-9200, 8400-7900 and 7700-7000 cal yr BP, reflecting northwards migration of the westerlies that bring moisture towards southern parts of Australia (Meneghini et al., 2007; Evans et al., 2009; Perren et al., 2020). These periods of weaker SWW all coincide with periods of increased P/E inferred from reconstructed $\delta^{18}O_{LW}$ at Lake Surprise. Our record also corresponds with Murray Canyons record that indicates relative cold phases at around 9200, 7300, and 5800 cal yr BP, which are reflective of more stratified waters in the early Holocene (weaker SWW on the Australian coast) and periods of stronger SWW on Australian coast as indicated by ocean mixing between 5200 – 4800 cal yr BP, both of which correspond with weakening (strengthening) of the SWW at Macquarie Island, as well as increased (decreased) P/E at Lake Surprise.

However, the marked variability after 4000 cal yr BP and the 1550-year climate cycle in the Murray Canyons record (Moros et al., 2009) is not reflected by similar variability at Lake Surprise, despite the proximity of these sites. Additionally, the subantarctic Indian Ocean and site temperature records from the EPICA ice core deuterium data show that Antarctica was shielded from and cooled by the northward shift of the subtropical/subantarctic front. This resulted in a colder source temperature of Antarctic precipitation between 9000 – 6000 cal yr BP (Masson-Delmotte et al., 2004). Previous studies have also inferred a major influence of SWW variability over southern Australia. For example, charcoal records from western Tasmania indicate periods of wetter climate existed from 9000 – 6000 cal yr BP, inferred to reflect stronger SWW impacting this region (Fletcher & Moreno, 2011; Beck et al., 2017; Mariani & Fletcher, 2017). Other records from the region have shown a concurrent increase in lake levels, subsequent decrease in salinity and aeolian activity with an increase in SWW-

derived precipitation (Jones et al., 1998; Xia et al., 2001; Stanley and De Deckker, 2002; Kemp et al., 2012; Wilkins et al., 2013). However, no previous records to date have indicated such a strong correlation between a record of SWW variability and centennial-scale hydroclimate variability in mainland Australia. The mid-Holocene wet period recorded at around 5600 – 4500 cal yr BP at Lake Surprise, also corresponds with a reduction of minerogenic input and DI conductivity measurements centred ~5500 cal yr BP at Macquarie Island record and also tally with cooling in Antarctica and weakening of westerlies at Murray Canyons record (Masson-Delmotte et al., 2004; Moros et al., 2009; Perner et al., 2018; Saunders et al., 2018). However, this period was not subjected to detailed discussion by Saunders et al., (2018). Relatively constant and intense winds recorded between 5300 – 0 cal yr BP at Macquarie Island indicate a continuous decline in SWW dominant rainfall which reflects lake drying (Saunders et al., 2018). This is well in place with continuous warming recorded after 5500 cal yr BP in EPICA ice core, Antarctica (Masson-Delmotte et al., 2004).

Variability in the ENSO as well as the IOD have also been invoked as major drivers of hydroclimate variability in south-east Australia (Cai et al., 2011b; Holgate et al., 2022; Reddy et al., 2022a; b). During the last millennium in particular IOD-ENSO interaction was identified to be the major cause of multi-decadal drought occurrence (Ummenhofer et al., 2009; Cai et al., 2011b, 2012; Abram et al., 2020a). It has been proposed that the frequent occurrence of El-Niño and La-Niña events overlap with drier and wetter events, respectively (Donders et al., 2008; Gliganic et al., 2014). The onset of persistently low P/E recorded at Lake Surprise agrees with the relatively high-resolution ENSO reconstruction from Murray Canyons based on planktonic foraminifer assemblages and alkenone-derived SST, which suggest a transition of La-Niña like state to El-Niño state after ~3500 cal yr BP (Perner et al., 2018). This gradual lake drying since 4500 cal yr BP also corresponds with an increase in El-Niño events in southern Ecuador and a decrease in rainfall at North Stradbroke Island (Moy et al., 2002; Barr et al., 2019). Lack of frequent active ENSO events approximately before 5000 cal yr BP, further influenced the predominance of SWW during this period (Moy et al., 2002). A slight increase in ENSO events from ~7000 to 5000 cal yr BP as recorded in Moy et al., (2002), disagrees with the relative wet period observed from 5600 – 4500 cal yr BP at Lake Surprise. However, prominent cooling due to La-Niña-like-state recorded from Murray Canyons records (5000 – 4500 cal yr BP) and concurrent increase in precipitation at swallow lagoon suggest south-east Australia may have the relatively wetter condition during this time (Perner et al., 2018; Barr et al., 2019).

The suppressed ENSO variability before 5000 cal yr BP, suggests that SWW are more likely to control the regional climate during this period (MacGregor and Gagan, 2004; Donders et al., 2008; Gouramanis et al., 2013; Barr et al., 2019). Wavelet coherence analysis based on the regional charcoal influx from western Tasmania and southern South America demonstrated that the period between 12000 – 6000 cal yr BP was synchronous with SWW-driven climate change and the same study between the regional Tasmania charcoal inflow and an ENSO proxy indicates a consistent pattern of frequency variations between both records from around 6000 cal yr BP, emphasising the role of ENSO in changing fire regimes in this area (Mariani & Fletcher, 2017). This is further supported by Paddy's Lake record (western Tasmania) that indicates a transition of SWW dominant climate to ENSO driven climate with the increase in fires (Beck et al., 2017). Even though, ENSO event reconstruction from Laguna Pallcacocha shows a gradual decrease in the intensity of ENSO peaks over the last millennium (Moy et al., 2002), more recent records from Murray Canyons show the occurrence of most intense El-Niño like conditions (Perner et al., 2018), suggesting that ENSO was predominant during the last millennium.

Correlation with precipitation variability and SST records from Sumatra Islands indicate relatively poor IOD influence with Lake Surprise isotope variability until at least the last millennium. However, the increase in precipitation amount at north-west Sumatra between 8000 – 6500 cal yr BP, is somewhat consistent with the wet period centred at 7300 cal yr BP at Lake Surprise. These rainfall excursions also coincide with the coral record or warming (cooling) in the eastern Indian Ocean, which reflects wetter (drier) conditions towards the mainland of Australia (Abram et al., 2009). This is followed by a lowering in precipitation from 6500 – 4500 cal yr BP and a considerable rise in precipitation from 2000 – 1000 cal yr BP. These wet (dry) episodes correspond with warming (cooling) in Sumatra and drying (wetting) in East Africa (Gasse, 2000; Thompson et al., 2002). From around 4500 – 2000 cal yr BP, rainfall variation does not show a significant transition as observed in lake isotope variability (Niedermeyer et al., 2014). Similarly, the SST anomaly illustrates a transition towards relative warming pattern disagreeing with the Lake Surprise record (Abram et al., 2009). However, a considerable decrease in precipitation amount and relative warming in the eastern tropical Indian Ocean since 1000 cal yr BP coincide with lake drying over the last millennium (Abram et al., 2009; Niedermeyer et al., 2014).

Apart from the ocean and atmospheric circulations, solar forcing also influences climate variability to some extent given that the sun's heating causes warming on Earth. It has been hypothesised that cyclical fluctuations in solar insolation may have an impact on millennial-scale climate variation in the late Quaternary period, given the ca. 2300 periodicity was observed in sediment proxy data from Lake Surprise which is synchronous with the ~2400-year solar activity (Hallstatt cycle) (Falster et al., 2018). Cosmic rays in the Earth's atmosphere create cosmogenic isotopes and the fluctuation of cosmogenic isotope production follows solar magnetic activity, which modulates cosmic rays, and vice versa (Usoskin et al., 2016). Even though $\delta^{18}O_{LW}$ at Lake Surprise does not exhibit a one-to-one relationship with the TSI, frequent occurrence of lower TSI values before 5000 cal yr BP is identified, especially coinciding with the wet periods discussed above. This is consistent with the TSI reconstruction developed for the past 9300 years based on ^{10}Be isotopes in polar ice cores and reconstruction of sun-spot numbers through Holocene using ^{14}C concentration in tree-ring chronologies (Solanki et al., 2004; Steinhilber et al., 2009; Usoskin et al., 2016). An increase in solar activity is observed along with a gradual transition to lake drying at around 4500 cal yr BP. It also implies that the solar irradiation peaked between 5000 and 4000 cal yr BP comparable to the present-day values (Vieira et al., 2011). However, a considerable reduction in TSI values during the last millennium reflects the Spȍrer (~550 – 400 cal yr BP) and Maunder minimum (~300 – 250 cal yr BP) events (Vieira et al., 2011; Usoskin et al., 2016; Wright et al., 2022). Even though this behaviour in TSI is not apparent in the $\delta^{18}O_{LW}$ variability at Lake Surprise, the previous reconstruction from Barr et al., (2014), provides evidence of a wet Little Ice Age that may correspond with the period of solar minimum. However, the steady increase in TSI record after ~300 cal yr BP represents a considerable transition towards warming or lake level decline as in the lake water isotope variability.

On observable timeframes, solar irradiance has previously been proposed as a significant driver of the SAM and variations in solar irradiance have been qualitatively interpreted to influence the temporal evolution of reconstructed SAM over the past millennium (Kuroda et al., 2007; Lu et al., 2011; Brehm et al., 2021; Wright et al., 2022). This has been investigated using the solar constant and simulations from the last millennium that encompass large amplitude solar variations and have shown that the SAM index significantly declines (increases) with a reduction (increase) in solar forcing (Wright et al., 2022). The most recent finding has suggested that at least a $7Wm^{-2}$ reduction in TSI should be required to differentiate the impact of solar forcing on the SAM index from a wide range of uncontrolled SAM fluctuations (Wright

et al., 2022). Even though Holocene climate proxies and atmospheric/oceanic circulations show a correlation with solar variations, the physical mechanisms related to solar forcing are still unclear since there are disparities in these records because they are based on different approaches and estimates. Furthermore, it is challenging to comprehend these linkages since there are only a limited number of studies available for solar and climate driver simulations that cover a short period.

Based on the $\delta^{18}O$ variability from Lake Surprise, this study suggests that the Holocene climate did not simply transition from a completely wet period to a dry period, but instead a period with a series of three or four multi-centennial wet periods, which presumably sustained the lakes and groundwater in the region. Additionally, the relative increase in $\delta^{18}O$ isotopes from 9000 – 5600 cal yr BP, may correspond with the warm/wet environment as suggested in De Deckker, (2022). Unlike previous studies (Kemp et al., 2012; Wilkins et al., 2013), data from this study also illustrate that the transition to persistent long-term drying at Lake Surprise initiated later than 5000 cal yr BP. Progressive drying in Lake Surprise seems to agree with stronger SWW intensity and intensification of ENSO events. However, increased variability at Lake Surprise before 5000 cal yr BP and a relatively stable climate during the late Holocene are in good agreement with (Saunders et al., 2018) that identified greater amplitude changes in SWW intensity from 9200 – 5300 cal yr BP, resulting extreme events of wet/dry intervals and smaller fluctuations after 5000 cal yr BP leading to a relatively persistent climate during the late Holocene. This is also true when considering the last wet period in Lake Surprise (5600 – 4500 cal yr BP), where all three climate modes are available for comparison, presence of El-Niño and positive IOD-like events exhibit that the moisture increase in the region during this period was driven by westerlies. Therefore, the influence of SWW overrides any effect of IOD and ENSO before 4500 cal yr BP when the western Victorian climate was enriched with frequent wet intervals. In addition, late Holocene drying also corresponds with the increasing frequency of ENSO events. TSI/solar forcing is likely to impact changes in climate through Holocene. Yet, high-resolution recordings of both climate and solar activity are necessary to discover the connection between TSI and climate drivers. Although Lake Surprise isotope variability shows a greater coherence to weakening/strengthening of SWW intensity through the Holocene, over the last two millennium lake seems to respond to the frequent occurrence of ENSO and IOD events.

5.6 Conclusions

Holocene climate reconstruction developed from cellulose inferred lake water isotopes at Lake Surprise, provides detailed insight into the south-east Australian hydroclimate, given the well-constrained chronological control and application of more reliable climate proxies such as lacustrine cellulose and decadal to the centennial-scale resolution used in sediment analysis. Monitoring of modern water and sediment traces from Lake Surprise provides indications of the lake's response to the P/E ratio and allows us to test the ability of aquatic cellulose to infer past climate change. In agreement with the previous lake studies from western Victoria and elsewhere in the region, Lake Surprise represents a relatively wetter early-mid Holocene and a significant transition to a prolonged arid climate ~4500 cal yr BP. However, three extensive wet intervals existing from ~10850 – 10000 cal yr BP, 7400 – 7000 cal yr BP and 5600 – 4500 cal yr BP and relative warming observed in between were not well defined elsewhere in the region detail. The earliest wet phase existed before 10000 cal yr BP is possibly a novel finding for the region given that many available Holocene records do not extend that far.

Lake isotope record illustrates the frequent occurrence of dry episodes after 4500 cal yr BP, associated with a small incidence of short wet intervals. Lake Surprise records its peak aridity from ~2100 – 1550 cal yr BP. Although climate over the last 1000 years remains nearly constant for most of the period, the last century illustrates high amplitude changes in climate, that are synchronous with two major historical droughts that existed at the beginning and end of the last century and intermittent moisture phase corresponding to a period of high rainfall. The correlation of Lake Surprise record with major climate drivers indicates that long-term drying in Lake Surprise corresponds with the changes in SWW intensity, intensification of ENSO events and changes in solar irradiation. Yet, changes in SWW intensity from high amplitude to more stable conditions through time fully agree with this record, demonstrating the dominance of SWW over other drivers. IOD remains a weaker driver at least until the past millennium. However, more detailed research is required for an in-depth understanding of the influence of these climate modes and their mechanisms. Overall, the Lake Surprise record provides a more variable, yet descriptive picture than generally accepted in south-east Australia.

5.7 List of references cited

Abbott, M. B., Wolfe, B. B., Aravena, R., Wolfe, A. P., & Seltzer, G. O. (2000). Holocene hydrological reconstructions from stable isotopes and paleolimnology, Cordillera Real, Bolivia. *Quaternary Science Reviews*, *19*(17–18), 1801–1820. https://doi.org/10.1016/S0277-3791(00)00078-0

Abram, N. J., Gagan, M. K., Cole, J. E., Hantoro, W. S., & Mudelsee, M. (2008). Recent intensification of tropical climate variability in the Indian Ocean. *Nature Geoscience*, *1*(12), 849–853. https://doi.org/10.1038/ngeo357

Abram, N. J., Gagan, M. K., Liu, Z., Hantoro, W. S., McCulloch, M. T., & Suwargadi, B. W. (2007a). Seasonal characteristics of the Indian Ocean Dipole during the Holocene epoch. *Nature*, *445*(7125), 299–302. https://doi.org/10.1038/nature05477

Abram, N. J., Hargreaves, J. A., Wright, N. M., Thirumalai, K., Ummenhofer, C. C., & England, M. H. (2020a). Palaeoclimate perspectives on the Indian Ocean Dipole. *Quaternary Science Reviews*, *237*, 106302. https://doi.org/10.1016/j.quascirev.2020.106302

Abram, N. J., Henley, B. J., Gupta, A. Sen, Lippmann, T. J. R., Clarke, H., Dowdy, A. J., Sharples, J. J., Nolan, R. H., Zhang, T., Wooster, M. J., Wurtzel, J. B., Meissner, K. J., Pitman, A. J., Ukkola, A. M., Murphy, B. P., Tapper, N. J., & Boer, M. M. (2021). Connections of climate change and variability to large and extreme forest fires in southeast Australia. *Communications Earth and Environment*, *2*. https://doi.org/10.1038/s43247-020-00065-8

Abram, N. J., McGregor, H. V., Gagan, M. K., Hantoro, W. S., & Suwargadi, B. W. (2009). Oscillations in the southern extent of the Indo-Pacific Warm Pool during the mid-Holocene. *Quaternary Science Reviews*, *28*(25–26), 2794–2803. https://doi.org/10.1016/j.quascirev.2009.07.006

Abram, N. J., Wright, N. M., Ellis, B., Dixon, B. C., Wurtzel, J. B., England, M. H., Ummenhofer, C. C., Philibosian, B., Cahyarini, S. Y., Yu, T. L., Shen, C. C., Cheng, H., Edwards, R. L., & Heslop, D. (2020b). Coupling of Indo-Pacific climate variability over the last millennium. *Nature*, *579*(7799), 385–392. https://doi.org/10.1038/s41586-020-2084-4

Ankor, M. J. (2020). *Hydrologic and Isotopic Lake Modelling for Palaeoclimate Research*. *January*.

Ankor, M. J., & Tyler, J. J. (2022). A computational method for rapid orthographic photography of lake sediment cores. *Journal of Paleolimnology*, *0123456789*. https://doi.org/10.1007/s10933-022-00241-0

Ankor, M. J., Tyler, J. J., & Hughes, C. E. (2019). Development of an autonomous , monthly and daily , rainfall sampler for isotope research. *Journal of Hydrology*, *575*(April), 31–41. https://doi.org/10.1016/j.jhydrol.2019.04.074

Aquino-López, M. A., Blaauw, M., Christen, J. A., & Sanderson, N. K. (2018). Bayesian Analysis of 210 Pb Dating. *Journal of Agricultural, Biological, and Environmental Statistics*, *23*(3), 317–333. https://doi.org/10.1007/s13253-018-0328-7

Aquino-López, M. A., Ruiz-Fernández, A. C., Blaauw, M., & Sanchez-Cabeza, J. A. (2020). Comparing classical and Bayesian 210Pb dating models in human-impacted aquatic environments. *Quaternary Geochronology*, *60*(November 2019). https://doi.org/10.1016/j.quageo.2020.101106

Ashcroft, L., Gergis, J., & Karoly, D. J. (2014). A historical climate dataset for southeastern Australia, 1788–1859. *Geoscience Data Journal*, *1*(2), 158–178. https://doi.org/10.1002/gdj3.19

Atahan, P., Heijnis, H., Dodson, J., Grice, K., Le Métayer, P., Taffs, K., Hembrow, S., Woltering, M., & Zawadzki, A. (2015). Pollen, biomarker and stable isotope evidence of late Quaternary environmental change at Lake McKenzie, southeast Queensland. *Journal of Paleolimnology*, *53*(1), 139–156. https://doi.org/10.1007/s10933-014-9813-3

Barr, C., Tibby, J., Gell, P., Tyler, J., Zawadzki, A., & Jacobsen, G. E. (2014). Climate variability in south-eastern Australia over the last 1500 years inferred from the high-resolution diatom records of two crater lakes. *Quaternary Science Reviews*, *95*, 115–131. https://doi.org/10.1016/j.quascirev.2014.05.001

Barr, C., Tibby, J., Leng, M. J., Tyler, J. J., Henderson, A. C. G., Overpeck, J. T., Simpson, G. L., Cole, J. E., Phipps, S. J., Marshall, J. C., McGregor, G. B., Hua, Q., & McRobie, F. H. (2019). Holocene El Niño–Southern Oscillation variability reflected in subtropical Australian precipitation. *Scientific Reports*, *9*(1), 1–9. https://doi.org/10.1038/s41598-019-38626-3

Barras, V., & Simmonds, I. (2009). Observation and modeling of stable water isotopes as diagnostics of rainfall dynamics over southeastern Australia. *Journal of Geophysical Research Atmospheres*, *114*(23). https://doi.org/10.1029/2009JD012132

Beck, K. K., Fletcher, M. S., Gadd, P. S., Heijnis, H., & Jacobsen, G. E. (2017). TITLE: An early onset of ENSO influence in the extra-tropics of the southwest Pacific inferred from a 14, 600 year high resolution multi-proxy record from Paddy's Lake, northwest Tasmania. *Quaternary Science Reviews*, *157*, 164–175. https://doi.org/10.1016/j.quascirev.2016.12.001

Bell, D., & Johnston, C. (2008). Budj Bim; Caring for the spirit and the people. *Finding the Spirit of Place : Between Tangible and Intangible Heritage. (16th ICOMOS General Assembly and International Scientific Symposium, Quebec, 2008)*, 213-224. http://openarchive.icomos.org/12/%5Cnhttp://openarchive.icomos.org/12/1/77-7xnf-104.pdf

Beuning, K. R. M., Kelts, K., Russell, J., & Wolfe, B. B. (2002). Reassessment of Lake Victoria-Upper Nile River paleohydrology from oxygen isotope records of lake-sediment cellulose. *Geology*, *30*(6), 559–562. https://doi.org/10.1130/0091-

7613(2002)030<0559:ROLVUN>2.0.CO;2

Bowler, J. M. (1981). 30. Australian salt lakes - A palaeohydrologic approach. *Hydrobiologia*, *81–82*(1), 431–444. https://doi.org/10.1007/BF00048730

Brahney, J., Clague, J. J., Edwards, T. W. D., & Menounos, B. (2010). Late Holocene paleohydrology of Kluane Lake, Yukon Territory, Canada. *Journal of Paleolimnology*, *44*(3), 873–885. https://doi.org/10.1007/s10933-010-9459-8

Brehm, N., Bayliss, A., Christl, M., Synal, H. A., Adolphi, F., Beer, J., Kromer, B., Muscheler, R., Solanki, S. K., Usoskin, I., Bleicher, N., Bollhalder, S., Tyers, C., & Wacker, L. (2021). Eleven-year solar cycles over the last millennium revealed by radiocarbon in tree rings. *Nature Geoscience*, *14*(1), 10–15. https://doi.org/10.1038/s41561-020-00674-0

Buhay, W. M., Wolfe, B. B., & Schwalb, A. (2012). Lakewater paleothermometry from Deep Lake, Minnesota during the deglacial-Holocene transition from combined δ 18O analyses of authigenic carbonate and aquatic cellulose. *Quaternary International*, *260*, 76–82. https://doi.org/10.1016/j.quaint.2011.11.034

Builth, H., Kershaw, A. P., White, C., Roach, A., Hartney, L., McKenzie, M., Lewis, T., & Jacobsen, G. (2008). Environmental and cultural change on the Mt Eccles lava-flow landscapes of southwest Victoria, Australia. *Holocene*, *18*(3), 413–424. https://doi.org/10.1177/0959683607087931

Cadd, H. R., Tibby, J., Barr, C., Tyler, J., Unger, L., Leng, M. J., Marshall, J. C., McGregor, G., Lewis, R., Arnold, L. J., Lewis, T., & Baldock, J. (2018). Development of a southern hemisphere subtropical wetland (Welsby Lagoon, south-east Queensland, Australia) through the last glacial cycle. *Quaternary Science Reviews*, *202*, 53–65. https://doi.org/10.1016/j.quascirev.2018.09.010

Cadd, H., Sherborne-Higgins, B., Becerra-Valdivia, L., Tibby, J., Barr, C., Forbes, M., Cohen, T. J., Tyler, J., Vandergoes, M., Francke, A., Lewis, R., Arnold, L. J., Jacobsen, G., Marjo, C., & Turney, C. (2022). the Application of Pollen Radiocarbon Dating and Bayesian Age-Depth Modeling for Developing Robust Geochronological Frameworks of Wetland Archives. *Radiocarbon*, *64*(2), 213–235. https://doi.org/10.1017/RDC.2022.29

Cai, W., Sullivan, A., & Cowan, T. (2011a). Interactions of ENSO, the IOD, and the SAM in CMIP3 models. *Journal of Climate*, *24*(6), 1688–1704. https://doi.org/10.1175/2010JCLI3744.1

Cai, W., van Rensch, P., Cowan, T., & Hendon, H. H. (2011b). Teleconnection pathways of ENSO and the IOD and the mechanisms for impacts on Australian rainfall. *Journal of Climate*, *24*(15), 3910–3923. https://doi.org/10.1175/2011JCLI4129.1

Cai, W., Van Rensch, P., Cowan, T., & Hendon, H. H. (2012). An Asymmetry in the IOD and ENSO teleconnection pathway and its impact on australian climate. *Journal of Climate*, *25*(18), 6318–6329. https://doi.org/10.1175/JCLI-D-11-00501.1

Cleverly, J., Eamus, D., Luo, Q., Coupe, N. R., Kljun, N., Ma, X., Ewenz, C., Li, L., Yu, Q., & Huete, A. (2016). The importance of interacting climate modes on Australia's contribution to global carbon cycle extremes. *Scientific Reports*, *6*(November 2015), 1–10. https://doi.org/10.1038/srep23113

Cohen, T. J., & Nanson, G. C. (2007). Mind the gap: An absence of valley-fill deposits identifying the Holocene hypsithermal period of enhanced flow regime in southeastern Australia. *Holocene*, *17*(3), 411–418. https://doi.org/10.1177/0959683607076475

Conroy, J. L., Overpeck, J. T., Cole, J. E., Shanahan, T. M., & Steinitz-Kannan, M. (2008). Holocene changes in eastern tropical Pacific climate inferred from a Galápagos lake sediment record. *Quaternary Science Reviews*, *27*(11–12), 1166–1180. https://doi.org/10.1016/j.quascirev.2008.02.015

Cook, E. R., Buckley, B. M., D'Arrigo, R. D., & Peterson, M. J. (2000). Warm-season temperatures since 1600 BC reconstructed from Tasmanian tree rings and their relationship to large-scale sea surface temperature anomalies. *Climate Dynamics*, *16*(2–3), 79–91. https://doi.org/10.1007/s003820050006

Cook, E. R., Palmer, J. G., & D'Arrigo, R. D. (2002). Evidence for a "Medieval Warm Period" in a 1,100 year tree-ring reconstruction of past austral summer temperatures in New Zealand. *Geophysical Research Letters*, *29*(14), 14–17. https://doi.org/10.1029/2001GL014580

Craig, H. (1961). Isotopic variations in meteoric waters. *Science*, *133*(3465), 1702–1703. https://doi.org/10.1126/science.133.3465.1702

Crawford, J., Hughes, C. E., & Parkes, S. D. (2013). Is the isotopic composition of event based precipitation driven by moisture source or synoptic scale weather in the Sydney Basin, Australia? *Journal of Hydrology*, *507*, 213–226. https://doi.org/10.1016/j.jhydrol.2013.10.031

da Silveira Lobo Sternberg, L. (1989). *Oxygen and Hydrogen Isotope Ratios in Plant Cellulose: Mechanisms and Applications*. 124–141. https://doi.org/10.1007/978-1-4612-3498-2_9

De Deckker, P. (1982). Late quaternary ostracods from lake george, new south wales. *Alcheringa*, *6*(4), 305–318. https://doi.org/10.1080/03115518208619640

De Deckker, P. (2022). The Holocene hypsithermal in the Australian region. *Quaternary Science Advances*, *7*(July), 100061. https://doi.org/10.1016/j.qsa.2022.100061

Dean, J. R., Eastwood, W. J., Roberts, N., Jones, M. D., Yig, H., Allcock, S. L., Woodbridge, J., Metcalfe, S. E., & Leng, M. J. (2014). *Tracking the hydro-climatic signal from lake to sediment : A field study from central Turkey*. https://doi.org/10.1016/j.jhydrol.2014.11.004

Delmonte, B., Petit, J., & Maggi, V. (2002). Glacial to Holocene implications of the new 27000-year dust record from the EPICA Dome C (East Antarctica) ice core. *Climate*

Dynamics, *18*(8), 647–660. https://doi.org/10.1007/s00382-001-0193-9

Dixon, B. C., Tyler, J. J., Lorrey, A. M., Goodwin, I. D., Gergis, J., & Drysdale, R. N. (2017). Low-resolution Australasian palaeoclimate records of the last 2000 years. *Climate of the Past*, *13*(10), 1403–1433. https://doi.org/10.5194/cp-13-1403-2017

Dixon, B., Tyler, J., Henley, B. J., & Drysdale, R. (2019). Regional patterns of hydroclimate variability in southeastern Australia over the past 1200 years. *Earth and Space Science Open Archive*. https://doi.org/10.1002/essoar.10501482.1

Dodson, J. (1974). Calcium carbonate formation by Enteromorpha nana algae in a hypersaline volcanic crater lake. *Hydrobiologia*, *44*(2–3), 247–255. https://doi.org/10.1007/BF00187274

Donders, T. H., Wagner-Cremer, F., & Visscher, H. (2008). Integration of proxy data and model scenarios for the mid-Holocene onset of modern ENSO variability. *Quaternary Science Reviews*, *27*(5–6), 571–579. https://doi.org/10.1016/j.quascirev.2007.11.010

Edwards, T. W. D., & McAndrews, J. H. (1989). Paleohydrology of a Canadian Shield land inferred from 18O in sediment cellulose. *Canadian Journal of Earth Sciences*, *26*(9), 1850–1859. https://doi.org/10.1139/e89-158

Emile-Geay, J., & Tingley, M. (2016). Inferring climate variability from nonlinear proxies: Application to palaeo-ENSO studies. *Climate of the Past*, *12*(1), 31–50. https://doi.org/10.5194/cp-12-31-2016

Evans, A. D., Bennett, J. M., & Ewenz, C. M. (2009). South Australian rainfall variability and climate extremes. *Climate Dynamics*, *33*(4), 477–493. https://doi.org/10.1007/s00382-008-0461-z

Falster, G., Tyler, J., Grant, K., Tibby, J., Turney, C., Löhr, S., Jacobsen, G., & Kershaw, A. P. (2018). Millennial-scale variability in south-east Australian hydroclimate between 30,000 and 10,000 years ago. *Quaternary Science Reviews*, *192*, 106–122. https://doi.org/10.1016/j.quascirev.2018.05.031

Fitzsimmons, K. E., & Barrows, T. T. (2010). Holocene hydrologic variability in temperate southeastern Australia: An example from Lake George, New South Wales. *Holocene*, *20*(4), 585–597. https://doi.org/10.1177/0959683609356589

Flack, A., Kiem, A., Vance, T., Tozer, C., & Roberts, J. (2020). Comparison of published palaeoclimate records suitable for reconstructing annual to sub-decadal hydroclimatic variability in eastern Australia: implications for water resource management and planning. *Hydrology and Earth System Sciences Discussions*, *June*, 1–25. https://doi.org/10.5194/hess-2020-314

Fletcher, M. S., & Moreno, P. I. (2011). Zonally symmetric changes in the strength and position of the Southern Westerlies drove atmospheric CO2 variations over the past 14 k.y. *Geology*, *39*(5), 419–422. https://doi.org/10.1130/G31807.1

Fletcher, M. S., Wolfe, B. B., Whitlock, C., Pompeani, D. P., Heijnis, H., Haberle, S. G.,

Gadd, P. S., & Bowman, D. M. J. S. (2014). The legacy of mid-holocene fire on a Tasmanian montane landscape. *Journal of Biogeography*, *41*(3), 476–488. https://doi.org/10.1111/jbi.12229

Fowler, A. M., Boswijk, G., Lorrey, A. M., Gergis, J., Pirie, M., McCloskey, S. P. J., Palmer, J. G., & Wunder, J. (2012). Multi-centennial tree-ring record of ENSO-related activity in New Zealand. *Nature Climate Change*, *2*(3), 172–176. https://doi.org/10.1038/nclimate1374

Gagan, M. K., Ayliffe, L. K., Beck, J. W., Cole, J. E., Druffel, E. R. M., Dunbar, R. B., & Schrag, D. P. (2000). New views of tropical paleoclimates from corals. *Quaternary Science Reviews*, *19*(1–5), 45–64. https://doi.org/10.1016/S0277-3791(99)00054-2

Gagan, M. K., Hendy, E. J., Haberle, S. G., & Hantoro, W. S. (2004). Post-glacial evolution of the Indo-Pacific Warm Pool and El Niño-Southern oscillation. *Quaternary International*, *118–119*, 127–143. https://doi.org/10.1016/S1040-6182(03)00134-4

Gasse, F. (2000). Hydrological changes in the African tropics since the Last Glacial Maximum. *Quaternary Science Reviews*, *19*(1–5), 189–211. https://doi.org/10.1016/S0277-3791(99)00061-X

Gergis, J., Gallant, A. J. E., Braganza, K., Karoly, D. J., Allen, K., Cullen, L., D'Arrigo, R., Goodwin, I., Grierson, P., & McGregor, S. (2012). On the long-term context of the 1997-2009 "Big Dry" in South-Eastern Australia: Insights from a 206-year multi-proxy rainfall reconstruction. *Climatic Change*, *111*(3), 923–944. https://doi.org/10.1007/s10584-011-0263-x

Gergis, J., & Henley, B. J. (2017). Southern Hemisphere rainfall variability over the past 200 years. *Climate Dynamics*, *48*(7–8), 2087–2105. https://doi.org/10.1007/s00382-016-3191-7

Gergis, J., Neukom, R., Gallant, A. J. E., & Karoly, D. J. (2016). Australasian temperature reconstructions spanning the Last Millennium. *Journal of Climate*, *29*(15), 5365–5392. https://doi.org/10.1175/JCLI-D-13-00781.1

Gibson, J. J., Birks, S. J., & Edwards, T. W. D. (2008). Global prediction of δA and δ2H-δ18O evaporation slopes for lakes and soil water accounting for seasonality. *Global Biogeochemical Cycles*, *22*(2), 1–12. https://doi.org/10.1029/2007GB002997

Gibson, J. J., Birks, S. J., & Yi, Y. (2016). Stable isotope mass balance of lakes: A contemporary perspective. *Quaternary Science Reviews*, *131*, 316–328. https://doi.org/10.1016/j.quascirev.2015.04.013

Gibson, J. J., & Edwards, T. W. D. (2002). Regional water balance trends and evaporation-transpiration partitioning from a stable isotope survey of lakes in northern Canada. *Global Biogeochemical Cycles*, *16*(2), 10-1-10–14. https://doi.org/10.1029/2001gb001839

Gingele, F., De Deckker, P., & Norman, M. (2007). Late Pleistocene and Holocene climate of

SE Australia reconstructed from dust and river loads deposited offshore the River Murray Mouth. *Earth and Planetary Science Letters*, *255*(3–4), 257–272. https://doi.org/10.1016/j.epsl.2006.12.019

Gliganic, L. A., Cohen, T. J., May, J. H., Jansen, J. D., Nanson, G. C., Dosseto, A., Larsen, J. R., & Aubert, M. (2014). Late-Holocene climatic variability indicated by three natural archives in arid southern Australia. *Holocene*, *24*(1), 104–117. https://doi.org/10.1177/0959683613515732

Gouramanis, C., Deckker, P. De, Switzer, A. D., & Wilkins, D. (2013). Earth-Science Reviews Cross-continent comparison of high-resolution Holocene climate records from southern Australia — Deciphering the impacts of far- fi eld teleconnections. *Earth Science Reviews*, *121*, 55–72. http://dx.doi.org/10.1016/j.earscirev.2013.02.006

Gouramanis, C., Wilkins, D., & De Deckker, P. (2010). 6000years of environmental changes recorded in Blue Lake, South Australia, based on ostracod ecology and valve chemistry. *Palaeogeography, Palaeoclimatology, Palaeoecology*, *297*(1), 223–237. https://doi.org/10.1016/j.palaeo.2010.08.005

Grant, S. B., Fletcher, T. D., Feldman, D., Saphores, J. D., Cook, P. L. M., Stewardson, M., Low, K., Burry, K., & Hamilton, A. J. (2013). Adapting urban water systems to a changing climate: Lessons from the millennium drought in southeast Australia. *Environmental Science and Technology*, *47*(19), 10727–10734. https://doi.org/10.1021/es400618z

Hancock, G. J., Leslie, C., Everett, S. E., Tims, S. G., Brunskill, G. J., & Haese, R. (2011). Plutonium as a chronomarker in Australian and New Zealand sediments: A comparison with 137Cs. *Journal of Environmental Radioactivity*, *102*(10), 919–929. https://doi.org/10.1016/j.jenvrad.2009.09.008

Harris, D., Horwáth, W. R., & Van Kessel, C. (2001). Acid fumigation of soils to remove carbonates prior to total organic carbon or carbon-13 isotopic analysis. *Soil Science Society of America Journal*, *65*(6), 1853–1856. https://doi.org/10.2136/sssaj2001.1853

Harrison, J. J., Saunders, K. M., Child, D. P., & Hotchkis, M. A. C. (2021). A record of fallout 239Pu and 240Pu at World Heritage Bathurst Harbour, Tasmania, Australia. *Journal of Environmental Radioactivity*, *237*(June). https://doi.org/10.1016/j.jenvrad.2021.106679

Harrison, S. P. (1993). Late Quaternary lake-level changes and climates of Australia. *Quaternary Science Reviews*, *12*(4), 211–231. https://doi.org/10.1016/0277-3791(93)90078-Z

Hassan, K. M., James B., S. B., & Spalding, R. F. (1997). Evidence for holocene environmental change from C/N ratios, and δ13C and δ15N values in Swan Lake sediments, western Sand Hills, Nebraska. *Journal of Paleolimnology*, *18*(2), 121–130. https://doi.org/10.1023/A:1007993329040

Head, L., Adams, M., Mcgregor, H. V., & Toole, S. (2014). Climate change and Australia.

Wiley Interdisciplinary Reviews: Climate Change, *5*(2), 175–197. https://doi.org/10.1002/wcc.255

Heikkilä, M., Edwards, T. W. D., Seppä, H., & Sonninen, E. (2010). Sediment isotope tracers from Lake Saarikko, Finland, and implications for Holocene hydroclimatology. *Quaternary Science Reviews*, *29*(17–18), 2146–2160. https://doi.org/10.1016/j.quascirev.2010.05.010

Henderson, A. K., & Shuman, B. N. (2009). Hydrogen and oxygen isotopic compositions of lake water in the western United States. *Bulletin of the Geological Society of America*, *121*(7–8), 1179–1189. https://doi.org/10.1130/B26441.1

Henley, B. J., Gergis, J., Karoly, D. J., Power, S., Kennedy, J., & Folland, C. K. (2015). A Tripole Index for the Interdecadal Pacific Oscillation. *Climate Dynamics*, *45*(11–12), 3077–3090. https://doi.org/10.1007/s00382-015-2525-1

Heyng, A. M., Mayr, C., Lücke, A., Wissel, H., & Striewski, B. (2014). Late Holocene hydrologic changes in northern New Zealand inferred from stable isotope values of aquatic cellulose in sediments from Lake Pupuke. *Journal of Paleolimnology*, *51*(4), 485–497. https://doi.org/10.1007/s10933-014-9769-3

Holgate, C., Evans, J. P., Taschetto, A. S., Gupta, A. Sen, & Santoso, A. (2022). The Impact of Interacting Climate Modes on East Australian Precipitation Moisture Sources. *Journal of Climate*, *35*(10), 3147–3159. https://doi.org/10.1175/JCLI-D-21-0750.1

Hope, G., Kershaw, A. P., van der Kaars, S., Xiangjun, S., Liew, P. M., Heusser, L. E., Takahara, H., McGlone, M., Miyoshi, N., & Moss, P. T. (2004). History of vegetation and habitat change in the Austral-Asian region. *Quaternary International*, *118–119*, 103–126. https://doi.org/10.1016/S1040-6182(03)00133-2

Hua, M., Zhang, X., Yao, T., Luo, Z., Zhou, H., Rao, Z., & He, X. (2019). Dual effects of precipitation and evaporation on lake water stable isotope composition in the monsoon region. *Hydrological Processes*, *33*(16), 2192–2205. https://doi.org/10.1002/hyp.13462

Hughes, C. E., & Crawford, J. (2013). Spatial and temporal variation in precipitation isotopes in the Sydney Basin, Australia. *Journal of Hydrology*, *489*, 42–55. https://doi.org/10.1016/j.jhydrol.2013.02.036

Hughes, L. (2003). *Climate change and Australia : Trends , projections and impacts*. 423–443.

Jones, M. D., Cuthbert, M. O., Leng, M. J., Mcgowan, S., Mariethoz, G., Arrowsmith, C., Sloane, H. J., Humphrey, K. K., & Cross, I. (2016a). Comparisons of observed and modelled lake d 18 O variability. *JQSR*, *131*, 329–340. https://doi.org/10.1016/j.quascirev.2015.09.012

Jones, M. D., Dee, S., Anderson, L., Baker, A., Bowen, G., & Noone, D. C. (2016b). Water isotope systematics: Improving our palaeoclimate interpretations. *Quaternary Science Reviews*, *131*, 243–249. https://doi.org/10.1016/j.quascirev.2015.11.014

Jones, M. D., Leng, M. J., Roberts, C. N., & Tu, M. (2005). *A coupled calibration and modelling approach to the understanding of dry-land lake oxygen isotope records*. 391–411. https://doi.org/10.1007/s10933-005-6743-0

Jones, R. N., McMahon, T. A., & Bowler, J. M. (2001). Modelling historical lake levels and recent climate change at three closed lakes, Western Victoria, Australia (c.1840-1990). *Journal of Hydrology*, *246*(1–4), 159–180. https://doi.org/10.1016/S0022-1694(01)00369-9

Jones, T. R., Roberts, W. H. G., Steig, E. J., Cuffey, K. M., Markle, B. R., & White, J. W. C. (2018). Southern Hemisphere climate variability forced by Northern Hemisphere ice-sheet topography. *Nature*, *554*(7692), 351–355. https://doi.org/10.1038/nature24669

Jonsson, C. E., Andersson, S., Rosqvist, G. C., & Leng, M. J. (2010). Reconstructing past atmospheric circulation changes using oxygen isotopes in lake sediments from Sweden. *Climate of the Past*, *6*(1), 49–62. https://doi.org/10.5194/cp-6-49-2010

Kemp, J., Radke, L. C., Olley, J., Juggins, S., & De Deckker, P. (2012). Holocene lake salinity changes in the Wimmera, southeastern Australia, provide evidence for millennial-scale climate variability. *Quaternary Research*, *77*(1), 65–76. https://doi.org/10.1016/j.yqres.2011.09.013

Kiem, A. S., Johnson, F., Westra, S., van Dijk, A., Evans, J. P., O'Donnell, A., Rouillard, A., Barr, C., Tyler, J., Thyer, M., Jakob, D., Woldemeskel, F., Sivakumar, B., & Mehrotra, R. (2016). Natural hazards in Australia: droughts. *Climatic Change*, *139*(1), 37–54. https://doi.org/10.1007/s10584-016-1798-7

Kiem, A. S., Vance, T. R., Tozer, C. R., Roberts, J. L., Dalla Pozza, R., Vitkovsky, J., Smolders, K., & Curran, M. A. J. (2020). Learning from the past – Using palaeoclimate data to better understand and manage drought in South East Queensland (SEQ), Australia. *Journal of Hydrology: Regional Studies*, *29*(April), 100686. https://doi.org/10.1016/j.ejrh.2020.100686

Kirono, D. G. C., Jones, R. N., Kent, D., & Leahy, P. (2009). Modelling lake levels under climate change conditions: Three closed lakes in Western Victoria. *18th World IMACS Congress and MODSIM 2009 - International Congress on Modelling and Simulation: Interfacing Modelling and Simulation with Mathematical and Computational Sciences, Proceedings*, *July*, 4312–4318.

Kirono, D. G. C., Round, V., Heady, C., Chiew, F. H. S., & Osbrough, S. (2020). Drought projections for Australia: Updated results and analysis of model simulations. *Weather and Climate Extremes*, *30*, 100280. https://doi.org/10.1016/j.wace.2020.100280

Kuroda, Y., Deushi, M., & Shibata, K. (2007). Role of solar activity in the troposphere-stratosphere coupling in the Southern Hemisphere winter. *Geophysical Research Letters*, *34*(21), 1–5. https://doi.org/10.1029/2007GL030983

Kwiatkowski, C., Prange, M., Varma, V., Steinke, S., Hebbeln, D., & Mohtadi, M. (2015). Holocene variations of thermocline conditions in the eastern tropical Indian Ocean.

Quaternary Science Reviews, *114*, 33–42. https://doi.org/10.1016/j.quascirev.2015.01.028

Leake, L., Present, B. P., & Dodson, J. R. (1974). Vegetation History and Water Fluctuations. *Australian Journal of Botany*, *22*(1862), 719–741.

Lehmann, M. F., Bernasconi, S. M., Barbieri, A., & McKenzie, J. A. (2002). Preservation of organic matter and alteration of its carbon and nitrogen isotope composition during simulated and in situ early sedimentary diagenesis. *Geochimica et Cosmochimica Acta*, *66*(20), 3573–3584. https://doi.org/10.1016/S0016-7037(02)00968-7

Leng, M. J., Lamb, A. L., Lamb, H. F., & Telford, R. J. (1999). Palaeoclimatic implications of isotopic data from modern and early Holocene shells of the freshwater snail Melanoides tuberculata, from lakes in the Ethiopian Rift Valley. *Journal of Paleolimnology*, *21*(1), 97–106. https://doi.org/10.1023/A:1008079219280

Leng, M. J., & Marshall, J. D. (2004). Palaeoclimate interpretation of stable isotope data from lake sediment archives. *Quaternary Science Reviews*, *23*(7–8), 811–831. https://doi.org/10.1016/j.quascirev.2003.06.012

Li, H., Liu, X., Tripati, A., Feng, S., Elliott, B., Whicker, C., Arnold, A., & Kelley, A. M. (2020). Factors controlling the oxygen isotopic composition of lacustrine authigenic carbonates in Western China: implications for paleoclimate reconstructions. *Scientific Reports*, *10*(1), 1–17. https://doi.org/10.1038/s41598-020-73422-4

Lu, H., Jarvis, M. J., Gray, L. J., & Baldwin, M. P. (2011). High- and low-frequency 11-year solar cycle signatures in the Southern Hemispheric winter and spring. *Quarterly Journal of the Royal Meteorological Society*, *137*(659), 1641–1656. https://doi.org/10.1002/qj.852

Mariani, M., & Fletcher, M. S. (2017). Long-term climate dynamics in the extra-tropics of the South Pacific revealed from sedimentary charcoal analysis. *Quaternary Science Reviews*, *173*, 181–192. https://doi.org/10.1016/j.quascirev.2017.08.007

Mariani, M., Fletcher, M. S., Haberle, S., Chin, H., Zawadzki, A., & Jacobsen, G. (2019). Climate change reduces resilience to fire in subalpine rainforests. *Global Change Biology*, *25*(6), 2030–2042. https://doi.org/10.1111/gcb.14609

Masson-Delmotte, V., Stenni, B., & Jouzel, J. (2004). Common millennial-scale variability of Antarctic and Southern Ocean temperatures during the past 5000 years reconstructed from the EPICA Dome C ice core. *Holocene*, *14*(2), 145–151. https://doi.org/10.1191/0959683604hl697ft

Matchan, E. L., Phillips, D., Jourdan, F., & Oostingh, K. (2020). Early human occupation of southeastern Australia: Newinsights from 40Ar/39Ar dating of young volcanoes. *Geology*, *48*(4), 390–394. https://doi.org/10.1130/G47166.1

Maxson, C., Tibby, J., Marshall, J., Kent, M., Tyler, J., Barr, C., McGregor, G., Cadd, H., Schulz, C., & Lomax, B. H. (2021). Fourier transform infrared spectroscopy as a tracer

of organic matter sources in lake sediments. *Palaeogeography, Palaeoclimatology, Palaeoecology*, *581*(August), 110622. https://doi.org/10.1016/j.palaeo.2021.110622

Mayr, C., Lücke, A., Maidana, N. I., Wille, M., Haberzettl, T., Corbella, H., Ohlendorf, C., Schäbitz, F., Fey, M., Janssen, S., & Zolitschka, B. (2009). Isotopic fingerprints on lacustrine organic matter from Laguna Potrok Aike (southern Patagonia, Argentina) reflect environmental changes during the last 16,000 years. *Journal of Paleolimnology*, *42*(1), 81–102. https://doi.org/10.1007/s10933-008-9249-8

Meneghini, B., Simmonds, I., & Smith, I. N. (2007). Association between Australian rainfall and the Southern Annular Mode. *International Journal of Climatology*, *27*(1), 109–121. https://doi.org/10.1002/joc.1370

Meyers, P. A. (1997). Organic geochemical proxies of paleoceanographic, paleolimnologic, and paleoclimatic processes. *Organic Geochemistry*, *27*(5–6), 213–250. https://doi.org/10.1016/S0146-6380(97)00049-1

Meyers, P. A., & Ishiwatari, R. (1993). Lacustrine organic geochemistry-an overview of indicators of organic matter sources and diagenesis in lake sediments. *Organic Geochemistry*, *20*(7), 867–900. https://doi.org/10.1016/0146-6380(93)90100-P

Meyers, P. A., & Lallier-Vergès, E. (1999). Lacustrine sedimentary organic matter records of Late Quaternary paleoclimates. *Journal of Paleolimnology*, *21*(3), 345–372. https://doi.org/10.1023/A:1008073732192

Mooney, S. D., Harrison, S. P., Bartlein, P. J., Daniau, A. L., Stevenson, J., Brownlie, K. C., Buckman, S., Cupper, M., Luly, J., Black, M., Colhoun, E., D'Costa, D., Dodson, J., Haberle, S., Hope, G. S., Kershaw, P., Kenyon, C., McKenzie, M., & Williams, N. (2011). Late Quaternary fire regimes of Australasia. *Quaternary Science Reviews*, *30*(1–2), 28–46. https://doi.org/10.1016/j.quascirev.2010.10.010

Moros, M., De Deckker, P., Jansen, E., Perner, K., & Telford, R. J. (2009). Holocene climate variability in the Southern Ocean recorded in a deep-sea sediment core off South Australia. *Quaternary Science Reviews*, *28*(19–20), 1932–1940. https://doi.org/10.1016/j.quascirev.2009.04.007

Moy, C. M., Seltzer, G. O., Rodbell, D. T., & Anderson, D. M. (2002). Variability of El Niño/Southern Oscillation activity at millennial timescales during the Holocene epoch. *Nature*, *420*(6912), 162–165. https://doi.org/10.1038/nature01194

Neukom, R., & Gergis, J. (2012). Southern Hemisphere high-resolution palaeoclimate records of the last 2000 years. *Holocene*, *22*(5), 501–524. https://doi.org/10.1177/0959683611427335

Neukom, R., Gergis, J., Karoly, D. J., Wanner, H., Curran, M., Elbert, J., González-Rouco, F., Linsley, B. K., Moy, A. D., Mundo, I., Raible, C. C., Steig, E. J., Van Ommen, T., Vance, T., Villalba, R., Zinke, J., & Frank, D. (2014). Inter-hemispheric temperature variability over the past millennium. *Nature Climate Change*, *4*(5), 362–367. https://doi.org/10.1038/nclimate2174

Nicholls, N. (2004). The changing nature of Australian droughts. *Climatic Change*, *63*(3), 323–336. https://doi.org/10.1023/B:CLIM.0000018515.46344.6d

Niedermeyer, E. M., Sessions, A. L., Feakins, S. J., & Mohtadi, M. (2014). Hydroclimate of the western Indo-Pacific Warm Pool during the past 24,000 years. *Proceedings of the National Academy of Sciences of the United States of America*, *111*(26), 9402–9406. https://doi.org/10.1073/pnas.1323585111

Parks Victoria. (1996). *Mount eccles national park and mount napier state park; Management plan*.

Pauly, M., Turney, C. S. M., Palmer, J. G., Büntgen, U., Brauer, A., & Helle, G. (2021). Kauri Tree-Ring Stable Isotopes Reveal a Centennial Climate Downturn Following the Antarctic Cold Reversal in New Zealand. *Geophysical Research Letters*, *48*(2), 1–13. https://doi.org/10.1029/2020GL090299

Perner, K., Moros, M., De Deckker, P., Blanz, T., Wacker, L., Telford, R., Siegel, H., Schneider, R., & Jansen, E. (2018). Heat export from the tropics drives mid to late Holocene palaeoceanographic changes offshore southern Australia. *Quaternary Science Reviews*, *180*, 96–110. https://doi.org/10.1016/j.quascirev.2017.11.033

Perren, B. B., Hodgson, D. A., Roberts, S. J., Sime, L., Van Nieuwenhuyze, W., Verleyen, E., & Vyverman, W. (2020). Southward migration of the Southern Hemisphere westerly winds corresponds with warming climate over centennial timescales. *Communications Earth and Environment*, *1*(1), 1–8. https://doi.org/10.1038/s43247-020-00059-6

Petherick, L., Bostock, H., Cohen, T. J., Fitzsimmons, K., Tibby, J., Fletcher, M. S., Moss, P., Reeves, J., Mooney, S., Barrows, T., Kemp, J., Jansen, J., Nanson, G., & Dosseto, A. (2013). Climatic records over the past 30ka from temperate Australia - a synthesis from the Oz-INTIMATE workgroup. *Quaternary Science Reviews*, *74*, 58–77. https://doi.org/10.1016/j.quascirev.2012.12.012

Reddy, P. J., Perkins-Kirkpatrick, S. E., Ridder, N. N., & Sharples, J. J. (2022a). Combined role of ENSO and IOD on compound drought and heatwaves in Australia using two CMIP6 large ensembles. *Weather and Climate Extremes*, *37*(December 2021), 100469. https://doi.org/10.1016/j.wace.2022.100469

Reddy, P. J., Perkins-Kirkpatrick, S. E., & Sharples, J. J. (2022b). Interactive influence of ENSO and IOD on contiguous heatwaves in Australia. *Environmental Research Letters*, *17*(1). https://doi.org/10.1088/1748-9326/ac3e9a

Risbey, J. S., Pook, M. J., McIntosh, P. C., Wheeler, M. C., & Hendon, H. H. (2009). On the remote drivers of rainfall variability in Australia. *Monthly Weather Review*, *137*(10), 3233–3253. https://doi.org/10.1175/2009MWR2861.1

Rozanski, K., Klisch, M. A., Wachniew, P., Gorczyca, Z., Goslar, T., Edwards, T. W. D., & Shemesh, A. (2010). Oxygen-isotope geothermometers in lacustrine sediments: New insights through combined δ18O analyses of aquatic cellulose, authigenic calcite and biogenic silica in Lake Gościaz, central Poland. *Geochimica et Cosmochimica Acta*,

74(10), 2957–2969. https://doi.org/10.1016/j.gca.2010.02.026

Saunders, K. M., Grosjean, M., & Hodgson, D. A. (2013). A 950 yr temperature reconstruction from Duckhole Lake, southern Tasmania, Australia. *Holocene*, *23*(6), 771–783. https://doi.org/10.1177/0959683612470176

Saunders, K. M., Kamenik, C., Hodgson, D. A., Hunziker, S., Siffert, L., Fischer, D., Fujak, M., Gibson, J. A. E., & Grosjean, M. (2012). Late Holocene changes in precipitation in northwest Tasmania and their potential links to shifts in the Southern Hemisphere westerly winds. *Global and Planetary Change*, *92–93*, 82–91. https://doi.org/10.1016/j.gloplacha.2012.04.005

Saunders, K. M., Roberts, S. J., Perren, B., Butz, C., Sime, L., Davies, S., Van Nieuwenhuyze, W., Grosjean, M., & Hodgson, D. A. (2018). Holocene dynamics of the Southern Hemisphere westerly winds and possible links to CO2 outgassing. *Nature Geoscience*, *11*(9), 650–655. https://doi.org/10.1038/s41561-018-0186-5

Savage, C. A. M., Remmer, C. R., Telford, J. V., Kay, M. L., Mehler, E., Wolfe, B. B., & Hall, R. I. (2021). Field testing cellulose-water oxygen isotope relations in periphyton for paleohydrological reconstructions. *Journal of Paleolimnology*, *66*(3), 297–312. https://doi.org/10.1007/s10933-021-00207-8

Scroxton, N., Walczak, M., Markowska, M., Zhao, J. X., & Fallon, S. (2020). Historical droughts in Southeast Australia recorded in a New South Wales stalagmite. *Holocene*. https://doi.org/10.1177/0959683620981717

Solanki, S. K., Usoskin, I. G., Kromer, B., Schüssler, M., & Beer, J. (2004). Unusual activity of the Sun during recent decades compared to the previous 11,000 years. *Nature*, *431*(7012), 1084–1087. https://doi.org/10.1038/nature02995

Stahle, L. N., Chin, H., Haberle, S., & Whitlock, C. (2017). Late-glacial and Holocene records of fire and vegetation from Cradle Mountain National Park, Tasmania, Australia. *Quaternary Science Reviews*, *177*, 57–77. https://doi.org/10.1016/j.quascirev.2017.09.010

Stahle, L. N., Whitlock, C., & Haberle, S. G. (2016). A 17,000-year-long record of vegetation and fire from Cradle Mountain National Park, Tasmania. *Frontiers in Ecology and Evolution*, *4*(JUL), 1–17. https://doi.org/10.3389/fevo.2016.00082

Stanley, S., & De Deckker, P. (2002). A holocene record of allochthonous, aeolian mineral grains in an australian alpine lake; implications for the history of climate change in southeastern australia. *Journal of Paleolimnology*, *27*(2), 207–219. https://doi.org/10.1023/A:1014249404845

Steinhilber, F., Beer, J., & Fröhlich, C. (2009). Total solar irradiance during the Holocene. *Geophysical Research Letters*, *36*(19), 1–5. https://doi.org/10.1029/2009GL040142

Steinman, B. A., Rosenmeier, M. F., Abbott, M. B., & Bain, D. J. (2010). The isotopic and hydrologic response of small, closed-basin lakes to climate forcing from predictive

models: Application to paleoclimate studies in the upper Columbia River basin. *Limnology and Oceanography*, *55*(6), 2231–2245. https://doi.org/10.4319/lo.2010.55.6.2231

Stenni, B., Masson-Delmotte, V., Selmo, E., Oerter, H., Meyer, H., Röthlisberger, R., Jouzel, J., Cattani, O., Falourd, S., Fischer, H., Hoffmann, G., Iacumin, P., Johnsen, S. J., Minster, B., & Udisti, R. (2010). The deuterium excess records of EPICA Dome C and Dronning Maud Land ice cores (East Antarctica). *Quaternary Science Reviews*, *29*(1–2), 146–159. https://doi.org/10.1016/j.quascirev.2009.10.009

Stephens, C. M., McVicar, T. R., Johnson, F. M., & Marshall, L. A. (2018). Revisiting Pan Evaporation Trends in Australia a Decade on. *Geophysical Research Letters*, *45*(20), 11,164-11,172. https://doi.org/10.1029/2018GL079332

Sternberg, L., Deniro, M. J., & Keeley, J. E. (1984). Hydrogen, oxygen, and carbon isotope ratios of cellulose from submerged aquatic crassulacean acid metabolism and non-crassulacean acid metabolism plants. *Plant Physiology*, *76*(1), 68–70. https://doi.org/10.1104/pp.76.1.68

Street-Perrott, F. A., Holmes, J. A., Robertson, I., Ficken, K. J., Koff, T., Loader, N. J., Marshall, J. D., & Martma, T. (2018). The Holocene isotopic record of aquatic cellulose from Lake Äntu Sinijärv, Estonia: Influence of changing climate and organic-matter sources. *Quaternary Science Reviews*, *193*, 68–83. https://doi.org/10.1016/j.quascirev.2018.05.010

The Bureau of Meteorology, & CSIRO. (2020). *Report at a glance Key points*.

Thomas, E. R., Allen, C. S., Etourneau, J., King, A. C. F., Severi, M., Winton, V. H. L., Mueller, J., Crosta, X., & Peck, V. L. (2019). Antarctic sea ice proxies from marine and ice core archives suitable for reconstructing sea ice over the past 2000 years. *Geosciences (Switzerland)*, *9*(12). https://doi.org/10.3390/geosciences9120506

Thomas, Z. A., Mooney, S., Cadd, H., Baker, A., Turney, C., Schneider, L., Hogg, A., Haberle, S., Green, K., Weyrich, L. S., Pérez, V., Moore, N. E., Zawadzki, A., Kelloway, S. J., & Khan, S. J. (2022). Late Holocene climate anomaly concurrent with fire activity and ecosystem shifts in the eastern Australian Highlands. *Science of the Total Environment*, *802*, 149542. https://doi.org/10.1016/j.scitotenv.2021.149542

Thompson, L. G., Mosley-Thompson, E., Davis, M. E., Henderson, K. A., Brecher, H. H., Zagorodnov, V. S., Mashiotta, T. A., Lin, P. N., Mikhalenko, V. N., Hardy, D. R., & Beer, J. (2002). Kilimanjaro ice core records: Evidence of holocene climate change in tropical Africa. *Science*, *298*(5593), 589–593. https://doi.org/10.1126/science.1073198

Tibby, J., Penny, D., Leahy, P., & Kershaw, A. P. (2012). Vegetation and water quality responses to Holocene climate variability in Lake Purrumbete, western Victoria. *Peopled Landscapes: Archaeological and Biogeographic Approaches to Landscapes*, *May*. https://doi.org/10.22459/ta34.01.2012.17

Timms, B. V. (1975). Basic limnology of two crater lakes in western Victoria.

Torres, I. C., Inglett, P. W., Brenner, M., Kenney, W. F., & Reddy, K. R. (2012). Stable isotope (δ 13C and δ 15N) values of sediment organic matter in subtropical lakes of different trophic status. *Journal of Paleolimnology*, *47*(4), 693–706. https://doi.org/10.1007/s10933-012-9593-6

Treble, P. C., Baker, A., Hellstrom, J. C., Abram, N. J., & Crawford, J. (2021). *Quantification of the hydrological control on speleothem oxygen isotopic variability*. *April*, 1–39.

Turney, C., Becerra-Valdivia, L., Sookdeo, A., Thomas, Z. A., Palmer, J., Haines, H. A., Cadd, H., Wacker, L., Baker, A., Andersen, M. S., Jacobsen, G., Meredith, K., Chinu, K., Bollhalder, S., & Marjo, C. (2021). Radiocarbon protocols and first intercomparison results from the CHRONOS 14Carbon-cycle facility, University of New south wales, Sydney, Australia. *Radiocarbon*, *63*(3), 1003–1023. https://doi.org/10.1017/RDC.2021.23

Tweed, S., Leblanc, M., & Cartwright, I. (2009). Groundwater-surface water interaction and the impact of a multi-year drought on lakes conditions in South-East Australia. *Journal of Hydrology*, *379*(1–2), 41–53. https://doi.org/10.1016/j.jhydrol.2009.09.043

Tyler, J. J., Marshall, J. C., Schulz, C., Barr, C., Hofmann, H., Blessing, J. J., Mccoy, K., Mcgregor, G. B., & Tibby, J. (2022). *Hydrological and Isotopic Variability of Perched Wetlands on North Stradbroke Island (Minjerribah), Australia : Implications for Understanding the Effects of Past and Future Climate Change*. *10*(July), 1–21. https://doi.org/10.3389/fenvs.2022.868114

Tyler, J. J., Mills, K., Barr, C., Sniderman, J. M. K., Gell, P. A., & Karoly, D. J. (2015). Identifying coherent patterns of environmental change between multiple, multivariate records: an application to four 1000-year diatom records from Victoria, Australia. *Quaternary Science Reviews*, *119*, 94–105. https://doi.org/10.1016/j.quascirev.2015.04.010

Ummenhofer, C. C., England, M. H., Mcintosh, P. C., Meyers, G. A., Pook, M. J., Risbey, J. S., & Gupta, A. Sen. (2009). *What causes southeast Australia ' s worst droughts ? 36*, 1–5. https://doi.org/10.1029/2008GL036801

Usoskin, I. G., Gallet, Y., Lopes, F., Kovaltsov, G. A., & Hulot, G. (2016). Solar activity during the Holocene: The Hallstatt cycle and its consequence for grand minima and maxima. *Astronomy and Astrophysics*, *587*(27295), 1–9. https://doi.org/10.1051/0004-6361/201527295

Vance, T. R., Roberts, J. L., Plummer, C. T., Kiem, A. S., & Ommen, T. D. Van. (2015a). *Interdecadal Pacific variability and eastern Australian megadroughts over the last millennium*. 129–137. https://doi.org/10.1002/2014GL062447.Abstract

Vieira, L. E. A., Solanki, S. K., Krivova, N. A., & Usoskin, I. (2011). Evolution of the solar irradiance during the Holocene. *Astronomy and Astrophysics*, *531*, 1–20. https://doi.org/10.1051/0004-6361/201015843

Wilkins, D., Gouramanis, C., de Deckker, P., Fifield, L. K., & Olley, J. (2013). Holocene lake-level fluctuations in Lakes Keilambete and Gnotuk, southwestern Victoria, Australia. *Holocene*, *23*(6), 784–795. https://doi.org/10.1177/0959683612471983

Wissel, H., Mayr, C., & Lücke, A. (2008). A new approach for the isolation of cellulose from aquatic plant tissue and freshwater sediments for stable isotope analysis. *Organic Geochemistry*, *39*(11), 1545–1561. https://doi.org/10.1016/j.orggeochem.2008.07.014

Wolfe, B. B., Aravena, R., Abbott, M. B., Seltzer, G. O., & Gibson, J. J. (2001). Reconstruction of paleohydrology and paleohumidity from oxygen isotope records in the Bolivian Andes. *Palaeogeography, Palaeoclimatology, Palaeoecology*, *176*(1–4), 177–192. https://doi.org/10.1016/S0031-0182(01)00337-6

Wolfe, B. B., Edwards, T. W. D., Aravena, R., Forman, S. L., Warner, B. G., Velichko, A. A., & MacDonald, G. M. (2000). Holocene paleohydrology and paleoclimate at treeline, north-central Russia, inferred from oxygen isotope records in lake sediment cellulose. *Quaternary Research*, *53*(3), 319–329. https://doi.org/10.1006/qres.2000.2124

Wolfe, B. B., Falcone, M. D., Clogg-Wright, K. P., Mongeon, C. L., Yi, Y., Brock, B. E., Amour, N. A. S., Mark, W. A., & Edwards, T. W. D. (2007). Progress in isotope paleohydrology using lake sediment cellulose. *Journal of Paleolimnology*, *37*(2), 221–231. https://doi.org/10.1007/s10933-006-9015-8

Wright, H. E. (1967). A square-rod piston sampler for lake sediments. *Journal of Sedimentary Research*, *37*(3), 975–976. https://doi.org/10.1306/74d71807-2b21-11d7-8648000102c1865d

Wright, N. M., Krause, C. E., Phipps, S. J., Boschat, G., & Abram, N. J. (2022). Influence of long-term changes in solar irradiance forcing on the Southern Annular Mode. *Climate of the Past, Preprint*, 1–32. https://cp.copernicus.org/preprints/cp-2021-156/

Wu, H., Li, X., Li, J., Jiang, Z., Li, G., & Liu, L. (2015). Evaporative enrichment of stable isotopes (δ18o and δd) in lake water and the relation to lake-level change of lake qinghai, northeast tibetan plateau of China. *Journal of Arid Land*, *7*(5), 623–635. https://doi.org/10.1007/s40333-015-0048-6

Xia, Q., Zhao, J. xin, & Collerson, K. D. (2001). Early-mid Holocene climatic variations in Tasmania, Australia: Multi-proxy records in a stalagmite from Lynds Cave. *Earth and Planetary Science Letters*, *194*(1–2), 177–187. https://doi.org/10.1016/S0012-821X(01)00541-6

Yang, G., Zheng, J., Tagami, K., & Uchida, S. (2015). Plutonium concentration and isotopic ratio in soil samples from central-eastern Japan collected around the 1970s. *Scientific Reports*, *5*, 1–8. https://doi.org/10.1038/srep09636

Zhang, Y., Jones, M., Zhang, J., McGowan, S., & Metcalfe, S. (2021). Can δ18O help indicate the causes of recent lake area expansion on the western Tibetan Plateau? A case study from Aweng Co. *Journal of Paleolimnology*, *65*(1), 169–180. https://doi.org/10.1007/s10933-020-00158-6

Zhao, J. xin, Xia, Q., & Collerson, K. D. (2001). Timing and duration of the Last Interglacial inferred from high resolution U-series chronology of stalagmite growth in Southern Hemisphere. *Earth and Planetary Science Letters*, *184*(3–4), 635–644. https://doi.org/10.1016/S0012-821X(00)00353-8

Supplementary data

Section 1: Comparison of precipitation data between Macarthur and Melbourne stations

In the absence of $\delta^{18}O_P$ data for Macarthur station, we compared Melbourne's $\delta^{18}O_P$ with precipitation data from both stations to determine how well they corresponded.

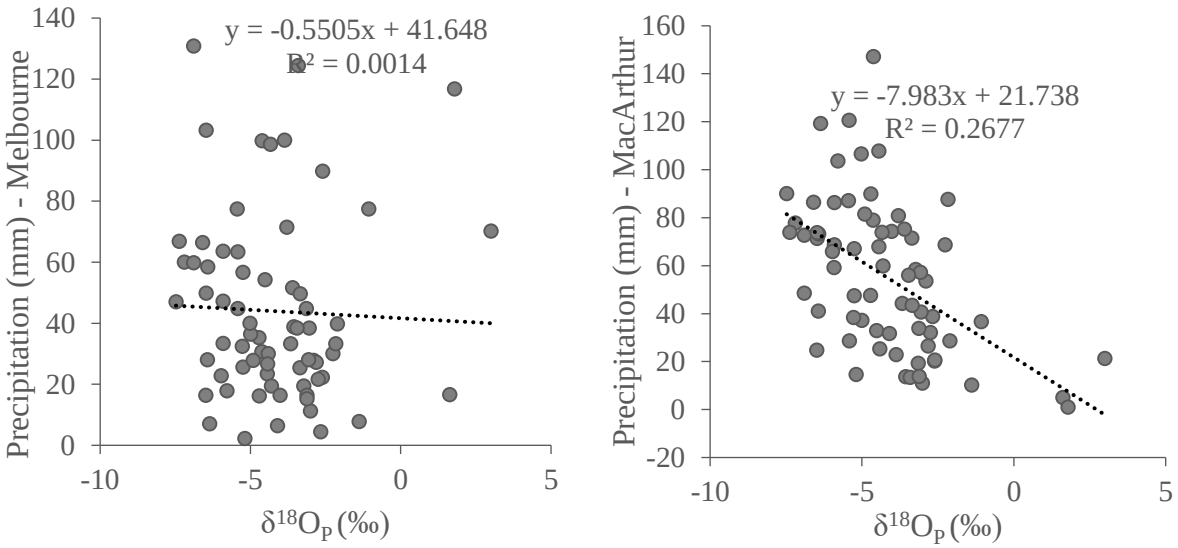

Figure I. Linear correlation between $\delta^{18}O_P$ data and precipitation amount of both weather stations.

Accordingly, a better correlation was observed between Macarthur rainfall and Melbourne isotope data compared to Melbourne isotope vs rainfall data. This is further confirmed by the opposite relationship between rainwater isotopes and precipitation as shown in figure II.

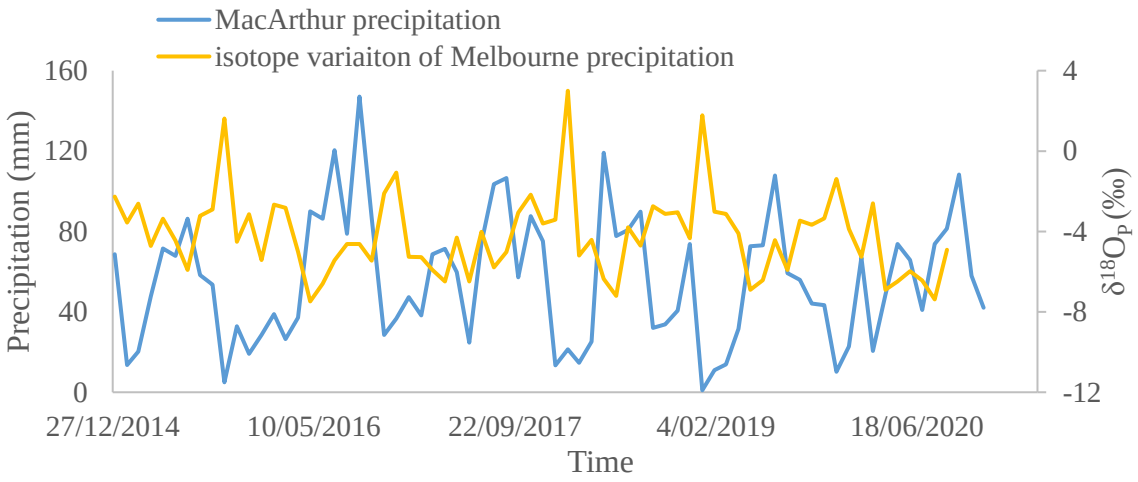

Figure II. Variation between $\delta^{18}O_P$ from Melbourne and precipitation data from Macarthur.

Section 2: External standards (Pinewood and cellulose powder) used in cellulose oxygen isotope analysis

Cellulose extraction was performed in pinewood and cellulose powder samples along with each batch of sediment extraction as a reference for methodological accuracy. Except for the sieving step, all other steps were followed for cellulose extraction in freeze-dried, powdered pinewood and cellulose. Cellulose extraction in sediment was initially performed at 10 cm (lower) resolution and increased to 5 cm resolution late. Therefore, Pinewood and cellulose powder are illustrated in two sets of batches here.

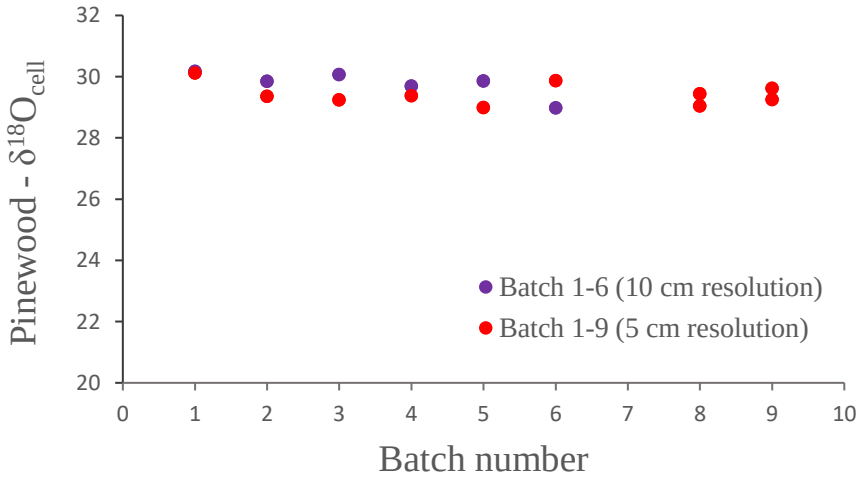

Figure I. Distribution of Pinewood samples measured with the separate batches of sediment samples

As illustrated in Figure I, $\delta^{18}O_{cell}$ in pinewood show a relatively lower deviation of 0.4 with no significant bias between different samples. This indicates that the cellulose extraction procedure followed across the sediment depth was relatively consistent and accurate.

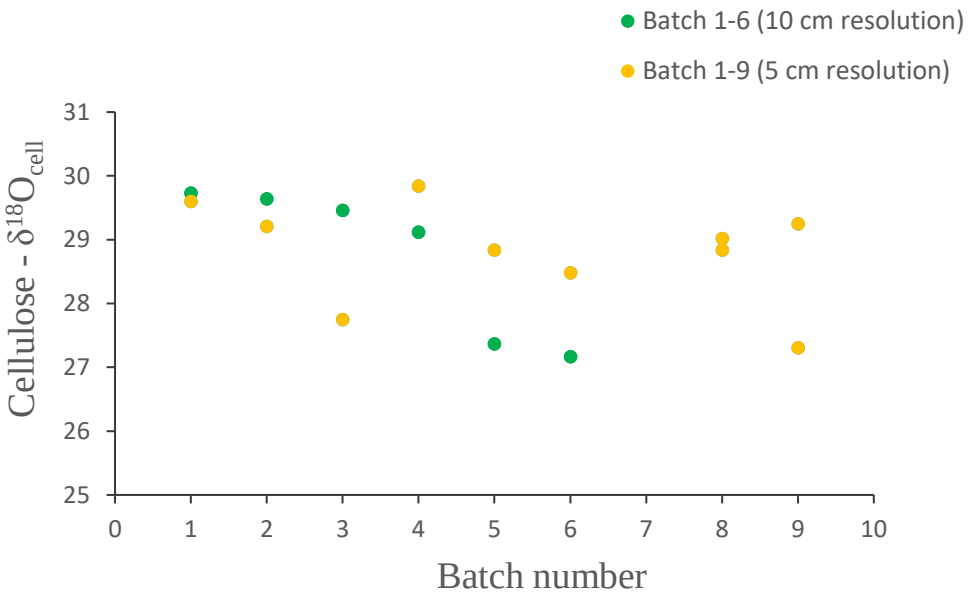

Figure II. Distribution of Cellulose powder samples measured with the separate batches of sediment samples

$\delta^{18}O_{cell}$ in cellulose powder illustrate inconsistent distribution between different batches with an approximately 1‰ deviation. However, considering the consistency observed in both the pinewood and international standards (e.g. cellulose, Sucrose and silver phosphate) it is apparent that this bias is most likely due to the inhomogeneity of the cellulose powder or maybe these samples may have adsorbed moisture from the atmosphere due to their hygroscopic nature. Therefore, this cannot be accounted for as a methodological error. In addition to international standards, this adds a tie-point to validate the consistency and replicability of the methodology.

	Batch number		$\delta^{18}O_{cell}$
10 cm resolution sample batches	1	cellulose	29.73
	2	cellulose	29.64
	3	cellulose	29.46
	4	cellulose	29.12
	5	cellulose	27.37
	6	cellulose	27.17
5 cm resolution sample batches	1	cellulose	29.6
	2	cellulose	29.21
	3	cellulose	27.75
	4	cellulose	29.84
	5	cellulose	28.84
	6	cellulose	28.48
	7	cellulose	28.84
	7	cellulose	29.02
	8	cellulose	27.31
	8	cellulose	29.25

Table I. $\delta^{18}O_{cell}$ values of cellulose powder processed along with sediment samples

	Batch number	sample	$\delta^{18}O_{cell}$
10 cm resolution sample batches	1	wood	30.18
	2	wood	29.85
	3	wood	30.07
	4	wood	29.7
	5	wood	29.87
	6	wood	28.99
	1	wood	30.13
5 cm resolution sample batches	2	wood	29.36
	3	wood	29.25
	4	wood	29.38
	5	wood	29
	6	wood	29.88
	7	wood	29.05
	7	wood	29.45
	8	wood	29.26
	8	wood	29.62

Table II. $\delta^{18}O_{cell}$ values of Pinewood samples processed along with sediment samples

Section 3: Equipment set up used in monitoring of modern rainwater and sediment samples from the Lake Surprise,

Figure I. Automated rainfall sampler (Ankor et. al. (2019), installed at Wannon water treatment plant, McArthur

Figure II. Lake sediment trap used to collect sediment samples from the lake bottom. Each end collects two 125 ml sediment column

Section 4: PCA analysis of ITRAX data

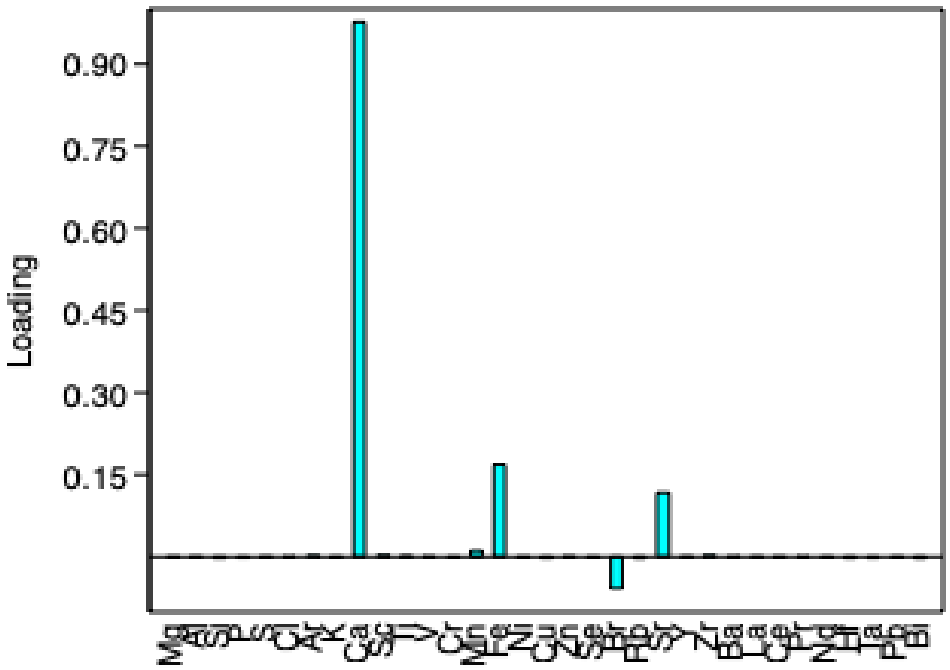

Figure I. Representation of PC1 (Ca abundance), the graph is obtained from Barr et al., in preparation.

CHAPTER 6

Key outcomes and suggestions for future research

6 Key outcomes and suggestions for future research

The main objective of this thesis was to develop a palaeoclimate record for south-eastern Australia to contribute to understanding long-term climate variability, supported by a robust understanding of the contemporary proxy system that links climate processes to lake sediment geochemistry. In this chapter, the key outcomes of this thesis will be discussed in light of three distinct outcomes. Furthermore, limitations and ideas for future research based on the findings of this thesis will be discussed.

6.1 Key outcomes

i. Understanding the hydrological balance of Lake Surprise, Victoria, the role of groundwater and the influence of climate

The main focus of Chapter 2 of this thesis was to better understand the modern hydrological system at Lake Surprise, a crater lake in Victoria, Australia. Results obtained from a seven-year monitoring program (2015 – 2022) of lake water and rainwater samples, collected at monthly and three-monthly intervals, were utilised to assess the groundwater influence and lake water oxygen isotope response to climate variability. Analysis of lake water major ionic composition interpreted using Piper and Gibbs plots, indicates that the lake water salts are mainly Na-HCO_3 type, most likely sourced from groundwater derived by basalt weathering and carbonate dissolution. This observation was further supported by similar groundwater chemistry data observed from nearby borehole locations and also by considering the similar water chemistry measured by Timms, (1975). A comparison of water chemistry over ~50 years indicates that the lake's composition appears to have been relatively constant for that time. The Lake Surprise groundwater regime was further assessed using HCO_3^-/Cl^- and deuterium-excess (d-excess) in lake waters, whereby HCO_3^-/Cl^- is used to differentiate if the source of the water is primarily groundwater or surface and interflow, and d-excess is used to infer lake residence time (Barton et al., 2013).

Variability in $\delta^{18}O$ and $\delta^{2}H$ in Lake Surprise waters is dominated by evaporation, as indicated by paired $\delta^{18}O$ and $\delta^{2}H$ values defining a 'local evaporation line' (LEL) when plotted against each other, exhibiting a slope of 3.93 (Chapter 2, Figure 7). The processes driving variability in $\delta^{18}O$ and $\delta^{2}H$ of lake water were investigated using an isotope mass balance model, driven

by climate data from a nearby weather station (Macarthur), and isotopes in precipitation data monitored in Melbourne (GNIP database). Overlapping monthly rainfall $\delta^{18}O$ data from Macarthur and Melbourne exhibit similar trends and values, lending confidence in the use of Melbourne data to estimate Macarthur rainwater isotopes. The isotope mass balance model further highlighted groundwater influence on the lake water mass balance, whereby estimated Index Lake $\delta^{18}O$ and $\delta^{2}H$ values plots at the maximum end of the projected LEL and away from the measured lake water values. Using a steady-state isotope mass balance model (Lacey & Jones, 2018) fluxes of groundwater into and out of the lake were estimated. Hence, the lake can be therefore characterised as a groundwater-dominant through-flow lake. This understanding of lake hydrology and the major controls of lake water oxygen isotope variability provides a basis for the robust interpretation of lake sediment oxygen isotopes as a palaeoclimate proxy (Jones et al., 2016; Jones & Dee, 2018).

ii. Development of a more accurate chronology for the Holocene period by evaluating different age-models

The generation of palaeoclimate proxy records with improved chronological control is essential to develop a deeper understanding of Holocene climate variability (Dixon et al., 2019; De Deckker, 2022). Multiple methods were employed to develop a robust chronology of sediment accumulation at Lake Surprise. Younger sediments collected from the upper 1 m of sediment were dated using ^{210}Pb activity and Pu concentration and isotope ratios. Deeper sediments were dated using pollen (33 samples), macrofossils (17 samples) and a limited number of bulk sediment dates (3 samples). Pu is a marker for historical nuclear weapons testing and based on the total Pu concentration, depths corresponding to the maximum atmospheric global fall-out, which was recorded ~1964 CE in the Southern Hemisphere and the first detection of Pu, which was considered to be ~ 1954 in southern latitudes were estimated (Leslie & Hancock, 2008; Harrison et al., 2021). These historical chronomarkers were used to validate the ^{210}Pb chronology, and thus lend confidence in the dating of sediments aged <100 years. With respect to radiocarbon dates, an age offset was identified between the radiocarbon ages of pollen and macrofossil samples, with pollen dates being older than the macrofossil dates by 340±50 ^{14}C years. This age offset was interpreted to reflect the possible incorporation of algal spores within the pollen extracts, which in turn may have assimilated groundwater-derived radiometrically 'old' carbon.

A Holocene sediment age-depth model for Lake Surprise was created using the Bayesian *Plum* model (Aquino-López et al., 2018, 2020). ~10,850 cal yr BP is thus captured by 11.4 m of sediment, with an estimated sedimentation rate of ~9.5 cm/year. This age model provides the foundation both for the climate reconstruction presented in this thesis, as well as future work on Lake Surprise. The detailed analysis of pollen radiocarbon dating further provide useful insights for others who consider applying this technique to similar lake sediments.

iii. Contributing to the knowledge of Holocene climate variability in the south-east Australian region through the application of stable isotope data

In order to expand the number of high-quality palaeoclimate records for south-eastern Australia, Chapters 4 and 5 in this thesis focused on validating and applying oxygen isotopes in lake sediment cellulose as a proxy for past hydroclimate at Lake Surprise, building on the modern hydrological research in Chapter 2 and the age model development in Chapter 3.

- Validation of palaeoclimate assumptions using sediment proxy-climate relationship

In principle, oxygen isotopes in aquatic cellulose preserved in lake sediment provide a direct archive of palaeo-lake water oxygen isotope composition, which in turn is physically linked to lake water mass balance (Edwards & McAndrews, 1989; Rozanski et al., 2010; Street-Perrott et al., 2018). However, despite the widespread use of oxygen isotopes as a palaeoclimate proxy, several factors raise uncertainties around the interpretation of such data in the palaeo-context, including seasonal biases in sedimentation and possible diagenetic alteration. As a consequence, to validate the use of cellulose oxygen isotopes ($\delta^{18}O_{cell}$) as a palaeoclimate proxy, $\delta^{18}O_{cell}$ data spanning the last ~130 years were analysed and compared to instrumental climate data for the same period. Carbon isotopes in bulk organic matter ($\delta^{13}C_{org}$) and calcium carbonate concentration, reflected by Ca content, were also analysed for comparison. $\delta^{18}O_{cell}$ inversely correlated with changes in effective moisture (P-E), consistent with the outcomes from Chapter 2, as well as evaporation and mean annual air temperature, and as such was validated as a robust proxy for past hydrological balance. $\delta^{13}C_{org}$ also exhibited a positive correlation to both evaporation and air temperature, whereas Ca content illustrated a negative correlation to evaporation and temperature and a positive correlation with rainfall. Changes in $\delta^{13}C_{org}$ were interpreted to reflect changes in lake productivity, possibly associated with the nutrient influx and lake water mixing. Carbonate concentration may fluctuate due to changes in groundwater inflow, or possibly also due to changes in productivity or carbonate dissolution

in acidic and anoxic bottom waters. For example, increased groundwater inflow during times of heavy rainfall or lake processes like photosynthesis and stratification/mixing regimes may have an impact on enhanced carbonate formation in wet periods. The findings from Chapter 4, therefore, lay the foundation for the interpretation of $\delta^{18}O_{cell}$ as a palaeoclimate proxy. Additionally, this study enhances the knowledge of lake environmental changes over decadal timescales, the role of climate and the generation of sedimentary proxies.

- A new record of Holocene hydroclimate based on cellulose oxygen isotopes from Lake Surprise

A decadal to centennial-scale lake water oxygen isotope record that spans over ~10,850 cal yr BP was produced using sedimentary cellulose from Lake Surprise. The record was supported by the chronology developed in Chapter 3, which consists of two or more dates per millennium. Previous research has identified a relatively wet early-mid Holocene and a tendency towards late Holocene drying (Kemp et al., 2012; Wilkins et al., 2013; De Deckker, 2022). The record from Lake Surprise broadly supports these records, however, it also indicates that the early Holocene was characterised by three wet intervals from ~ 10850 – 10000 cal yr BP, 7400 – 7000 cal yr BP and 5600 – 4500 cal yr BP, with the intervening periods being relatively dry. This is the first time this early Holocene centennial-millennial scale variability has been documented for south-eastern Australia.

The Lake Surprise hydroclimate reconstruction from Lake Surprise is similar to reconstructed changes in the Southern Westerly Winds (SWW) (Moros et al., 2009; Saunders et al., 2018), particularly during the relatively wet periods in the early to mid-Holocene period. Further, a prolonged period of relatively dry climate during the late Holocene (after ~4,500 cal yr BP) generally corresponds with evidence for the increased frequency of El-Niño events (Moy et al., 2002; Perner et al., 2018; Barr et al., 2019). At least until the last millennium, the influence of the Indian Ocean Dipole (IOD) on lake isotope variations was less evident (Abram et al., 2009; Niedermeyer et al., 2014). Considering the decadal to centennial-scale resolution, well-constrained chronology and use of validated palaeoclimate proxies, the Lake Surprise record offers valuable new insights into the timing and nature of hydroclimate changes in south-eastern Australia, which in turn can be used to investigate the drivers of long term climate variability.

6.2 Suggestions for future research

This thesis has demonstrated the potential of stable oxygen isotopes in lacustrine cellulose as a palaeoclimate proxy and provided new data and tools for examining the nature of south-eastern Australian climate change over decades to centuries. Further, this study well-addressed the key elements that are necessary for a reliable climate reconstruction such as a chronological framework that is well-constrained, a better understanding of the contemporary lake system and its response to climate variables and evaluation of palaeoclimate hypotheses and sediment proxy data prior to being used as a palaeoclimate proxy. Therefore the Lake water oxygen isotope record developed in this thesis can be used in the future, for detailed comparison with other regional records and remote climate drivers. Provided that the majority of the climate model simulations rely on the resolution and chronological framework of the datasets, this may also be applied in the numerical approaches to enhance the accuracy of climate projections for the region.

One major limitation throughout Chapter 2 was the lack of sufficient monitoring data (e.g. groundwater isotope data, intermittent sampling due to COVID-19 disruptions) and poor integrity between climate data (i.e. precipitation data were obtained from two weather stations), which confined modelled outcomes. Another limitation was the instrumental errors in the rainfall sampler, partly also due to COVID-19 disruption, which caused the loss of rainfall isotope data. The model can be improved in the future by extending the monitoring period, especially throughout more extreme climate changes (droughts, pluvial), increasing sampling resolution and minimising any instrumental or analytical errors, which enable increased accuracy of the model outputs. The stratification regime may have contributed to the relative differences between model predictions and observed data at times of enriched lake water isotopes because it may have reflected changes in lake water isotopes in the epilimnion rather than the entire water column. This can be eliminated by monitoring water samples along the depth profile for their isotope values, thereby, application of average lake water isotope values in the model. Despite these drawbacks, modelled hydrology remained consistent with the observational data, in particular related to the groundwater dominance in the lake.

An important future application of the steady-state modelling approach used in this thesis would be a quantitative reconstruction of precipitation variability through the Holocene by combining the contemporary lake water balance and lake water isotope record developed in Chapters 2 and 5. This has previously been employed in lakes in Macedonia (Lacey & Jones,

2018). The relative hydrological inputs and outputs of the lake can be assumed to be consistent with the present-day ratios and parameters like evaporation (temperature), precipitation and the isotope composition of precipitation can either be estimated using palaeoclimate model simulations or alternative palaeoclimate proxies. Accordingly, groundwater inflow and outflow can be calculated for the early Holocene, mid-Holocene and late-Holocene periods by averaging the isotope record (Lacey & Jones, 2018). Another potential future study would be the extension of this lake model for the past 130 years through the instrumental period, in order to explore the change in lake water isotopes and water depth in response to annual and decadal-scale changes in precipitation and evaporation. Further, the sediment proxy-climate relationship employed in Chapter 4 can be replicated in other western Victorian lakes to elucidate the reliability of the sediment proxies and to validate palaeoclimate assumptions used in these studies, thereby, increasing the accuracy of these records and their application to future sediment proxy reconstructions.

6.3 List of references cited

Abram, N. J., McGregor, H. V., Gagan, M. K., Hantoro, W. S., & Suwargadi, B. W. (2009). Oscillations in the southern extent of the Indo-Pacific Warm Pool during the mid-Holocene. *Quaternary Science Reviews*, *28*(25–26), 2794–2803. https://doi.org/10.1016/j.quascirev.2009.07.006

Aquino-López, M. A., Blaauw, M., Christen, J. A., & Sanderson, N. K. (2018). Bayesian Analysis of 210 Pb Dating. *Journal of Agricultural, Biological, and Environmental Statistics*, *23*(3), 317–333. https://doi.org/10.1007/s13253-018-0328-7

Aquino-López, M. A., Ruiz-Fernández, A. C., Blaauw, M., & Sanchez-Cabeza, J. A. (2020). Comparing classical and Bayesian 210Pb dating models in human-impacted aquatic environments. *Quaternary Geochronology*, *60*(November 2019). https://doi.org/10.1016/j.quageo.2020.101106

Barr, C., Tibby, J., Leng, M. J., Tyler, J. J., Henderson, A. C. G., Overpeck, J. T., Simpson, G. L., Cole, J. E., Phipps, S. J., Marshall, J. C., McGregor, G. B., Hua, Q., & McRobie, F. H. (2019). Holocene El Niño–Southern Oscillation variability reflected in subtropical Australian precipitation. *Scientific Reports*, *9*(1), 1–9. https://doi.org/10.1038/s41598-019-38626-3

Barton, A. B., Herczeg, A. L., Dahlhaus, P. G., & Cox, J. W. (2013). A geochemical approach to determining the hydrological regime of wetlands in a volcanic plain, South-Eastern Australia. *Groundwater and Ecosystems*, 69–79. https://doi.org/10.1201/b15003-12

De Deckker, P. (2022). The Holocene hypsithermal in the Australian region. *Quaternary Science Advances*, *7*(July), 100061. https://doi.org/10.1016/j.qsa.2022.100061

Dixon, B., Tyler, J., Henley, B. J., & Drysdale, R. (2019). Regional patterns of hydroclimate variability in southeastern Australia over the past 1200 years. *Earth and Space Science Open Archive*. https://doi.org/10.1002/essoar.10501482.1

Edwards, T. W. D., & McAndrews, J. H. (1989). Paleohydrology of a Canadian Shield land inferred from 18O in sediment cellulose. *Canadian Journal of Earth Sciences*, *26*(9), 1850–1859. https://doi.org/10.1139/e89-158

Harrison, J. J., Saunders, K. M., Child, D. P., & Hotchkis, M. A. C. (2021). A record of fallout 239Pu and 240Pu at World Heritage Bathurst Harbour, Tasmania, Australia. *Journal of Environmental Radioactivity*, *237*(June). https://doi.org/10.1016/j.jenvrad.2021.106679

Jones, M. D., Cuthbert, M. O., Leng, M. J., McGowan, S., Mariethoz, G., Arrowsmith, C., Sloane, H. J., Humphrey, K. K., & Cross, I. (2016). Comparisons of observed and modelled lake δ18O variability. *Quaternary Science Reviews*, *131*, 329–340. https://doi.org/10.1016/j.quascirev.2015.09.012

Jones, M. D., & Dee, S. G. (2018). Global-scale proxy system modelling of oxygen isotopes in lacustrine carbonates: New insights from isotope-enabled-model proxy-data comparison. *Quaternary Science Reviews*, *202*, 19–29. https://doi.org/10.1016/j.quascirev.2018.09.009

Kemp, J., Radke, L. C., Olley, J., Juggins, S., & De Deckker, P. (2012). Holocene lake salinity changes in the Wimmera, southeastern Australia, provide evidence for millennial-scale climate variability. *Quaternary Research*, *77*(1), 65–76. https://doi.org/10.1016/j.yqres.2011.09.013

Lacey, J. H., & Jones, M. D. (2018). Quantitative reconstruction of early Holocene and last glacial climate on the Balkan Peninsula using coupled hydrological and isotope mass balance modelling. *Quaternary Science Reviews*, *202*, 109–121. https://doi.org/10.1016/j.quascirev.2018.09.007

Leslie, C., & Hancock, G. J. (2008). Estimating the date corresponding to the horizon of the first detection of 137Cs and 239+240Pu in sediment cores. *Journal of Environmental Radioactivity*, *99*(3), 483–490. https://doi.org/10.1016/j.jenvrad.2007.08.016

Moros, M., De Deckker, P., Jansen, E., Perner, K., & Telford, R. J. (2009). Holocene climate variability in the Southern Ocean recorded in a deep-sea sediment core off South Australia. *Quaternary Science Reviews*, *28*(19–20), 1932–1940. https://doi.org/10.1016/j.quascirev.2009.04.007

Moy, C. M., Seltzer, G. O., Rodbell, D. T., & Anderson, D. M. (2002). Variability of El Niño/Southern Oscillation activity at millennial timescales during the Holocene epoch. *Nature*, *420*(6912), 162–165. https://doi.org/10.1038/nature01194

Niedermeyer, E. M., Sessions, A. L., Feakins, S. J., & Mohtadi, M. (2014). Hydroclimate of the western Indo-Pacific Warm Pool during the past 24,000 years. *Proceedings of the National Academy of Sciences of the United States of America*, *111*(26), 9402–9406. https://doi.org/10.1073/pnas.1323585111

Perner, K., Moros, M., De Deckker, P., Blanz, T., Wacker, L., Telford, R., Siegel, H., Schneider, R., & Jansen, E. (2018). Heat export from the tropics drives mid to late Holocene palaeoceanographic changes offshore southern Australia. *Quaternary Science Reviews*, *180*, 96–110. https://doi.org/10.1016/j.quascirev.2017.11.033

Rozanski, K., Klisch, M. A., Wachniew, P., Gorczyca, Z., Goslar, T., Edwards, T. W. D., & Shemesh, A. (2010). Oxygen-isotope geothermometers in lacustrine sediments: New insights through combined δ18O analyses of aquatic cellulose, authigenic calcite and biogenic silica in Lake Gościaz, central Poland. *Geochimica et Cosmochimica Acta*, *74*(10), 2957–2969. https://doi.org/10.1016/j.gca.2010.02.026

Saunders, K. M., Roberts, S. J., Perren, B., Butz, C., Sime, L., Davies, S., Van Nieuwenhuyze, W., Grosjean, M., & Hodgson, D. A. (2018). Holocene dynamics of the Southern Hemisphere westerly winds and possible links to CO2 outgassing. *Nature Geoscience*, *11*(9), 650–655. https://doi.org/10.1038/s41561-018-0186-5

Street-Perrott, F. A., Holmes, J. A., Robertson, I., Ficken, K. J., Koff, T., Loader, N. J., Marshall, J. D., & Martma, T. (2018). The Holocene isotopic record of aquatic cellulose from Lake Äntu Sinijärv, Estonia: Influence of changing climate and organic-matter sources. *Quaternary Science Reviews*, *193*, 68–83. https://doi.org/10.1016/j.quascirev.2018.05.010

Wilkins, D., Gouramanis, C., de Deckker, P., Fifield, L. K., & Olley, J. (2013). Holocene lake-level fluctuations in Lakes Keilambete and Gnotuk, southwestern Victoria, Australia. *Holocene*, *23*(6), 784–795. https://doi.org/10.1177/0959683612471983

APPENDICES

Appendix 1

This appendix contains the preliminary lake model developed for Lake Surprise using the lake bathymetry measurements obtained in 2019, which accompany in Chapters 1, 2, 4 and 5

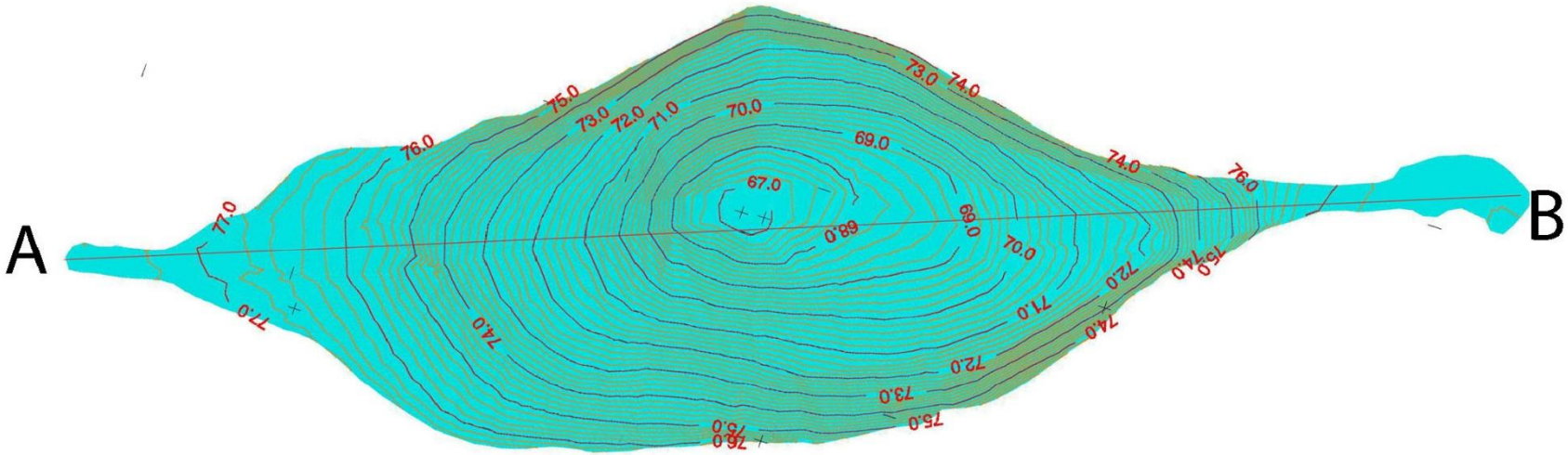

Figure I. The preliminary lake model of Lake Surprise developed using the bathymetry measurements obtained in 2019 (developed by Martin Ankor).

Detailed methodology of lake bathymetry is given in Chapter 2 (Section 2.3.1). The 3D-view of the lake cross-section illustrated in this thesis was developed using contour measurements along the AB line.

Appendix 2

This appendix contains data tables resulting from the lake monitoring and sampling program, which accompany Chapters 2 and 5.

Table I. Major ion data used in the piper plot and Gibbs analysis

Date	Depth (m)	Ca (mg/L)	Mg (mg/L)	Na (mg/L)	K (mg/L)	Cl (mg/L)	SO4 (mg/L)	HCO_3+CO_3(mg/L)	Source
1976		15.04	16.32	80.96	7.8	102.5	10.08	161.04	Timms, 1975
2016-04-16		19.21	27.09	88.5	9.7	118.0	1.24	206.4	Ankor, 2020
2016-08-03		26.52	25.33	80.35	8.98	109.0	1.6	214.0	Ankor, 2020
2016-09-20		22.49	23.94	72.76	8.31	96.7	3.64	188.0	Ankor, 2020
2016-11-18		27.59	24.39	72.81	8.39	94.2	4.77	202.0	Ankor, 2020
2017-01-06		28.97	25.05	77.88	8.78	104.0	4.64	190.0	Ankor, 2020
2017-03-12		26.6	26.3	83.2	9.59	98.5	4.1	196.0	Ankor, 2020
2017-04-25		26.4	24.8	78.7	9.2	93.5	3.25	188.0	Ankor, 2020
2017-06-29		30.8	25.3	79.2	9.01	95.3	2.31	204.0	Ankor, 2020
2017-09-03		31.1	24.5	79.4	9.09	92.1	2.24	180.0	Ankor, 2020
2017-11-07		25.5	24.3	76.6	8.64	90.2	2.82	158.0	Ankor, 2020
2018-01-22		27.4	24.8	82.3	9.55	94.9	2.66	212.0	Ankor, 2020
2018-03-06		26.6	26.4	81.8	9.43	102.0	2.55	232.0	Ankor, 2020
2018-05-07		27.0	26.3	80.3	9.42	103.0	2.25	204.0	Ankor, 2020
2018-07-09		29.9	25.7	80.2	9.16	102.0	2.26	235.0	Ankor, 2020
2018-09-11		29.7	24.6	76.1	8.41	95.6	2.41	224.0	Ankor, 2020
2020-02-13	0.5 m	13.0	21.0	84.0	11.0	112.0	4.0	210.0	
	10 m	33.0	23.0	84.0	12.0	106.0	4.0	298.0	
2020-06-24	0.5 m	28.0	26.0	82.0	10.0	98.0	2.0	206.0	
2020-12-09	0.5 m	15.0	21.0	76.0	10.0	98.0	2.0	212.0	
	10 m	27.0	23.0	76.0	10.0	104.0	2.0	273.0	
2021-03-21	0.5 m	12.0	20.0	80.0	10.0	110.0	5.0	204.0	
	10 m	30.0	21.0	78.0	10.0	108.0	3.0	298.0	
2022-04-14	0.5 m	24.0	25.0	84.0	9.0	100.0	4.5	162.0	

Table II. Lake water isotope and physical measurements obtained during the monitoring period. Data from 2015 – 2018 are accessed from Ankor, (2020). Data from 2019 – 2022 were measured by the author.

Date	$\delta^{18}O$ (‰)	$\delta^{2}H$ (‰)	Water level (m)	Altitude (AHD)	EC (µS/cm)	PH	T (ºC)	Source
23/05/2015	3.1	11.9						Ankor, 2020
29/08/2015	2.67	10.7						Ankor, 2020
6/04/2016	4.23	17.32	11.02	77.816	680	8.77	17.75	Ankor, 2020
3/08/2016	3	12.9	11.05	77.854				Ankor, 2020
20/09/2016	1.7	6.7						Ankor, 2020
18/11/2016	1.68	6.8	12.04	78.843	553	9.26	21.45	Ankor, 2020
6/01/2017	2.35	9.2			676	8.98	25.09	Ankor, 2020
12/03/2017	2.96	10.76	11.77	78.571	587	9.1	21.7	Ankor, 2020
25/04/2017	2.54	9.03						Ankor, 2020
29/06/2017	2.52	8.67	11.62	78.42	597	7.7	10.8	Ankor, 2020
3/09/2017	2.08	7.26	11.61	78.41	604	9.2	12.8	Ankor, 2020
7/11/2017	2.15	8.75	11.92	78.72	584	9.26	18.12	Ankor, 2020
22/01/2018	3.04	11.56	11.86	78.66	588	8.9	26	Ankor, 2020
6/03/2018	3.4	13.33	11.71	78.51	686	8.9	21.3	Ankor, 2020
7/05/2018	3.3	12.61	11.54	78.34	647	8.7	15	Ankor, 2020
9/07/2018	2.67	9.52	11.52	78.32	639	7.97	10.44	Ankor, 2020
11/09/2018	2.26	8.11	11.67	78.47	661	9.28	12.7	Ankor, 2020
30/10/2019	2.70	11.23	11.2	78	702	8.91	13.88	
17/12/2019	3.16	12.63						
20/01/2020	3.75	15.79						
12/02/2020	2.72	11.40						
31/03/2020	4.41	16.07						
6/05/2020	3.28	12.94						

Date	$\delta^{18}O$ (‰)	$\delta^{2}H$ (‰)	Water level (m)	Altitude (AHD)	EC (µS/cm)	PH	T (ºC)	Source
12/06/2020	3.42	12.71						
23/06/2020	2.94	10.83			790	8.6		
6/07/2020	3.58	13.03						
2/09/2020	2.71	10.11						
29/09/2020	2.75	9.45						
1/11/2020	2.86	9.86						
8/12/2020	2.71	9.94	11.2	78	635	7.7	18.75	
6/01/2021	3.01	11.42						
4/02/2021	3.22	11.72						
11/03/2021	3.79	13.84			686	8.84	19.7	
3/04/2021	3.26	12.20						
5/05/2021	3.06	12.40						
1/06/2021	3.21	12.30						
7/07/2021	2.62	9.40						
14/04/2022	3.24	12.50			640	8.86	18.84	

Table III. Rainfall isotope measurements obtained from the automated rainfall sampler from November 2019 – March 2021 (Note that these values are obtained from the daily collected samples)

Sample ID	$\delta^{18}O$ (‰)	$\delta^{2}H$ (‰)
2SUR	1.53	15.52
3SUR	1.53	12.95
4SUR	-4.66	-25.09
5SUR	NA	NA
6SUR	1.89	12.38
7SUR	-4.90	-25.61
8SUR	-4.39	-26.58
9SUR	-1.21	0.36
10SUR	-3.89	-24.65
11SUR	-1.95	-22.00
12SUR	NA	NA
13SUR	NA	NA
14SUR	-2.68	-15.09
15SUR	-0.14	0.30
16SUR	-0.54	-4.66
17SUR	-1.32	-6.21
18SUR	-2.50	-22.05
19SUR	-2.63	-20.78
20SUR	1.86	8.78
21SUR	-1.57	-1.54
22SUR	-2.23	-6.08
23SUR	-1.23	-3.12
24SUR	0.83	8.52
25SUR	-0.20	6.25
26SUR	-3.31	-21.75
27SUR	-1.37	-6.18
34SUR	-1.40	0.90
35SUR	0.65	9.85
37SUR	NA	NA
36SUR	1.65	3.59
38SUR	1.43	1.27
42SUR	1.87	7.15
45SUR	-4.82	-39.53
46SUR	0.78	-1.99
60SUR	-1.98	-8.02
LS-6-1	-4.18	-33.82
LS-6-2	-1.21	-3.67
LS-6-3	-5.14	-34.28
LS-6-4	-4.14	-21.96
LS-6-5	0.02	2.05
LS-6-6	-3.48	-18.42
LS-6-7	-4.16	-22.55
LS-6-8	-3.53	-17.94
LS-6-9	-5.98	-38.18
LS-6-10	-1.38	-1.58
LS-6-11	-0.41	-0.19
LS-6-12	0.13	4.28

Sample ID	$\delta^{18}O$ (‰)	$\delta^{2}H$ (‰)
LS-6-13	-5.08	-31.64
LS-6-14	-2.36	-17.13
LS-6-15	-8.92	-67.65
LS-6-16	-5.47	-26.88
LS-6-17	-3.23	-12.29
LS-6-18	-1.75	-8.47
LS-6-19	-1.19	-1.20
LS-6-20	-1.77	-5.51
LS-6-21	1.37	7.69
LS-6-34	0.32	2.52
LS-6-35	-1.32	0.28
LS-6-36	-3.47	-25.71
LS-6-37	-4.40	-39.61
LS-6-38	-2.44	-13.75
LS-6-39	-6.24	-36.67
LS-6-40	-7.33	-43.57
LS-6-41	-7.85	-47.52
LS-6-42	-1.44	-0.14
LS-6-43	-1.56	0.64
LS-6-44	-2.14	-7.61
LS-6-45	-8.92	-59.21
LS-6-46	-4.56	-17.35
LS-12-1	-1.26	-8.06
LS-12-2	-2.60	-8.55
LS-12-3	-2.40	-10.64
LS-12-4	-4.42	-24.90
LS-12-5	-3.90	-23.40
LS-12-6	-2.94	-6.30
LS-12-7	-2.12	-3.72
LS-12-8	-2.05	-4.67
LS-12-9	-5.36	-30.75
LS-12-10	-4.85	-28.23
LS-12-11	-1.60	-9.04
LS-12-12	-4.24	-21.37
LS-12-13	-3.33	-15.82
LS-12-14	-2.09	-5.28
LS-12-15	-3.35	-12.33
LS-12-16	-3.26	-15.76
LS-12-17	-1.36	0.91
LS-12-18	-6.76	-32.11
LS-12-19	-3.17	-7.09
LS-12-20	-3.80	-15.82
LS-12-21	-3.86	-21.00
LS-12-22	-0.55	3.32
LS-12-23	-3.33	-20.29
LS-12-24	-3.86	-19.12
LS-12-25	-5.07	-26.90
LS-12-32	-5.57	-36.15
LS-12-36	-2.48	-10.51
LS-12-37	-7.15	-47.43
LS-12-38	-4.25	-24.37
LS-12-39	-3.52	-19.19

Sample ID	$\delta^{18}O$ (‰)	$\delta^{2}H$ (‰)
LS-12-40	-5.97	-35.69
LS-12-41	0.15	0.53
LS-12-43	-3.62	-11.26
LS-12-44	-2.91	-15.33
LS-12-45	-3.50	-14.99
LS-12-46	-2.44	-10.33
LS-12-47	-4.26	-20.14
LS-12-49	-5.30	-21.11
LS-12-50	-6.98	-31.61
LS-12-51	-2.75	-8.67
LS-12-52	-3.67	-7.62
LS-12-53	-3.11	-19.01
LS-12-54	-4.83	-24.62
LS-12-55	-3.85	-15.47

Table IV: Rainfall isotope measurements of obtained from the monthly collected samples

Month	$\delta^{18}O$ (‰)	$\delta^{2}H$ (‰)
October 2019	-3.92	-20.17
November 2019	-3.44	-17.02
December 2019	-1.63	-8.02
January 2020	-4.37	-25.36
April 2020	-6.12	-37.30
May 2020	-6.42	-39.61
July 2020	-4.98	-24.09
September 2020	-5.10	-26.52
November 2020	-6.35	-35.12

Appendix 3

This appendix contains data tables resulting from the XRF analysis of sediment core samples, which accompany Chapter 4.

Section 1: XRF data

Table I. Major element concentrations of the SUR-19-01 sediment core measured using the XRF handheld analyser (Note that LE refers to light element concentration (C, H,O))

Field depth	composite depth	Age	Age	Ca	Sr	Fe	S	Si	Cl	LE
cm	cm	cal yr BP	CE	%	%	%	%	%	%	%
0.5	0.35	-69	2019.0	0.4281	0.002	0.0749	0.0725	1.1233	0.8166	97.3661
1.0	1.05	-67.95	2018.0	0.3663	0.0016	0.0862	0.0671	1.0756	0.7315	97.22
1.5	1.75	-66.9	2016.9	0.3687	0.0016	0.075	0.068	1.0736	0.7288	97.5584
2.0	2.45	-65.85	2015.9	0.4869	0.0018	0.1747	0.0736	1.0771	0.6686	97.3273
2.5	3.15	-64.8	2014.8	0.4395	0.0017	0.1486	0.0793	1.0434	0.7092	97.3981
3.0	3.85	-63.8	2013.8	0.3566	0.0018	0.0894	0.0658	1.035	0.7095	97.3181
3.5	4.55	-62.75	2012.8	0.5228	0.002	0.1532	0.0777	1.0754	0.6983	97.308
4.0	5.25	-61.7	2011.7	0.3807	0.0016	0.0739	0.0613	1.0941	0.6985	97.4336
4.5	5.95	-60.65	2010.7	0.4043	0.0021	0.0674	0.059	1.0503	0.7153	97.5189
5.0	6.65	-59.6	2009.6	0.4358	0.0021	0.0737	0.0581	1.0689	0.7015	97.2
5.5	7.35	-58.6	2008.6	0.4516	0.0018	0.0621	0.0595	1.1208	0.7281	97.4674
6.0	8.05	-57.55	2007.6	0.601	0.0019	0.1254	0.0659	0.962	0.633	97.14
6.5	8.75	-56.75	2006.8	0.5315	0.0019	0.0814	0.0568	1.0582	0.6906	97.4658
7.0	9.45	-55.95	2006.0	0.7541	0.0023	0.1197	0.062	1.0063	0.6328	97.2521
7.5	10.15	-55.15	2005.2	0.7335	0.0022	0.123	0.0607	1.0462	0.6419	97.2501
8.0	10.85	-54.35	2004.4	0.5474	0.0017	0.0735	0.057	1.014	0.6837	97.09
8.5	11.55	-53.55	2003.6	0.6247	0.002	0.1005	0.0591	1.0339	0.6631	97.3769
9.0	12.25	-52.75	2002.8	0.6951	0.0025	0.1268	0.0735	0.9868	0.6727	96.98
9.5	12.95	-51.95	2002.0	0.7166	0.0024	0.123	0.0587	0.987	0.6306	97.09
10.0	13.65	-51.15	2001.2	0.8279	0.0027	0.1115	0.0626	1.0352	0.6398	97.1932
10.5	14.35	-50.35	2000.4	0.8741	0.0026	0.1114	0.0625	0.9953	0.6931	97.0997
11.0	15.05	-49.55	1999.6	1.0551	0.0033	0.1439	0.0625	0.9795	0.6272	96.9344
11.5	15.75	-48.75	1998.8	0.8129	0.0027	0.0955	0.0575	0.9382	0.6845	97.2017

Field depth	composite depth	Age	Age	Ca	Sr	Fe	S	Si	Cl	LE
cm	cm	cal yr BP	CE	%	%	%	%	%	%	%
12.0	16.45	-46.05	1996.1	1.2994	0.0041	0.1481	0.0621	0.9058	0.5884	96.7907
12.5	17.15	-42.25	1992.3	1.6091	0.0049	0.1586	0.0724	0.9319	0.6088	96.4965
13.0	17.85	-38.45	1988.5	1.0298	0.0034	0.1195	0.0656	0.9673	0.6528	96.9685
13.5	18.55	-34.65	1984.7	1.5832	0.0037	0.1657	0.0643	0.9619	0.6442	96.3927
14.0	19.25	-30.95	1981.0	1.1477	0.0037	0.1113	0.0575	0.9783	0.621	96.9612
14.5	19.95	-27.3	1977.3	1.5707	0.0046	0.151	0.0644	0.9134	0.6158	96.27
15.0	20.65	-23.8	1973.8	1.1393	0.0037	0.1276	0.0659	0.9343	0.6495	96.8942
15.5	21.35	-20.6	1970.6	1.3697	0.0044	0.1495	0.0562	0.9875	0.6071	96.7349
16.0	22.05	-17.85	1967.9	1.4849	0.0044	0.1381	0.0591	0.9547	0.5976	96.39
16.5	22.75	-15.55	1965.6	1.4066	0.0044	0.1481	0.0577	0.9045	0.5893	96.7907
17.0	23.45	-13.25	1963.3	1.5802	0.0041	0.1977	0.076	0.9246	0.6078	96.4963
17.5	24.15	-10.75	1960.8	1.5016	0.0041	0.1839	0.0773	0.9614	0.6143	96.32
18.0	24.85	-8.8	1958.8	1.3016	0.0039	0.123	0.0743	0.9355	0.6546	96.48
18.5	25.55	-6.75	1956.8	1.4138	0.0044	0.1627	0.0662	0.9472	0.5887	96.6701
19.0	26.25	-4.55	1954.6	1.543	0.0047	0.1639	0.0713	0.9932	0.5983	96.4899
19.5	26.95	-2.35	1952.4	1.1243	0.0037	0.1532	0.0732	1.0374	0.6156	96.9476
20.0	27.65	-0.15	1950.2	1.0542	0.0033	0.1333	0.0755	1.2699	0.63	96.42
20.5	28.3	1.8	1948.2	1.3152	0.0043	0.1591	0.0716	0.9699	0.6029	96.7297
21.0	28.95	3.85	1946.2	1.2125	0.004	0.1485	0.0794	0.9636	0.6345	96.7948
21.5	29.6	5.8	1944.2	1.2105	0.004	0.183	0.1008	0.9587	0.6579	96.8389
22.0	30.25	7.75	1942.3	0.8296	0.003	0.1728	0.0952	0.9035	0.6328	97.2103
22.5	30.9	9.7	1940.3	0.9697	0.0029	0.2031	0.0856	0.9609	0.636	96.9666
23.0	31.55	11.55	1938.5	0.9672	0.0031	0.2313	0.0904	0.9528	0.6527	97.005
23.5	32.2	13.4	1936.6	0.913	0.003	0.2725	0.0846	0.9821	0.614	96.9503
24.0	32.85	15.15	1934.9	0.7089	0.0026	0.2028	0.0944	0.9958	0.6484	97.1856
24.5	33.5	16.8	1933.2	0.9656	0.0034	0.3269	0.1109	0.947	0.5927	96.889
25.0	34.15	18.6	1931.4	0.7599	0.0028	0.2416	0.1044	0.9572	0.5979	97.1468
25.5	34.8	20.3	1929.7	0.702	0.0023	0.1868	0.1161	1.0076	0.6329	97.1518

Field depth	composite depth	Age	Age	Ca	Sr	Fe	S	Si	Cl	LE
cm	cm	cal yr BP	CE	%	%	%	%	%	%	%
26.0	35.45	21.95	1928.1	0.8804	0.0029	0.2203	0.1103	0.9638	0.6048	97.0448
26.5	36.1	23.7	1926.3	0.7996	0.0021	0.2431	0.1294	0.9974	0.6357	96.89
27.0	36.75	25.8	1924.2	0.7992	0.0025	0.2392	0.1123	0.9772	0.6259	96.86
27.5	37.4	28.2	1921.8	0.7923	0.0021	0.2849	0.1083	0.9398	0.6149	96.83
28.0	38.05	30.6	1919.4	0.6439	0.0023	0.1663	0.086	0.9996	0.6794	97.03
28.5	38.7	32.8	1917.2	0.7986	0.0024	0.209	0.0821	1.0084	0.6409	97.2113
29.0	39.35	35	1915.0	0.786	0.0024	0.1903	0.0882	0.988	0.6349	97.2138
29.5	40	37.1	1912.9	0.7205	0.0021	0.1646	0.0886	1.0034	0.6475	97.2348
30.0	40.65	38.2	1911.8	0.6581	0.0022	0.152	0.0772	0.981	0.6302	97.1
30.5	41.2	39.1	1910.9	0.6425	0.0021	0.1394	0.0761	1.0436	0.684	97.3682
31.0	41.75	40	1910.0	0.6177	0.0021	0.1151	0.0786	1.0139	0.7006	97.06
31.5	42.3	40.9	1909.1	0.7017	0.0029	0.1853	0.0955	1.0827	0.8132	96.74
32.0	42.85	41.8	1908.2	0.6401	0.0022	0.1804	0.083	1.0126	0.6676	97.08
32.5	43.4	42.7	1907.3	0.7161	0.0024	0.2282	0.0989	1.039	0.6381	96.88
33.0	43.95	43.6	1906.4	0.6366	0.002	0.1927	0.0832	0.9957	0.6165	97.09
33.5	44.5	44.5	1905.5	0.5252	0.0018	0.1645	0.0848	1.0398	0.6449	97.03
34.0	45.05	45.5	1904.5	0.7746	0.0022	0.208	0.104	1.01	0.6274	96.88
34.5	45.6	46.4	1903.6	0.6612	0.002	0.2057	0.0997	1.0247	0.6341	97.04
35.0	46.15	47.35	1902.7	0.6347	0.0019	0.1762	0.1042	1.0489	0.6556	96.95
35.5	46.7	48.3	1901.7	0.6037	0.0018	0.3103	0.1124	1.0426	0.6067	96.95
36.0	47.25	49.3	1900.7	0.5416	0.002	0.2575	0.106	1.0687	0.6562	97.06
36.5	47.8	50.2	1899.8	0.4239	0.0013	0.232	0.1089	0.9796	0.6062	97.28
37.0	48.35	51.1	1898.9	0.4309	0.0015	0.1895	0.0819	1.0461	0.6409	97.2
37.5	48.9	51.9	1898.1	0.4195	0.0016	0.1984	0.0867	1.0368	0.672	97.14
38.0	49.45	52.8	1897.2	0.4883	0.0016	0.1548	0.0755	1.0724	0.6637	97.4194
38.5	50	53.6	1896.4	0.4744	0.0017	0.1747	0.0905	1.0438	0.6608	97.3865
39.0	50.55	54.55	1895.5	0.5033	0.0021	0.2044	0.0887	1.0959	0.8112	97.244
39.5	51.1	55.4	1894.6	0.4489	0.002	0.1525	0.0895	1.0434	0.7646	97.12

Field depth	composite depth	Age	Age	Ca	Sr	Fe	S	Si	Cl	LE
cm	cm	cal yr BP	CE	%	%	%	%	%	%	%
40.0	51.65	56.3	1893.7	0.4713	0.0018	0.1533	0.091	1.0397	0.773	97.3802
40.5	52.15	57.1	1892.9	0.5934	0.002	0.2024	0.0974	1.036	0.6897	97.07
41.0	52.65	57.9	1892.1	0.5881	0.0021	0.194	0.0911	1.0549	0.6856	97.01
41.5	53.15	58.8	1891.2	0.6143	0.0021	0.201	0.092	1.0318	0.6438	97.2706
42.0	53.65	59.6	1890.4	0.533	0.0021	0.2302	0.0884	0.993	0.628	97.3268
42.5	54.15	60.4	1889.6	0.5398	0.0021	0.2113	0.0867	0.9846	0.6538	97.3572
43.0	54.65	61.3	1888.7	0.4914	0.0018	0.2159	0.091	0.9984	0.7316	97.3203
43.5	55.15	62.1	1887.9	0.5419	0.0019	0.2394	0.0898	1.0062	0.6439	97.03
44.0	55.65	62.9	1887.1	0.4644	0.0016	0.1614	0.0783	0.9761	0.6426	97.26
44.5	56.15	63.8	1886.2	0.4773	0.002	0.1718	0.0852	1.0626	0.7035	97.4071
45.0	56.65	64.85	1885.2	0.49	0.0018	0.1679	0.0757	1.019	0.6403	97.4445
45.5	57.15	65.95	1884.1	0.4894	0.0018	0.1464	0.0753	0.9964	0.6736	97.4735
46.0	57.65	67.1	1882.9	0.5033	0.0019	0.1681	0.0856	1.0149	0.7068	97.24
46.5	58.15	68.25	1881.8	0.5861	0.002	0.1625	0.0767	0.9851	0.6192	97.4043
47.0	58.65	69.55	1880.5	0.5237	0.0018	0.1402	0.0819	1.006	0.6525	97.22
47.5	59.15	70.85	1879.2	0.5606	0.002	0.1759	0.0832	1.0233	0.6314	97.3574
48.0	59.65	72.25	1877.8	0.5582	0.002	0.1691	0.0821	0.9973	0.6772	97.3803
48.5	60.15	73.65	1876.4	0.5459	0.0019	0.1731	0.0831	0.9705	0.6715	97.14
49.0	60.65	75.05	1875.0	0.5477	0.0019	0.1903	0.0844	0.994	0.6429	97.14
49.5	61.15	76.45	1873.6	0.5381	0.0021	0.1743	0.0827	0.9973	0.6681	97.37
50.0	61.65	77.85	1872.2	0.5593	0.0021	0.1582	0.0837	1.0599	0.6641	97.09
50.5	62.15	79.15	1870.9	0.5224	0.0016	0.1278	0.067	0.9747	0.6335	97.5414
51.0	62.65	80.45	1869.6	0.5584	0.0021	0.1301	0.0849	0.9969	0.7105	97.4686
51.5	63.15	81.65	1868.4	0.5876	0.002	0.1579	0.0845	1.0061	0.654	97.18
52.0	63.65	82.8	1867.2	0.5391	0.0019	0.1433	0.0814	0.9892	0.6657	97.15
52.5	64.15	84.1	1865.9	0.6596	0.0024	0.1749	0.0848	1.0254	0.6158	97.02
53.0	64.65	85.9	1864.1	0.5622	0.002	0.1584	0.0904	1.0821	0.6972	97.1
53.5	65.15	87.75	1862.3	0.5294	0.0019	0.1282	0.0855	1.0149	0.6843	97.16

Field depth	composite depth	Age	Age	Ca	Sr	Fe	S	Si	Cl	LE
cm	cm	cal yr BP	CE	%	%	%	%	%	%	%
54.0	65.65	89.6	1860.4	0.6288	0.0024	0.1746	0.0851	0.9801	0.6206	97.12
54.5	66.15	91.5	1858.5	0.5347	0.0021	0.1452	0.0809	0.9988	0.6701	97.4216
55.0	66.65	93.35	1856.7	0.5696	0.0019	0.1482	0.0834	1.0022	0.6459	97.3768
55.5	67.15	95.2	1854.8	0.5203	0.0019	0.1426	0.0892	1.0366	0.6938	97.23
56.0	67.65	97.05	1853.0	0.6342	0.0021	0.1865	0.093	0.9659	0.6682	97.12
56.5	68.15	98.85	1851.2	0.6583	0.0023	0.2181	0.0974	0.9736	0.6436	97.05
57.0	68.65	100.55	1849.5	0.5727	0.002	0.1881	0.0895	1.0211	0.6494	97.14
57.5	69.15	102.4	1847.6	0.6063	0.0018	0.1751	0.0878	0.9891	0.638	97.09
58.0	69.65	104.1	1845.9	0.6568	0.0023	0.2309	0.0898	1.0125	0.6857	97.2009
58.5	70.15	105.8	1844.2	0.5513	0.002	0.1756	0.09	0.9895	0.6785	97.4143
59.0	70.65	107.55	1842.5	0.567	0.0019	0.1846	0.0878	1.0234	0.6681	97.3023
59.5	71.15	109.2	1840.8	0.627	0.0027	0.2146	0.0892	0.9869	0.6762	96.96
60.0	71.65	110.9	1839.1	0.6469	0.0022	0.1945	0.0866	1.0016	0.6444	96.98
60.5	72.25	112.85	1837.2	0.6836	0.0023	0.1879	0.0867	0.9664	0.6462	96.99
61.0	72.85	114.65	1835.4	0.7337	0.0024	0.1638	0.0848	0.9278	0.6528	97.04
61.5	73.45	116.3	1833.7	0.7415	0.0023	0.1766	0.0808	1.0114	0.6521	96.97
62.0	74.05	118	1832.0	0.8086	0.0024	0.1643	0.0792	0.9355	0.6256	96.99
62.5	74.65	119.55	1830.5	0.8326	0.0026	0.1731	0.0785	0.9194	0.6104	97
63.0	75.25	121.1	1828.9	0.8491	0.0026	0.1726	0.0747	0.9115	0.6195	97.2394
63.5	75.85	122.75	1827.3	0.8949	0.0026	0.2029	0.0899	1.0478	0.6901	96.78
64.0	76.45	124.4	1825.6	0.9135	0.0027	0.2264	0.077	0.94	0.5922	96.89
64.5	77.05	126.15	1823.9	0.8273	0.0026	0.1924	0.0733	0.9458	0.5753	97.2146
65.0	77.65	127.85	1822.2	0.8584	0.0025	0.1956	0.0736	0.9779	0.5927	97.1858
65.5	78.25	129.55	1820.5	0.9261	0.0031	0.2414	0.08	0.9523	0.577	96.82
66.0	78.85	131.25	1818.8	0.9203	0.0032	0.2443	0.0896	0.9755	0.5521	97.0691
66.5	79.45	132.85	1817.2	0.8311	0.0028	0.2015	0.0774	0.9577	0.5671	97.01
67.0	80.05	134.6	1815.4	0.7769	0.0024	0.1639	0.0809	0.9832	0.5953	97.08
67.5	80.65	136.5	1813.5	1.1232	0.0034	0.2944	0.0825	0.9699	0.5375	96.63

Field depth	composite depth	Age	Age	Ca	Sr	Fe	S	Si	Cl	LE
cm	cm	cal yr BP	CE	%	%	%	%	%	%	%
68.0	81.25	138.55	1811.5	0.8125	0.0026	0.1655	0.0816	0.9881	0.6076	97.2055
68.5	81.85	140.5	1809.5	0.8966	0.0024	0.1837	0.0779	1.0363	0.5834	96.73
69.0	82.45	142.55	1807.5	0.8087	0.0026	0.1428	0.0725	1.0147	0.6092	97.03
69.5	83.05	144.45	1805.6	0.952	0.0031	0.2201	0.0851	1.1306	0.6842	96.53
70.0	83.65	146.25	1803.8	0.8278	0.0023	0.1619	0.0756	1.0123	0.6053	96.89
70.5	84.25	148.05	1802.0	0.7925	0.0026	0.1462	0.0699	0.9644	0.5879	97.2352
71.0	84.85	150.05	1800.0	0.9859	0.0028	0.2133	0.0715	0.9724	0.5501	97.0026
71.5	85.45	151.95	1798.1	0.9905	0.0028	0.1848	0.0735	0.989	0.5754	97.0309
72.0	86.05	153.85	1796.2	0.9403	0.0026	0.151	0.0714	1.0415	0.5814	97.0289
72.5	86.65	155.65	1794.4	1.1363	0.0033	0.195	0.0886	1.2286	0.5953	96.41
73.0	87.25	157.55	1792.5	1.318	0.0041	0.2291	0.0785	0.9576	0.5126	96.7104
73.5	87.85	159.45	1790.6	1.0658	0.0032	0.1803	0.0714	1.0513	0.5586	96.8626
74.0	88.45	161.25	1788.8	1.3163	0.0042	0.2407	0.0801	0.9687	0.5529	96.45
74.5	89.05	163.3	1786.7	1.3321	0.004	0.2333	0.0698	0.9887	0.5365	96.41
75.0	89.65	165.45	1784.6	1.3672	0.0036	0.2191	0.0759	1.0008	0.5422	96.6868
75.5	90.25	167.65	1782.4	1.1272	0.0039	0.1975	0.0699	0.9614	0.5622	96.6
76.0	90.85	169.85	1780.2	1.1772	0.0036	0.2036	0.0709	0.9815	0.5508	96.8448
76.5	91.45	172.15	1777.9	1.114	0.0032	0.2132	0.0879	0.9886	0.5613	96.61
77.0	92.05	174.4	1775.6	0.8834	0.0028	0.1571	0.081	0.9799	0.6161	97.1525
77.5	92.65	176.55	1773.5	1.0114	0.0029	0.2282	0.0856	0.9912	0.5611	96.9307
78.0	93.25	178.65	1771.4	1.1883	0.0032	0.2017	0.0778	0.955	0.5702	96.8669
78.5	93.85	180.65	1769.4	1.1056	0.0028	0.256	0.0834	0.9598	0.5517	96.66
79.0	94.45	182.55	1767.5	0.9837	0.0029	0.2479	0.0822	0.9802	0.5672	96.76
79.5	95.05	184.65	1765.4	1.017	0.0028	0.2342	0.0847	0.9943	0.5716	96.72
80.0	95.65	186.5	1763.5	0.9293	0.0029	0.2432	0.0818	1.0382	0.5627	96.82
80.5	96.2	188.4	1761.6	0.8703	0.0026	0.1909	0.0852	1.0111	0.6029	97.1885
81.0	96.75	190.65	1759.4	0.9436	0.0031	0.1972	0.0949	1.0614	0.7348	96.62
81.5	97.3	193.5	1756.5	0.9004	0.0026	0.2238	0.0802	0.9774	0.5628	96.92

Field depth	composite depth	Age	Age	Ca	Sr	Fe	S	Si	Cl	LE
cm	cm	cal yr BP	CE	%	%	%	%	%	%	%
82.0	97.85	196.45	1753.6	0.934	0.0028	0.2178	0.0825	0.9491	0.5579	96.88
82.5	98.4	199.1	1750.9	0.9682	0.0029	0.2509	0.0772	0.9314	0.5597	97.0211
83.0	98.95	201.45	1748.6	1.1415	0.0029	0.2929	0.0828	0.9673	0.5622	96.59
83.5	99.5	203.7	1746.3	1.0667	0.0031	0.2832	0.0808	0.9412	0.5631	96.9008
84.0	100.05	206.1	1743.9	1.1368	0.0033	0.3276	0.0806	0.9813	0.5653	96.61
84.5	100.6	208.3	1741.7	1.3728	0.0034	0.3166	0.087	0.9569	0.5515	96.24
85.0	101.15	210.5	1739.5	1.2	0.0025	0.2606	0.0776	0.9345	0.5635	96.8592
85.5	101.7	212.6	1737.4	0.78	0.0026	0.2435	0.0836	1.0049	0.5969	97.142
86.0	102.25	214.55	1735.5	0.7365	0.0023	0.2424	0.077	0.9999	0.5904	97.1922
86.5	102.8	216.6	1733.4	0.9398	0.0024	0.2502	0.08	0.9671	0.574	97.0918
87.0	103.35	218.65	1731.4	0.8705	0.0023	0.2518	0.0817	0.9895	0.5667	96.85
87.5	103.9	220.8	1729.2	0.7243	0.002	0.2823	0.0915	1.0006	0.6046	97
88.0	104.45	224.2	1725.8	0.716	0.0023	0.2617	0.0873	1.0016	0.5952	96.96
88.5	105	227.9	1722.1	0.6274	0.0024	0.285	0.0852	1.0019	0.6126	96.96
89.0	105.55	231.9	1718.1	0.5771	0.0023	0.2287	0.0767	1.0081	0.5992	97.19
89.5	106.1	236.1	1713.9	0.6441	0.0022	0.2366	0.0735	0.9837	0.5819	97.11
90.0	106.65	240.15	1709.9	0.7273	0.0026	0.2663	0.0775	0.9817	0.5794	97.2036
90.5	107.15	243.85	1706.2	0.9085	0.0026	0.3026	0.0776	0.94	0.5565	96.81
91.0	107.65	247.65	1702.4	0.7918	0.0024	0.2675	0.0859	1.0058	0.5995	97.075
91.5	108.15	250.9	1699.1	0.7454	0.0025	0.307	0.0939	0.9997	0.6355	96.77
92.0	108.65	254.45	1695.6	1.0302	0.0032	0.2692	0.0761	1.0308	0.596	96.57
92.5	109.15	257.7	1692.3	1.1498	0.003	0.2867	0.0887	0.9826	0.6012	96.6951
93.0	109.65	260.8	1689.2	1.1388	0.0034	0.2787	0.0824	0.9808	0.5826	96.57
93.5	110.15	263.85	1686.2	1.3297	0.0037	0.3254	0.0875	0.9419	0.5726	96.5777
94.0	110.65	266.95	1683.1	1.2951	0.0035	0.2967	0.0866	0.9654	0.5764	96.588
94.5	111.15	269.8	1680.2	1.345	0.0032	0.2857	0.0824	0.9956	0.5806	96.5356
95.0	111.65	272.6	1677.4	1.0444	0.0029	0.2313	0.0763	0.9774	0.5889	96.74
95.5	112.15	275.6	1674.4	0.8852	0.0027	0.1969	0.0915	1.006	0.6208	96.78

Field depth	composite depth	Age	Age	Ca	Sr	Fe	S	Si	Cl	LE
cm	cm	cal yr BP	CE	%	%	%	%	%	%	%
96.0	112.65	279.3	1670.7	0.8684	0.0027	0.2093	0.0768	0.991	0.6094	97.0742
96.5	113.15	282.8	1667.2	0.8499	0.0024	0.1976	0.0764	1.0132	0.629	97.1123
97.0	113.65	286.4	1663.6	0.7713	0.0026	0.1809	0.0764	0.9969	0.6173	96.95
97.5	114.15	290	1660.0	0.7625	0.0023	0.1909	0.0748	1.0354	0.6122	96.89
98.0	114.65	293.4	1656.6	0.7561	0.0021	0.2011	0.0812	1.0166	0.6009	96.96
98.5	115.15	297.1	1652.9	0.6292	0.0023	0.1858	0.0759	1.0013	0.6308	97.03
99.0	115.65	301	1649.0	0.5468	0.0018	0.1756	0.0799	1.041	0.6449	97.3507
99.5	116.15	305.05	1645.0	0.566	0.0019	0.1805	0.0798	1.031	0.6459	97.03
100.0	116.65	309.15	1640.9	0.5308	0.0017	0.1961	0.0797	1.0828	0.5968	97.11
100.5	117.2	313.9	1636.1	0.5345	0.0018	0.1897	0.0761	1.0636	0.6183	97.15
101.0	117.75	318.7	1631.3	0.5769	0.0019	0.1958	0.0796	1.0418	0.6131	97.12
101.5	118.3	323.6	1626.4	0.5104	0.0021	0.1938	0.0823	1.0461	0.6451	97.17
102.0	118.85	328.35	1621.7	0.5144	0.0019	0.1993	0.0849	1.0229	0.6116	97.4114
102.5	119.4	333.3	1616.7	0.6631	0.0023	0.2827	0.1057	1.0822	0.7	96.89
103.0	119.95	338.4	1611.6	0.5135	0.0018	0.2171	0.0839	1.0051	0.6039	97.15
103.5	120.5	346.6	1603.4	0.6453	0.0022	0.2253	0.1011	1.2047	0.7477	97.0047
104.0	121.05	355.3	1594.7	0.519	0.0019	0.2205	0.0839	1.0221	0.6117	97.24
104.5	121.6	364.4	1585.6	0.5189	0.0019	0.2113	0.0892	1.0145	0.6219	97.11
105.0	122.15	373.5	1576.5	0.5365	0.0018	0.2261	0.0896	1.0405	0.6338	97.4196
105.5	122.7	382.9	1567.1	0.5421	0.0018	0.2227	0.0884	1.0049	0.5979	97.19
106.0	123.25	392.35	1557.7	0.6094	0.002	0.2703	0.1027	0.9817	0.6878	96.92
106.5	123.8	402.1	1547.9	0.5216	0.0019	0.2068	0.0783	0.9817	0.5843	97.4842
107.0	124.35	411.9	1538.1	0.5604	0.0022	0.2632	0.0855	0.9916	0.6138	97.09
107.5	124.9	422	1528.0	0.6115	0.0022	0.2671	0.0989	1.0546	0.6169	97.293
108.0	125.45	432	1518.0	0.5027	0.002	0.1915	0.083	1.0348	0.6425	97.16
108.5	126	441.8	1508.2	0.4863	0.0019	0.1879	0.0829	0.9994	0.6374	97.27
109.0	126.55	451.25	1498.8	0.4893	0.0021	0.201	0.0834	1.0494	0.6145	97.4549
109.5	127.1	459.8	1490.2	0.4937	0.0017	0.2037	0.0831	0.9945	0.6642	97.19

Field depth	composite depth	Age	Age	Ca	Sr	Fe	S	Si	Cl	LE
cm	cm	cal yr BP	CE	%	%	%	%	%	%	%
110.0	127.65	467.35	1482.7	0.479	0.0019	0.1846	0.0763	1.035	0.6186	97.4895
110.5	128.2	473.1	1476.9	0.5285	0.0018	0.1911	0.0919	1.1063	0.6804	97.2893
111.0	128.75	475.85	1474.2	0.5252	0.0019	0.2028	0.0838	1.0588	0.6118	97.2
111.5	129.3	478.8	1471.2	0.496	0.0017	0.1756	0.0792	1.019	0.6281	97.23
112.0	129.85	481.65	1468.4	0.5184	0.0019	0.1833	0.0849	1.0047	0.6414	97.17
112.5	130.4	484.6	1465.4	0.529	0.002	0.1586	0.0785	1.0421	0.6434	97.14
113.0	130.95	487.6	1462.4	0.5636	0.0019	0.1666	0.0856	1.0242	0.6514	97.09
113.5	131.5	490.5	1459.5	0.7016	0.0023	0.1756	0.0914	1.2451	0.7266	96.9409
114.0	132.05	493.45	1456.6	0.5275	0.0019	0.1641	0.0854	0.9859	0.7178	97.14
114.5	132.6	496.3	1453.7	0.5318	0.002	0.1888	0.0772	1.0516	0.6228	97.4032
115.0	133.15	498.95	1451.1	0.5256	0.0019	0.1979	0.0784	1.0377	0.6446	97.4187
115.5	133.7	501.4	1448.6	0.5006	0.0018	0.1851	0.0824	1.0677	0.6319	97.4782
116.0	134.25	503.95	1446.1	0.505	0.0019	0.1874	0.0795	1.0234	0.619	97.16
116.5	134.8	506.5	1443.5	0.5155	0.0019	0.1855	0.0863	1.0318	0.6333	97.2
117.0	135.35	509.4	1440.6	0.5512	0.002	0.2093	0.0817	1.0281	0.6229	97.4036
117.5	135.9	512.8	1437.2	0.5372	0.002	0.2175	0.0811	0.9824	0.614	97.2
118.0	136.45	516	1434.0	0.5285	0.0019	0.2096	0.0814	0.9866	0.6223	97.425
118.5	137	519.4	1430.6	0.5895	0.0021	0.2139	0.0782	1.015	0.6148	97.3345
119.0	137.55	522.75	1427.3	0.6194	0.002	0.2294	0.0861	0.9654	0.5959	97.09
119.5	138.1	526	1424.0	0.6437	0.002	0.2225	0.0844	0.9776	0.6054	97.09
120.0	138.65	529.2	1420.8	0.643	0.0019	0.2108	0.0836	1.0036	0.6067	97.2961
120.5	139.29	532.85	1417.2	0.5283	0.0018	0.1997	0.0861	1.0012	0.6002	97.4547
121.0	139.94	536.3	1413.7	0.5709	0.002	0.2137	0.0942	1.039	0.6487	97.3788
121.5	140.58	539.7	1410.3	0.555	0.0019	0.225	0.0934	1.0125	0.6253	97.11
122.0	141.22	543.1	1406.9	0.5477	0.0019	0.2106	0.0897	0.9824	0.6399	97.3522
122.5	141.86	546.5	1403.5	0.5427	0.0017	0.2252	0.0898	1.028	0.645	97.2988
123.0	142.51	549.85	1400.2	0.6034	0.002	0.2558	0.0957	1.0023	0.616	97.3249
123.5	143.15	553.2	1396.8	0.5609	0.0018	0.2043	0.0882	1.0199	0.6008	97.23

Field depth	composite depth	Age	Age	Ca	Sr	Fe	S	Si	Cl	LE
cm	cm	cal yr BP	CE	%	%	%	%	%	%	%
124.0	143.79	556.55	1393.5	0.6376	0.0017	0.202	0.0874	0.9805	0.5804	97.14
124.5	144.44	560.68	1389.3	0.5658	0.0021	0.2125	0.0865	1.0372	0.6559	97.15
125.0	145.08	565.26	1384.7	0.5087	0.0019	0.232	0.0927	1.038	0.5995	97.22
125.5	145.72	570.14	1379.9	0.5252	0.0016	0.2107	0.0831	0.9811	0.5653	97.4635
126.0	146.36	575.02	1375.0	0.4764	0.0016	0.196	0.0788	0.9933	0.5947	97.27
126.5	147.01	580.08	1369.9	0.5314	0.0023	0.2363	0.0919	1.0618	0.6824	97.2293
127.0	147.65	584.9	1365.1	0.5365	0.0018	0.222	0.0852	0.9893	0.6158	97.08
127.5	148.29	589.73	1360.3	0.5383	0.0018	0.2507	0.0823	0.9571	0.6106	97.11
128.0	148.94	594.48	1355.5	0.5514	0.0018	0.2545	0.0876	1.0148	0.5763	97.3395
128.5	149.58	599.14	1350.9	0.5051	0.0018	0.229	0.0763	0.9875	0.5965	97.21
129.0	150.22	603.74	1346.3	0.4957	0.0016	0.1943	0.077	1.0464	0.6345	97.4593
129.5	150.86	608.06	1341.9	0.5681	0.0019	0.2255	0.0852	0.9796	0.6056	97.13
130.0	151.51	612.27	1337.7	0.6631	0.002	0.2592	0.09	1.0022	0.5656	97.01
130.5	152.15	617.05	1333.0	0.5593	0.0022	0.2132	0.0846	0.9789	0.7018	97.2703
131.0	152.79	623.9	1326.1	0.5414	0.0018	0.2366	0.084	0.9631	0.668	97.3368
131.5	153.44	630.26	1319.7	0.5761	0.0022	0.2179	0.0821	1.0336	0.579	97.11
132.0	154.08	636.02	1314.0	0.5455	0.0016	0.2157	0.0858	0.9774	0.5894	97.4459
132.5	154.72	641.7	1308.3	0.5662	0.0022	0.2073	0.0903	1.0135	0.5688	97.4242
133.0	155.36	647.7	1302.3	0.5443	0.002	0.2257	0.0741	1.0216	0.548	97.3974
133.5	156.01	653.6	1296.4	0.6537	0.0022	0.2446	0.0886	1.0066	0.5521	97.09
134.0	156.65	659.65	1290.4	0.5565	0.0022	0.2269	0.0838	1.0267	0.6073	97.13

Appendix 4

This appendix contains data tables resulting from the stable isotope analysis of sediment core samples, which accompany Chapters 4 and 5.

Table I: Cellulose $\delta^{18}O$ lake water $\delta^{18}O$ values of the composite sediment core

Sample depth	Age (cal yr BP)	$\delta^{18}O$ in cellulose	$\delta^{18}O$ in lake water
5.25	-61.4	30.57	2.54
15.05	-48.85	31.30	3.26
19.05	-31.15	30.12	2.11
22.75	-12.45	30.99	2.95
28.3	3.4	28.94	0.96
36.75	24.5	29.93	1.92
43.4	40	30.41	2.39
46.7	45.9	29.99	1.98
52.15	55.7	31.13	3.09
56.15	63.1	30.85	2.81
57.15	65.15	31.63	3.58
62.15	77.2	31.24	3.20
65.65	88.2	31.34	3.29
71.15	109.35	31.09	3.05
77.05	126.05	30.95	2.91
83.65	145.35	30.87	2.84
90.85	168.35	30.56	2.53
98.4	196.9	31.16	3.12
102.8	214.9	31.32	3.27
109.65	261.6	30.74	2.71
116.15	306.45	31.28	3.24
123.25	394.15	31.07	3.03
128.75	476.35	31.06	3.02
133.7	501.9	30.85	2.82
138.65	529.5	30.6	2.57
144.44	560.88	31.2	3.16
150.86	607.72	31.34	3.29
156.01	654.79	31.01	2.97
160.5	698.6	31.03	2.99
169.5	807.3	31.41	3.36
175.5	881.8	31.11	3.07
181	938.8	31.26	3.22
186.5	987.1	31.35	3.30
191.5	1021.8	31.09	3.05
197	1050.2	31.34	3.29
202	1074.8	31.52	3.47
207	1100.4	31.03	2.99
211.5	1122.1	30.53	2.51
216.5	1147.9	30.32	2.30
221.5	1182.3	30.82	2.79
226.5	1222.8	30.07	2.06
231.5	1271.8	30.25	2.23
236.5	1315.7	31.2	3.16
242	1362.1	30.67	2.64
252.5	1445.4	30.97	2.93
255.5	1468.9	28.96	0.98
258	1485.3	30.52	2.50
261	1503.6	31.49	3.44
267	1541	30.96	2.92
272	1570.9	31.64	3.59

Sample depth	Age (cal yr BP)	$\delta^{18}O$ in cellulose	$\delta^{18}O$ in lake water
277	1617.7	30.66	2.63
281.5	1665.1	31.66	3.61
286.5	1716.7	31.05	3.01
291.5	1762.3	31.32	3.27
296	1799.1	30.97	2.93
301	1841	31.06	3.02
306	1879.6	29.81	1.81
311	1916.8	31.43	3.38
316	1945.2	30.55	2.53
321	1969.2	31.55	3.50
331	2020	31.32	3.27
336	2045.6	30.39	2.37
341.5	2073.6	31.37	3.32
348	2106.5	30.19	2.17
354	2135.2	30.12	2.11
359.5	2160.6	29.56	1.56
370.5	2210.9	31.42	3.37
376	2235.9	30.7	2.67
380.5	2283.3	31.09	3.05
385.5	2331.4	30.16	2.15
390.5	2375	30.64	2.61
396	2426.6	30.08	2.07
401	2474.1	30.94	2.90
406	2523.5	30.19	2.17
411.5	2577	30.6	2.57
416.5	2624.9	30.72	2.69
421	2668.4	30.94	2.90
426	2716.4	30.31	2.29
431	2766.8	31.04	3.00
436	2816	30.6	2.57
441	2864.2	30.72	2.69
446.5	2916.3	30.39	2.37
450.5	2947.4	30.94	2.90
454.5	2974.6	30.52	2.50
458.5	2999.6	30.9	2.87
467.5	3054	30.37	2.35
472.5	3084.8	30.11	2.10
475.5	3103	29.43	1.44
478.5	3121.7	30.3	2.28
481.5	3140.1	30.81	2.78
485.5	3165.4	29.36	1.37
490	3193	30.85	2.82
495	3221.4	30.46	2.44
500	3248.1	30.73	2.70
505	3274.1	30.77	2.74
510	3301.4	31.07	3.03
514.5	3325.8	30.6	2.57
519	3349.9	30.2	2.18
523	3371.6	29.8	1.80
528	3398.5	30.86	2.83
533.5	3426.5	31.37	3.32
539	3457.8	31.33	3.28

Sample depth	Age (cal yr BP)	$\delta^{18}O$ in cellulose	$\delta^{18}O$ in lake water
544.5	3495.2	30.95	2.91
550	3567.4	30.74	2.71
561.5	3685.1	30.38	2.36
566.5	3726.9	30.44	2.42
571.5	3754.6	30.32	2.30
576.5	3776.1	30.56	2.53
581.5	3797.2	29.82	1.81
586.5	3821.3	31.44	3.39
591.5	3845.9	29.9	1.89
596.5	3866.8	30.76	2.73
601.5	3888.8	29.96	1.95
606.5	3910.8	30.09	2.08
611	3932.7	30.17	2.16
616	3957.7	30.45	2.43
621	3992.3	30.74	2.71
626	4033.2	30.93	2.89
631	4077.2	30.54	2.52
636	4121.9	31.09	3.05
641	4167.9	30.92	2.89
646	4219.4	31.35	3.30
650.5	4266.1	30.51	2.49
657.5	4349.9	29.88	1.87
662.5	4411.1	29.49	1.49
667.5	4470.6	29.39	1.40
672.5	4531.2	28.57	0.60
677.5	4592.9	30.15	2.14
682.5	4653.2	29.98	1.97
687.5	4713.5	30.06	2.05
693	4779.8	30.14	2.13
698	4839.4	28.97	0.99
703	4897.8	29.31	1.32
707.5	4950.3	28.61	0.64
712.5	5007.5	29.23	1.24
717.5	5067.8	29.54	1.54
723	5151.9	29.29	1.30
728	5229.6	29.1	1.11
733	5292.2	28.1	0.14
738.5	5357	29.07	1.09
743	5430.8	27.88	-0.07
747	5470.4	28.59	0.62
755.5	5550.4	29.51	1.51
758	5575.6	29.94	1.93
763	5621.3	30.78	2.75
767.5	5662.9	30.85	2.82
771.5	5695.1	31.14	3.10
775.5	5727.1	30.5	2.48
779.5	5769.8	30.5	2.48
783.5	5822	30.88	2.85
788	5880.2	30.22	2.20
793	5937	29.68	1.68
797.5	5990.4	31.01	2.97
802.5	6046.8	30.89	2.86

Sample depth	Age (cal yr BP)	$\delta^{18}O$ in cellulose	$\delta^{18}O$ in lake water
807.5	6108.9	29.19	1.20
812.5	6184.5	30.87	2.84
817.5	6260.1	30.33	2.31
822.5	6346.9	30	1.99
827.5	6434	29.62	1.62
832.5	6523	30.75	2.72
848.5	6801.8	30.34	2.32
855.5	6900.8	30.24	2.22
866	6982.3	30.42	2.40
870.5	7015.3	28.19	0.23
874.5	7043.9	30.27	2.25
879	7076.7	29.31	1.32
884.5	7116.5	30.39	2.37
891	7162.1	28.38	0.41
896.5	7202.7	28.82	0.84
901.5	7238.4	29.5	1.50
906.5	7272	27.38	-0.56
911.5	7307	27.97	0.01
916.5	7343.7	29.87	1.86
921.5	7384.3	29.82	1.81
926.5	7432.8	29.9	1.89
932	7496.6	31.08	3.04
937.5	7562	28.62	0.65
942.5	7625.9	30.55	2.53
948	7689.5	30.62	2.59
953	7745.3	30.23	2.21
958.5	7793.7	30.77	2.74
968.5	7860.4	30.84	2.81
973.5	7891	29.51	1.51
978.5	7923.1	30.02	2.01
984	7965	30.18	2.17
989	8047.8	29.99	1.98
994	8128.2	29.27	1.28
999	8215.5	29.24	1.25
1004	8295.7	29.97	1.96
1009.5	8381.4	29.95	1.94
1014.5	8454.4	28.13	0.17
1019.5	8544.8	31.13	3.09
1024.5	8630.3	30.13	2.12
1030	8743.5	29.34	1.35
1035	8842.8	31.23	3.19
1040	8946.2	30.21	2.19
1045	9043.8	29.66	1.66
1050	9140	29.29	1.30
1055	9238.3	29.93	1.92
1057	9278.2	29.68	1.68
1058	9296.7	30.14	2.13
1062	9371.1	28.68	0.71
1067	9464	29.62	1.62
1072	9557.2	29.25	1.26
1077	9661.1	28.61	0.64
1082	9760.8	29.42	1.43

Sample depth	Age (cal yr BP)	$\delta^{18}O$ in cellulose	$\delta^{18}O$ in lake water
1087	9860.8	29.5	1.50
1092	9965.9	29.7	1.70
1097	10069.8	29.05	1.07
1102	10175.2	26.8	-1.12
1107	10279	28.74	0.76
1112	10384.4	28.34	0.38
1117	10492.8	29.59	1.59
1122	10597.9	28.04	0.08
1127	10705.4	28.91	0.93
1132	10786.4	29.49	1.49
1137	10848.8	29.12	1.13

Table II: Stable carbon and nitrogen isotope data of the composite sediment core

Sample ID	Field depth (cm)	Composite depth (cm)	Age (cal yr BP)	$\delta^{13}C$ (‰)	TOC (%)	TN (%)	C/N ratio
SUR-19-01	1.0	1.75	-66.9	-27.88	34.60	3.20	10.93
	2.0	3.15	-64.8	-27.97	35.30	3.30	10.86
	4.0	5.95	-60.65	-27.66	33.50	3.60	9.31
	6.0	8.75	-56.75	-28.01	33.30	3.20	10.58
	8.0	11.55	-53.55	-27.71	30.90	3.40	9.10
	10.5	14.35	-50.35	-28.37	25.80	2.40	10.76
	12.0	17.85	-38.45	-28.16	24.50	2.60	9.42
	14.0	22.05	-17.85	-28.42	24.00	2.10	11.41
	16.0	23.45	-13.25	-28.15	21.60	2.40	9.02
	18.0	27.65	-0.15	-29.01	23.60	2.00	11.86
	22.0	30.25	7.75	-29.65	25.90	2.10	12.48
	24.0	32.85	15.15	-28.60	29.50	3.10	9.52
	26.0	35.45	21.95	-28.92	30.60	2.50	12.34
	28.0	38.05	30.6	-28.33	30.30	3.00	10.10
	30.0	40.65	38.2	-28.62	32.10	2.60	12.45
	32.0	42.85	41.8	-28.16	33.70	3.30	10.23
	34.0	45.05	45.5	-28.96	34.10	2.80	12.18
	36.0	47.25	49.3	-29.34	38.70	3.50	11.07
	38.0	49.45	52.8	-27.82	35.00	2.90	12.14
	40.0	51.65	56.3	-27.68	36.10	3.60	10.02
	42.0	53.65	59.6	-28.07	33.60	2.90	11.79
	44.0	55.65	62.9	-28.07	33.30	3.30	10.09
	46.0	57.65	67.1	-28.36	32.70	2.80	11.75
	48.0	59.65	72.25	-28.27	34.00	3.10	10.97
	50.0	61.65	77.85	-28.43	32.60	2.80	11.73
	52.0	63.65	82.8	-28.32	30.20	3.10	9.75
	54.0	65.65	89.6	-28.76	33.00	2.80	11.87
	56.0	67.65	97.05	-28.20	33.70	3.30	10.20
	58.0	69.65	104.1	-28.61	34.10	2.80	12.23
	60.0	71.65	110.9	-28.61	33.60	3.20	10.51
	62.0	74.05	118	-28.58	33.30	2.80	11.76
	64.0	76.45	124.4	-27.72	31.50	3.00	10.49
	66.0	78.85	131.25	-28.26	31.20	2.70	11.76
	68.0	81.25	138.55	-27.98	27.70	2.90	9.57

Sample ID	Field depth (cm)	Composite depth (cm)	Age (cal yr BP)	$\delta^{13}C$ (‰)	TOC (%)	TN (%)	C/N ratio
	70.0	83.65	146.25	-28.30	31.30	2.70	11.79
	72.0	86.05	153.85	-27.91	30.10	3.00	10.02
	74.0	88.45	161.25	-28.26	28.80	2.40	11.79
	76.0	90.85	169.85	-27.94	26.60	2.70	9.84
	78.0	93.25	178.65	-28.90	28.70	2.30	12.58
	80.0	95.65	186.5	-29.33	32.30	3.10	10.42
	82.0	97.85	196.45	-29.35	33.00	2.50	13.00
	84.0	100.05	206.1	-28.64	30.00	2.90	10.35
	86.0	102.25	214.55	-28.53	32.30	2.60	12.39
	88.0	104.45	224.2	-28.79	35.50	3.40	10.39
	90.0	106.65	240.15	NA	NA	NA	NA
	92.0	110.65	266.95	-27.30	29.30	2.80	10.48
	94.0	112.65	279.3	-28.16	30.70	2.50	12.38
	96.0	114.65	293.4	-28.81	31.80	2.90	10.96
	98.0	116.65	309.15	-28.65	33.20	2.70	12.22
	100.0	118.85	328.35	-28.56	34.60	3.40	10.18
	102.0	121.05	355.3	-29.15	29.10	2.30	12.44
	104.0	123.25	392.35	-28.81	35.30	3.40	10.38
	106.0	125.45	432	-29.10	36.10	2.90	12.29
	108.0	127.65	467.35	-28.70	34.50	3.30	10.46
	110.0	129.85	481.65	-28.94	37.20	3.00	12.53
	112.0	132.05	493.45	-29.11	33.90	3.30	10.29
	114.0	134.25	503.95	-29.43	35.60	2.80	12.54
	116.0	136.45	516	-29.17	36.10	3.40	10.62
	118.0	138.65	529.2	-29.27	36.70	2.90	12.44
	120.0	143.79	556.55	-28.61	NA	NA	NA
	124.0	146.36	575.02	-28.70	NA	NA	NA
	126.0	148.94	594.48	-29.20	33.10	2.60	12.58
	128.0	151.51	612.27	-28.67	34.60	3.20	10.80
	130.0	154.08	636.02	-29.21	34.70	2.80	12.35
	132.0	155.36	647.7	-28.76	28.90	2.80	10.30
	134.0	156.65	659.65	-29.14	35.70	2.90	12.53
SUR-19-02	110	62.15		-28.66	36.70	3.30	11.12
	120	71.15		-28.22	33.70	3.10	10.87
	130	83.65		-28.19	30.50	2.80	10.89
	140	98.40		-28.72	31.40	2.70	11.63
	150	109.65		-28.08	31.90	2.90	11.00
	160	123.25		-28.87	37.90	3.30	11.48
	170	133.70		-29.51	38.80	3.30	11.76
	180	144.44		-28.85	36.40	3.00	12.13
	190	156.01		-29.28	33.40	2.80	11.93
	210	175.50		-28.15	23.80	2.10	11.33
	220	186.50		-29.83	34.50	2.90	11.90
	230	197.00		-29.94	37.60	3.50	10.74
	240	207.00		-29.05	37.50	3.40	11.03
	250	216.50		-29.54	39.10	3.40	11.50
	260	226.50		-28.14	29.20	2.40	12.17
	270	236.50		-29.53	30.30	2.40	12.63
	280	252.50		-30.00	29.70	2.50	11.88
	290	258.00		-27.59	25.40	2.10	12.10

Sample ID	Field depth (cm)	Composite depth (cm)	Age (cal yr BP)	$\delta^{13}C$ (‰)	TOC (%)	TN (%)	C/N ratio
	310	272.00		-28.88	27.20	2.20	12.36
	320	281.50		-29.63	23.60	1.80	13.11
	330	291.50		-30.03	30.60	2.40	12.75
	340	301.00		-30.26	31.20	2.60	12.00
	350	311.00		-29.30	36.30	3.00	12.10
	360	321.00		-30.00	33.20	2.70	12.30
	370	331.00		-29.55	31.00	2.60	11.92
	380	341.50		-30.37	29.80	2.10	14.19
	390	354.00		-29.09	32.10	2.50	12.84
	410	376.00		-30.16	37.30	3.00	12.43
	420	385.50		-29.73	33.40	2.50	13.36
	430	396.00		-28.83	34.30	2.70	12.70
	440	406.00		-29.23	31.00	2.50	12.40
	450	416.50		-30.02	29.60	2.40	12.33
	460	426.00		-28.15	29.80	2.50	11.92
	470	436.00		-28.84	30.00	2.40	12.50
	480	446.50		-30.34	26.00	2.10	12.38
	490	454.50		-28.75	26.30	2.10	12.52
	510	472.50		-29.53	20.20	1.70	11.88
	520	478.50		-29.27	19.90	1.60	12.44
	530	485.50		-28.84	19.10	1.60	11.94
	540	495.00		-29.05	23.30	1.90	12.26
	550	505.00		-29.66	25.50	2.00	12.75
	560	514.50		-29.25	27.40	2.20	12.45
	570	523.00		-29.39	23.00	1.70	13.53
	580	533.50		-30.07	23.00	1.80	12.78
	590	544.50		-29.22	28.20	2.20	12.82
	610	566.50		-30.82	26.10	1.80	14.50
	620	576.50		-29.81	25.90	2.00	12.95
	630	586.50		-29.91	28.60	2.10	13.62
	640	596.50		-29.37	27.70	2.00	13.85
	650	606.50		-29.69	26.70	2.00	13.35
	660	616.00		-29.65	22.00	1.60	13.75
	670	626.00		-29.58	27.00	2.10	12.86
	680	636.00		-29.33	28.70	2.10	13.67
	690	646.00		-29.69	26.00	1.90	13.68
	710	665.00		-29.04	29.70	2.80	10.61
	720	675.00		-30.36	32.70	2.90	11.28
	730	685.00		-30.23	30.90	2.90	10.66
	740	695.50		-30.21	27.70	2.70	10.26
	750	705.00		-29.48	29.60	2.90	10.21
	760	715.00		-30.14	26.80	2.70	9.93
	770	725.50		-29.60	28.50	2.70	10.56
	780	736.00		-30.03	31.60	2.90	10.90
	790	745.00		-30.71	32.40	3.00	10.80
	810	763.00		-28.95	27.50	2.70	10.19
	820	771.50		-29.26	22.30	2.20	10.14
	830	779.50		-30.72	28.00	2.60	10.77
	840	788.00		-28.35	25.90	2.50	10.36
	850	797.50		-29.96	25.20	2.60	9.69

Sample ID	Field depth (cm)	Composite depth (cm)	Age (cal yr BP)	$\delta^{13}C$ (‰)	TOC (%)	TN (%)	C/N ratio
	860	807.50		-27.99	25.10	2.60	9.65
	870	817.50		-29.14	25.10	2.50	10.04
	880	827.50		-30.35	21.50	2.30	9.35
	890	848.50		-31.91	19.10	2.20	8.68
	910	870.50		-28.83	17.10	2.10	8.14
	920	879.00		-30.07	19.10	2.10	9.10
	930	891.00		-32.28	21.00	2.10	10.00
	940	901.50		-31.35	23.10	2.30	10.04
	950	911.50		-31.77	21.00	2.00	10.50
	960	921.50		NA	NA	NA	NA
	970	932.00		-29.65	34.30	2.90	11.83
	980	942.50		-32.36	26.50	2.30	11.52
	990	953.00		-32.02	29.10	2.60	11.19
	1010	973.50		-31.67	29.70	2.60	11.42
	1020	984.00		-31.23	30.60	2.60	11.77
	1030	994.00		-30.21	35.90	2.90	12.38
	1040	1004.00		-31.22	37.10	3.10	11.97
	1050	1014.50		-29.95	34.50	2.90	11.90
	1060	1024.50		-30.74	38.70	3.20	12.09
	1070	1035.00		-31.21	43.10	3.40	12.68
	1080	1045.00		-31.67	41.00	3.30	12.42
	1090	1055.00		-31.69	41.40	3.10	13.35

Appendix 5

This appendix contains stratigraphic log of Lake Surprise sediment cores, which accompany Chapters 3, 4 and 5.

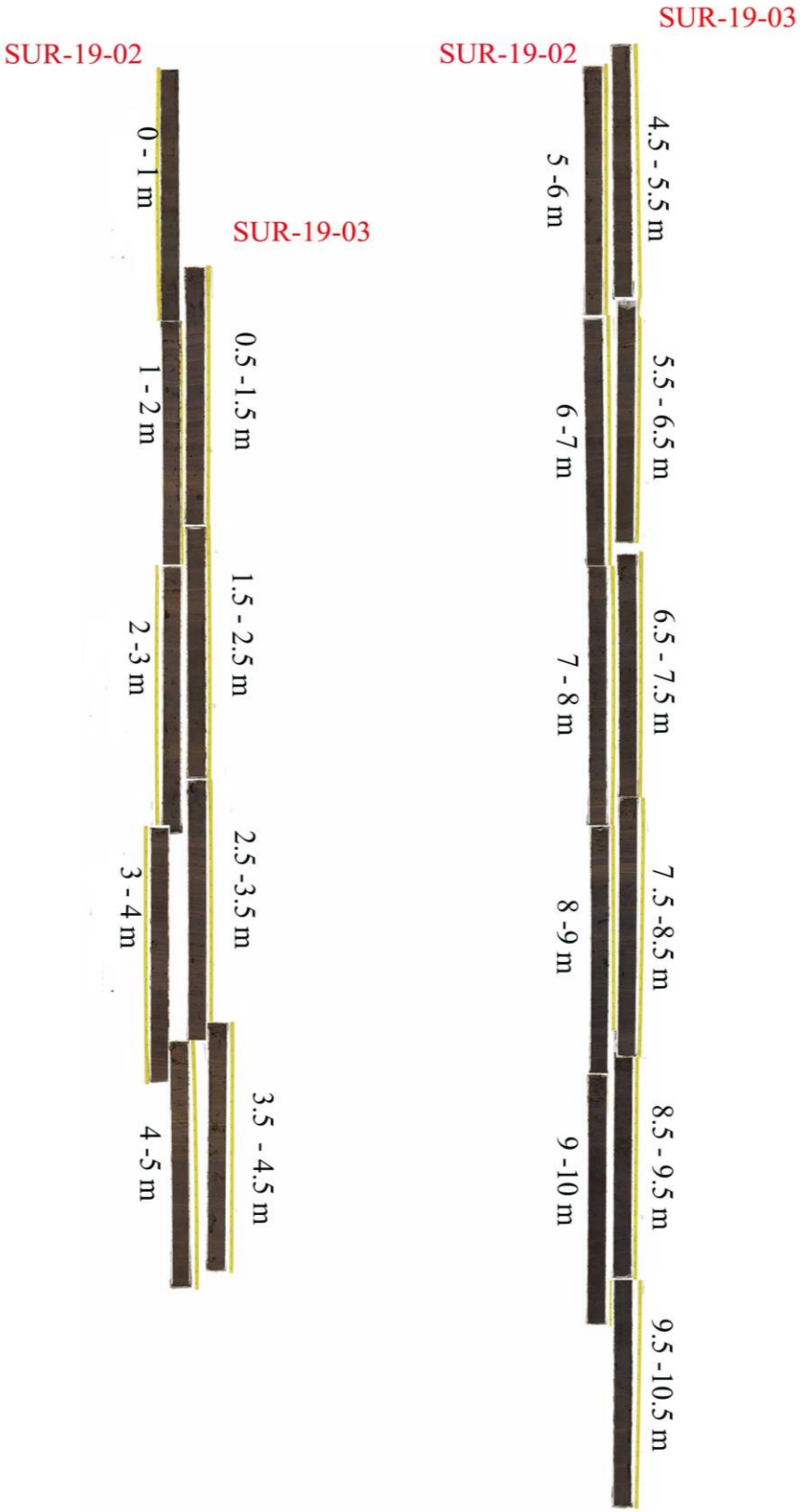

Figure I. Stratigraphic representation of Lake Surprise sediment (SUR-19-02 and SUR-19-03). Both cores were taken in 1 m drive sections with a 0.5 m depth difference between two cores.